A NEW FRAMEWORK FOR FLOODING CONTROL IN REGULATED RIVER SYSTEMS

by

Elizabeth A. Kanashiro

A thesis

submitted in partial fulfillment

of the requirements for the degree of

Master of Science in Civil Engineering

Boise State University

August 2013

BOISE STATE UNIVERSITY GRADUATE COLLEGE

DEFENSE COMMITTEE AND FINAL READING APPROVALS

of the thesis submitted by

Elizabeth A. Kanashiro

Thesis Title: A New Framework for Flooding Control in Regulated River Systems

Date of Final Oral Examination: 10 December 2010

The following individuals read and discussed the thesis submitted by student Elizabeth A. Kanashiro, and they evaluated her presentation and response to questions during the final oral examination. They found that the student passed the final oral examination.

Arturo S. Leon, Ph.D.	Chair, Supervisory Committee
Murgel George, Ph.D.	Member, Supervisory Committee
Venkataramana Sridhar, Ph.D.	Member, Supervisory Committee

The final reading approval of the thesis was granted by Arturo S. Leon, Ph.D., Chair of the Supervisory Committee. The thesis was approved for the Graduate College by John R. Pelton, Ph.D., Dean of the Graduate College.

ACKNOWLEDGMENTS

The author gratefully acknowledge the financial support of the NSF Idaho EPSCoR Program and the National Science Foundation under award number EPS-0814387.

ABSTRACT

This thesis presents a case study on the application of a dynamic framework for the intelligent control of flooding in the Boise River system in Idaho. This framework couples a robust and numerically efficient hydraulic routing approach with the popular multi-objective, non-dominated Sorting Genetic Algorithm II (NSGA-II). The novelty of this framework is that it allows for controlled flooding when the conveyance capacity of the river system is exceeded or is about to exceed. Controlled flooding is based on weight factors assigned to each reach of the system depending on the amount of damage that would occur should a flood occur. For example, an urban setting would receive a higher weight factor than a rural or agricultural area. The weight factor for a reach doesn't need to be constant as it can be made a function of the flooding volume (or water stage) in the reach. The optimization algorithm minimizes flood damage by favoring low weighted floodplain areas (e.g., rural areas) rather than high weighted areas (e.g., urban areas) for the overbank flows. The proposed framework has the potential to improve water management and use of flood-prone areas in river systems, especially of those systems subjected to frequent flooding. The Hydraulic Performance Graph (HPG) of a channel reach graphically summarizes the dynamic relation between the flow through and the stages at the ends of the reach under gradually varied flow (GVF) conditions, while the Volume Performance Graph (VPG) summarizes the corresponding storage. The Rating Performance Graph (RPG) summarizes the dynamic relation between the flow through and the stages at the ends of the in-line structure under gradually varied flow or rapidly varied flow

conditions. The use of HPGs, VPGs, and RPGs in the proposed approach results in a robust and numerically efficient model because the hydraulics for all river reaches are pre-computed (i.e., any error attained during the computation of the water profiles for each reach-e.g., due to instability-can be detected and therefore corrected before the river system routing) and most of the computations for the system routing involve only interpolation steps. The latter makes this approach highly numerically efficient. The proposed framework is the first model of its kind that uses the HPG/VPG/RPG approach for intelligent control of river flooding and has been applied to the Boise River system of Idaho. In order to test the hydraulic routing approach, a model for unsteady flow routing through dendritic and looped river networks based on performance graphs is presented in this thesis. The application presented in this thesis is limited to subcritical flows; however, it can be extended to supercritical flows. The model builds upon the application of Hydraulic Performance Graph (HPG) to unsteady flow routing introduced by [12] and adopts the Volume Performance Graph (VPG) introduced by [16]. The HPG of a channel reach graphically summarizes the dynamic relation between the flow through and the stages at the ends of the reach under gradually varied flow (GVF) conditions, while the VPG summarizes the corresponding storage. Both, the HPG and VPG are unique to a channel reach with a given geometry and roughness, and can be computed decoupled from unsteady boundary conditions by solving the GVF equation for all feasible conditions in the reach. Hence, in the proposed approach, the performance graphs can be used for different boundary conditions without the need to recompute them. Previous models based on the performance graph concept were formulated for routing through single channels or channels in series. The new approach expands on the use of HPG/VPGs and adds the use of rating performance graphs for unsteady flow routing in dentritic

and looped networks. We exemplify the applicability of the proposed model to a looped network and contrast its simulation results with those from the well-known unsteady HEC-RAS model. Our results show that the present extension of application of the HPG/VPGs appears to inherit the robustness of the HPG routing approach in [12].

TABLE OF CONTENTS

LIST OF TABLES

LIST OF FIGURES

LIST OF ABBREVIATIONS

BC – Boundary Condition

CIB – Controlled In-line structure Boundary

CPU – Central Processing Unit

CWMS – Corps Water Management System

EBC – External Boundary Condition

GVF – Gradually Varied Flow

HEC – Hydrologic Engineering Center

HECFloodOpt – Hydrologic Engineering Center Reservoir Flood Control Optimization

HEC-RAS – Hydrologic Engineering Centers River Analysis System

HEC-ResSim – Hydrologic Engineering Center Reservoir Simulation

HEC-PRM – Hydrologic Engineering Center Prescriptive Reservoir model

HPG – Hydraulic Performance Graph

HPC – Hydraulic Performance Curve

IBC – Internal Boundary Condition

InflowHydro – Inflow hydrograph

LFPG – Left Flooding Performance Graph

MCM – Million Cubic Meter

NSGA-II – Non-dominated Sorting Genetic Algorithm II

RIBASIM – River Basin Simulation

RFPG – Right Flooding Performance Graph

RPG – Rating Performance Graph

SWAT – Soil and Water Assessment Tool

UNHVPG – Unsteady flow routing model for complex river networks based on HPG and VPG

VPG – Volume Performance Graph

LIST OF SYMBOLS

A	Constant (> 1)
c	Coefficient
$\overline{c}$	Average gravity wave celerity
d	Downstream end index
f	Function
FV	Flooding volume
G	Discrete gate position
i	Node index
I	Inflow
$\forall i$	For all i
j	River reach index
k	Total number of river reaches linked to the node
max	Maximum
min	Minimum
n	Discrete-time index
N	Set of nodes
NB	Set of downstream boundary nodes

NS Set of source nodes

O Outflow

p Number of outflowing river reaches linked to the node

Q_{d_j} Flow discharge at downstream end of reach j

$Q_{u_{\mathbf{CIB}}}$ storage of a river reach or reservoir located upstream of the CIB

Q_{u_j} Flow discharge at upstream end of reach j

RR Total number of river reaches

s Slope

S Storage

Δt Time step

u Upstream end index

$\overline{u}$ Average reach velocity

v Number of inflowing river reaches linked to the node

V Cumulative outflow volume

w Weight factor

WS Water stage

Δx Length of river reach

y_{d_j} Water depth at downstream end of reach j

y_{u_j} Water depth at upstream end of reach j

z_{d_j} Channel bottom elevation at downstream end of reach j

z_{u_j} Channel bottom elevation at upstream end of reach j

CHAPTER 1

INTRODUCTION

River flooding is a recurrent threat that normally ensues a huge cost, both in terms of human suffering and economic losses associated with damage to infrastructure, loss of business, and the cost of insurance claims. From 2005 to 2009, the National Weather Service [28] estimated 63 billion dollars in losses in the U.S. associated with flooding. The catastrophic disasters associated with river flooding urge the re-evaluation of current strategies for flood control for most appropriate frameworks.

Recent studies on flood mitigation indicate that major emphasis must be given to flood control projects under the greater framework of basin-wide ecosystem rehabilitation (e.g., [35], [6]). These studies also aim for improving structural measures for minimizing the impact of floods while emphasizing the importance of risk management in flood control projects. A review of common structural measures used for flood control (e.g., levees, dams) reveals most of these measures are passive (static), with dams being the most important structural measure for flood control (e.g., [37]).

Most dams built for flood control have gates that are operated based on rule curves, which are determined based on annual estimates of system loads, reservoir storages, and resources provided by stakeholders. Rule curves neglect the flow dynamics in the entire river system, which makes this approach a "slow-response" method for flood control. This is particularly true in complex river systems when parts of the river

system may have enough in-line storage capacity, while other portions of the system may be overflowing.

A flooding process may be highly dynamic and may start from anywhere in the river system ([26]). It may start from upstream (e.g., large inflows), downstream (i.e., high water levels at downstream), or laterally from the connecting reaches (e.g., water levels at river junctions near the reach banks). It may change for the same river system depending on inflows to the river system and antecedent boundary conditions. Accounting for system flow dynamics is also important because flow conveyance from one reservoir to another is not instantaneous but depends on the capacity of the connecting reaches, the capacity of associated gates, outlet structures, and the dynamic hydraulic gradients. Clearly, rule curves are insufficient for making system-wide operational decisions.

For instance, consider the schematic in Figure 1.1, which shows that reach 1 upstream of Dam "A" is about to flood in a high risk area, while reaches 2, 3 (medium and low risk area) have enough capacity for storage. Under these conditions, the rule curve approach would open the gates of dam "A" but not those of dams B and C. In Figure 1.1, FV is a flood volume and the sub-indexes "L" and "R" represents left and right, respectively. The gates of dam C would open only after reach 3 is almost full, and the gates of dam B would open after reach 2 is almost full. This near-passive approach is far from being the most optimal flood control method. Another flaw with the rule curve approach for flood control is that it does not take into account hydraulic gradient (e.g., water surface profile). In dynamic conditions (e.g., under flooding occurrence), the water elevations upstream and downstream of a dam are not constant, and have a significant hydraulic gradient. In many circumstances, this hydraulic gradient by itself may cause flooding. Clearly, rule curves are insufficient

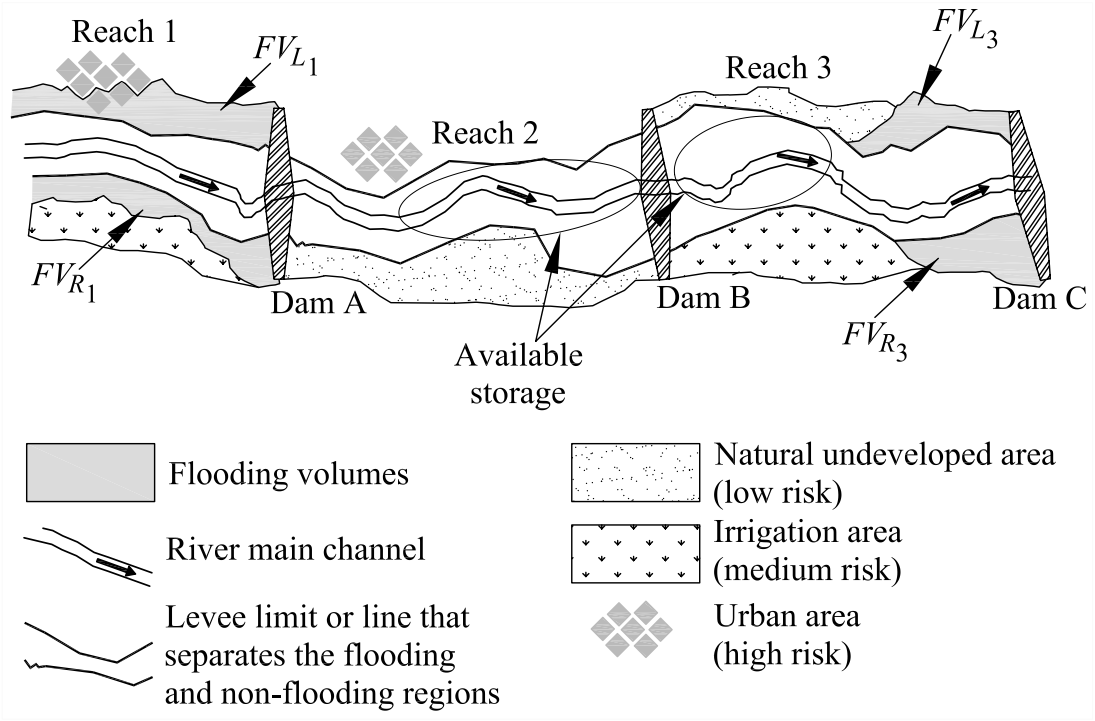

Figure 1.1: Schematic that illustrates the need for real-time control and the need for accounting for system flow dynamics

for making system-wide operational decisions.

Several engineers and academicians (e.g., [36], [9], [5]), justified the need of real-time operation of gates installed in dams for flood control. In fact, strategies and models for real-time flood control for a multi-reservoir operation system have been developed for more than 30 years ([29]). However, none of the frameworks combining simulation and optimization (necessary for obtaining the optimal system-wide operational decision), accounts for system flow dynamics, which is of utmost importance in flood control because a flooding process is highly dynamic and may start from anywhere in the river system ([26]). It may start from upstream (e.g., large inflows), downstream (i.e., high water levels at downstream), or laterally from the connecting reaches (e.g., water levels at river junctions near the reach banks). It may change

for the same river system depending on inflows to the river system and antecedent boundary conditions. Accounting for system flow dynamics is also important because flow conveyance from one reservoir to another is not instantaneous but depends on the capacity of the connecting reaches, the capacity of associated gates, outlet structures, and the dynamic hydraulic gradients. The author is not aware of a single river system in the world that has a real-time flood control framework combining simulation and optimization to account for system flow dynamics.

Various models for reservoir operation are available. These include optimization models, simulation models, and combined simulation-optimization models. For achieving an optimal system-wide operational decision for flood control, it was recognized that optimization and simulation components must be combined (e.g., [19]). Within the category of models that combine simulation and optimization, there are various models intended for reservoir operation including flood control. One of these models is the "Generalized Real-Time Flood Control System Model" ([9]) that was developed by the Hydrologic Engineering Center (HEC). Currently, HEC supports three individual reservoir modeling tools for the simulation and optimization of reservoir system operations ([20], [19]). The tools include: 1) Reservoir Simulation (HEC-ResSim), 2) Multi-Objective Reservoir Optimization (Prescriptive Reservoir Model, HEC-PRM), and 3) Reservoir Flood Control Optimization (HECFloodOpt). HEC-ResSim is a reservoir simulation model that makes operation decisions following the user-specified operating rules or guidelines. HEC-PRM and HEC-FloodOpt are optimization models that make operation decisions to maximize system objectives and values as defined by the user. HEC combines these three modeling tools into one package, the Reservoir Evaluation System (HEC-RES). The simulation component of HEC-RES, ResSim, is used extensively in real-time water control as part of the Corps

Water Management System (CWMS). The RIBASIM (RIver BAsin SIMulation) [[7]] model is another comprehensive and flexible tool for reservoir operation. Since 1985, RIBASIM has been applied in more than 20 countries world wide and is used by a wide range of both national and regional agencies. RIBASIM enables the user to evaluate a variety of measures related to infrastructure, operational, and demand management in order to see results in terms of water quantity and flow composition.

Recently, many more combined simulation-optimization models were formulated for reservoir operation including flood control. [30] proposed to optimize the control strategies for the Hoa Binh reservoir operation. The control strategies were set up in the MIKE 11 simulation model to guide the releases of the reservoir system according to the current storage level, the hydro-meteorological conditions, and the time of the year. [23] refined an existing optimization/simulation procedure for rebalancing flood control and refill objectives for the Columbia River Basin for anticipated global warming. To calibrate the optimization model for the 20th century flow, the objective function was tuned to reproduce the current reliability of reservoir refill, while providing comparable levels of flood control to those produced by current flood control practices. After the optimization model was calibrated using the 20th century, flow the same objective function was used to develop flood control curves for a global warming scenario.

Current frameworks combining simulation (e.g., hydraulic routing) and optimization neglect system flow dynamics and instead simply perform mass balance in the reservoirs while assuming that reservoir's water levels are horizontal. The reasons for neglecting system flow dynamics are due to a lack of robustness (first limitation) and computational burden (second limitation) of current unsteady flow models (e.g., [12]). It is pointed out that currently there are dozens of one-, two-, and three-dimensional

models having the capability to perform hydraulic routing of any river system. In the authors experience, some of the existing routing models, especially those that are one-dimensional, are highly robust for a wide range of conditions. This is the first limitation of these models because they are not robust for all conditions. For instance, the widely known unsteady HEC-RAS model ([18]) provides accurate results for a large range of conditions but may fail for some others. It is pointed out that when the HEC-RAS model finds problems of convergence, the simulation is not stopped but rather continues assuming pre-specified conditions (e.g., critical flow). Certainly the results after the convergence problems cannot be trusted.

Most free surface flows (also called open-channel flows) are unsteady and non-uniform. Hence, in many applications the spatial and temporal variation of water stages and flow discharges need to be determined. Unsteady flows in river systems are typically simulated using one-dimensional models although two and three-dimensional models are now being used more frequently. In a one-dimensional framework, unsteady flows in rivers are typically simulated by the Saint-Venant equations, the pair of partial differential equations representing conservation of mass and momentum for a control volume are:

$$\frac{\partial A}{\partial t} + \frac{\partial Q}{\partial x} = 0 \tag{1.1}$$

$$\frac{1}{g}\frac{\partial V}{\partial t} + \frac{\partial}{\partial x}\left(\frac{V^2}{2g}\right) + \cos\theta\frac{\partial y}{\partial x} + S_f - S_o = 0 \tag{1.2}$$

where x = distance along the channel in the longitudinal direction; t = time; Q = discharge; A = cross-sectional area; y = flow depth normal to x; θ = angle between the longitudinal bed slope and a horizontal plane; g = acceleration of gravity; S_o = bed

slope and S_f = friction slope. In Eq. (1.2) [momentum equation], the first, second, third, fourth, and fifth terms represent the local acceleration, convective acceleration, pressure gradient, friction, and gravity terms, respectively.

The Saint-Venant equations are typically solved for appropriate initial and boundary conditions to simulate the spatial and temporal variation of water stages and flow discharges resulting from flood routing. At present, no analytical solution for the Saint-Venant equations is known, except for special conditions (e.g., dam break flow over a dry bed in a frictionless and horizontal channel). Hence, solutions of general open-channel flow conditions such as those found in practical applications are sought numerically. Solutions to the full dynamic, one dimensional Saint-Venant Equations and their quasi-steady, noninertia (or diffusion), and kinematic wave approximations (details on these approximations can be found for example in [39]) have been sought based on several numerical schemes and methods (e.g., [1]). As emphasized in [12] and [14], despite the wide array of methods available for the solution of the Saint-Venant equations, the lack of robustness and accuracy issues still pose a problem.

The computational burden of hydraulic routing models constitutes a second limitation because the implementation of a real-time strategy that combines simulation and optimization may require hundreds or even thousands of simulations for each operational decision. To illustrate why a large number of simulations is needed, let's assume that a river system has five dams, and each of these dams has two gates that will be operated for flood control. For simplicity of operation of these gates, let's assume that each of these gates can adopt eighty different positions (If gate height is 4 meters, the gate can be closed or opened in intervals of 5 cm). Thus, for a system analysis of this hypothetical regulated river system, we would need to perform at least 400 runs. For this system, if we were to use the unsteady HEC-RAS model, it would

take between five to ten minutes for performing the unsteady flow computations.

An important issue with unsteady flow models is computational burden, especially when an unsteady model is used for optimization problems such as real-time operation of regulated river systems (e.g., [25]). In this case, hundreds or even thousands of runs need to be performed for each operational decision ($\sim$ 30 minutes), which would require numerically efficient models for unsteady flow routing or a large number of computer processors (clusters). Even if the simulations are run on computer clusters, there is no guarantee that hydraulic routing models will work for all ranges of conditions (e.g., low stage flows up to flows in the floodplains). In the authors' experience, under some simulation conditions most of the existing routing models fail to converge to a solution. In particular, the widely known unsteady HEC-RAS model ([18]), which has been found to converge for a range of conditions, fails to converge under some conditions. When HEC-RAS fails to converge, it proceeds with the simulation based on assumed pre-specified conditions (e.g., critical flow), which may yield questionable results.

In the last three decades, Ben Chie Yen's research group at the University of Illinois at Urbana-Champaign extended the concept of delivery curves introduced by [3]. Yen's group proposed a general approach to summarize the dynamic relation between the water surface elevations (stages) or depths at the ends of a channel reach (e.g., rivers or canals) for different constant discharges under gradually varied flow (GVF) conditions (e.g., [40]; [32]). This approach was called the Hydraulic Performance Graph (HPG). The HPG is a set of curves of constant discharge known as hydraulic performance curves (HPCs). Each HPC defines the locus of the upstream and downstream water depths in a channel reach for a given constant flow discharge. An example of an HPG for a mild-sloped channel is depicted in Figure 2.1. The

HPG shown in Figure 2.1 has few HPCs; in actual applications, the number of HPCs must be set based on a precision goal. This must be decided based on a convergence analysis, which consists of successive refinement of the resolution of the set of HPCs to a resolution such that the solution for the conditions of interest (e.g., stage and flow hydrographs at a given station) becomes nearly independent of the number of HPCs used. The procedure to determine the optimal resolution of HPCs to ensure that a prescribed accuracy is afforded is outside the scope of this thesis.

HPGs can be used to summarize gradually varied subcritical and supercritical flows. However, they have been mostly applied to summarize subcritical GVF in channel reaches with steep, mild, adverse, and horizontal slopes (see methodology in [40]; and [32]). The construction of the HPG for each reach may involve hundreds of GVF simulations, each simulation corresponding to one discrete point on the HPG. When using a one-dimensional model for constructing the performance graphs, any GVF model can be used. In the present application, the steady HEC-RAS model was used to generate the HPG's/VPG's.

HPGs have been applied to solve problems in open-channel flows including the (a) evaluation of hydraulic performance of floodplain channels under pre- and post-breached levee conditions ([13]), (b) assessment of the carrying capacity of channel systems in series ([40]), and (c) theoretical development of discharge ratings based on the hydrodynamics of unsteady and nonuniform flows ([32]). [12] assessed the applicability of HPG's for unsteady flow routing in single prismatic channels and channel systems in series with successful results. The unsteady approach of [12] assumes that the flow is steady at the different time steps of the simulation. More recently, [16] relied on the Volume Performance Graph (VPG) instead of a finite-difference scheme like the four-point implicit finite difference scheme used by [12]

to satisfy the reach-wise mass conservation during routing. The VPG approach is equivalent to enforcing Equation (1.1) [conservation of mass] in a reach (see details in [16]). An example of a VPG for a mild-sloped channel is depicted in Figure 2.2. The HPG and VPG are unique to a channel reach with a given geometry and roughness, and can be computed decoupled from unsteady boundary conditions by solving the GVF equation for all feasible conditions in the reach. They are essentially a fingerprint of all gradually varied flow conditions in a channel reach. Consequently, HPG/VPGs need to be revised only when geomorphic changes modify the geometry or roughness characteristics of the channel ([40]). A significant advantage of the HPG approach with respect to other routing models is that the results are little sensitive to space and time discretization ([12]).

To address the complexity of river flooding and to overcome the limitations of current frameworks for flood control, a coupled optimization-simulation framework is proposed that accounts for system flow dynamics and that makes possible the intelligent control of river flooding (e.g., automatic operation of gates and locks in river systems). This framework is robust and enough fast so that it will allow its application to actual complex river systems in real-time.

The main benefit of the proposed framework is that it will maximize the in-line storage of the entire river system and it will allow controlled flooding only after the capacity of the river system has been exceeded. This controlled flooding will be based on weight factors assigned to each reach of the system depending on a hierarchy of risk to losses associated with flooding. Naturally, river reaches that are less prone to losses are assigned smaller weight factors and reaches that are more prone to losses are assigned larger weight factors.

Using the premise that a good operation model must combine a good optimization

model with a good simulation model, the proposed framework couples the well-known multi-objective, non-dominated Sorting Genetic Algorithm II (NSGA-II) with the concept of Hydraulic Performance Graph, Volume Performance Graph, and Rating Performance Graph.

This thesis is presented in two major parts, the first is the unsteady flow routing in complex river networks and the second is the intelligent control of river flooding.

The present work extends the application of the performance graph approach for unsteady flow routing in river networks. In a similar fashion to the unsteady approach of [12], the model introduced here, to which we refer to as UNHVPG model, assumes that the flow is timewise steady at the different time steps of the routing. The application presented in this thesis is limited to subcritical flows; however, it can be extended to supercritical flows. Besides relying on the HPG/VPG concept, the UNHVPG model also makes use of what we refer to as Rating Performance Graph (RPG). RPGs graphically summarize the dynamic relation between the flow through and the stages upstream and downstream of an in-line structure. RPG's are conceptually similar to look-up tables such as those utilized to characterize the dynamics of hydraulic structures in the FEQ model of [10]. However, RPG's are described with an adaptive spacing so as to capture changes smoothly, which leads to better interpolation estimates. Further details on RPGs are presented in the next section. Results of these models are compared and discussed in Chapter 2.

The Intelligent control of river flooding couples the hydraulic and optimization components of the proposed framework. This framework is applied to the Boise River system and results of this application are discussed in Chapter 3.

This thesis presents a case study on the application of a dynamic framework for the intelligent control of flooding in the Boise River system in Idaho. This framework

couples a robust and numerically efficient hydraulic routing approach with the popular multi-objective, non-dominated Sorting Genetic Algorithm II (NSGA-II). The novelty of this framework is that it allows for controlled flooding when the conveyance capacity of the river system is exceeded or is about to exceed. Controlled flooding is based on weight factors assigned to each reach of the system depending on the amount of damage that would occur, should a flood occur. For example, an urban setting would receive a higher weight factor than a rural or agricultural area. The weight factor for a reach doesn't need to be constant as it can be made a function of the flooding volume (or water stage) in the reach. The optimization algorithm minimizes flood damage by favoring low weighted floodplain areas (e.g., rural areas) rather than high weighted areas (e.g., urban areas) for the overbank flows. In an actual river system, presumably, rural areas are already more prone to flooding (flood more frequently), because of existing planning and land management practices. However, the proposed framework has the potential to refine and improve water management and use of flood-prone areas in river systems, especially of those systems subjected to frequent flooding.

CHAPTER 2

UNSTEADY FLOW ROUTING MODEL FOR COMPLEX RIVER NETWORKS BASED ON HPG AND VPG: UNHVPG

This chapter presents a highly robust model for unsteady flow routing through dentritic and looped river network. The application presented in this chapter is limited to subcritical flows; however, it can be extended to supercritical flows. The model builds upon the application of the Hydraulic Performance Graph (HPG) to unsteady flow routing introduced by González-Castro [12] and adopts the Volume Performance Graph (VPG) introduced by Hoy and Schmidt [16].

The hydraulic component of the proposed framework consists in dividing the river system into reaches and pre-computing the hydraulics for each of these reaches independently using any gradually varied flow model (one-, two-, or three-dimensional model). The pre-computed hydraulics for each reach is stored in matrices and is accessed as look-up tables. The Hydraulic routing adopted for each river reach is performed using the Hydraulic Performance Graph (HPG) and Volume Performance Graph (VPG).

According with Yen and González-Castro [40], the HPG is an efficient approach for summarizing the backwater profiles of all possible gradually varied flow conditions in an open-channel reach, expressed in the form of water surface elevations (stages) or

depths at the ends of the channel reach for different constant discharges. A significant advantage of the HPG approach with respect to other routing models is that any error attained during the pre-computation of the hydraulics (e.g., due to instability) can be detected and therefore corrected before the optimization process (e.g., redo simulations with other discretization parameters). For a detailed description of HPGs, see Yen and González-Castro [40]. An example of an HPG and a VPG for a mild-sloped channel are depicted in Figures 2.1 and 2.2, respectively. These HPG and VPG intentionally show a few performance curves (constant discharge curves). In actual applications, the number of discharges must be commensurate to the desired interpolation precision.

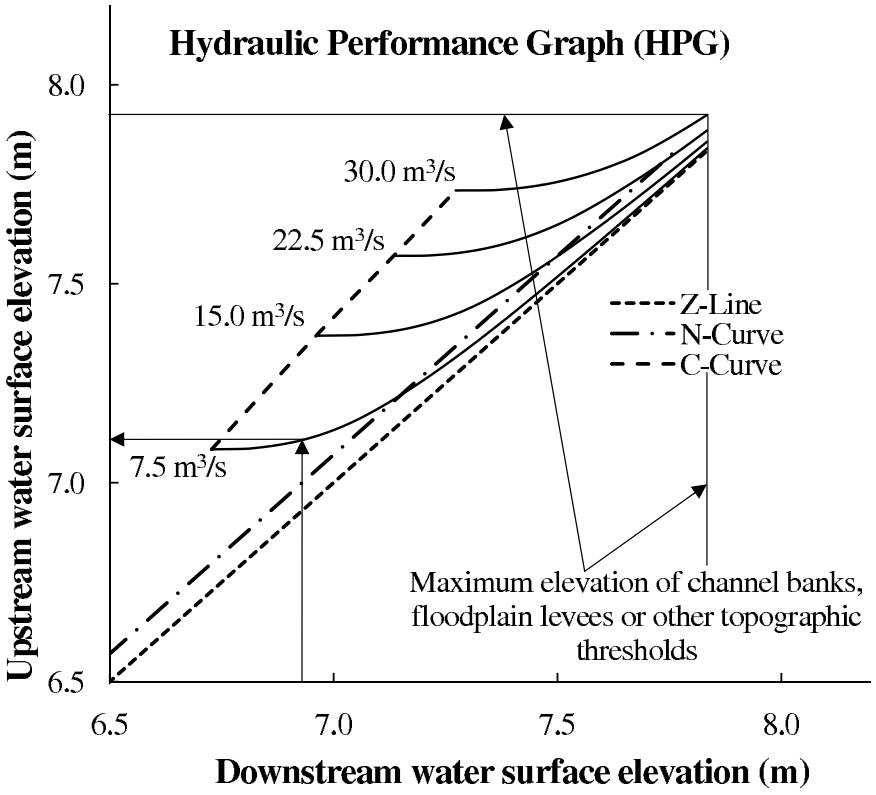

Figure 2.1: Example of a Hydraulic Performance Graph (HPG).

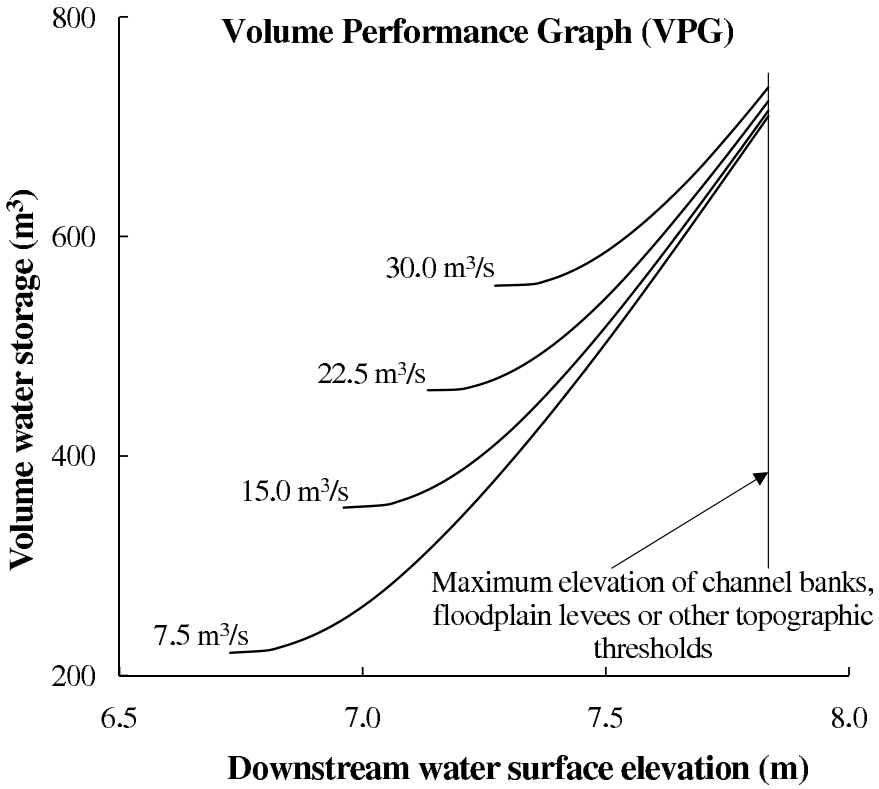

Figure 2.2: Example of a Volumetric Performance Graph (VPG).

The HPG of a channel reach graphically summarizes the dynamic relation between the flow through and the stages at the ends of the reach under gradually varied flow (GVF) conditions, while the VPG summarizes the corresponding storage. Both the HPG and VPG are unique to a channel reach with a given geometry and roughness, and can be computed decoupled from unsteady boundary conditions by solving the GVF equation for all feasible conditions in the reach. Hence, in the proposed approach, the performance graphs can be used for different boundary conditions without the need to recompute them. Previous models based on the performance graph concept were formulated for routing through single channels or channels in series.

They are essentially a fingerprint of all possible gradually varied flow conditions in

a channel reach. Consequently, HPG/VPGs need to be revised only when geomorphic changes modify the geometry or roughness characteristics of the channel ([40]). The HPG/VPG are obtained for as many flows and downstream boundary conditions as necessary to cover the region of possible pairs of upstream and downstream stages in the channel reach.

The performance graphs approach applies to flow routing when the local acceleration is negligible. This condition is met by flows in many natural and man-made systems [[15] showed that the local acceleration term is small compared to the gravity and friction terms even for a steep river with a "very fast-rising flood"]. Actually, the relative contribution of the local acceleration with respect to the pressure gradient is in the order of the Froude number squared ([15]). Typically, the maximum Froude number of mild-slope unregulated river systems and regulated river systems is much smaller than one. According to Hoy and Schmidt [16] and Xia [38], the pressure gradient term may be of the same order of magnitude of those of the gravity and friction terms, however its magnitude decreases with increasing slope. Furthermore, the ratio of the local acceleration term with respect to the pressure gradient term is in the order of the Froude number squared. For instance, for a Froude number of 0.2, the local acceleration term would be on the order of 4% of that of the pressure gradient term. Typically, the maximum Froude number in regulated river systems is much smaller than one.

HPGs have been used extensively for evaluating the hydraulic performance of floodplain channels under pre- and post-breached levee conditions ([13]). And more recently, Yen and González-Castro [40] assessed the applicability of HPGs for open-channel unsteady flow routing with successful results. Hoy and Schmidt [16] used the concept of the Volume Performance Graph (VPG) instead of a finite-difference

scheme used by Gonzalez-Castro [12] for the reach-wise conservation of mass. The approaches proposed by Yen and González-Castro [40], Hoy and Schmidt [16], and others were not formulated for a general river network, in particular they cannot address looped and dendritic networks ([16]).

The hydraulic routing adopted for each in-line structure is performed using the Rating Performance Graph (RPG). RPG construction is very similar to the HPG. An RPG is different to an HPG in that the latter is restricted to GVF conditions, while the former can be used in GVF or rapidly varied flow conditions. For constructing an RPG, physical measurements of flow discharge and water stages, or a one-, two-, or three-dimensional numerical model can be used. In the UNHVPG, an all internal nodes (uncontrolled and controlled in-line structures and channel junctions) are assumed to have no storage. The water depth immediately upstream of the in-line structure is computed using the RPG built for the structure. For building the RPG, the upstream and downstream stages are assumed to be as close as possible to the in-line structure to minimize errors in mass conservation.

In this framework, a system of nonlinear equations is solved, assembled based on information summarized in the systems' HPGs and VPGs, continuity and compatibility conditions at the union of reaches (nodes), and the system boundary conditions. The proposed framework was applicability to a looped network and contrast its simulation results with those from the well-known unsteady HEC-RAS model.

2.1 Integration and Linking of Modules

The UNHVPG model is composed of six main modules as illustrated in Figure 2.3. A brief description of these modules is presented next.

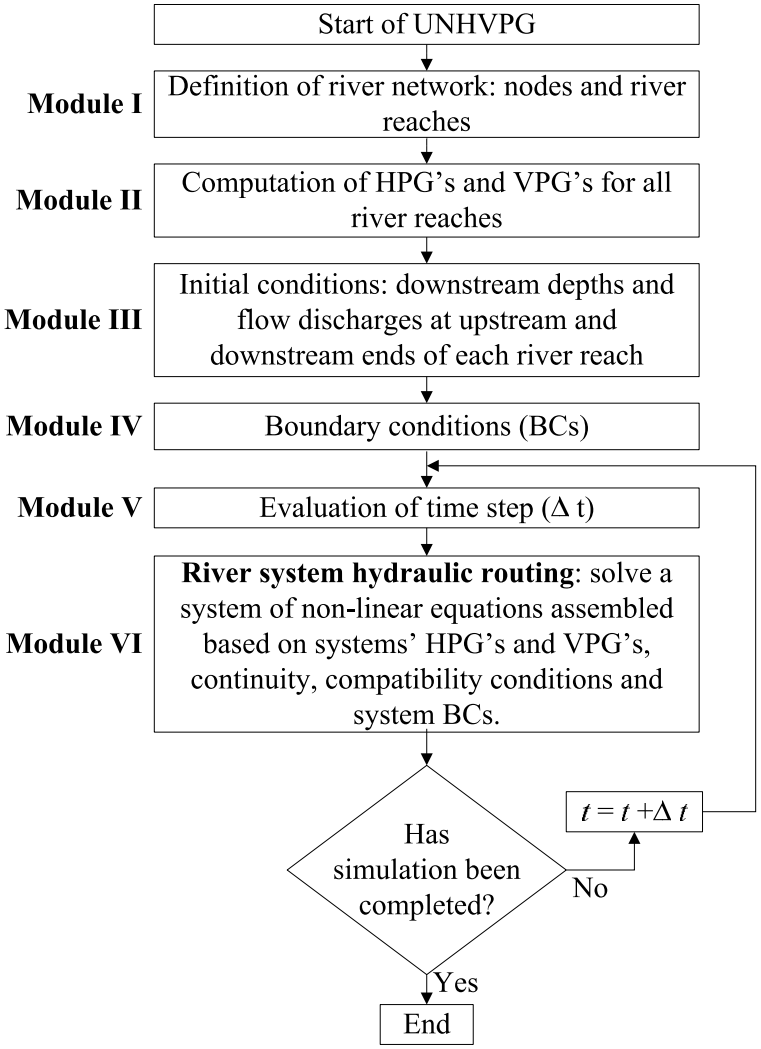

Figure 2.3: Flow chart of the UNHVPG

2.1.1 Module I: Definition of a River Network

In this module, data of nodes and river reaches that define the river system network are read and stored for later use. In the UNHVPG model, a river system is represented as a network where all components of the river system are defined by river reaches and nodes. A river reach is defined by its upstream and downstream nodes and should have similar geometric properties along the reach (e.g., prismatic channel) as

to ensure GVF conditions. Whether a channel reach is changing gradually enough so that flow through it can be treated as flow in a prismatic channel must be assessed based on a more general form of the ordinary differential equation (ODE) for GVF conditions. [12] discusses this issue based on the following more general ODE for GVF in nonprismatic channels:

$$\frac{dy}{dx} = \frac{S_o - S_f + \frac{Fr^2}{\cos^2\theta}\frac{D}{T}\frac{dT}{dx}}{\cos\theta - Fr^2} \tag{2.1}$$

The third term in the numerator of Eq. (2.1) accounts for changes in nonprismatic channels. From this equation, it is clear that for a canal to behave as prismatic

$$S_o - S_f \gg \frac{Fr^2}{\cos^2\theta}\frac{D}{T}\frac{dT}{dx} \tag{2.2}$$

where T = free surface width, D = hydraulic depth ($= A/T$), and Fr = Froude number. The criterion in Eq. (2.2) is met by subcritical flows in canals with mild bed slopes for which $Fr^2/\cos^2\theta = \mathcal{O}(0.1)$ and $D/T = \mathcal{O}(0.1)$, even when $dT/dx = \mathcal{O}$(So - Sf).

The flow direction in a river reach is assumed to be from its upstream node to its downstream node as shown in Fig. 2.4. A negative flow discharge in a river reach indicates that reverse flow occurs in that river reach.

In Figure 2.4, the subscript j and superscript n represent the river reach index and the discrete-time index, respectively, y and Q with the subscripts u and d denote the water depths and discharges at the upstream and downstream ends of the river reach, respectively.

A node, as depicted schematically in Figure 2.5, may have v inflowing river reaches and w outflowing river reaches, giving a total of k ($k = v + w$) reaches connected

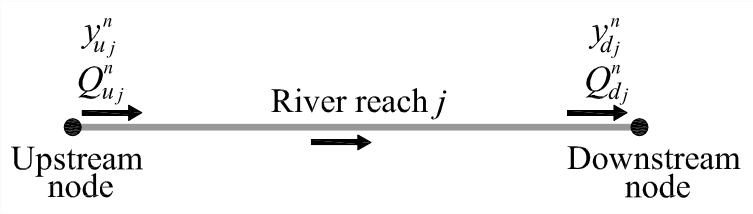

Figure 2.4: Schematic of a river reach

to the node. A river reach is denoted as inflowing (or outflowing) when it conveys to (or from) the node. A node in the proposed model refers to point nodes that have no storage. A node is used at the location of hydraulic structures, connection of reaches, and boundary conditions. It is worth mentioning that in the UNHVPG model, a reservoir is not represented by a node but by one or a series of reaches. The treatment of boundary conditions is presented in the Module IV section.

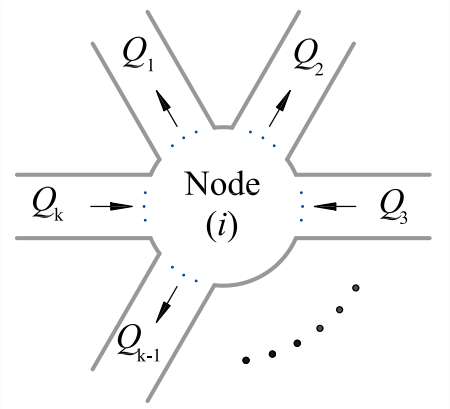

Figure 2.5: Schematic of a node

2.1.2 Module II: Computation of HPGs and VPGs

In this module, HPGs and VPGs for all the reaches of the river system and RPG's for the hydraulic structures are computed and stored for later use. An example of an HPG and a VPG for a mild-sloped channel (for few flow discharges) were depicted

previously in Figures 2.1 and 2.2, respectively. In the present application, a system's performance graphs (PGs) were constructed using the HEC-RAS steady module. The subcritical flow mode of the steady HEC-RAS model allows multiple steady subcritical flow simulations (e.g., using multiple discharges) with a fixed downstream water depth as initial condition. This allows a rapid construction of the performance graphs.

Once the PGs are constructed, they are plotted to ensure that they are free of numerically induced errors. Numerical errors may result in the superposition of PCs or in PCs that display oscillatory patterns. For the discrete points of a HPC that present apparent problems, the simulations must be repeated with more stringent criteria. These require decreasing Δx (interpolation between cross-sections) and adjusting convergence parameters for the GVF simulations. This initial screening of the PGs results in the elimination of the aforementioned oscillatory patterns and superposition of HPCs. For a detailed description on the construction of HPGs, the reader is referred to [40] and [32].

2.1.3 Module III: Initial Conditions

The initial conditions in the UNHVPG model for each river reach in the steady case can be specified by two of the variables describing the reach's HPG (i.e., the water stages at the reach's end, or one of the stages and the flow discharge in the reach). In the case that the simulation starts from nonsteady conditions, the initial conditions must be defined as the combination of the stages at the reach's end and the flow at one of its ends, or the flows at the reach's ends and the stage at one of its ends.

2.1.4 Module IV: Boundary Conditions

The following types of boundaries are supported by the UNHVPG model:

1. External Boundary Condition (EBC), which is defined at the most upstream and downstream ends of the river system. An EBC can have either an inflowing or outflowing river reach connected to the node. An external boundary includes an inflow hydrograph, a stage hydrograph, or a rating curve.

2. Internal Boundary Condition (IBC), which is defined at internal nodes whenever two or more reaches meet. Three types of IBCs are supported in the UNHVPG model. These are:

    - A fixed in-line structure BC (e.g., weirs or dams with fixed position of gates, see Figure 2.6). A single RPG is built for this BC. The water depth immediately upstream of the in-line structure is computed using the RPG built for this structure. For building the RPG of an in-line structure (fixed and mobile), the most upstream and downstream cross sections of the simulation must be kept close to the in-line structure to avoid large errors of conservation of mass. The criteria for the selection of cross sections for the construction of look-up tables can be found in [11]. This criteria also applies to the construction of RPGs. Under simple conditions, good rating equations are probably easier to manage than both RPG's and look-up tables. However, for the operation of multi-type hydraulic structures under complex flow conditions (e.g., downstream flow conditions ranging from low to high water stages, and/or viceversa), relying on RPGs (look-up tables) may expedite convergence during the simulation of unsteady flow. Both RPGs and look-up tables can be constructed based on measurements of flow discharge and water stages and/or results from computational fluid dynamics simulations. As pointed out by Franz and Melching ([11]; [10]),

the use of look-up tables (or RPGs) can be used to model the dynamics of a variety of hydraulic structures such weirs, culverts, spillways, bridges, and canal expansions and contractions. The analyst only needs an adequate description of the relation between the flow through the structure, and the water-surface elevation downstream and upstream of the structure. For an application of RPGs to the opening and closing of gates, the reader is referred to [25].

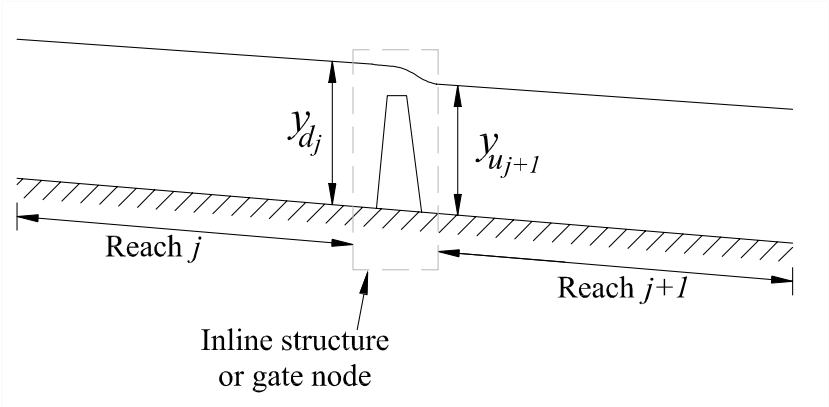

Figure 2.6: Schematic of an inline structure or gate node.

- A mobile in-line structure BC (e.g., spillways and culverts with control gates, and pumping stations with pumps of different capacities or operated at variable speeds). Dams with a combination of tainter and roller gates are often found in canal networks and dams. In some cases, the roller gates at dams can be raised (underflow gate) or lowered (overflow gate). These gates are often operated using pre-defined operating rules that specify the number of gates to open and percentage of openings while addressing issues such as scour, safety, outdraft, etc. Complex arrays and operations can be handled by using a group of RPGs (e.g., one for each gate opening) for

each gate or pre-specified combinations of gates depending on how they will be operated. The RPGs will need to encompass the entire range of gate openings and all possible ranges of downstream and upstream water levels. Naturally, a given flow discharge can be passed through the dam with more than one combination of operational settings. If there is any pre-specified order for the operation of gates, this should be linked to the order of use of the RPGs. For the application of RPGs to mobile in-line structures, the reader is referred to [25].

- Another IBC is a node without a hydraulic structure, which is used to connect two or more river reaches with different roughness or bed slopes, or where an abrupt bed drop or canal expansion occurs. This node is denoted as a junction BC and its schematic is depicted in Figure 2.7. As shown in Figure 2.5, a junction boundary may connect two or more river reaches.

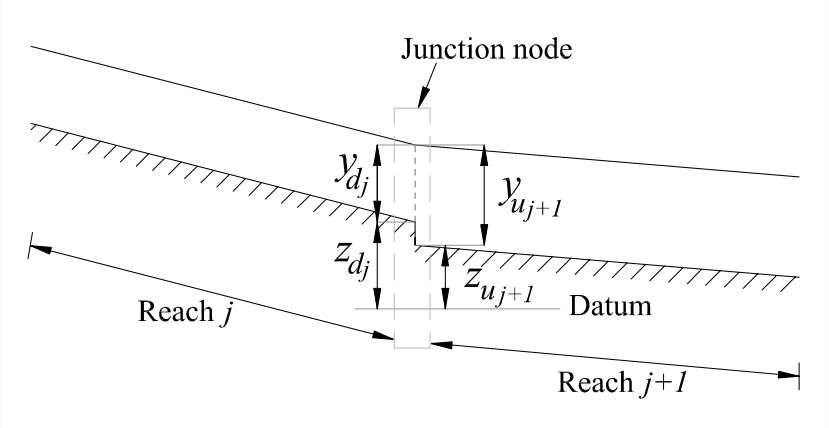

Figure 2.7: Schematic of a junction node

2.1.5 Module V: Evaluation of Time Step (Δt)

This module estimates the time step for advancing the solution to the next time level. In the PG approach, the reach-wise averaged flow discharge $[1/2 * (Q_u + Q_d)]$ and y_d are used to determine y_u. Hence, the time step must be long enough to ensure that disturbances generated at the ends of the reaches have enough time to arrive to the opposite end. This can be expressed as

$$\Delta t > \text{Max}\left\{ \frac{\Delta x_j}{\|\overline{u}_j^n\| + \overline{c}_j^n} \right\} \forall j \tag{2.3}$$

where j is a reach index, and $\overline{u}^n$ and $\overline{c}^n$ are the average reach velocity and gravity wave celerity at time level n, respectively. The average reach-wise gravity wave celerity and velocity are defined as $\overline{c} = (c_u + c_d)/2$ and $\overline{u} = (u_u + u_d)/2$, respectively. A Δt smaller to that of Eq. (2.3) would mean that disturbances in some of the reaches don't have enough time to travel from one end of the reach to the other, which would violate one of the HPG/VPG assumptions (HPG/VPG use reach-wise averaged flow variables). The time step presented in Eq. (2.3) can be expressed as

$$\Delta t = k\text{Max}\left\{ \frac{\Delta x_j}{\|\overline{u}_j^n\| + \overline{c}_j^n} \right\} \forall j \tag{2.4}$$

where k must be set larger than 1. Numerical tests we performed to evaluate the sensitivity of k for both simulations in section "Application to a looped river network" showed that the results are nearly insensitive to k. The simulation results presented in this thesis were generated using $k = 3$.

2.1.6 Module VI: River System Hydraulic Routing

This module assembles and solves a non-linear system of equations to perform the hydraulic routing of the river system. These equations are assembled based on information summarized in the reaches HPGs and VPGs, RPGs at nodes with hydraulic structures, continuity, and compatibility of water stages at junctions, and the system's initial and boundary conditions. The compatibility of water stages at a junction is a simplification of the energy equation ignoring losses and assuming that the differences in velocity heads $[u^2/(2g)]$ upstream and downstream of the junction are negligible. In general, for a river network consisting of N reaches, there is a total of $3N$ unknowns at each time level, namely the flow discharge at the upstream and downstream end of each reach and the water depth at the downstream end of each reach, hence $3N$ equations are required. The water depth at the upstream end (y_u) of each reach is estimated from the reach HPG using the water depth at its downstream end (y_d) and the spatially averaged flow discharge $[Q = (Q_u + Q_d)/2]$. This can be represented as

$$y_u^n = \text{HPG}[y_d^n, \frac{1}{2}(Q_u^n + Q_d^n)], \forall j \tag{2.5}$$

The application of Eq. (2.5) requires an interpolation process for determining y_u. Two cases of interpolation are possible. These are depicted in Figures 2.8 and 2.9. As illustrated in these figures, the locus of the upstream and downstream water depth for a given constant flow discharge is denoted as hydraulic performance curve (HPC).

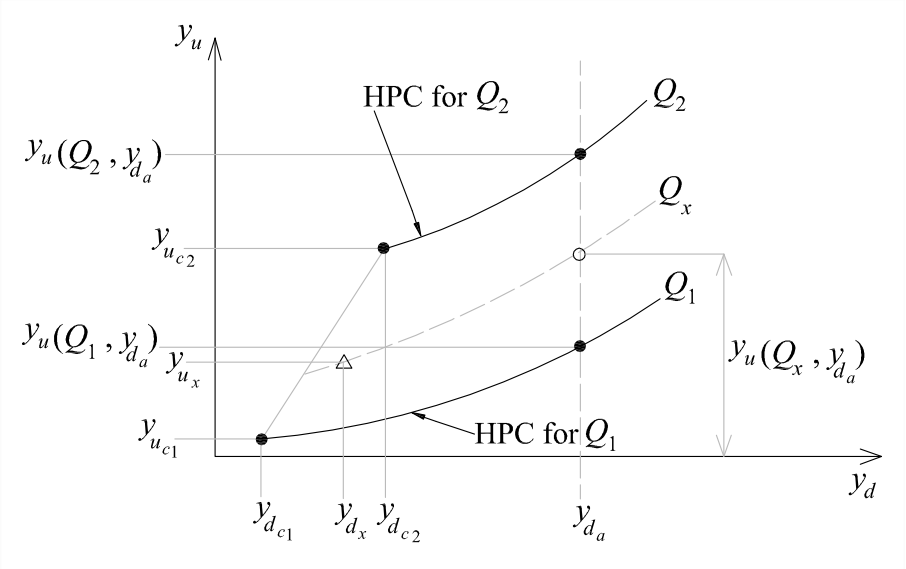

Figure 2.8: Schematic of first interpolation case

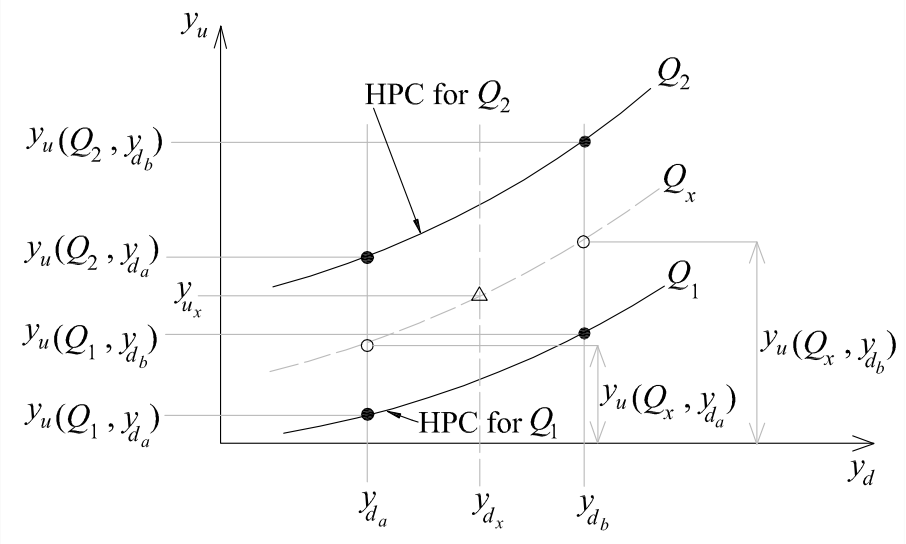

Figure 2.9: Schematic of second interpolation case

The first case of interpolation is used whenever y_{d_x} is located between two critical downstream water depths ($y_{d_{c1}}$ and $y_{d_{c2}}$) as shown in Figure 2.8. In this interpolation case (Figure 2.8), the discrete points (y_{d_a}, $y_u(Q_1, y_{d_a})$), (y_{d_b}, $y_u(Q_1, y_{d_b})$), ($y_{d_{c1}}, y_{u_{c1}}$), and ($y_{d_{c2}}, y_{u_{c2}}$) are known and y_{u_x} for a given y_{d_x} and Q_x is sought.

The second interpolation case is used for all conditions other than the first case (Figure 2.9). In the second interpolation case (Figure 2.9), the discrete points (y_{d_a}, $y_u(Q_1, y_{d_a})$), (y_{d_a}, $y_u(Q_2, y_{d_a})$), (y_{d_b}, $y_u(Q_1, y_{d_b})$), and (y_{d_b}, $y_u(Q_2, y_{d_b})$) are known and y_{u_x} for a given y_{d_x} and Q_x is sought.

The interpolation procedure to determine the upstream water depth y_{u_x} for a given Q_x and y_{d_x} for the first case (Figure 2.8) can be summarized as follows:

1. Determine coefficient c_1 as:

$$c_1 = \frac{Q_x - Q_1}{Q_2 - Q_1}$$

2. Determine slope s_1 of HPC for Q_1 as:

$$s_1 = \frac{y_u(Q_1, y_{d_a}) - y_{u_{c_1}}}{y_{d_a} - y_{d_{c_1}}}$$

3. Determine slope s_2 of HPC for Q_2 as:

$$s_2 = \frac{y_u(Q_2, y_{d_a}) - y_{u_{c_2}}}{y_{d_a} - y_{d_{c_2}}}$$

4. Determine slope s_x of HPC for Q_x as:

$$s_x = s_1(1 - c_1) + s_2 c_1$$

5. Determine $y_u(Q_x, y_{d_a})$ for Q_x and y_{d_a} as:

$$y_u(Q_x, y_{d_a}) = [1 - c_1][y_u(Q_1, y_{d_a})] + c_1[y_u(Q_2, y_{d_a})]$$

6. Determine y_{u_x} for Q_x and y_{d_x} as:

$$y_{u_x} = y_u(Q_x, y_{d_a}) - (y_{d_a} - y_{d_x})s_x$$

The interpolation procedure to determine the upstream water depth y_{u_x} for a given Q_x and y_{d_x} for the second case (Figure 2.9) can be summarized as follows:

1. Determine coefficient c_1 as:

$$c_1 = \frac{Q_x - Q_1}{Q_2 - Q_1}$$

2. Determine coefficient c_2 as:

$$c_2 = \frac{y_{d_x} - y_{d_a}}{y_{d_b} - y_{d_a}}$$

3. Determine $y_u(Q_x, y_{d_a})$ for Q_x and y_{d_a} as:

$$y_u(Q_x, y_{d_a}) = y_u(Q_1, y_{d_a}) + c_1[y_u(Q_2, y_{d_a}) - y_u(Q_1, y_{d_a})]$$

4. Determine $y_u(Q_x, y_{d_b})$ for Q_x and y_{d_b} as:

$$y_u(Q_x, y_{d_b}) = y_u(Q_1, y_{d_b}) + c_1[y_u(Q_2, y_{d_b}) - y_u(Q_1, y_{d_b})]$$

5. Determine y_{u_x} for Q_x and y_{d_x} as:

$$y_{u_x} = y_u(Q_x, y_{d_a}) + c_2[y_u(Q_x, y_{d_b}) - y_u(Q_x, y_{d_a})]$$

As mentioned earlier, $3N$ equations are required for a river system of N reaches. For illustration purposes without loosing generality, these equations are formulated for the simple network system depicted in Figure 2.10. The network system presented in Figure 2.10 has eight reaches and therefore has twenty four unknowns (3x8).

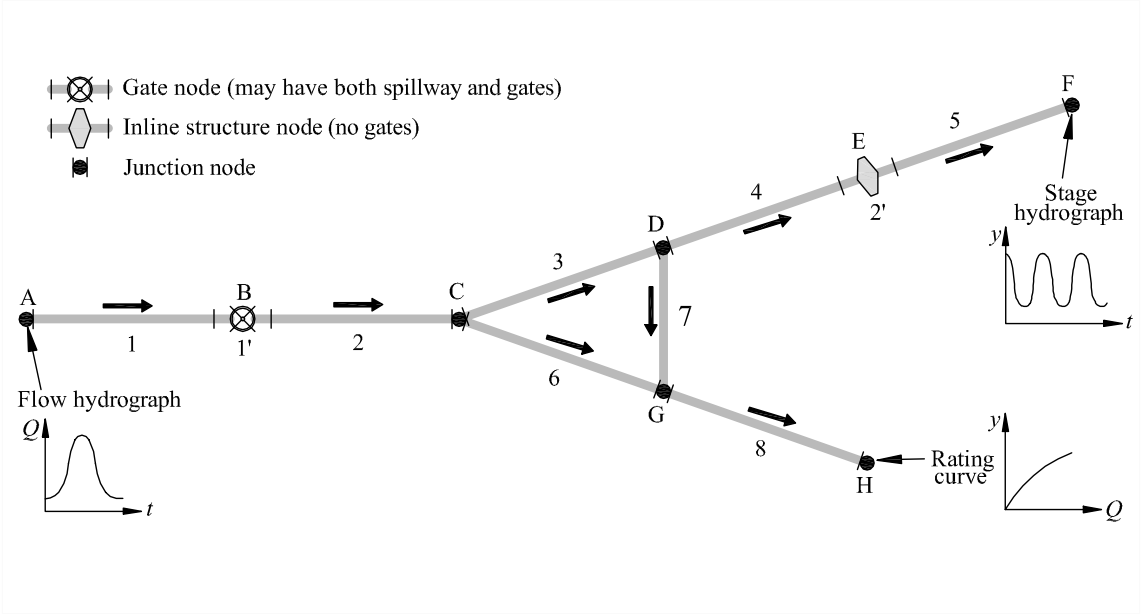

Figure 2.10: Schematic of a simple network system

The reach-wise conservation of mass provides one equation for each reach. This equation is typically discretized as follows:

$$\frac{I^n + I^{n+1}}{2} - \frac{O^n + O^{n+1}}{2} = \frac{S^{n+1} - S^n}{\Delta t}, \forall j \tag{2.6}$$

where I = inflow, O = outflow, S = storage, n = value at the current time level, t and $n+1$ = value at the next time level, $t + \Delta t$. It is worth mentioning that the storage

S is not considered an unknown because it can be related to y_d and Q through the VPG (VPG relates S, y_d and $Q \quad (Q_u + Q_d)/2$).

For our simple network (Figure 2.10), the application of Eq. (2.6) provides a total of eight equations. For an inflow hydrograph (external boundary), $(I^n + I^{n+1})/2$ is the average flow discharge computed from the hydrograph (integrated volume divided by Δt). The water storage (volume of water) at any time in a river reach is determined from the reach VPG using its downstream water depth and the spatially averaged flow discharge $(Q_u + Q_d)/2$ as input values, as

$$S^n = \text{VPG } [y_d^n, \frac{1}{2}(Q_u^n + Q_d^n)], \forall j \tag{2.7}$$

For more details on the VPG approach, the reader is referred to [16]. The application of Eq. (2.7) requires an interpolation process similar to that of the HPG presented earlier (see Eq. 2.5). Also, for the network in Figure 2.10, five continuity equations are available (nodes B, C, D, E and G). For instance, at node C, the continuity equation is given by

$$Q_{d2} = Q_{u3} + Q_{u6} \tag{2.8}$$

It can be also noticed that the system under study has three external boundary conditions (A, F, H). These external boundary conditions (EBCs) could be for instance inflow hydrographs $[Q(t)]$, stage hydrographs $[y(t)]$, overflow structures with hydraulic controls for which there is a flow-stage relation, or any other boundary pre-specified by the user. For each of these EBCs, a flow variable (e.g., $Q(t)$, $y(t)$) or an equation is available.

For this example, so far sixteen equations are available and eight more equations are needed. Six of the remaining eight equations can be obtained by enforcing water stage compatibility conditions at nodes that connect two or more river reaches and that don't have any hydraulic structure associated to the node. In this case, if a node is connected to k river reaches, k-1 water stage compatibility conditions are available for the junction node. These conditions enforce the same elevation for the water stages immediately upstream and downstream of the node (Figure 2.7). For instance, at node C, two water stage compatibility conditions are available as

$$\begin{aligned} z_{d2} + y_{d2} &= z_{u3} + y_{u3} \\ z_{d2} + y_{d2} &= z_{u6} + y_{u6} \end{aligned} \tag{2.9}$$

In Eq. (2.9), z_d and z_u are the reach bottom elevations immediately downstream and upstream of a junction node, respectively. In the case of an abrupt change in channel geometry or abrupt bed drop at the junction node, the energy equation instead of the water stage compatibility condition should be used. If a hydraulic structure is associated to the node, the equation is obtained from the RPG of the hydraulic structure. In our example, the last two equations are obtained from RPG's at in-line-structures (nodes B and E in Figure 2.10). The treatment of fixed and mobile in-line structures in the UNHVPG model are the same. The only difference is that a single RPG is used for a fixed in-line structure while as a group of RPG's (depending on discrete gate positions) are required for a mobile in-line structure. For instance at node B, the water stage upstream of the structure is obtained from the RPG of the structure as follows (see Figure 2.10)

$$y_{d_1} = \text{RPG}[y_{u_2}, \frac{1}{2}(Q_{d_1} + Q_{u_2})] \tag{2.10}$$

The application of Eq. (2.10) requires an interpolation process similar to that of the HPG for a river reach presented earlier (Eq. 2.5). For solving the resulting non-linear system of equations, the UNHVPG model uses the Open Source C/C++ MINPACK code. MINPACK solves systems of nonlinear equations, or carries out the least squares minimization of the residual of a set of linear or nonlinear equations. For more details on this library, the reader is referred to [27]

2.2 Application to a Looped River Network

For illustrating the use of the UNHVPG model, this model has been applied to a looped river system adapted from an example in the Applications Guide of the HEC-RAS model ([17]). The plan view of this system is depicted in Figure 2.11 and the geometric characteristics of the twenty six reaches that compose the system are presented in Table 2.1. The results of the UNHVPG model were compared with the results from the unsteady HEC-RAS model version 4.0. For this comparison, a flow hydrograph and a rating curve boundary conditions are specified at the most upstream (node 1) and most downstream (node 26) ends of the system, respectively (Figures 2.12 and 2.13, respectively). All performance graphs used in the applications (HPGs and VPGs) were generated using the steady HEC-RAS model.

Table 2.1: Geometric characteristics of river reaches of a looped river system

Reach ID	Length (m)	z_u (m)	z_d (m)	Slope (m/m)
1	35.05	6.2332	6.1631	0.002000
2	35.05	6.1631	6.0930	0.002000
3	38.10	6.0930	6.0198	0.001920
4	32.00	6.0198	5.9497	0.002190
5	24.38	5.9497	5.8887	0.002500
6	39.62	5.8887	5.8339	0.001385
7	39.62	5.8339	5.7790	0.001385
8	45.72	5.7790	5.7241	0.001200
9	44.20	5.7241	5.6693	0.001241
10	32.00	5.6693	5.6144	0.001714
11	36.58	5.6144	5.5596	0.001500
12	39.62	5.5596	5.5047	0.001385
13	25.91	5.5047	5.4712	0.001294
14	21.34	5.9497	5.8979	0.002429
15	51.82	5.8979	5.8491	0.000941
16	54.86	5.8491	5.7760	0.001333
17	48.16	5.7760	5.7638	0.000253
18	56.39	5.7638	5.7028	0.001081
19	56.39	5.7028	5.6510	0.000919
20	54.86	5.6510	5.5839	0.001222
21	57.00	5.5839	5.5535	0.000535
22	57.91	5.5535	5.5047	0.000842
23	21.34	5.5047	5.4712	0.001571
24	47.24	5.4712	5.4315	0.000839
25	42.67	5.4315	5.4132	0.000429
26	51.82	5.4132	5.3950	0.000353

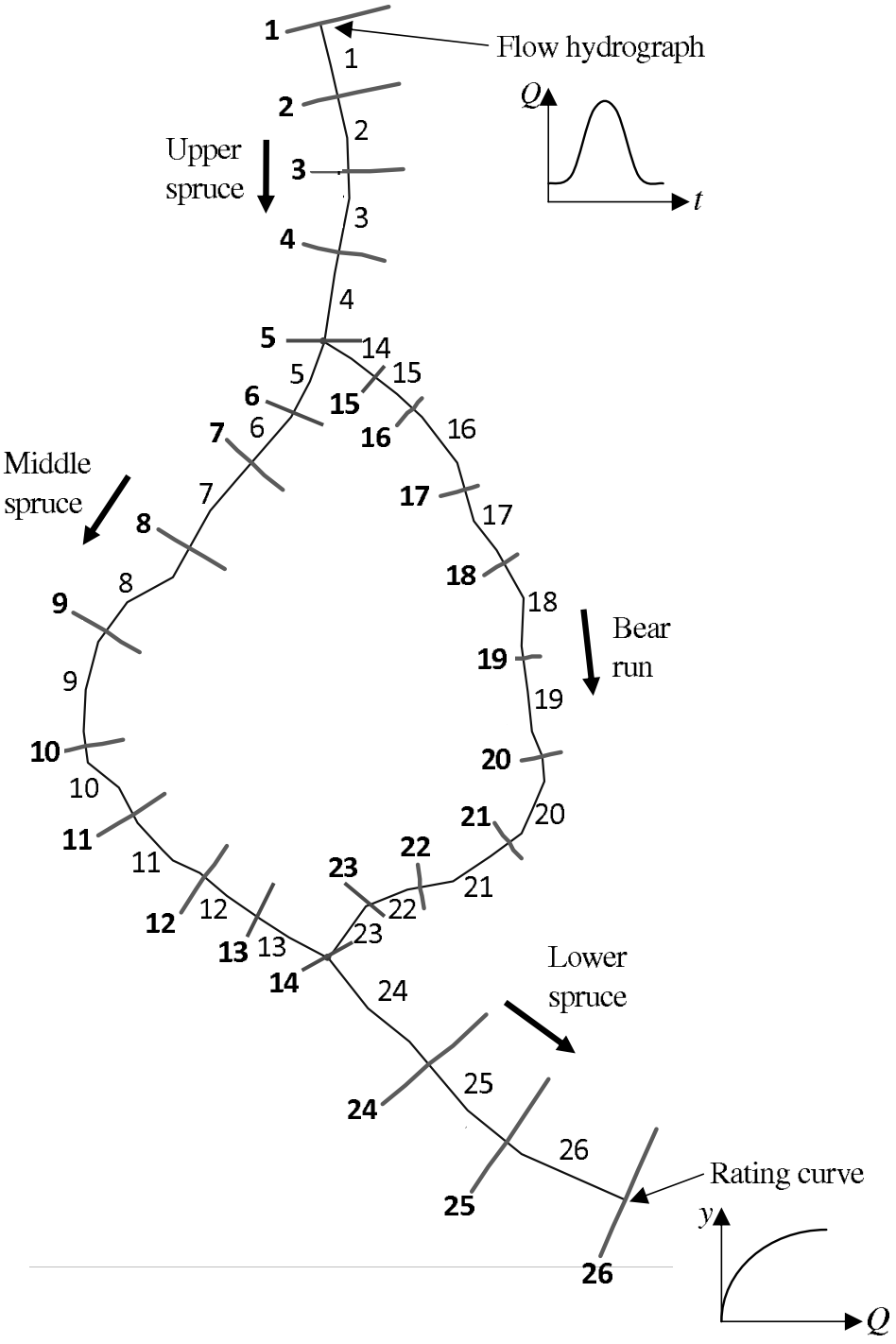

Figure 2.11: Plan view of HEC-RAS looped river system.

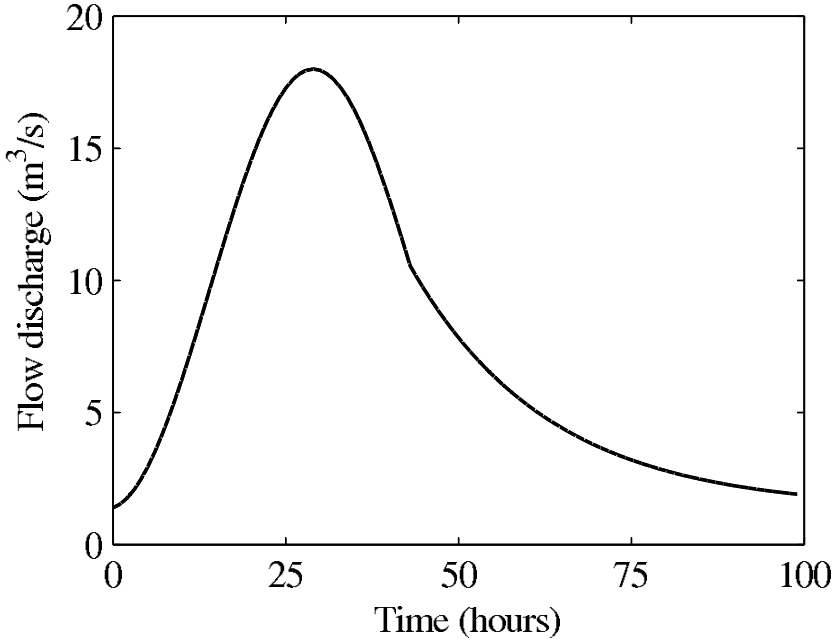

Figure 2.12: Inflow hydrograph at node 1 for case 1: slow flood-wave.

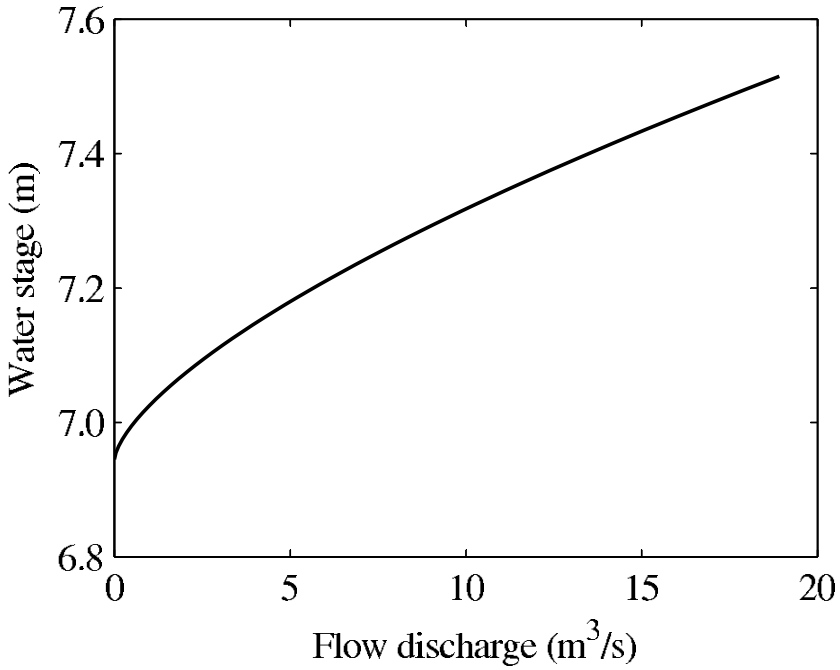

Figure 2.13: Rating curve boundary at node 26

To assess the UNHVPG model two test cases were simulated. The inflow hydrograph (node 1) for the first case represents a slow flood-wave, whereas the one for the second test case represents a fast flood-wave. To determine the initial conditions in the two subcritical flow test cases, a steady-flow discharge of 1.395 m^3/s with a water depth of 1.65 m at the downstream end of reach 26 (see Figure 2.11) was used. The values of water depth and flow discharge were used in turn for determining the water depths and flow discharges at the ends of every reach. The water depth and flow discharge at the ends of each reach are the necessary initial conditions.

2.2.1 Case 1: Slow Flood-Wave

The inflow hydrograph used for the first test case (slow flood-wave) is shown in Figure 2.12. The simulated flow and stage hydrographs at different locations obtained with the UNHVPG model are compared with the results obtained with HEC-RAS in Figures 2.14 - 2.15 and 2.16 - 2.17, respectively. As can be observed in these figures, the difference between the UNHVPG model results and the HEC-RAS results are rather small.

To evaluate the discrepancies in flow discharge, water stage, and volume between the UNHVPG and the HEC-RAS model results, the following relative differences were defined

$$\begin{aligned} E_Q(\%) &= 100\left(\frac{Q_{\text{UNHVPG}} - Q_{\text{HEC-RAS}}}{Q_{\text{Inflow Hidro}_{\max}} - Q_{\text{Inflow Hidro}_{\min}}}\right) \\ E_{WS}(\%) &= 100\left(\frac{WS_{\text{UNHVPG}} - WS_{\text{HEC-RAS}}}{WS_{\text{HEC-RAS}_{\max}} - WS_{\text{HEC-RAS}_{\min}}}\right) \\ E_V(\%) &= 100\left(\frac{V_{\text{UNHVPG}} - V_{\text{HEC-RAS}}}{V_{\text{HEC-RAS}}}\right) \end{aligned} \tag{2.11}$$

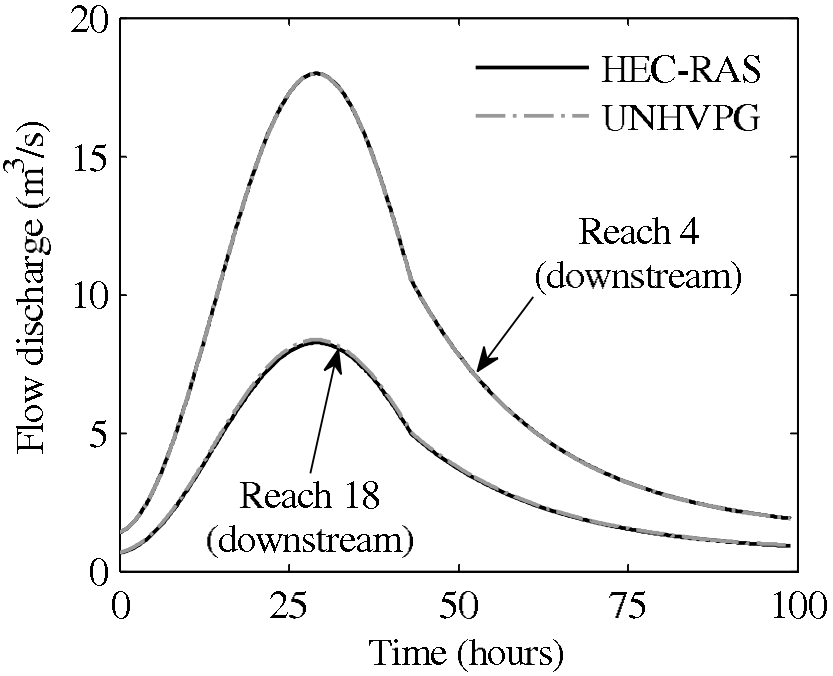

Figure 2.14: Flow hydrograph at downstream end of reaches 4 and 18 for case 1.

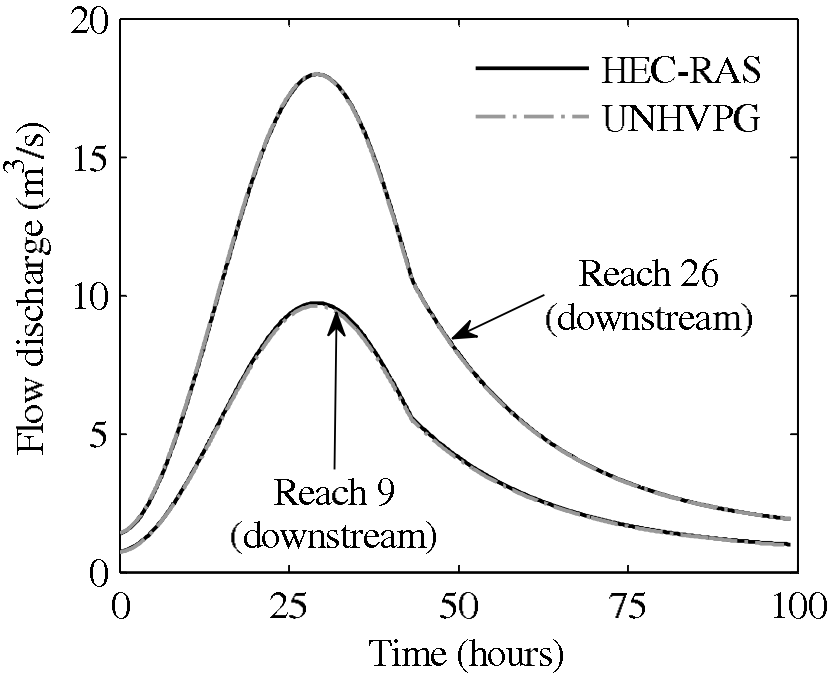

Figure 2.15: Flow hydrographs at downstream end of reaches 9 and 26 for case 1.

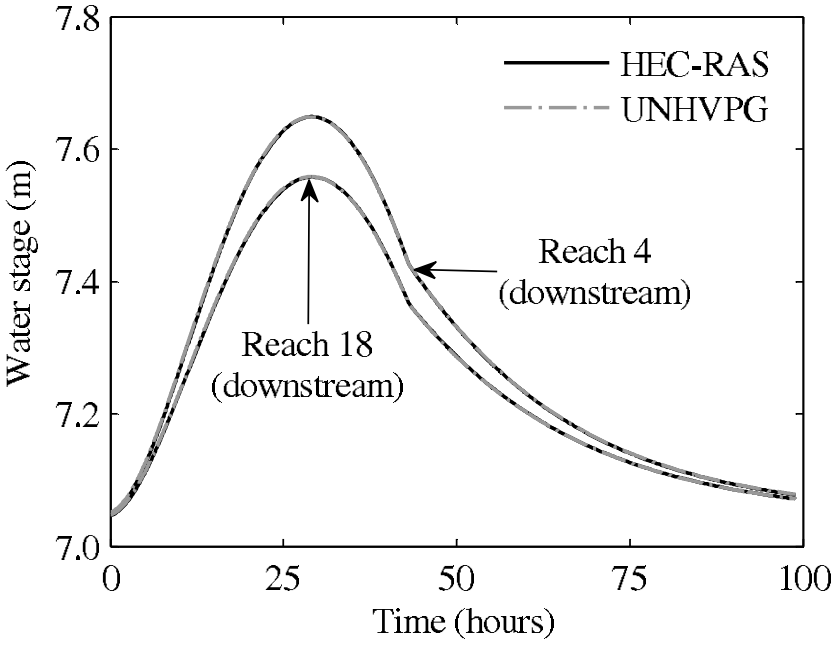

Figure 2.16: Stage hydrographs at downstream end of reaches 4 and 18 for case 1.

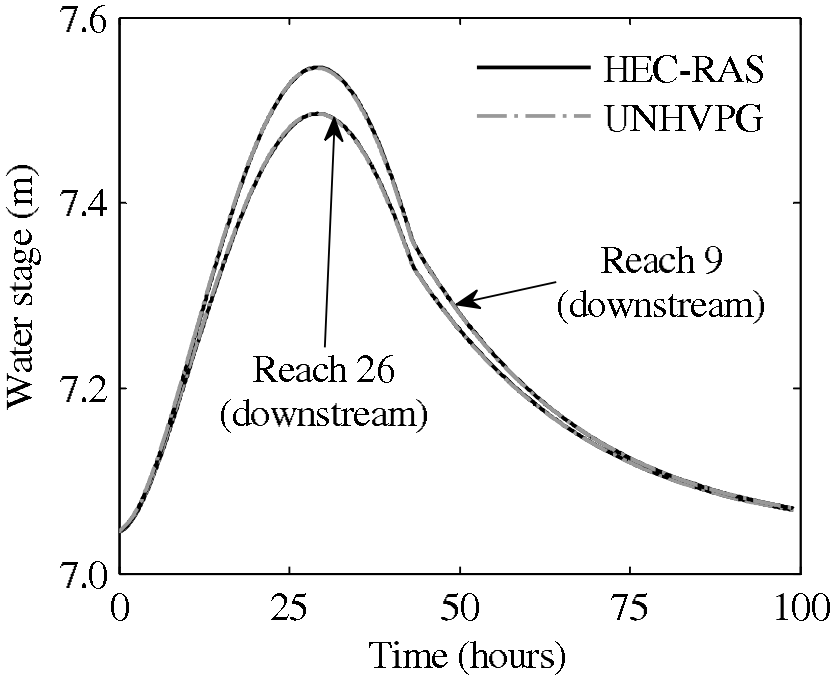

Figure 2.17: Stage hydrographs at downstream end of reaches 9 and 26 for case 1.

where E_Q, E_{WS}, and E_V are the relative differences in flow discharge, water stage and cumulative outflow volume, respectively. Note in Equation (2.11) that the discrepancies in flow discharge and water stage are defined as the difference of results between the two models normalized by the range of flow discharges or water stages.

The relative differences defined by Equation (2.11) are shown in Figures 2.18, 2.19, and 2.20 for the flow discharge, water stage, and cumulative outflow volume (V) at the downstream end of reaches 9 and 18, respectively. The relative differences in flow discharge ranged from -0.6 to 0.6 %, in water stage varied from -0.15 to 0.15 %, and in cumulative outflow volumes varied from -3.5 to 2.5 %. While the discrepancies between the results of HEC-RAS and the UNHVPG model are negligible, the maximum discrepancies in discharge and stage occur near the time of the peak discharge (see Figures 2.18 and 2.19). The local acceleration term may be responsible for the discrepancies, as the local acceleration term is more important in a sudden rising and falling of the flow (i.e., near peak flow). The unsteady HEC-RAS model accounts for the local acceleration term, while as the UNHVPG model neglects this term.

The results for the Central Processing Unit (CPU) times obtained using a Dell Precision T3500 2.67GHz, 1.00 GB of RAM for the UNHVPG, and the HEC-RAS models are presented in Table 2.2. In the UNHVPG model, for the slow flood-wave, the time step (Δt) ranged from 8.16 to 12.62 seconds, while for the fast flood-wave the time step ranged from 8.31 to 12.62 seconds. The average time steps were 9.77 and 10.27 seconds for the slow and fast flood-waves, respectively. For both flood-waves, the HEC-RAS model was simulated using a time step of 10 seconds. As can be observed in this table, the results obtained with the UNHVPG model are about 3 and 7 times faster than those of the HEC-RAS model for the slow and fast flood-waves, respectively.

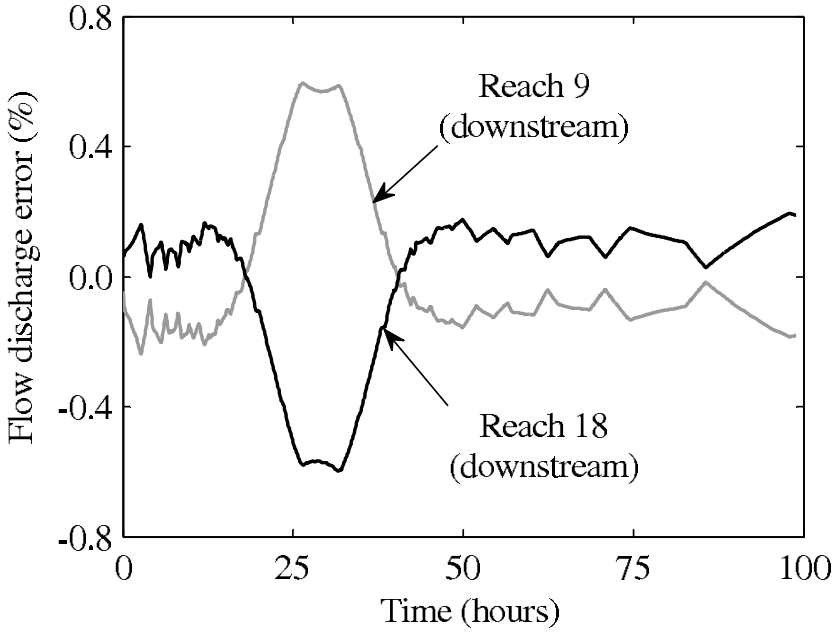

Figure 2.18: Difference in flow discharges at downstream end of reaches 9 and 18 for case 1.

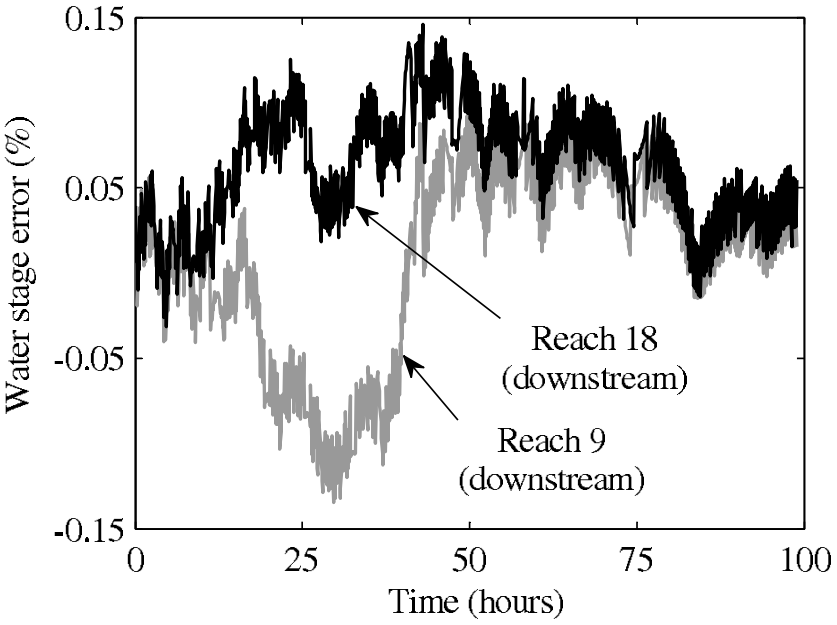

Figure 2.19: Difference in water stages at downstream end of reaches 9 and 18 for case 1.

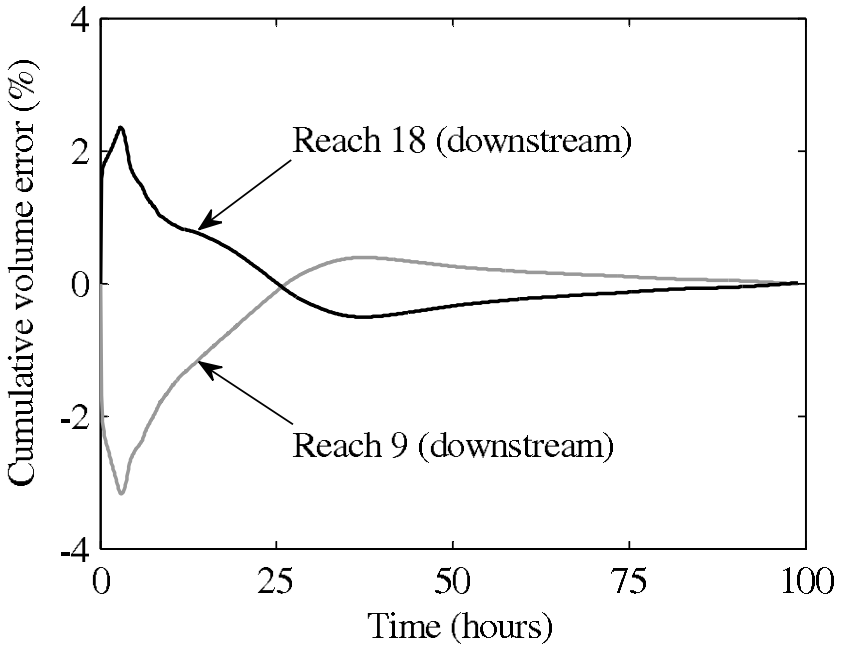

Figure 2.20: Difference in conservation of volume at downstream end of reaches 9 and 18 for case 1.

Table 2.2: Comparison of CPU times for the simulation of cases 1 and 2.

Description	UNHVPG Time (s)	HEC-RAS Time (s)
Case 1 (slow flood-wave)	218.8 ($\overline{\Delta t}$ = 9.77 s)	752.7 (Δt = 10 s)
Case 2 (fast flood-wave)	7.3 ($\overline{\Delta t}$ = 10.27 s)	52.6 (Δt = 10 s)

2.2.2 Case 2: Fast Flood-Wave

The inflow hydrograph used for the second test case (fast flood-wave conditions) is shown in Figure 2.21. The flow and stage hydrographs at different locations simulated with the UNHVPG and the HEC-RAS models are shown in Figures 2.22-2.23 and 2.24-2.25, respectively.

Simulation results obtained with both models appear to be similar. However, the differences are noticeably more significant for this case than those for slow flood-wave conditions of case 1. Figures 2.26, 2.27, and 2.28 show the differences in flow discharge, water stage, and cumulative outflow volume between UNHVPG and HEC-

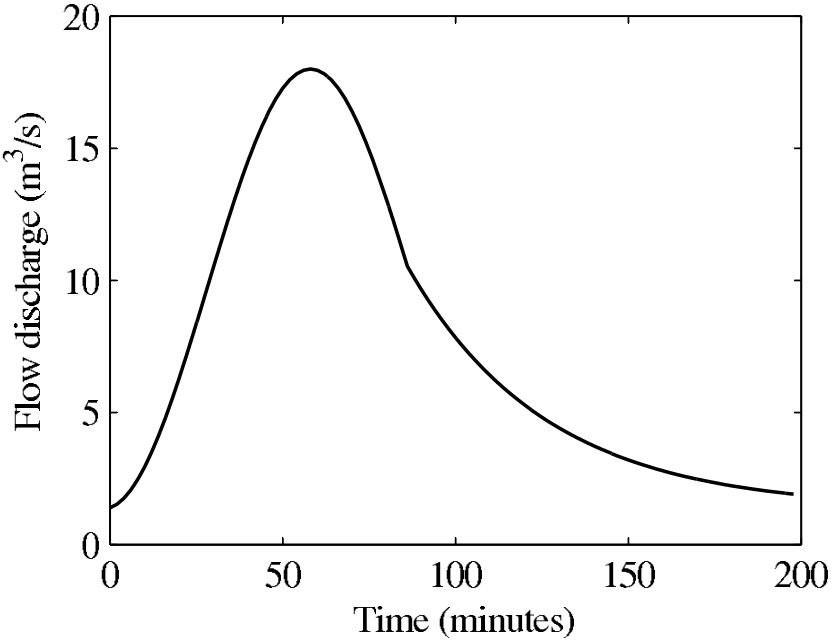

Figure 2.21: Inflow hydrograph at node 1 for case 2: fast flood-wave.

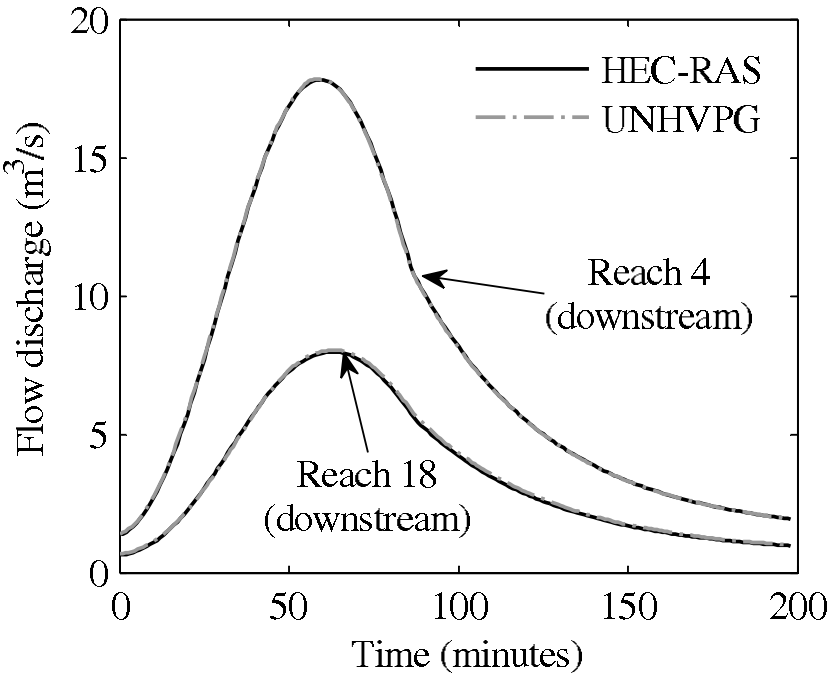

Figure 2.22: Flow hydrographs at downstream end of reaches 4 and 18 for case 2.

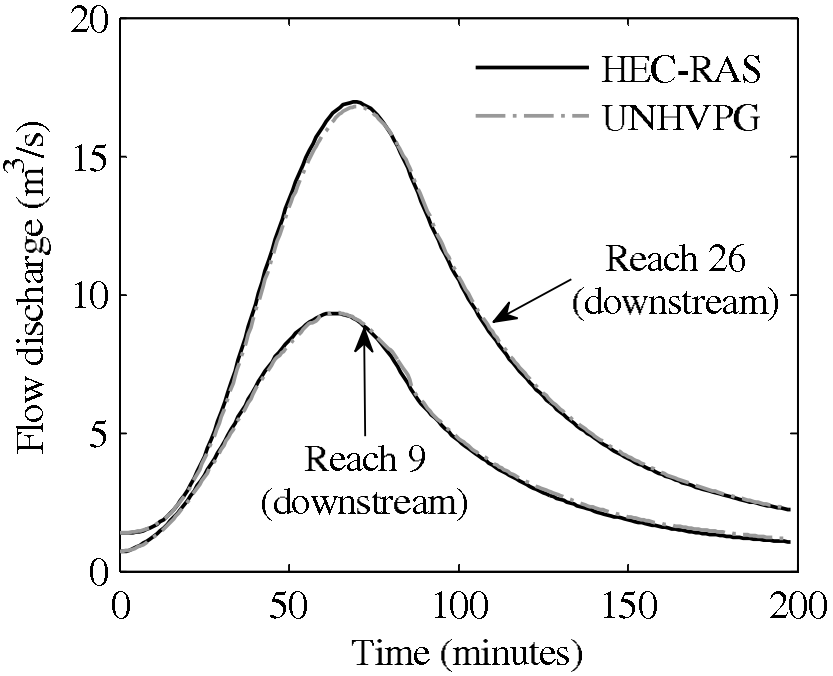

Figure 2.23: Flow hydrographs at downstream end of reaches 9 and 26 for case 2.

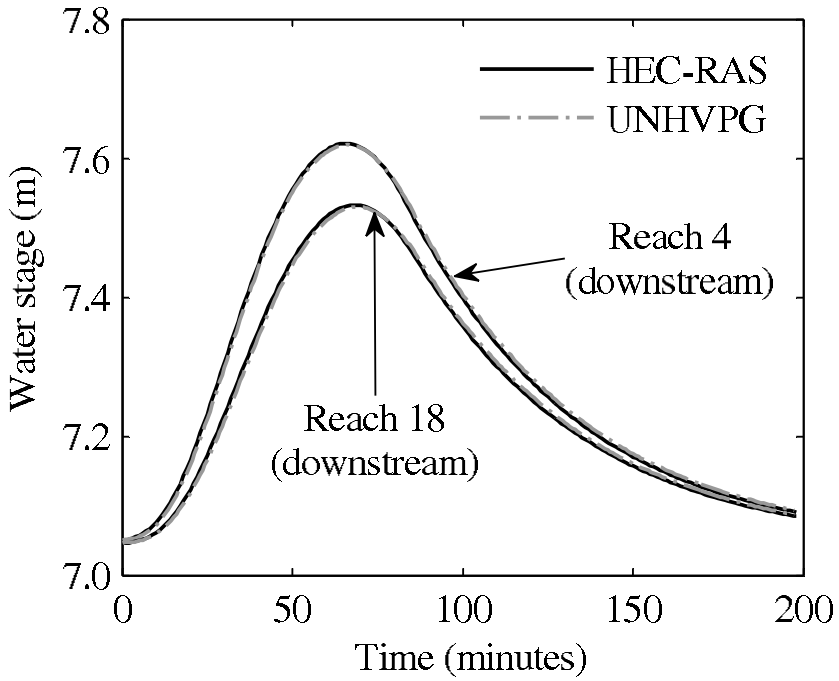

Figure 2.24: Stage hydrographs at downstream end of reaches 4 and 18 for case 2.

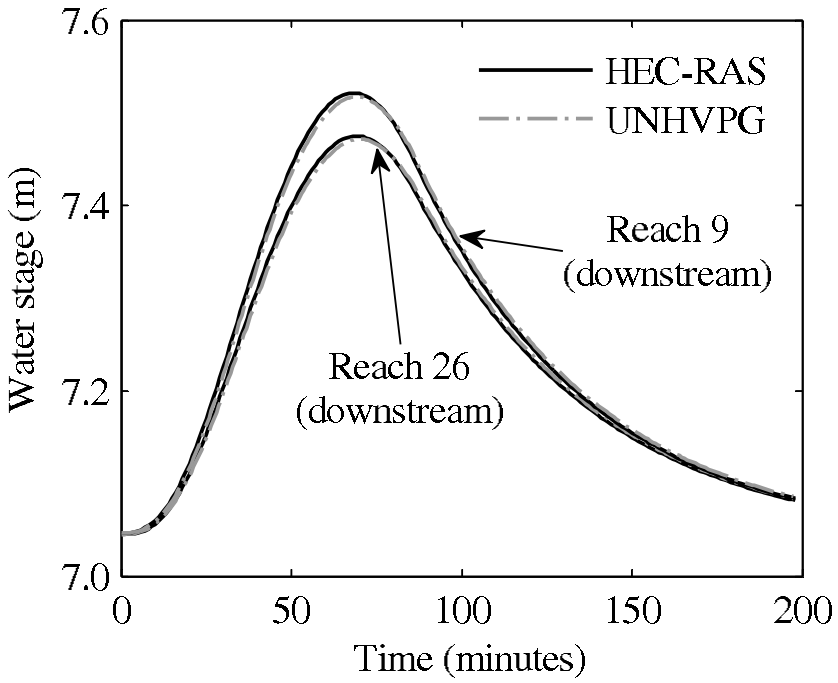

Figure 2.25: Stage hydrographs at downstream end of reaches 9 and 26 for case 2.

RAS (according with Eq. 2.11) at the downstream end of reaches 9 and 18. As shown in Figures 2.26, 2.27, and 2.28, the relative difference in flow discharge ranged from -2.5 to 1.5 %, in water stage from -1.5 to 1.0 %, and in cumulative outflow volume from -2.5 to 7.0 %. Figure 2.29 shows the plot of the flow discharge versus water stage (i.e., rating curve) at the downstream end of reach 18 for the fast flood-wave case (case 2). This figure shows a typical looped rating curve having greater flows at lower stages in the rising limb and smaller flows at higher stages in the receding limb. The rating curve for the slow flood-wave case is similar to that of the fast flood-wave case; however, it is not shown due to space limitations.

The results for the Central Processing Unit (CPU) times obtained using a Dell Precision T3500 2.67GHz, 1.00 GB of RAM for the UNHVPG, and the HEC-RAS models are presented in Table 2.2. The CPU time in Table 2.2 included the time of

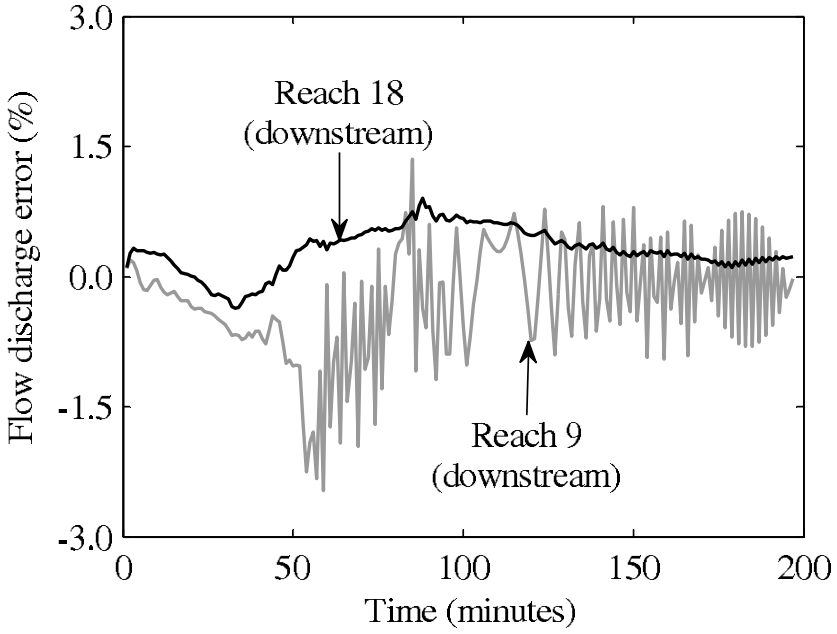

Figure 2.26: Difference in flow discharges at downstream end of reaches 9 and 18 for case 2.

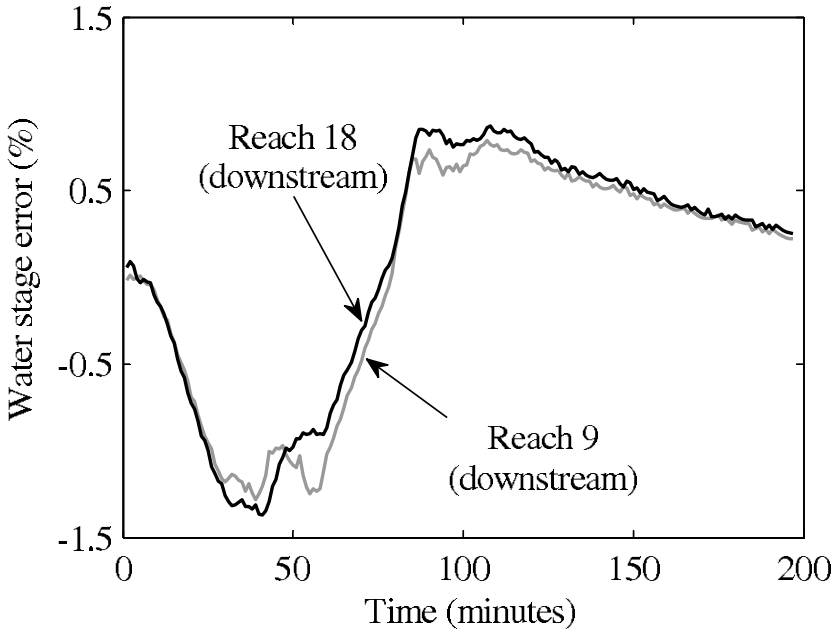

Figure 2.27: Difference in water stages at downstream end of reaches 9 and 18 for case 2.

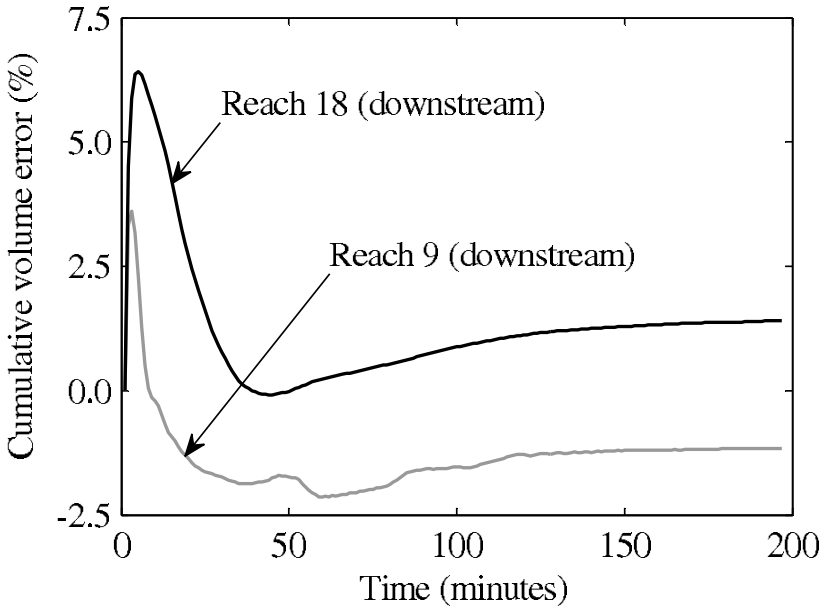

Figure 2.28: Difference in conservation of volume at downstream end of reaches 9 and 18 for case 2.

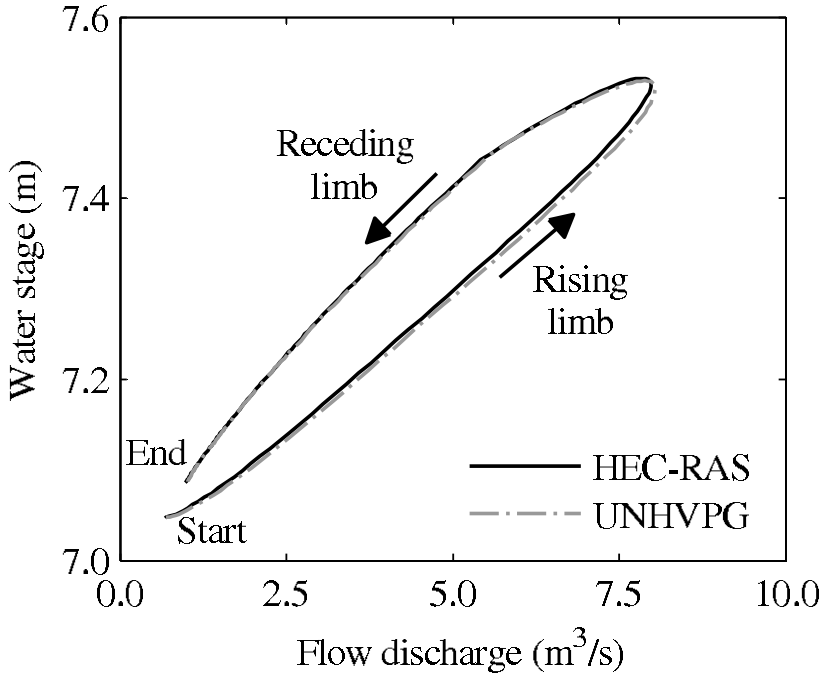

Figure 2.29: Flow discharge vs. water stage at downstream end of reach 18 for case 2.

pre-processing and computational engine but not that of post-processing. The pre-processing in the UNHVPG model involves the reading of performance graphs (from .dat files into matrices), while as in HEC-RAS it involves pre-processing geometric and hydraulic data for import into HEC-RAS. The post-processing typically demands more time and it depends on the user-specified outputs. As can be observed in Table 2, the results obtained with the UNHVPG model is about 700% faster than that of the HEC-RAS model. In the UNHVPG model, for the slow flood-wave the time step (Δt) ranged from 8.16 to 12.62 s, while as for the fast flood-wave, the time step ranged from 8.31 to 12.62 s. For both flood-waves, the HEC-RAS model was simulated using a time step of 10 seconds. Figure 2.30 shows the results of numerical accuracy of UNHVPG model due to time discretization for the upstream end of reach 14 and downstream end of reach 23. This figure appears to show that time discretization does not affect significantly the results. With regard to space and water depth discretization (Δx and Δy, respectively), the maximum value of Δx or Δy used to obtain a good accuracy is system dependent and should be obtained for each system by iteration. For instance, for Δx, two values of Δx can be used to check if the simulated results of discharge and water stage are similar for both discretizations. The process can be repeated to find the largest Δx that produces the desired accuracy and in turn the minimum CPU time. The reader is referred to [12] for an in-depth discussion on spatial discretization.

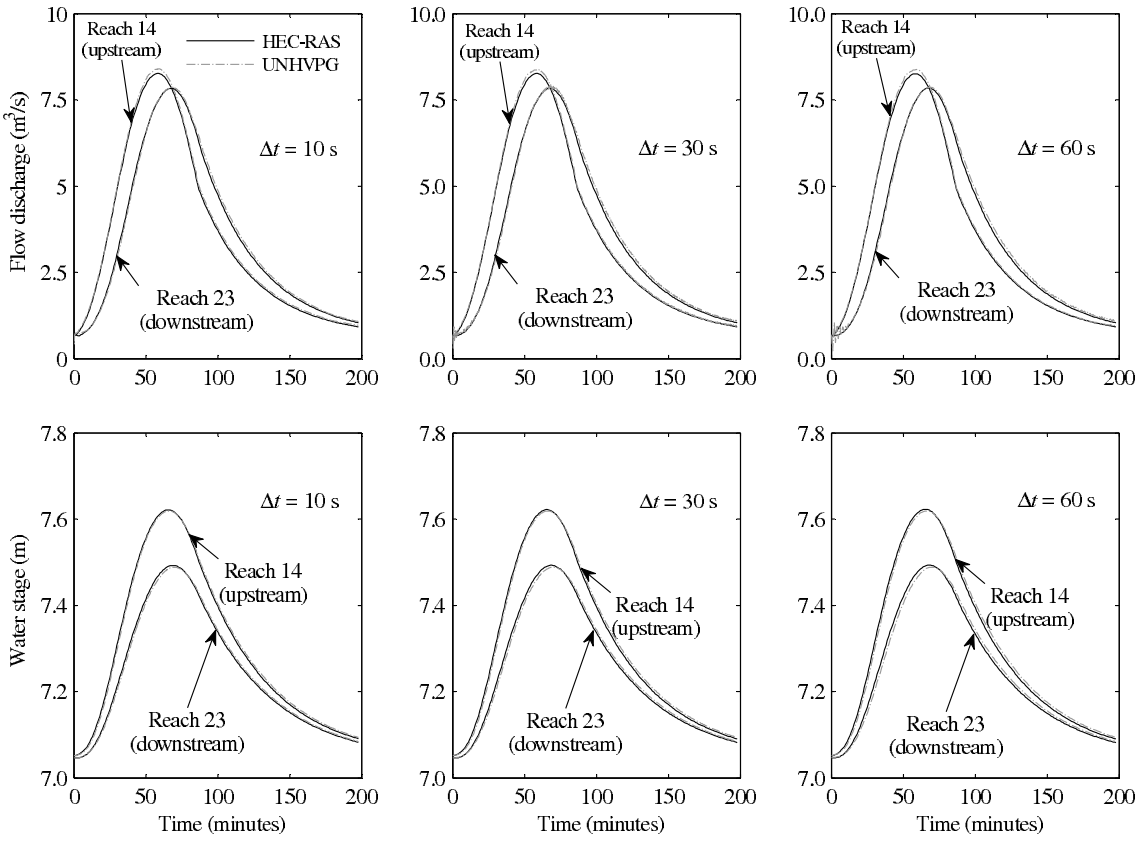

Figure 2.30: Numerical accuracy of UNHVPG due to time discretization for the upstream end of reach 14 and downstream end of reach 23

CHAPTER 3

INTELLIGENT CONTROL OF RIVER FLOODING

3.1 Components of the Proposed Framework

The proposed framework called the River Simulation and optimization Coupled Model (RSOCM) is essentially a real-time operational model that links two components: optimization and river system routing (simulation). The flow chart of the proposed framework is presented in Figure 3.1, which comprises two components and six modules.

3.1.1 Optimization Component: The Non-Dominated Sorting Genetic Algorithm-II (NSGA-II)

The optimization component of this framework uses the popular Non-dominated Sorting Genetic Algorithm-II (NSGA-II), which has been chosen based on its recent successful implementation in reservoir optimization analysis (e.g., [22]). The NSGA-II algorithm has been shown to be one of the most efficient algorithms for multi-objective optimization on a number of benchmark problems, including water resources engineering problems (e.g., [4]). Some of the recent applications to water resources engineering include multi-reservoir system optimization (e.g., [22]), optimal design of water distribution networks ([2]), long-term groundwater monitoring design ([31]), and watershed water quality management ([8]). The main features of these

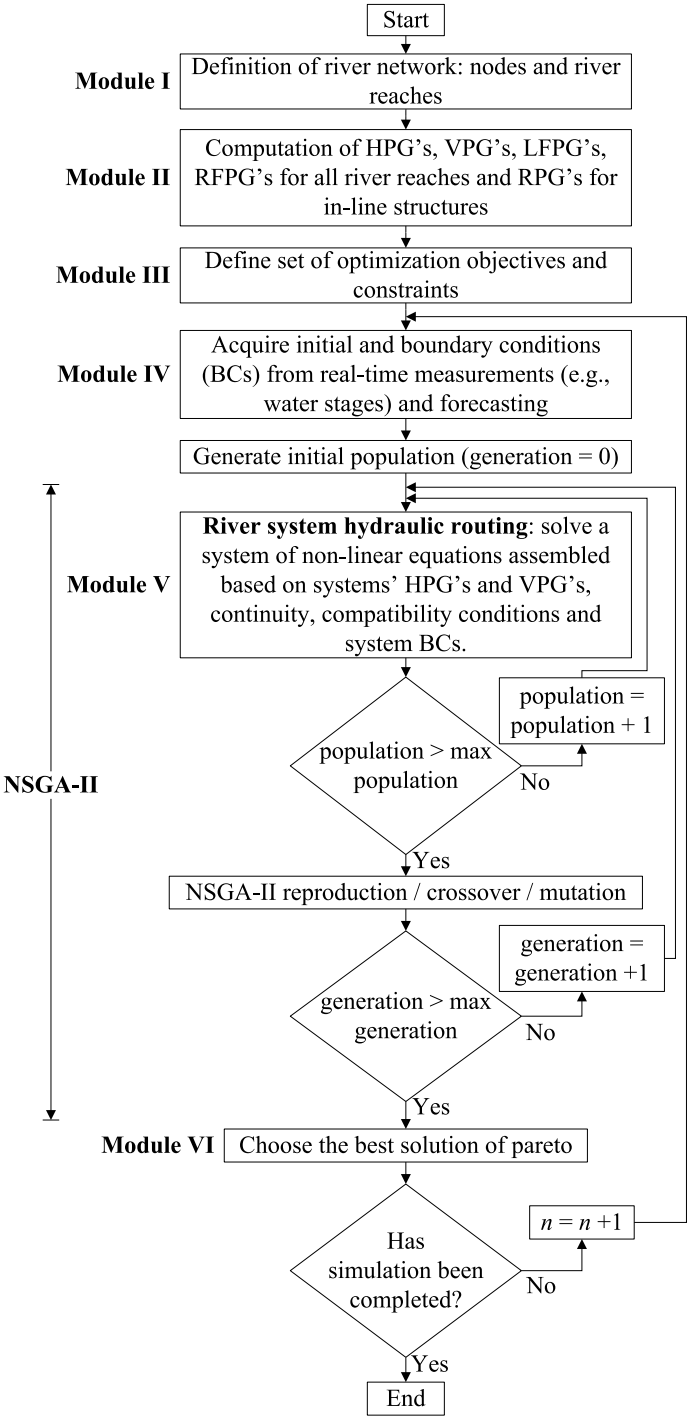

Figure 3.1: Flow chart of proposed framework for the intelligent control of river flooding.

algorithms are the implementation of a fast non-dominated sorting procedure and its ability to handle multiple objectives simultaneously without weight factors.

The reason for choosing a multi-objective optimization technique (i.e., NSGA-II) is that, under non-flooding conditions, this framework maximizes the benefits of the river system that may be multi-objective such as hydropower production, irrigation, and water supply. Under flooding conditions, the RSOCM framework uses a single-objective (minimize flooding), however to avoid using different algorithms, the multi-objective NSGA-II technique is used for both flooding and non-flooding conditions.

The NSGA-II algorithm places emphasis on moving towards the true Pareto-optimal region, which is essential in real-world credit structuring problems. The main feature of this algorithm is the implementation of a fast non-dominated sorting procedure and its ability to handle constraints without the use of penalty functions.

3.1.2 Simulation Component

The hydraulic component of the proposed framework consists of dividing the river system into reaches and pre-computing the hydraulics for each of these reaches independently using any gradually varied flow model (one-, two-, or three-dimensional model). The pre-computed hydraulics for each reach is stored in matrices and is accessed as look up tables. The hydraulic routing adopted for each river reach is performed using the Hydraulic Performance Graph (HPG) and Volume Performance Graph (VPG). The HPG of a channel reach graphically summarizes the dynamic relation between the flow through and the stages at the ends of the reach under gradually varied flow (GVF) conditions, while the VPG summarizes the corresponding storage. The storage volumes from VPGs are divided into left, right, and main channel storages volumes. The left and right inundation volumes are summarized into Left

Flooding Performance Graphs (LFPGs) and Right Flooding Performance Graphs (RFPGs), respectively. The LFPGs and RFPGs represent volumes of water outside of levee limits, channel banks or topographic thresholds that were used to define the limits of inundation (See Figure 3.2).

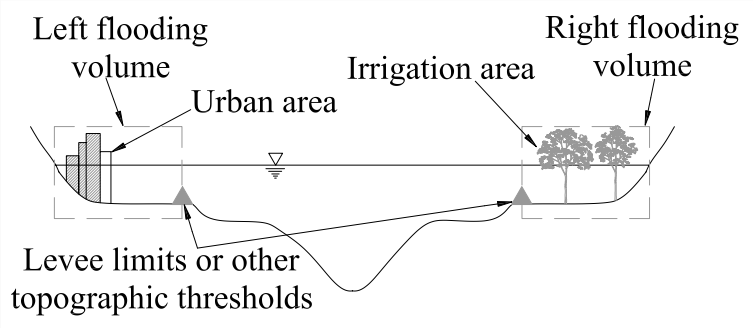

Figure 3.2: Cross-section schematic for definition of left and right flooding volumes.

The left and right storage volumes are summarized into LFPGs and RFPGs. Similarly, the VPGs, LFPGs and RVPGs of a channel reach graphically summarize the dynamic relation between the flow through, the stage at the downstream end and the corresponding left and right storage of the reach under gradually varied flow (GVF) conditions, respectively.

At the location of in-line structures (controlled and uncontrolled), the proposed framework makes use of Rating Performance Graphs (RPGs). An RPG graphically summarizes the dynamic relation between the flow through, and the stages upstream and downstream of an in-line structure under GVF conditions. Physical measurements of flow discharge and water stages or numerical simulations using one-, two-, or three-dimensional numerical models can be used for constructing RPGs. In this framework, all internal nodes (uncontrolled and controlled in-line structures, and channel junctions) are assumed to have no storage. The water depth immediately upstream of the in-line structure is computed using the RPG constructed for the

structure. For a detailed description of the hydraulic component of the proposed framework, the reader is referred to [24].

3.2 Integration and Linking of Components

The proposed framework is composed of six main modules as illustrated in Figure 3.1. A brief description of these modules is presented next.

3.2.1 Module I: Representation of a River Network

In the proposed model, a river system is represented by river reaches and nodes. A river reach is defined by its upstream and downstream nodes and must have more or less uniform properties along the reach (e.g., cross-section, bed slope). The flow direction in a river reach is assumed to be from its upstream node to its downstream node as shown in Figure 2.4. A negative flow discharge in a river reach indicates that reverse flow occurs in that river reach. In Figure 2.4, the subscript j and superscript n represent the river reach index and the discrete-time index, respectively. Also, y is water depth, Q is flow discharge, and the subscripts u and d denote the upstream and downstream ends of a river reach, respectively.

A node, which is depicted schematically in Figure 2.5, may have v inflowing river reaches and p outflowing river reaches, with $k = v + p$, where k is the total number of river reaches linked to the node. A river reach is denoted as inflowing (or outflowing) when it conveys to (or from) the node. Several types of boundaries conditions (BCs) are supported by the proposed model. A description of these boundaries is presented below.

1. External Boundary Conditions (EBC), which are prescribed at the most upstream and downstream ends of the river system. EBCs include inflow hydrographs, stage hydrographs, or stage-discharge ratings. An EBC can have either an inflowing or outflowing river reach connected to the node but not both.

2. Internal Boundary Conditions (IBCs), which are specified at internal nodes whenever two or more reaches meet. The three types of IBCs currently supported by the proposed framework are:

    - Uncontrolled in-line structures (e.g., dams without operation of gates, bridges). A single RPG, whose construction is very similar to that of the HPG, is built for this node.
    - Controlled in-line structures (e.g., gates, rising weirs). An array of RPGs is necessary for this type of structure, one for each discrete gate position so as to encompass the full range of operation of the gate(s). Typically, gates installed in dams are identical and have an equal invert elevation. For instance, if a dam has 10 identical gates that have the same invert elevation, all gates have the same RPG, which reduces drastically the number of RPGs needed for simulations.
    - Controlled in-line structures (e.g., gates, rising weirs). An array of RPGs is necessary for this type of structure, one for each discrete gate position so as to encompass the full range of operation of the gate(s). The water depth immediately upstream of the controlled in-line structure is computed using these RPGs. Typically, gates installed in dams are identical and have an equal invert elevation. For instance, if a dam has 10 identical gates that have the same invert elevation, all gates have the same RPG,

which reduces drastically the number of RPGs needed for simulations. In cases where gates have different invert elevations, the RPGs can be built for combined operations of one or more gates assuming that all gates are operated (opened or closed) using the same discrete levels.

- Junctions, which are schematically depicted in Figure 2.5, represent nodes without presence of hydraulic structures. A junction node is assumed not to have storage and may connect two or more river reaches.

For a detailed description of boundaries of the proposed framework, the reader is referred to Section 2.1.4.

3.2.2 Module II: Computation of HPGs, VPGs, LFPGs, RFPGs, and RPGs

In this module, HPGs, VPGs, LFPGs, and RFPGs are needed for all reaches of the river system, while RPGs are needed for all uncontrolled and controlled in-line structures. As mentioned in Section 2.1.2, the flow discharges used for constructing the performance graphs should range from near dry-bed states to high water stages (e.g., inundation, see Figure 3.2) using appropriate intervals between flow discharges. These intervals are set according to the desired precision by a trial and error process.

3.2.3 Module III: Definition of Optimization Objectives and Constraints for Flooding Control

Under flooding conditions, the first optimization objective proposed for flood control is given in Equation 3.1.

$$\text{Minimize } f = \sum_{j=1}^{\text{RR}} (w_{L_j} FV_{L_j} + w_{R_j} FV_{R_j}) \tag{3.1}$$

Where j denotes a river reach, RR is the total number of river reaches, and FV_{L_j} and FV_{R_j} are left and right flooding volume, respectively (see Figure 2). FV_{L_j} and FV_{R_j} are obtained from the corresponding LFPG and RFPG, respectively. w_L (or w_R) is a weight factor assigned to the left (or right) of each reach of the system depending on the amount of damage that would occur, should the left (or right) of the reach flood. In an actual application, weight factors should be determined from a social and economic study based on a hierarchy of losses that would be incurred as a result of flooding. It is worth mentioning that the weight factor for a reach doesn't need to be constant as it can be made a function of the flooding volume (or water stage) in the reach.

The percentage of opening of each of the gates and water stages are used as input values in RPGs. Consequently, flow discharges through controlled in-line structure BCs are a function of percentage of gates opening. These flow discharges together with water stages are used as input values to calculate flood volumes. Hence, the decision variables of the objective function presented in Equation 3.1 are the percentage of the opening of each of the gates in the entire river system.

Typically, the gates installed in dams are identical and have the same invert elevation. In the latter case, the number of decision variables can be significantly reduced. For instance, if a dam has 10 identical gates with the same invert elevation, the decision variables for each gate will be the same. Therefore, the decision variables of only one of these gates need to be considered. If the percentage of opening these 10 gates is divided in 20 parts (each 5% opening), only 20 decision variables would be

used for all the gates of this dam. As mentioned earlier, the optimization component of the proposed model is multi-objective. Therefore, various objectives can be defined besides flood control. The latter is outside the scope of this current model effort.

An additional optimization objective is aggregated into the proposed model for each controlled in-line structure boundary (CIB). An additional optimization objective for one CIB is given in Equation 3.2.

$$\text{Minimize} f_2 = S_{u_{\text{CIB}}} \tag{3.2}$$

In Equation 3.2, $S_{u_{\text{CIB}}}$ is the storage of a river reach or reservoir located right upstream of the CIB. This additional optimization objective is to minimize the storage in a river reach or reservoir located right upstream of a CIB in order to have available storage for the peak flow. The storage in the reservoir can be found using a stage-storage curve or a VPG, if the reservoir is composed of river reaches. The decision variable of this objective is the water stage in the reservoir if the storage in the reservoir is found using the stage-storage curve. The decision variable of this objective is the downstream water stage in the river reach located right upstream of the CIB if the reservoir is composed by river reaches.

During the optimization process, the water stage in the reservoir should be constrained between a minimum operation level and the spillway level. If the water stage in the reservoir is higher than the spillway level, the model will not optimize, as it will allow the flow to spill over the spillway.

3.2.4 Module IV: Initial and Boundary Conditions

The initial conditions in the proposed model are downstream water depths and flow discharges at upstream Q_u and downstream Q_d ends of each river reach. To check the consistency of initial conditions, continuity equations and compatibility conditions of water stages are verified for all internal nodes. The boundary conditions are basically the inflows to the river system and rating curves at the downstream ends of a river system. It is well known that hydrology predictions for inflow discharges have large uncertainties. However, this will not constitute a strong limitation of the proposed framework for the accurate operation of a river system because initial and boundary conditions can be continuously updated by real-time measurements in the river system (e.g., water stages). The latter means that any error in inflow discharge predictions at a previous time step will be minimized by real-time measurements of water stages at the next time step (e.g., mass balance will be conserved).

3.2.5 Module V: River System Hydraulic Routing

This module assembles and solves a non-linear system of equations to perform the hydraulic routing of the river system. These equations are assembled based on information summarized in the systems' HPGs, VPGs, and RPGs, the reach-wise equation of conservation of mass, continuity, and compatibility conditions of water stages at the union of reaches (nodes), and the system boundary conditions. For a detailed description of this hydraulic routing, the reader is referred to Section 2.1.6.

3.2.6 Module VI: Choose the Best Solution of Pareto

In NSGA-II, the number of optimal solutions provided in a pareto is equal to the number of individuals of the initial population. This module chooses the best solution of the paretos by adopting the following criterion. The gate opening belongs to rank 1 and produces the minimum first objective (flooding volume times weight factor). Solutions in rank 1 have the best objective functions and are the ones that least violate the constraints. In cases where more than one solution produces the same first objective, the solution that produces the minimum second objective will be chosen.

3.3 Application of the Proposed Model to the Boise River System

For demonstration purposes, this model was applied to the Boise River system in Idaho, the plan view of which is presented in Figure 3.3. The Boise River system was divided into twenty five river reaches, including three uncontrolled in-line structures, and one controlled in-line structure.

The controlled in-line structure consists of six sluice gates that are assumed to be operated automatically to fulfill the objective of the application. The upstream end of reach R1 is located right downstream of Boise River Diversion Dam and the downstream end of reach R25 is located approximately 2600 m downstream near Glenwood bridge.

3.3.1 Hydrologic Modeling

For the inflow to the Boise River system, an inflow hydrograph was obtained using the Soil and Water Assessment Tool (SWAT) for a climate change scenario. For

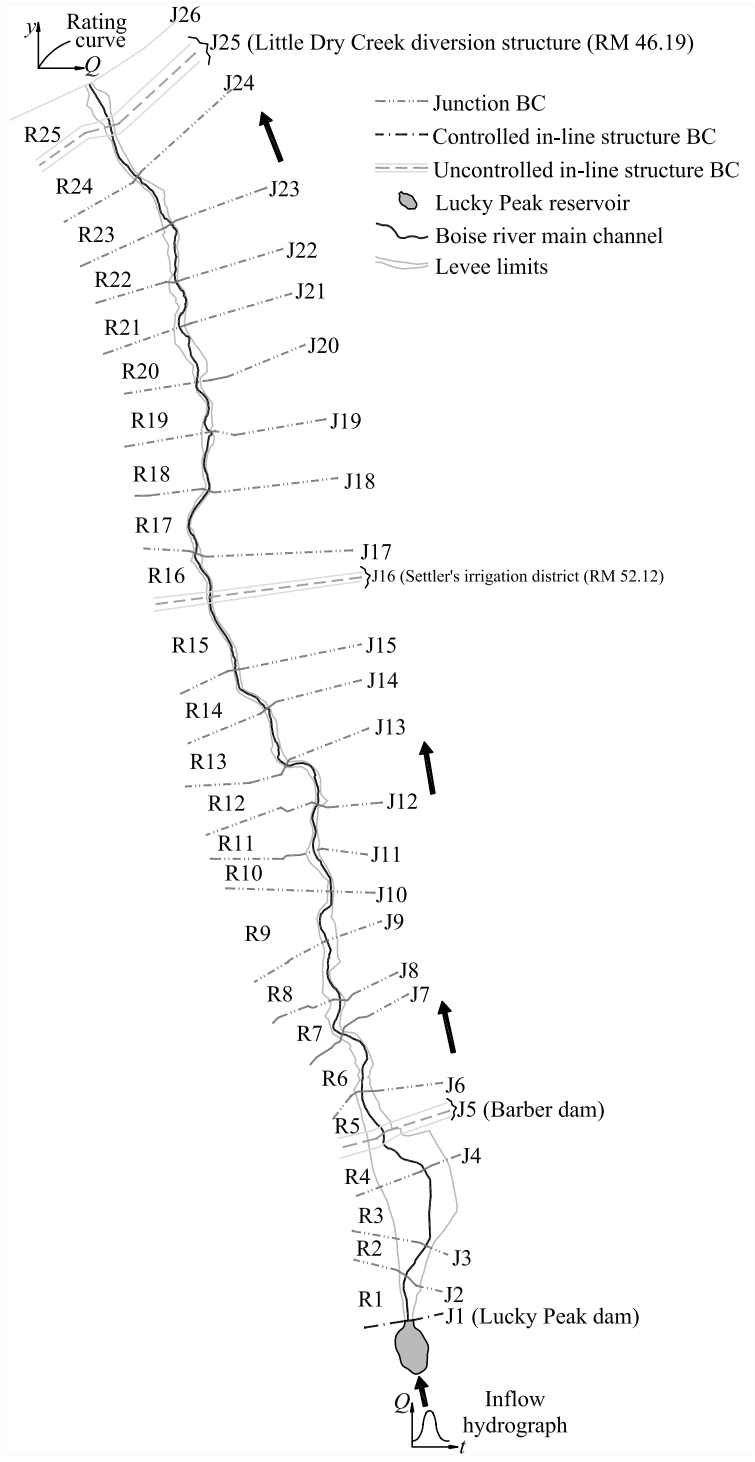

Figure 3.3: Schematic of Boise river's plan view

data-limited, complex terrain such as the Boise River basin, this model provides the best approximation of the basin's response to precipitation events. This model has been implemented for other Idaho watersheds earlier ([34], [33], [21]). The basic drivers for this model are USGS-derived Digital Elevation Model, STATSGO soil layer, National Land Cover Data 2001 for vegetation, and weather data. SWAT was used to quantify possible impacts of climate change due to anticipated precipitation and temperature increase as this is expected to cause a significant shift in the timing and magnitude of streamflow.

The climate change scenario used in this application is the IPSL-CM4 from the Institut Pierre Simon Laplace (IPSL), CNRS, CEA, France. This model in general projects a wetter winter for the study region. Based on the Special Report on Emission Scenarios (SRES) illustrative scenario, we chose A1B (750 parts per million CO_2) for deriving temperature and precipitation products. The spatial resolution of this model is $2.5^\circ \times 3.75^\circ$; however, we have downscaled the climate model-produced temperature and precipitation to 1/8th degree to drive the hydrology model. For details on the downscaling and SWAT model simulation, the readers are referred to [21]. The inflow hydrograph consisting of average daily and natural flows for a fifty year period (from 01/01/2010 to 12/19/2059) was generated at the Lucky Peak Reservoir. This inflow hydrograph represents natural flows, which means that the storage capacity of the Lucky Peak Reservoir and the flow diversions are not considered. For the present application, a period of nine months (274 days) between 11/30/2041 and 08/30/2042 from the fifty year period was selected and used in the simulations. This inflow hygrograph, which is depicted in Figure 3.4, corresponds to the largest volume of inflow during a period of nine months.

In this region, the snowpack in the higher mountains acts as a natural reservoir,

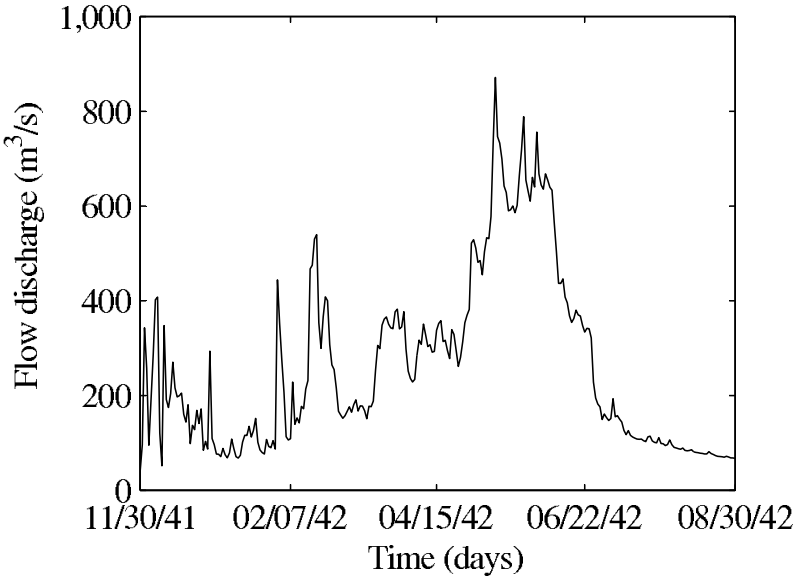

Figure 3.4: Inflow hydrograph (SWAT)

storing precipitation from the preceding winter. Most of this precipitation falls as snow and accumulates, and during the warm season, the snowpacks melt and release water as runoff into the rivers. In the Boise River system, the peak flow season starts in the spring and ends in the middle of the summer, from April through July (Figure 3.4). Also, Figure 3.4 shows that during December there is an increasing flow due to precipitation possibly as rain-on-snow, and between January to February and after July, the inflow hydrograph presents low flows. The rain-on-snow events and increasing temperature in the winter are potential triggers for flooding under future climate conditions.

In this application, Anderson Ranch reservoir, Arrow Rock reservoir, Lake Lowell, and Hubbard Dam could not be simulated because stage-storage curve of these storage facilities were not available to the authors. Anderson Ranch reservoir and Arrow Rock reservoir are located upstream of the Lucky Peak reservoir (See Figure 3.5).

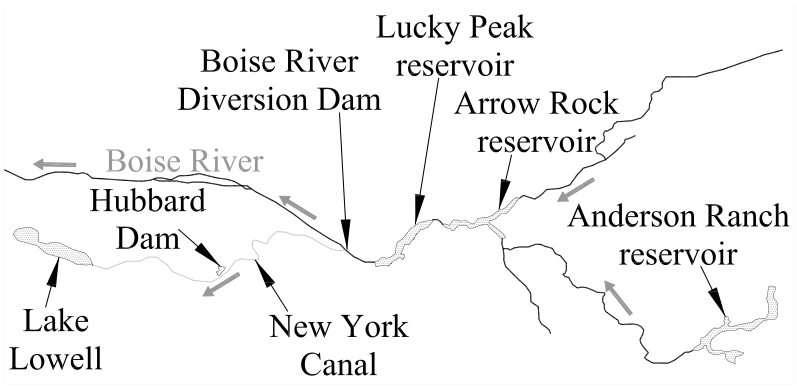

Figure 3.5: Plan view of major storage reservoirs in the Boise river basin.

The active storage capacity of Anderson Ranch and Arrow Rock reservoirs are 509.6 and 335.8 million cubic meters (MCM), respectively. In order to consider the active storage capacity of the aforementioned reservoirs, a constant flow discharge of 90 m^3/s was subtracted from the inflow hydrograph between 03/07/2042 and 05/11/2042 for filling Anderson Ranch reservoir, while a constant flow discharge of 84 m^3/s was subtracted from the inflow hydrograph between 03/25/2042 and 05/10/2042 for filling Arrow Rock reservoir. The Boise River Diversion Dam, an inline structure located downstream of Lucky Peak reservoir and upstream of river reach R1, diverts water into the New York Canal. The New York Canal feeds Lake Lowell (196.6 MCM) and Hubbard Dam (4.9 MCM), presented in Figure 3.5.

The geometry of the Boise River for this application starts downstream of the Boise River Diversion Dam. In order to consider the active storage capacity of Lake Lowell and Hubbard Dam, a constant flow discharge of 51.5 m^3/s was subtracted from the inflow hydrograph between 03/18/2042 and 04/30/2042 for filling Lake Lowell, while a constant flow discharge of 10 m^3/s was subtracted from the inflow hydrograph between 05/05/2042 and 05/09/2042 for filling Hubbard Dam.

The periods for filling the aforementioned storage facilities were chosen because a simply mass balance at Lucky Peak reservoir was performed using the inflow hydrograph obtained using SWAT, a maximum outflow from Lucky Peak of 150 m^3/s and a time step of one day. Results of this simple mass balance shows that water stage in Lucky Peak was 1 m below the spillway crest at date 03/06/2042. In order to increase the available storage capacity of Lucky Peak reservoir in the spring ahead of the snowmelt, the aforementioned flow discharges were subtracted from the inflow hydrograph beginning on 03/07/2042.

The flow hydrograph resulting from reducing the storage in Anderson Ranch reser-

voir, Arrow Rock reservoir, Lake Lowell, and Hubbard dam is depicted in Figure 3.6. This flow hydrograph was used as inflow to the river system at node J1 in the present application. The inflow reduction due to filling of the aforementioned storage facilities causes low flow between 03/07/2042 and 05/01/2042.

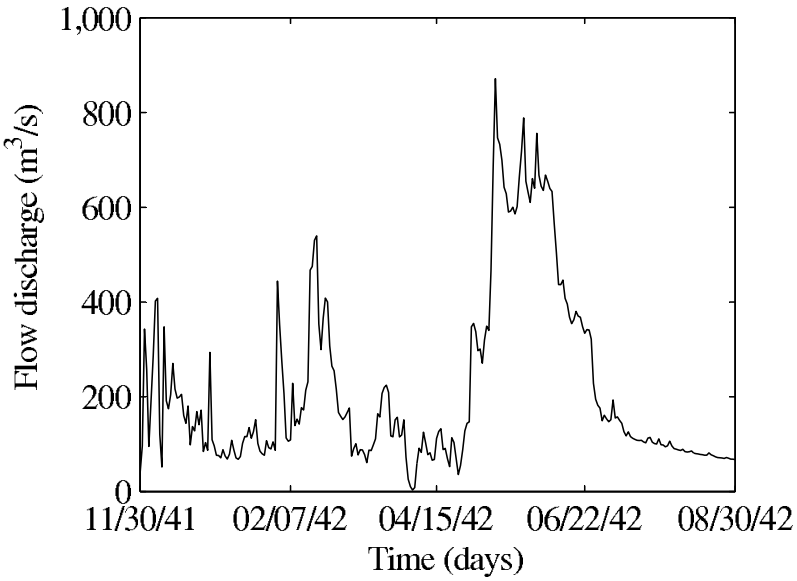

Figure 3.6: Inflow hydrograph subtracting active storage capacity of Anderson Ranch, Arrow Rock, Hubbard reservoirs and Lake Lowell.

Due to lack of river geometry between Lucky Peak reservoir and Boise Diversion Dam (node J1 in Figure 3.3), it was assumed that Lucky Peak reservoir is located immediately upstream of node J1 in Figure 3.3. In other words, the outflow of Lucky Peak reservoir discharges directly to river reach R1. The stage-storage curve for Lucky Peak reservoir is presented in Figure 3.7.

It is important to mention that this relationship was adjusted for elevation due to the fact that in this application Lucky Peak reservoir was moved from its original elevation to immediately upstream of node J1.

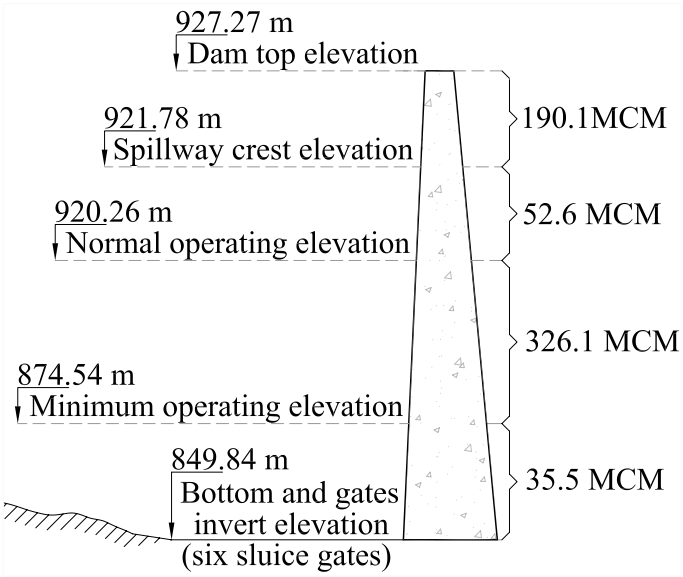

Figure 3.7: Stage-storage relationship of Lucky Peak reservoir.

3.3.2 Optimization Objective and Constraints

For this application, the optimization objectives were to minimize flooding according to Eq. 3.1 and to minimize the storage in Lucky Peak reservoir (Equation 3.2). Weight factors were assumed to be between one and three. These numbers were chosen for demonstration purposes and are not based on an actual social and economic study. In an actual application, weight factors should be determined from a social and economic study based on a hierarchy of losses that would be incurred as a result of flooding. As mentioned earlier, the weight factor for a reach doesn't need to be constant as it can be made a function of the flooding volume (or water stage) in the reach. A weight factor of one was assumed for the left and right sides of reaches R1 to R4. Reaches R1 to R4 correspond to the Barber pool conservation area (grasslands). A weight factor of two was assumed for the left side of reaches R5, R6, R16, and R17 and for the right side of reaches R6, R7, R9, R10, R11, R14, R17, R19, and R21. These regions correspond to parks and agricultural areas. Finally, a weight factor of three

was assumed for the rest of the river system. These regions correspond to residential, commercial, and business areas.

The storage in the Lucky Peak reservoir was found using the stage-storage curve presented in Figure 3.7. The water stage in the reservoir was constrained to the minimum operating level of 874.5 m. The outflow discharge at the Lucky Peak dam was constrained to the maximum flow discharge of 184 m^3/s, which is the maximum flow that the Boise River can convey without producing flooding under normal flow conditions. Note that this maximum flow discharge (184 m^3/s) corresponds to normal flow conditions (no backwater effects). In unsteady flow conditions, flooding may occur at smaller or larger discharges than that corresponding to the normal flow conditions. The outlet structure of the Lucky Peak reservoir consists of a 6.706 m diameter steel-lined pressure tunnel at the upstream end of the outlet structure and six sluice gates (1.6 m width and 3.048 m height) at the downstream end of the outlet. The hydraulic capacities of the upstream and downstream ends of the outlet structure were compared. The gate conveyance was smaller than that of the tunnel and hence it controls the flow discharge through the outlet structure. The RPGs were built assuming that all gates are operated (opened or closed) using the same discrete levels. The decision variable used in the optimization is the percentage of opening of the gates in a discrete fashion (discrete optimal control). Thirty-two discrete positions (each 10 cm) have been considered for all gates, and all gates were assumed to be operated identically (i.e., same gate invert elevation). The first position corresponded to the gate totally closed and the thirty-two position to the gate totally opened. The use of the opening of the gates as decision variable can be justified in this application because all gates were identical and they were assumed to be operated identically. However, when the inline structure has different controlled hydraulic structures (e.g.,

gates having different invert elevations), the total flow discharge at the inline structure rather than the percentage of opening of the gates should be used as decision variable. Once the optimized value of the flow discharge at the inline structure is determined, the RPG at the inline structure can be used for determining a combination of gates that satisfy this optimized flow discharge. Clearly, multiple combinations of gates may provide the same flow discharge. The plan view of Lucky Peak reservoir and the associated structures are shown in Figure 3.8. The characteristics of the river reaches are given in Table 3.1.

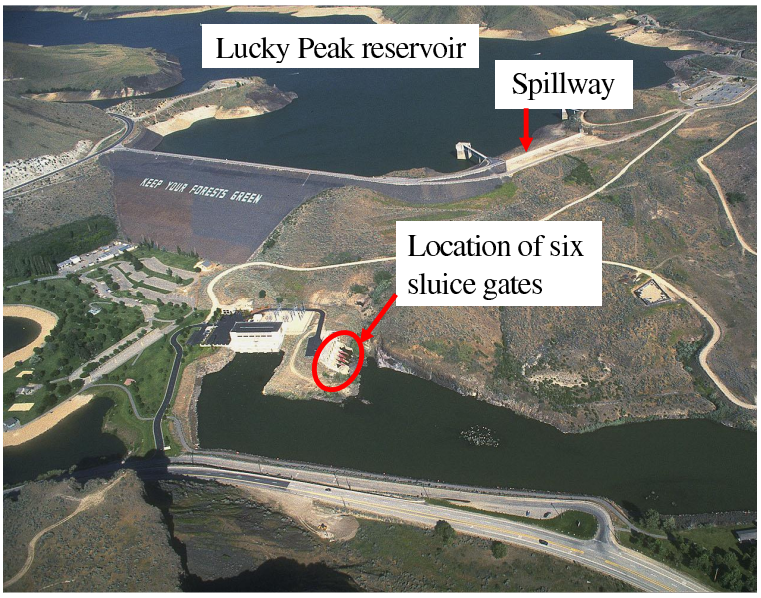

Figure 3.8: Plan view of Lucky Peak reservoir and associated structures.

The HEC-RAS file for the Boise River system along with the associated structures is available at the link http://coen.boisestate.edu/ce/faculty/aleon/index.html

3.3.3 Initial and Boundary Conditions

The system under consideration has two external boundary conditions (EBCs): the first BC is an inflow hydrograph at the upstream end of the Lucky Peak reservoir

Table 3.1: Geometric characteristics of Boise River reaches

Reach ID	Upstream node	Downstream node	Length (m)	z_u (m)	z_d (m)	Upstream station	Downstream station	Slope (m/m)
R1	J1	J2	1043.77	847.38	846.48	61.63999	61.03885	0.000859
R2	J2	J3	1000.07	846.48	845.05	61.03885	60.41834	0.001428
R3	J3	J4	998.86	845.05	844.81	60.41834	59.79479	0.000244
R4	J4	J5	877.72	844.81	844.74	59.79479	59.22549	0.000082
R5	J5	J6	991.77	838.26	837.17	59.10074	58.45808	0.001098
R6	J6	J7	1049.35	837.17	835.81	58.45808	57.84154	0.001300
R7	J7	J8	1007.67	835.81	832.18	57.84154	57.20452	0.003604
R8	J8	J9	990.85	832.18	831.26	57.20452	56.61452	0.000922
R9	J9	J10	914.63	831.26	828.76	56.61452	56.02100	0.002736
R10	J10	J11	1051.12	828.76	826.50	56.02100	55.38011	0.002153
R11	J11	J12	857.98	826.50	824.08	55.38011	54.83214	0.002815
R12	J12	J13	918.46	824.08	821.42	54.83214	54.21193	0.002901
R13	J13	J14	1174.63	821.42	818.79	54.21193	53.54053	0.002235
R14	J14	J15	1025.32	818.79	815.31	53.54053	52.84830	0.003398
R15	J15	J16	1160.85	815.31	814.27	52.84830	52.10631	0.000893
R16	J16	J17	1082.18	812.89	810.29	52.10631	51.42207	0.002408
R17	J17	J18	1218.60	810.29	807.08	51.42207	50.72177	0.002636
R18	J18	J19	1067.34	807.08	804.87	50.72177	50.03618	0.002071
R19	J19	J20	1089.71	804.87	802.69	50.03618	49.39323	0.001996
R20	J20	J21	1069.99	802.70	800.07	49.39323	48.73231	0.002448
R21	J21	J22	984.18	800.07	797.31	48.73231	48.10587	0.002806
R22	J22	J23	971.03	797.31	794.60	48.10587	47.48363	0.002794
R23	J23	J24	1075.16	794.60	792.05	47.48363	46.81672	0.002369
R24	J24	J25	982.00	792.05	790.90	46.81672	46.14800	0.001172
R25	J25	J26	643.77	789.14	787.37	46.14800	45.72556	0.002750

(see Figure 3.6) and the second BC is a flow-stage relation at the downstream end of the last river reach (see Figure 3.9). This flow-stage relation was built assuming critical flow conditions. The initial conditions are a constant flow discharge in the system of 166.7 m^3/s and a water stage in the Lucky Peak reservoir of 879.84 m. The simulation time step and the operational decision time used were one hour. The initial downstream water depths were calculated using the downstream boundary condition, constant flow discharge in the system, using HPGs, RPGs, continuity equations, and compatibility conditions of water stages for all internal nodes. The time step and the operational decision time used in the simulations were one hour.

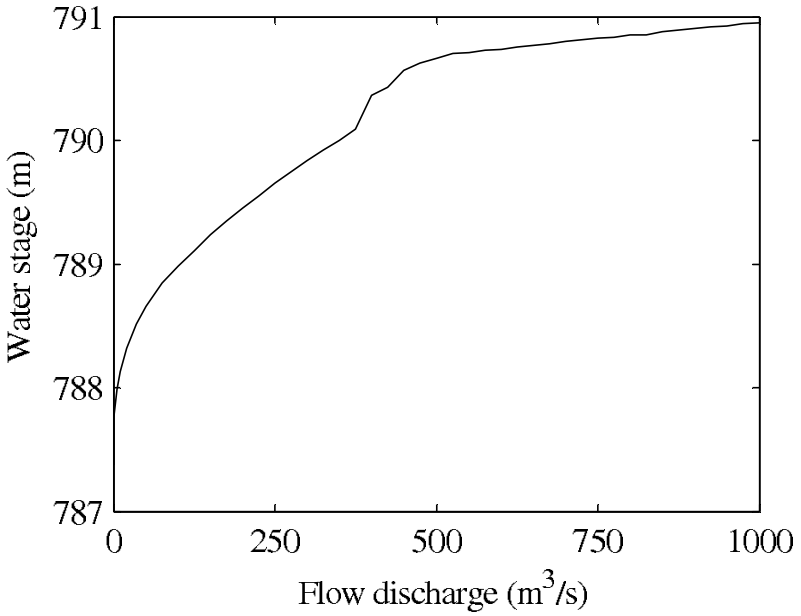

Figure 3.9: Rating curve at most downstream end of river system (node J26).

Three scenarios were simulated. The first scenario is with no gate operation (i.e., the gates are closed). The second scenario assumes that the Lucky Peak reservoir does not exist. The third scenario operates the gates according to the results of the proposed framework (minimizing the objective functions presented in Equation 3.1 and Equation 3.2).

3.3.4 Results and Analysis of Scenarios

The simulated results for flow and stage hydrographs for the three scenarios under consideration are presented in Figures 3.10 to 3.13 and 3.14 to 3.17, respectively. Reaches R1, R10, and R22 are located at upstream, downstream, and midway of the system, respectively. In the first scenario, the gates remain closed and hence the reservoir is rapidly filled. As expected, when the reservoir is full, the flow hydrograph downstream of the reservoir (flow over the spillway) is similar to that of the second scenario (no reservoir). The third scenario provides a better control of flooding, however flooding is not entirely avoided due to storage limitations.

Figures 3.12 and 3.16 show a zoom-in of results of flow and stage hydrographs from day 165 to day 180 at reach R10 for the three aforementioned scenarios.

The peak flow at reach R10 for scenario 3 is also shown in Figure 3.12. These figures show the flood attenuation due to the reservoir. As shown in Figure 3.12, the peak flow for scenario 3 arrives two hours later than in scenario 2. Results shows that the peak flow for scenario 3 is $7.76\,m^3/s$ smaller than that for scenario 2 (1% of the peak flow for scenario 3). As expected, the reservoir causes the attenuation of flow discharge and water stage for scenarios 1 and 3. Figure 3.13 and particularly Figure 3.12 show in detail for scenario 3, the rapid increase in flow discharge and water

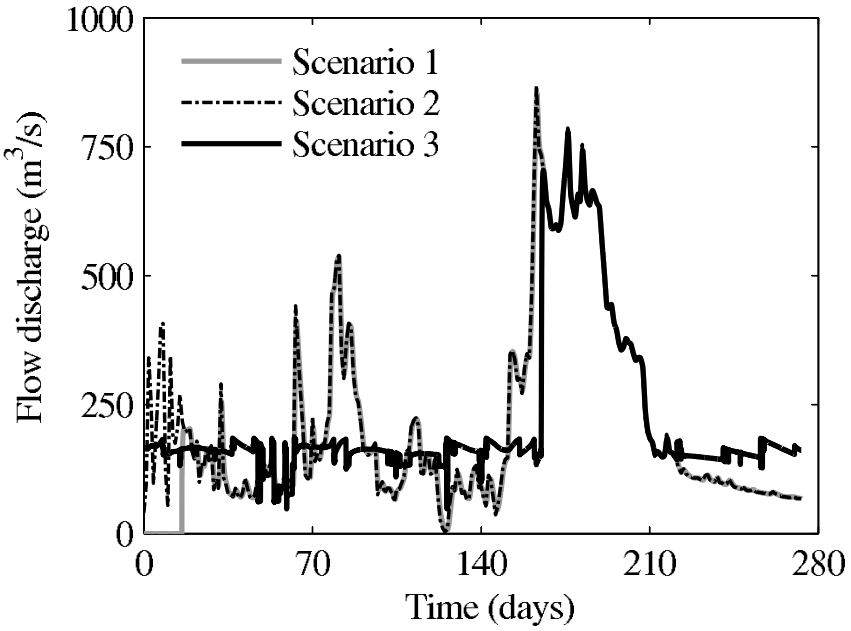

Figure 3.10: Flow hydrographs at downstream end of reach R1 for simulated scenarios.

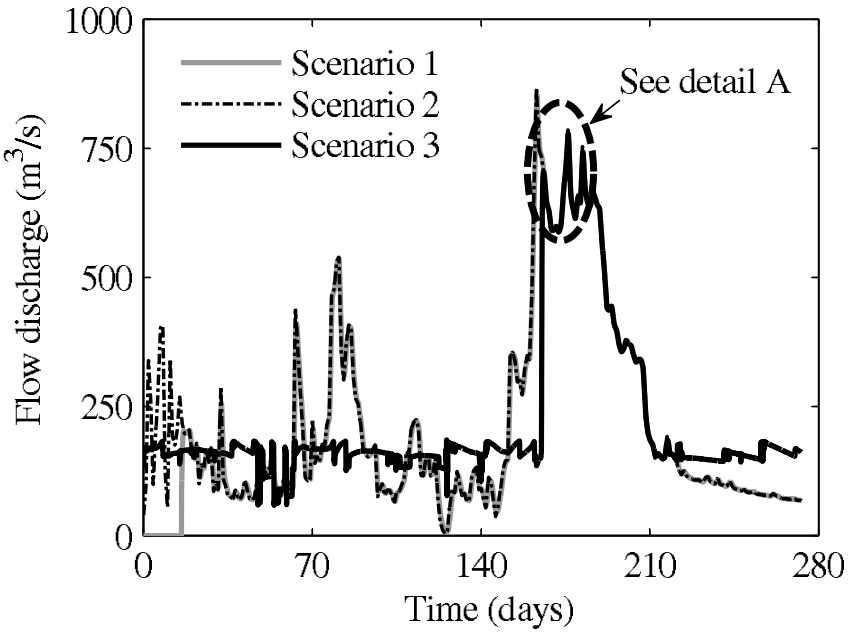

Figure 3.11: Flow hydrographs at downstream end of reach R10 for simulated scenarios.

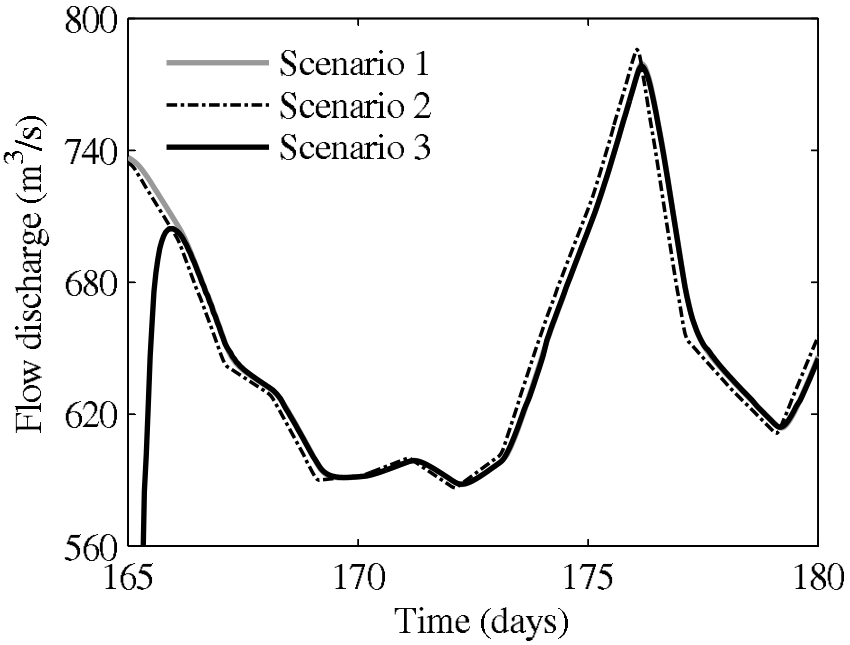

Figure 3.12: Detail A in Figure 3.11.

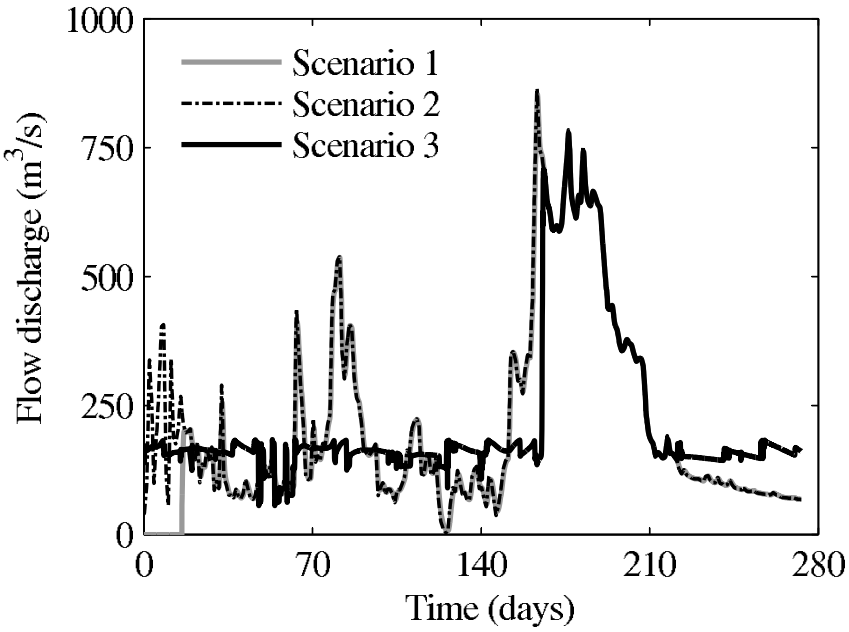

Figure 3.13: Flow hydrographs at downstream end of reach R22 for simulated scenarios.

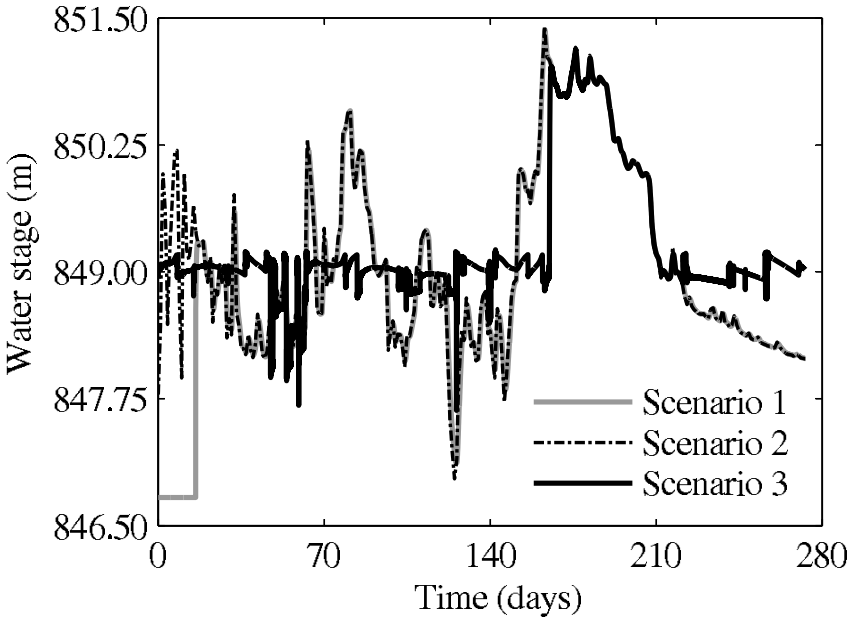

Figure 3.14: Stage hydrographs at downstream end of reach R1 for simulated scenarios.

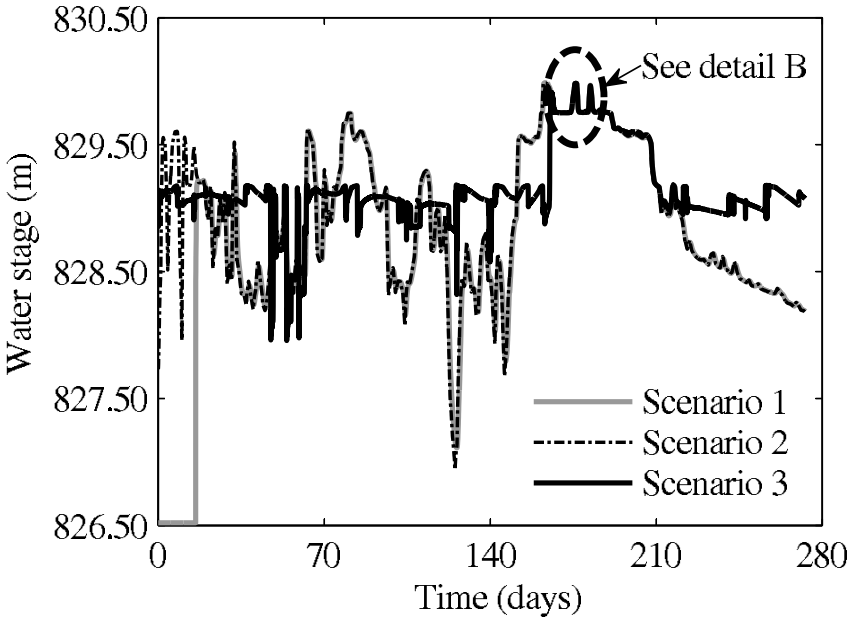

Figure 3.15: Stage hydrographs at downstream end of reach R10 for simulated scenarios.

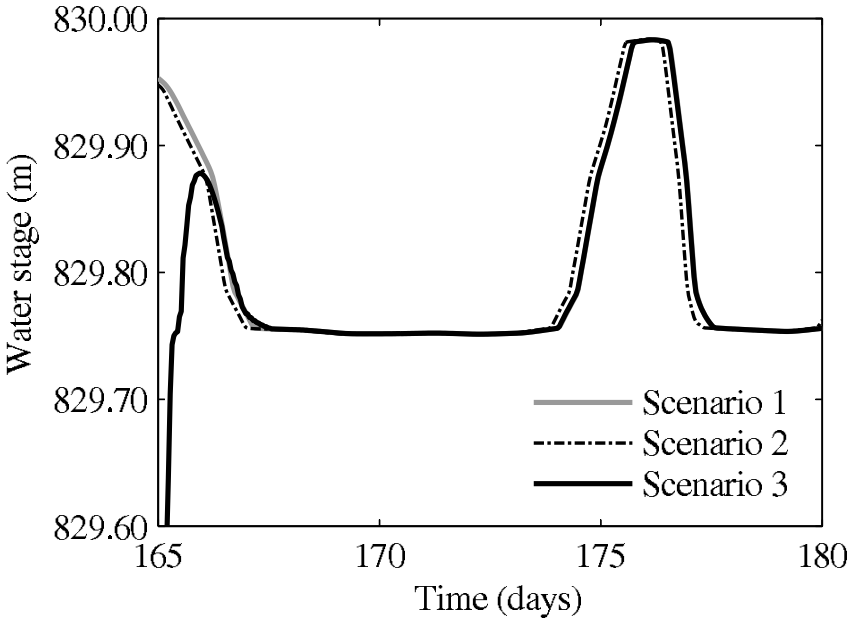

Figure 3.16: Detail B in Figure 3.15.

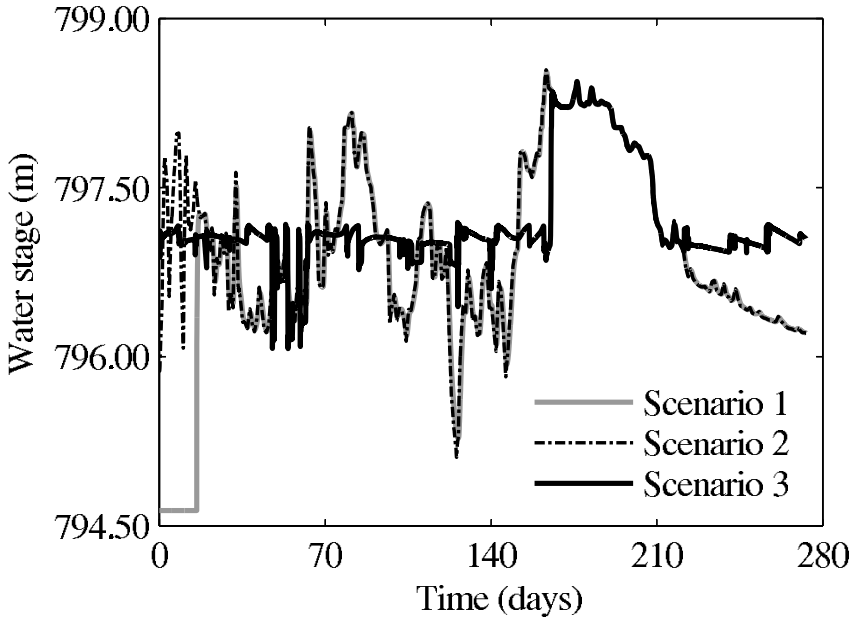

Figure 3.17: Stage hydrographs at downstream end of reach R22 for simulated scenarios.

stage after the reservoir was filled. Consequently, the flow hydrograph of scenario 3 has a similar shape to that of scenario 1 after the reservoir was filled.

To estimate the flood attenuation by the Boise River downstream of Lucky peak reservoir, an enlarged view of peak flows at the downstream ends of reaches R1, R10, and R22 for the second scenario (no reservoir) is presented in Figure 3.18. This figure shows the flood attenuation due to the river. The inflow hydrograph

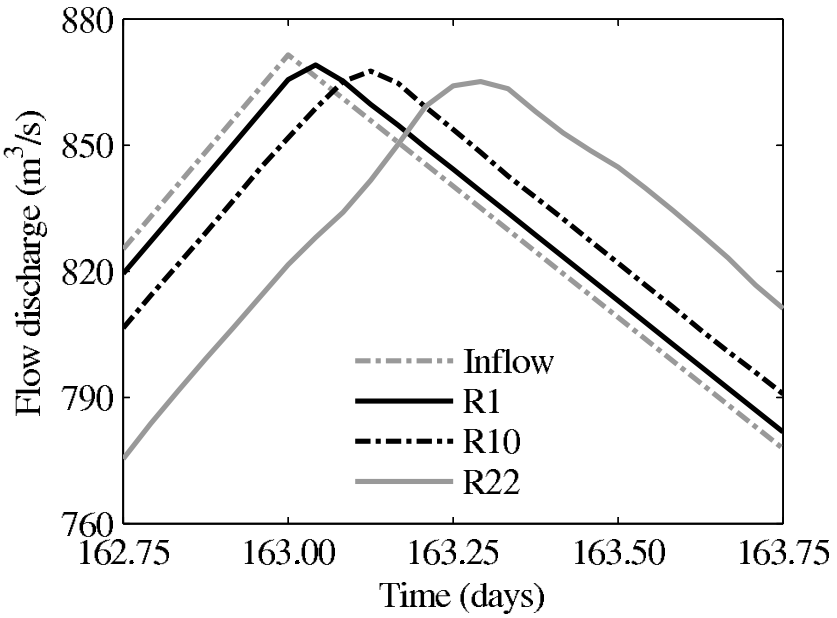

Figure 3.18: Peak flow at downstream end of reaches R1, R10 and R22 for scenario 2.

is also shown in Figure 3.18. As can be observed, the peak flow arrives to the downstream end of reaches R1, R10, and R22 after one, three, and seven hours, respectively. The attenuation of the peak inflow hydrograph was calculated to be 2.41 m^3/s (0.28%), 3.87 m^3/s (0.44%), and 6.35 m^3/s (0.73%) when the peak flow arrives at the downstream end of reaches R1, R10, and R22, respectively (see Figure 3.18). This small attenuation is because the storage capacity of the Boise River system downstream of Lucky peak reservoir is very small. The storage capacity of Boise

River downstream of the reservoir is about 0.7% of the maximum storage capacity of Lucky peak reservoir.

A zoom-in of results of flow hydrographs and stage hydrographs from time 175.75 to 176.75 days at the upstream end of reach R1 and at the downstream end of reaches R10 and R22 for scenario 3 are presented in Figure 3.19.

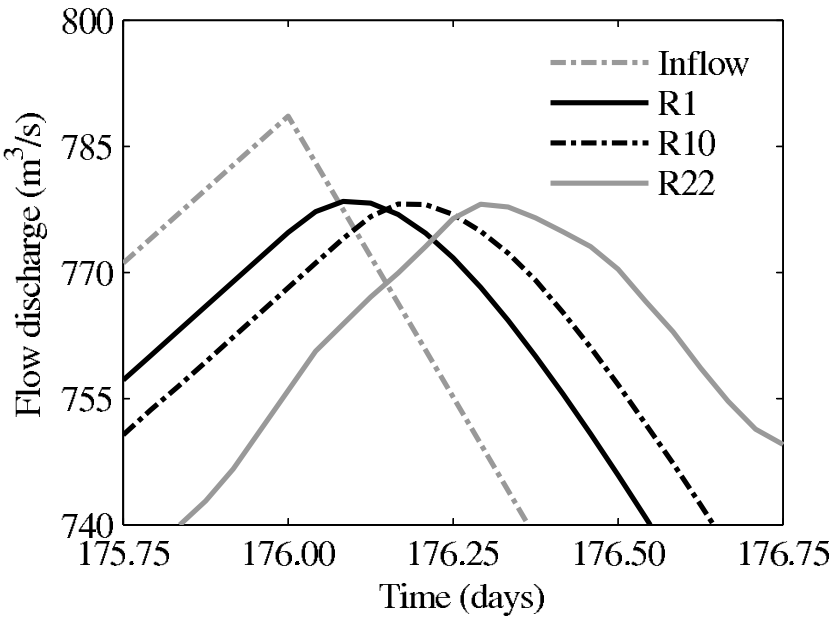

Figure 3.19: Peak flow at upstream end of reach R1 and at downstream end of reaches R10 and R22 for scenario 3.

This figure shows the flood attenuation due to the reservoir and the river. The inflow hydrograph from time 175.75 to 176.75 days is also shown in Figure 3.19. As can be observed in Figure 3.19, the peak flow of the inflow hydrograph arrives at the upstream end of reaches R1 after two hours and to the downstream end of reaches R10 and R22 after four and seven hours, respectively. The attenuation of the peak flow of the inflow hydrograph was calculated to be 10.13 m^3/s (1.29%) when it arrives at the upstream end of reaches R1 and 10.45 m^3/s (1.32%) and 10.48 m^3/s (1.33%) when it arrives at the downstream end of reaches R10 and R22, respectively.

The simulated results of objective function 1 (Equation 3.1), objective function 2 (Equation 3.2), and flooding volume using the three scenarios described above are compared in Figures 3.20, 3.21 and 3.22 respectively.

Results of flooding volume and objective function 1 show that the river starts to flood at day 16 for the first scenario, at day 2 for the second scenario, and at day 165 for the third scenario. When comparing the results of flooding volumes, results shows that the maximum flooding volumes for scenarios 3 and 1 are 86.97% and 98.71% of the maximum flooding volumes for scenario 2. Additionally, results of flooding volumes also show that the total flooding volume for scenarios 3 and 1 are 71.48% and 96.86% of the total flooding volumes for scenario 2. Also, the results show that the scenario without operation of gates (scenario 1) simply reduces flooding at the beginning of the simulation. This is because after the reservoir is filled, it does not help much for attenuating the peak flow discharge. Figure 3.21 plots objective function 2 versus time (proposed framework). Notice that for scenario 3, the reservoir is not full until day 165. For scenario 3, when a solution does not violate the constraints, the reservoir releases stored water from the reservoir due to objective function 2 (Equation 3.2). Note that for the simulated inflow hydrograph, the Boise River would flood for all scenarios. The operation of gates according to the proposed framework (third scenario) attenuates and delays the flood but does not avoid flooding due to lack of sufficient storage capacity. The storage capacity needed to avoid flooding for the inflow hydrograph under consideration is 1,323 MCM. This means that another reservoir with a capacity similar to that of Lucky peak reservoir (about 600 MCM) would be necessary to avoid flooding in this case.

Results for optimized outflow discharges and water stages at the Lucky Peak reservoir according to the proposed framework (third scenario) are presented in Fig-

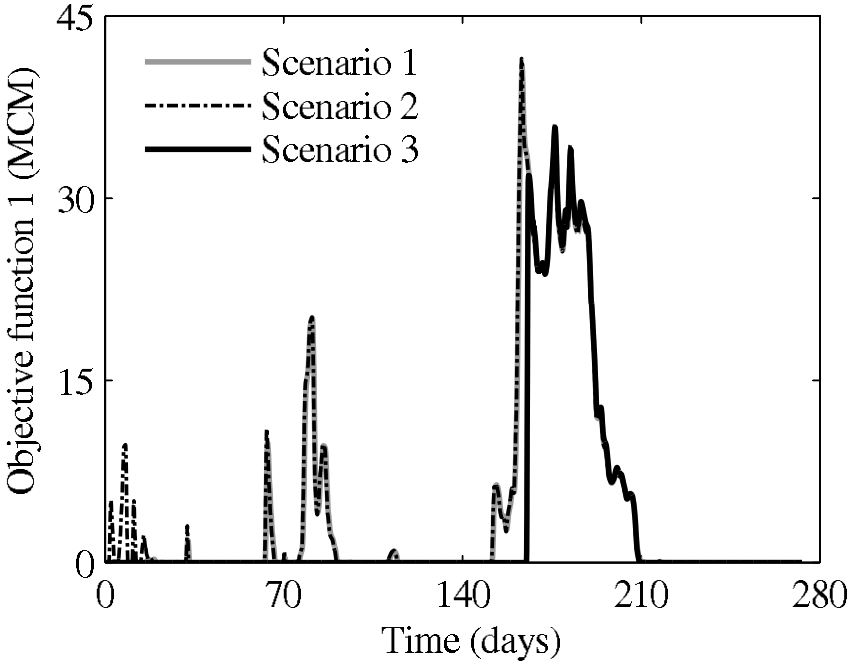

Figure 3.20: Objective function 1 (Equation 3.1) for simulated scenarios.

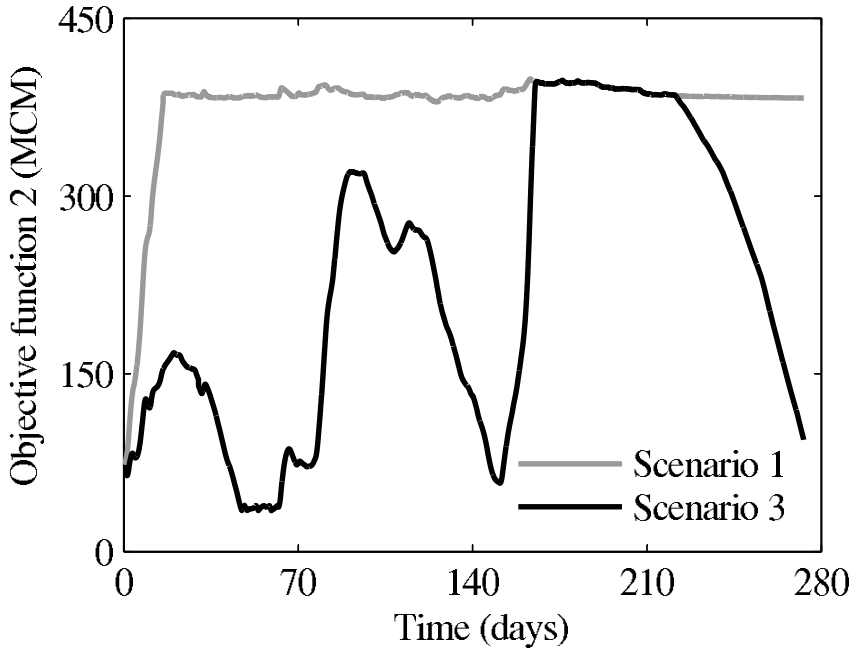

Figure 3.21: Objective function 2 (Equation 3.2) for simulated scenarios.

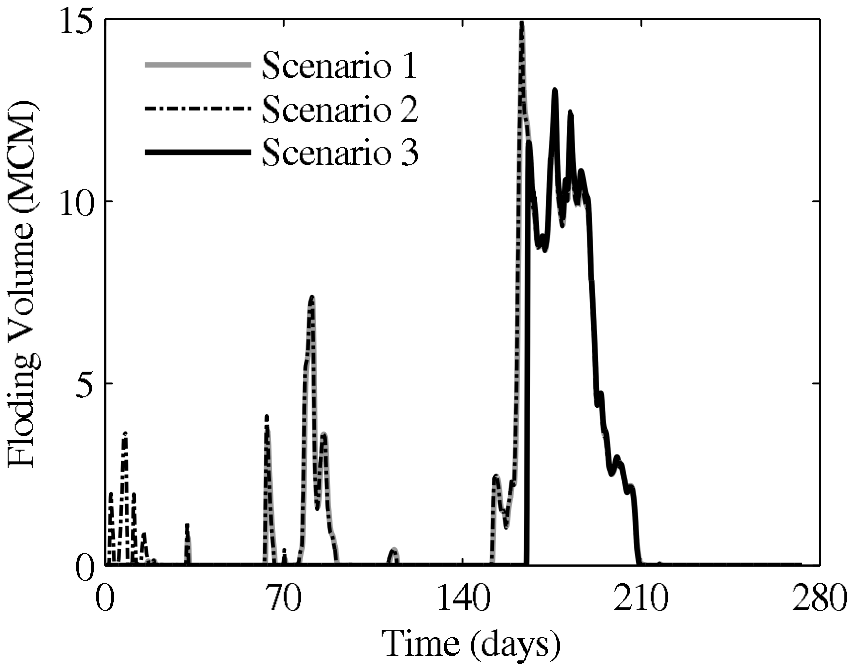

Figure 3.22: Total flooding volume for simulated scenarios.

ure 3.23. Figure 3.24 shows the corresponding trace of gate openings. Results of objective functions according to the proposed framework are shown in Figure 3.25.

For the third scenario, before the reservoir is full, operated gates release a flow discharge lower than 184 m^3/s, which is the maximum flow discharge without flooding under normal flow conditions. When the reservoir is full, the flow hydrograph is similar to the inflow hydrograph. The third scenario delayed and better controlled flooding; however, flooding is not entirely avoided due to storage limitations.

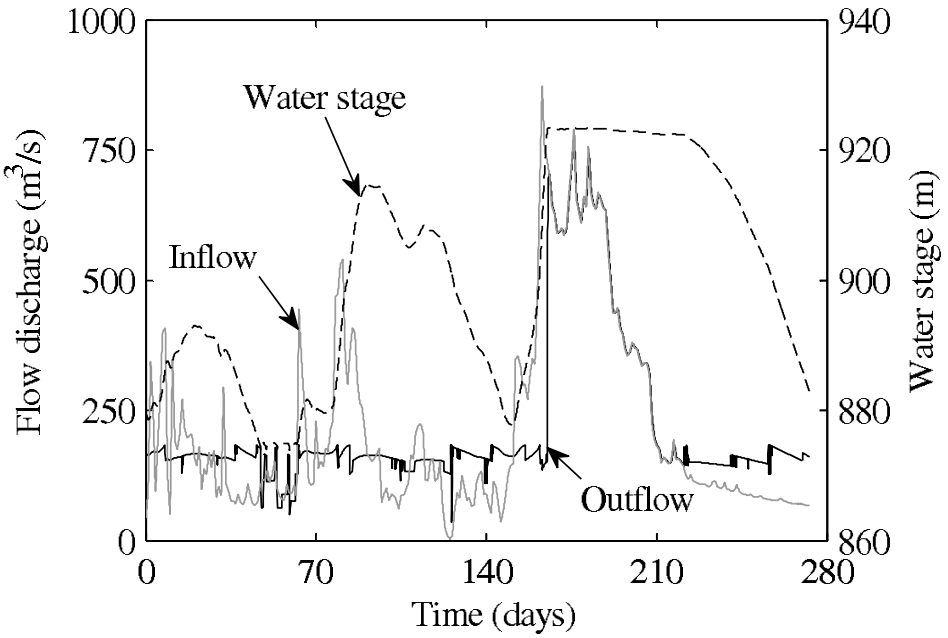

Figure 3.23: Inflow, outflow, and water stage hydrographs at Lucky Peak reservoir.

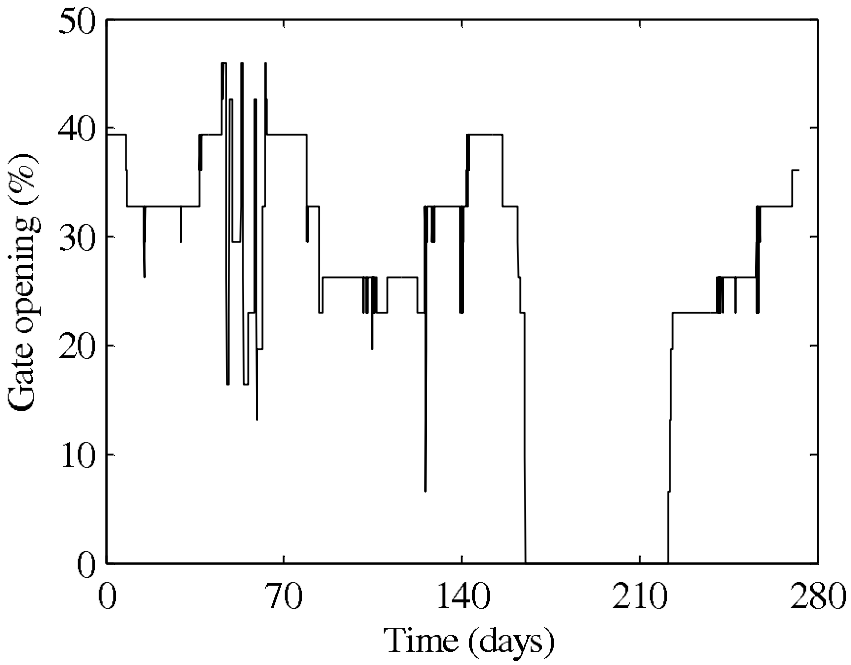

Figure 3.24: Operation of all gates (six) at Lucky Peak reservoir according to proposed framework.

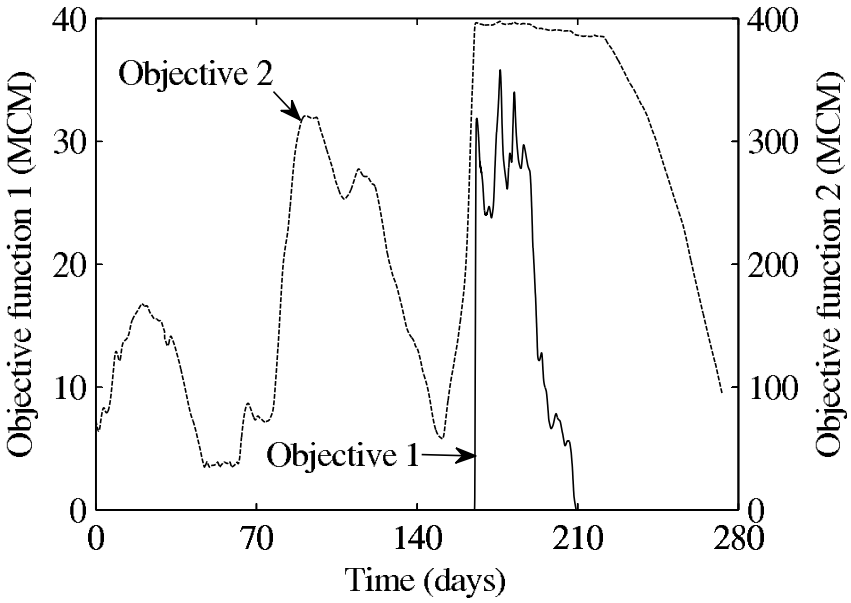

Figure 3.25: Results of objective functions according to proposed framework (Equation 3.1 and Equation 3.2).

CHAPTER 4

CONCLUSIONS

This thesis presents a computationally efficient model for unsteady flow routing through river networks with dendritic, looped, or a combination of dendritic and looped topologies. The application of the UNHVPG model focused on routing of subcritical flows; however, the model can be extended to include reaches susceptible to transition from subcritical to supercritical flow (and vice versa) during routing. The model builds upon the application of Hydraulic Performance Graph (HPG) to unsteady flow routing introduced by [12] and adopts the Volume Performance Graph (VPG) introduced by [16]. Moreover, in the UNHVPG model, we extend the concept of performance graphs to ratings and introduce the Rating Performance Graphs (RPGs), which graphically summarize the dynamic relation between the flow through and the stages upstream and downstream of in-line structures. The UNHVPG model solves a system of nonlinear equations assembled based on information summarized in the systems' HPG's, VPG's, and RPG's, continuity in junctions, water stage compatibility at junctions of reaches, and the system's initial and boundary conditions. We exemplify the applicability of the UNHVPG model to a looped network and contrast its simulation results with those from the well-known unsteady HEC-RAS model. The key findings are as follows:

1. Results show that agreement between UNHVPG and HEC-RAS models is very

good for slow and fast flood-wave conditions, with better agreement for slow flood-wave conditions.

2. The use of HPGs, VPGs, and RPGs for unsteady flow routing in a river system as proposed herein is a relatively robust and numerically efficient approach because the momentum and storage for all river reaches are computed prior to the system routing based on the momentum and mass conservation principles of GVF and most of the computations for the system routing only involves interpolation steps to satisfy the prescribed BC's. It is worth mentioning that the UNHVPG model provided an accurate solution for the looped system right the first time, while the unsteady HEC-RAS model required few adjustments to get the model to run properly. In addition, when using the performance graphs approach, instabilities or other problems due to discretization and numerical inaccuracies are removed as the system's HPGs, VPGs, and RPGs are being constructed.

3. The application examples presented here suggest that, overall, the proposed model is computationally more efficient and affords a numerical accuracy comparable to the unsteady HEC-RAS model for unsteady flow routing through river networks. It is clear that the CPU time for pre-computing the PGs can be computationally demanding but this is done only once. The advantage of the UNHVPG model may be significant when it is used for optimization problems such as real-time operation of regulated river systems. In this case, hundreds or even thousands of runs would be needed for each operational decision that may be as short as 30 minutes.

This thesis also presents a dynamic framework for the intelligent control of river flooding. The novelty of this framework is that it allows for controlled flooding when the conveyance capacity of the river system is exceeded or is about to exceed. The proposed approach links two components: river system routing (simulation) and optimization. The river system routing (simulation) component builds upon the application of Performance Graphs, while the optimization component uses the popular second generation multi-objective evolutionary algorithm Non-dominated Sorting Genetic Algorithm-II (NSGA-II). For illustration purposes, the proposed framework was applied to the Boise River system in Idaho. The key findings are as follows:

1. Results show that the Boise River would flood for all scenarios for the simulated inflow hydrograph. The operation of controlled in-line structures according to the results of the proposed framework delays the occurrence of flooding, but does not avoid it due to lack of sufficient storage capacity in the reservoir.

2. The use of performance graphs for river system routing results in a robust and numerically efficient model as most of the computations for the system routing only involves interpolation steps.

3. Overall, the results show a promising outcome in the application of this model for flood control.

REFERENCES

[1] Abbot, M. B., Basco, D. R., 1989. *Computational Fluid Dynamics. An Introduction for Engineers*. New York, Longman Scientific and Technical.

[2] Atiquzzaman, M., Liong, S., Yu, X., 2006. *Alternative decision making in water distribution network with NSGA-II*. Journal of Water Resources Planning and Management 132 (2), 122–126.

[3] Bakhmeteff, B. A., 1932. *Hydraulics of Open Channels*. New York, McGraw-Hill.

[4] Bekele, E. G., Nicklow, J. W., 2007. *Multi-objective automatic calibration of SWAT using NSGA-II*. Journal of Hydrology 341 (3-4), 165–176.

[5] Breckpot, M., Barjas Blanco, T., De Moor, B., jun 2010. *Flood control of rivers with Model Predictive Control - proof of concept based on the river Demer in Belgium*. Proc. 2010 American Control conf. 2983–2988.

[6] De Bruijn, K., Klijn, F., Mcgahey, C., Mens, M., Wolfert, H., 2008. *Long-term strategies for flood risk management: scenario definition and strategic alternative design*. FLOOD site report T14-07-02 Deltares.

[7] Delft Hydraulics, 2000. *RIBASIM user's manual and technical reference manual*. Delft, The Netherlands. Delft Hydraulics.

[8] Dorn, J. L., Ranji-Ranjithan, S., 2003. *Evolutionary multiobjective optimization in watershed water quality management*. EMO. pp. 692–706.

[9] Eichert, B. S., Pabst, A. F., 1998. *Generalized real-time flood control system model*. Davis, California. U.S. Army Corps of Engineers. Hydrologic Engineering Center.

[10] Franz, D. D., and Melching, C. S., 1997a. *Approximating the hydraulic properties of open channels and control structures, during unsteady flow using the Full Equations Utility (FEQUTL) program*. Water-Resources Investigations Report No. 97-4037. U.S. Geological Survey.

[11] Franz, D. D., and Melching, C. S., 1997b. *Full Equations (FEQ) model for the solution of the full, dynamic equations of motion for one-dimensional unsteady flow*

in open channels and through control structures. Water-Resources Investigations Report No. 96-4240. U.S. Geological Survey.

[12] González-Castro, J. A., 2000. *Applicability of the hydraulic performance graph for unsteady flow routing*. Urbana, Illinois, Ph.D. thesis, Univ. of Illinois at Urbana-Champaign.

[13] González-Castro, J. A., and Yen, B. C., 1996. *Hydraulic performance of open channel breaching*. California, 334–339. ASCE

[14] González-Castro, J. A., and Yen, B. C., 2012. *Open-channel unsteady flow routing by hydraulic performance graph*. Submitted for possible publication in the J. Hydraul. Eng.

[15] Henderson, F. M., 1966. *Open Channel Flow*. New York, Macmillan Publishing Co., Inc.

[16] Hoy, M. A., Schmidt, A. R., 2006. *Unsteady flow routing in sewers using hydraulic and volumetric performance graphs*. Nebraska, Proc. World Environmental and Water Resources Congress, 1–10.

[17] Hydrologic Engineering Center, 2010a. *HEC-RAS, River Analysis System, Applications Guide. Version 4.1.* California, U.S. Army Corps of Engineers, Davis.

[18] Hydrologic Engineering Center, 2010b. *HEC-RAS, River Analysis System, User's Manual. Version 4.1.* California, U.S. Army Corps of Engineers, Davis.

[19] Hydrologic Engineering Center, 2003. *Hydrologic engineering center's prescriptive reservoir model, program description*. Davis, California. U.S. Army Corps of Engineers.

[20] Hydrologic Engineering Center, 1996. *Developing Seasonal and Long-Term Reservoir System Operation Plans Using HEC-PRM Report RD-40*. Davis, California. U.S. Army Corps of Engineers.

[21] Jin, X. and Sridhar, V., 2011. *Impacts of climate change on hydrology and water resources in the Boise and Spokane River Basins*. Journal of American Water Resources Association. In press.

[22] Kim, T. and Heo, J.-H. and Jeong, C.-S., 2006. *Multireservoir system optimization in the Han River basin using multi-objective genetic algorithms*. Hydrol. Process. 20, 2057 - 2075.

[23] Lee S.-Y., Hamlet A. F., Fitzgerald C. J., Burges S. J., 2009. *Optimized Flood Control in the Columbia River Basin for a Global Warming Scenario*. J. of Water Resources Planning and Management. 135 (6), 440–450.

[24] Leon, A. S. and Kanashiro, E. A. and González-Castro, J. A., 2012. *A fast approach for unsteady flow routing in complex river networks*. ASCE J. Hydraul. Eng. Under review.

[25] Leon, A. S., and Kanashiro, E. A., and Valverde, R. and Sridhar V., 2012. *A Dynamic Framework for Intelligent Control of River Flooding - A Case Study*. Journal of Water Resources Planning and Management. Submitted.

[26] León, A. S., Kanashiro, E., 2010. *A new coupled optimization-hydraulic routing model for real-time operation of highly complex regulated river systems*. Presented in the 2010 Watershed Management Conference: "Innovations in Watershed Management Under Land Use and Climate Change".

[27] Moré, J. J., and Sorensen, D. C., and Hillstrom, K. E., and Garbow, B. S., 1984. *The MINPACK Project*. Sources and Development of Mathematical Software, W. J. Cowell, ed., Prentice-Hall, 88–111.

[28] National Weather Service, 2009. *Flood losses: Compilation of flood loss statistics*.

[29] Needham, T., Watkins, D. W., Lund, J. R., 2000. *Linear programming for flood control on the iowa and des moines rivers*. Journal of Water Resources Planning and Management 126, 118–127.

[30] Ngo, L. L., Madsen, H., Rosbjerg, D., 2007. *Simulation and optimization modelling approach for operation of the Hoa Binh reservoir, Vietnam*. J. of Hydrology 336 (3-4), 269–281.

[31] Reed, P. M., Minsker, B. S., 2004. *Striking the balance: Long-term groundwater monitoring design for conflicting objectives*. Journal of Water Resources Planning and Management 130 (2), 140–149.

[32] Schmidt, A. R., 2002. *Analysis of Stage-Discharge Relations for Open-Channel Flows and Their Associated Uncertainties*. Urbana, IL, Ph.D. thesis, Univ. of Illinois at Urbana-Champaign.

[33] Sridhar, V. and Nayak, A., 2010. *Implications of climate-driven variability and trends for the hydrologic assessment of the Reynolds Creek Experimental Watershed, Idaho*. Journal of Hydrology 385, 1-4, 183 - 202.

[34] Stratton, B. T. and Sridhar, V. and Gribb, M. M. and McNamara, J. P. and Narasimhan, B., 2009. *Modeling the Spatially Varying Water Balance Processes in a Semiarid Mountainous Watershed of Idaho*. Journal of the American Water Resources Association 45, 1390-1408, Blackwell Publishing Ltd.

[35] United Nations Environment Programme, 2003. *Taking it at the flood*.

[36] Unver, O. I., Mays, L. W., 1990. *Model for real-time optimal flood control operation of a reservoir system.* Journal Water Resources Management 4 (1), 21–46.

[37] Wei, C.-C., Hsu, N.-S., 2008. *Multireservoir flood-control optimization with neural-based linear channel level routing under tidal effects.* Water Resources Management 22, 1625–1647.

[38] Xia, R., 1992. *Sensitivity of flood routing models to variations of momentum equation coefficients and terms.* Urbana, Illinois. Ph.D. thesis, Univ. of Illinois at Urbana-Champaign.

[39] Yen, B. C., 1986. *Hydraulics of sewers.* London, Advances in Hydroscience 14, 1–115, Academic Press.

[40] Yen, B. C., González-Castro, J. A., 2000. *Open- channel capacity determination using hydraulic performance graph.* J. Hydraul. Eng. 126 (2), 112–122.

APPENDIX A

HYDRAULIC PERFORMANCE GRAPH

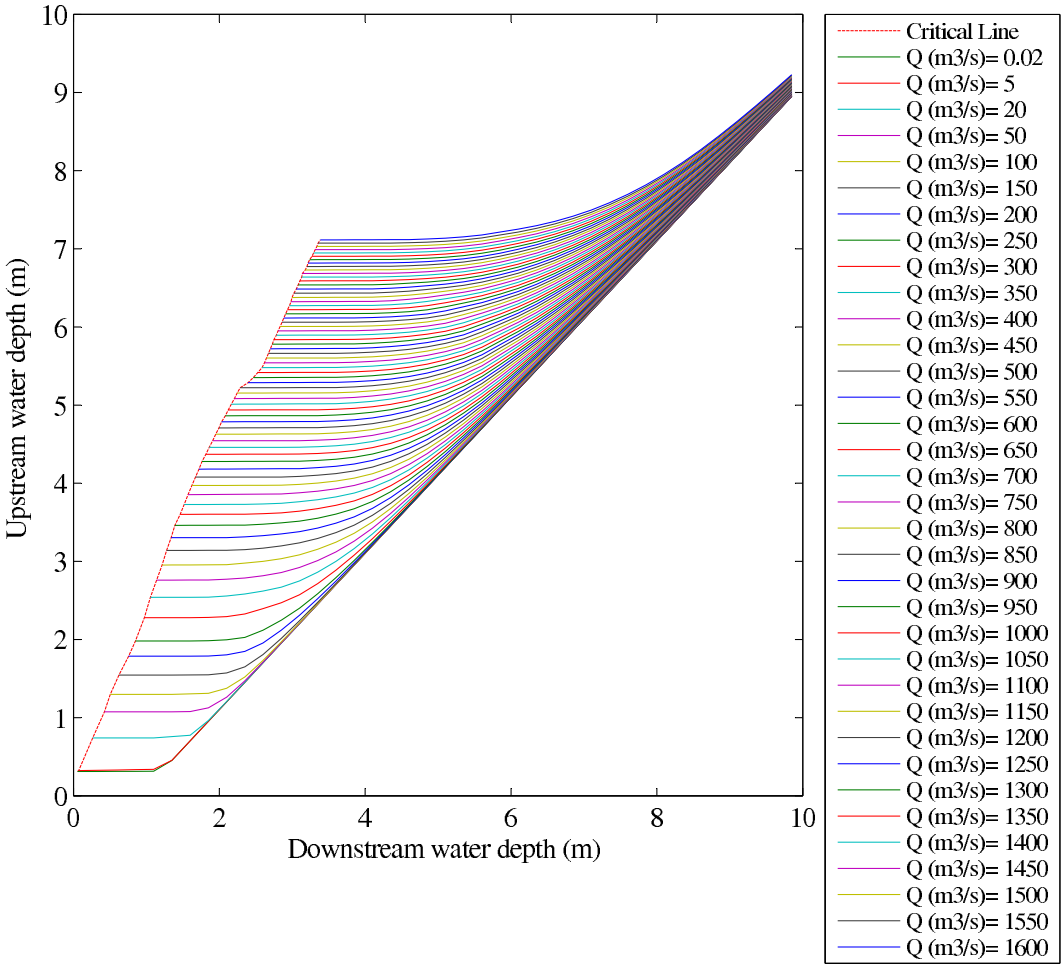

Figure A.1: Hydraulic Performance Graph - Reach R1

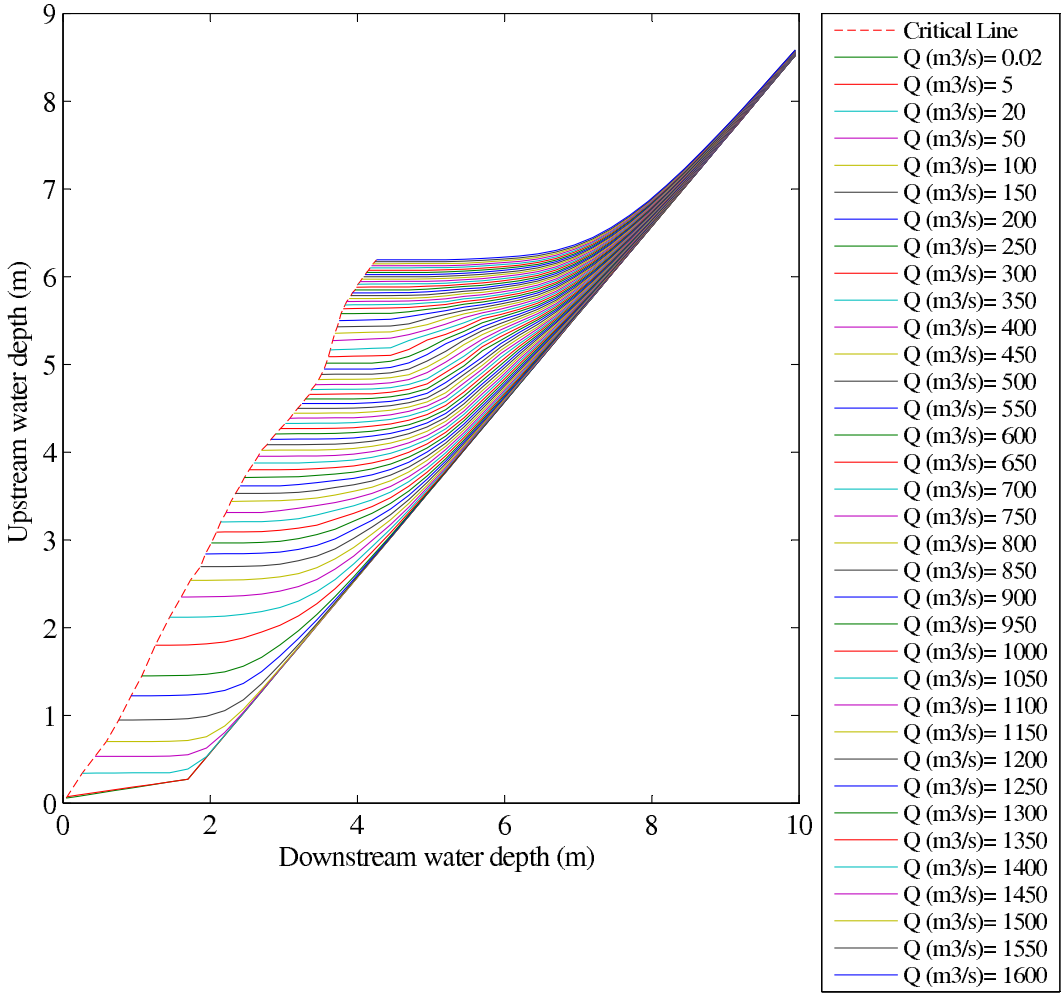

Figure A.2: Hydraulic Performance Graph - Reach R2

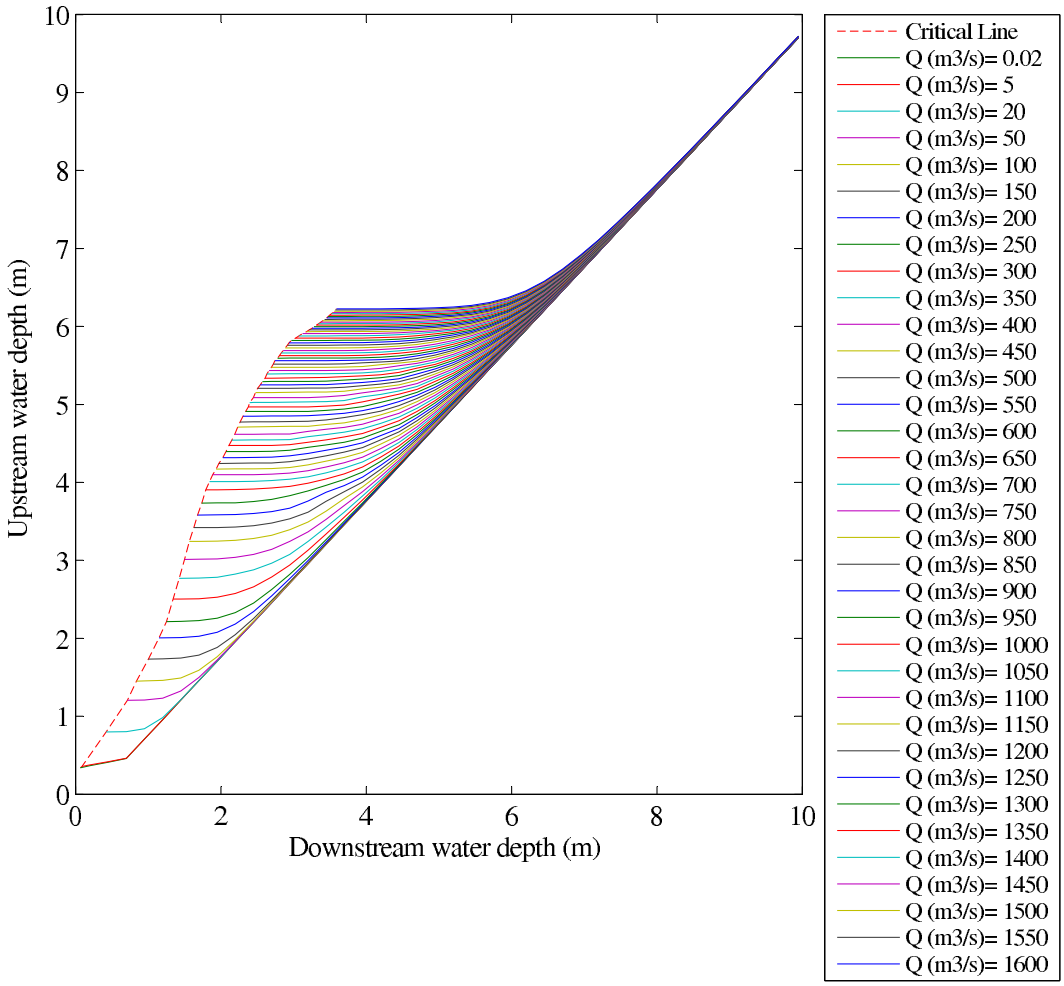

Figure A.3: Hydraulic Performance Graph - Reach R3

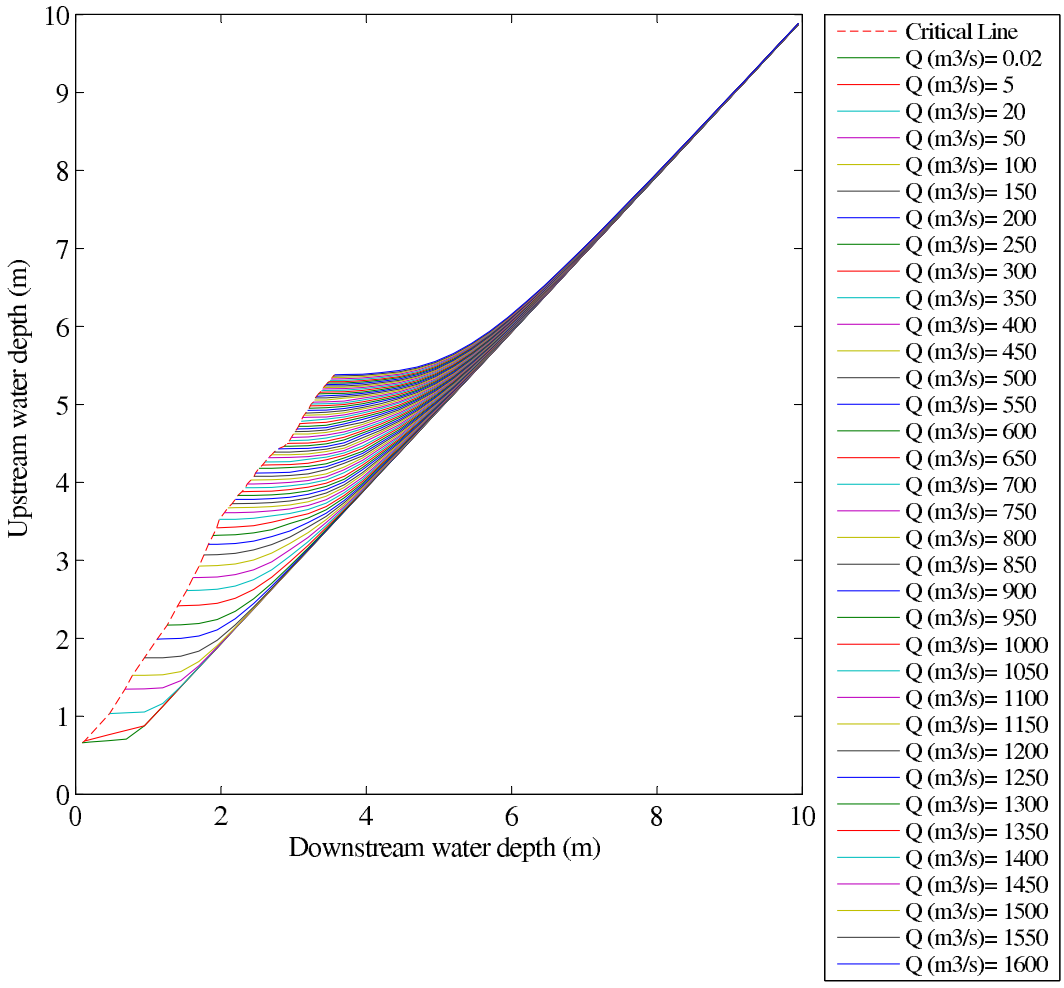

Figure A.4: Hydraulic Performance Graph - Reach R4

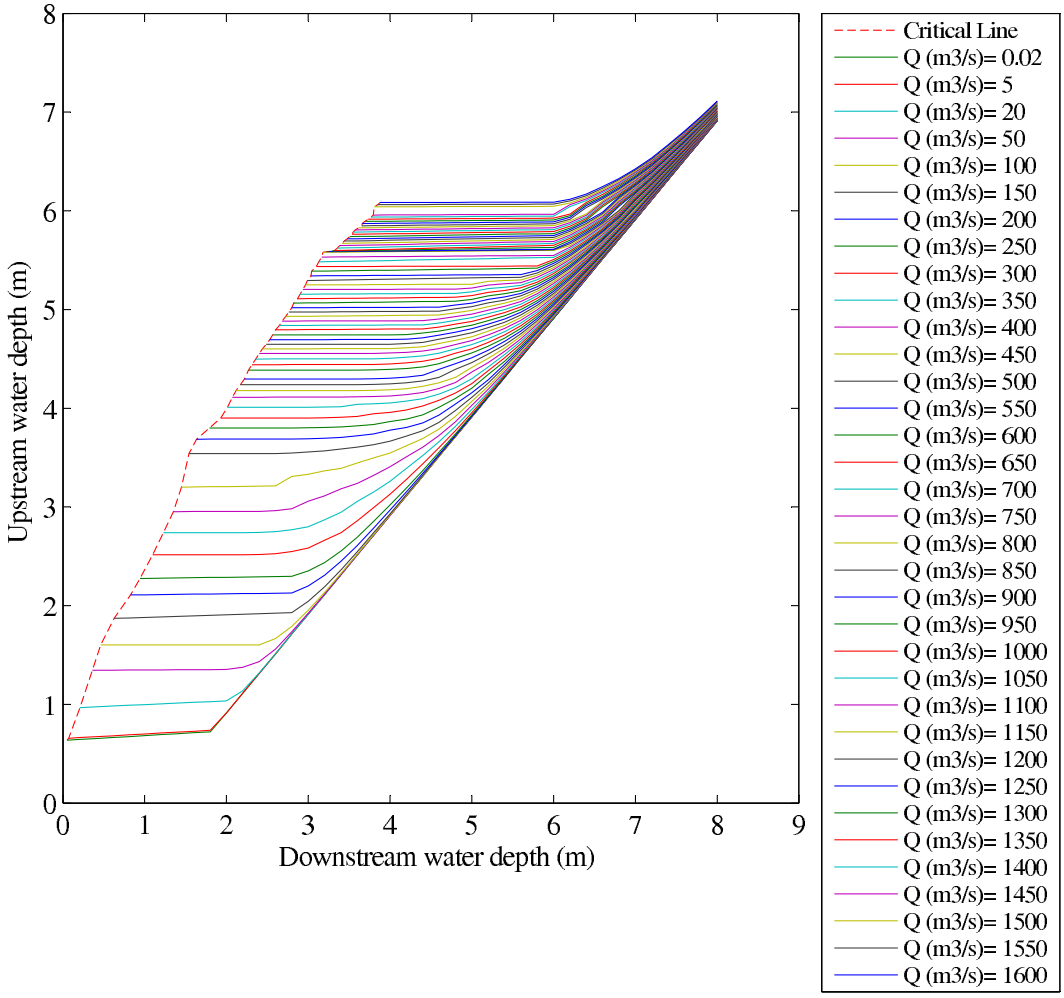

Figure A.5: Hydraulic Performance Graph - Reach R5

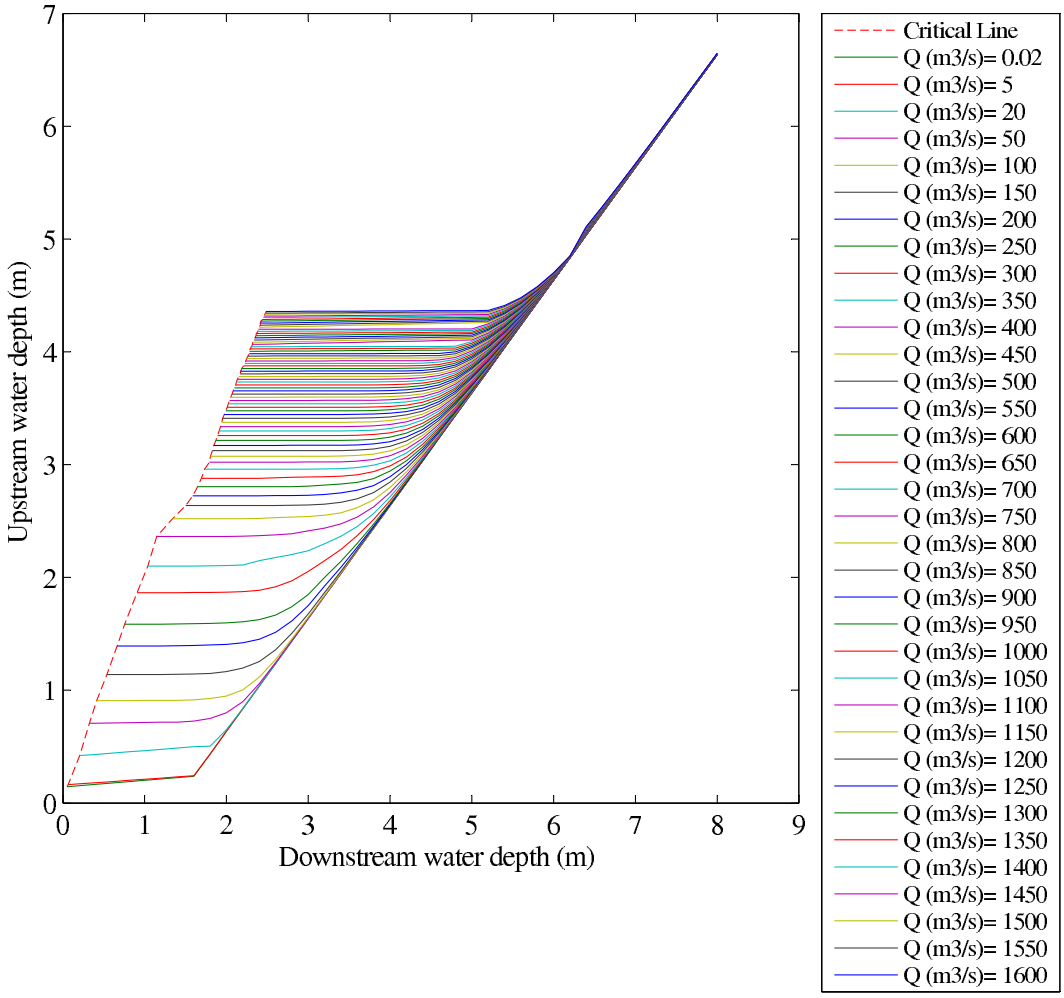

Figure A.6: Hydraulic Performance Graph - Reach R6

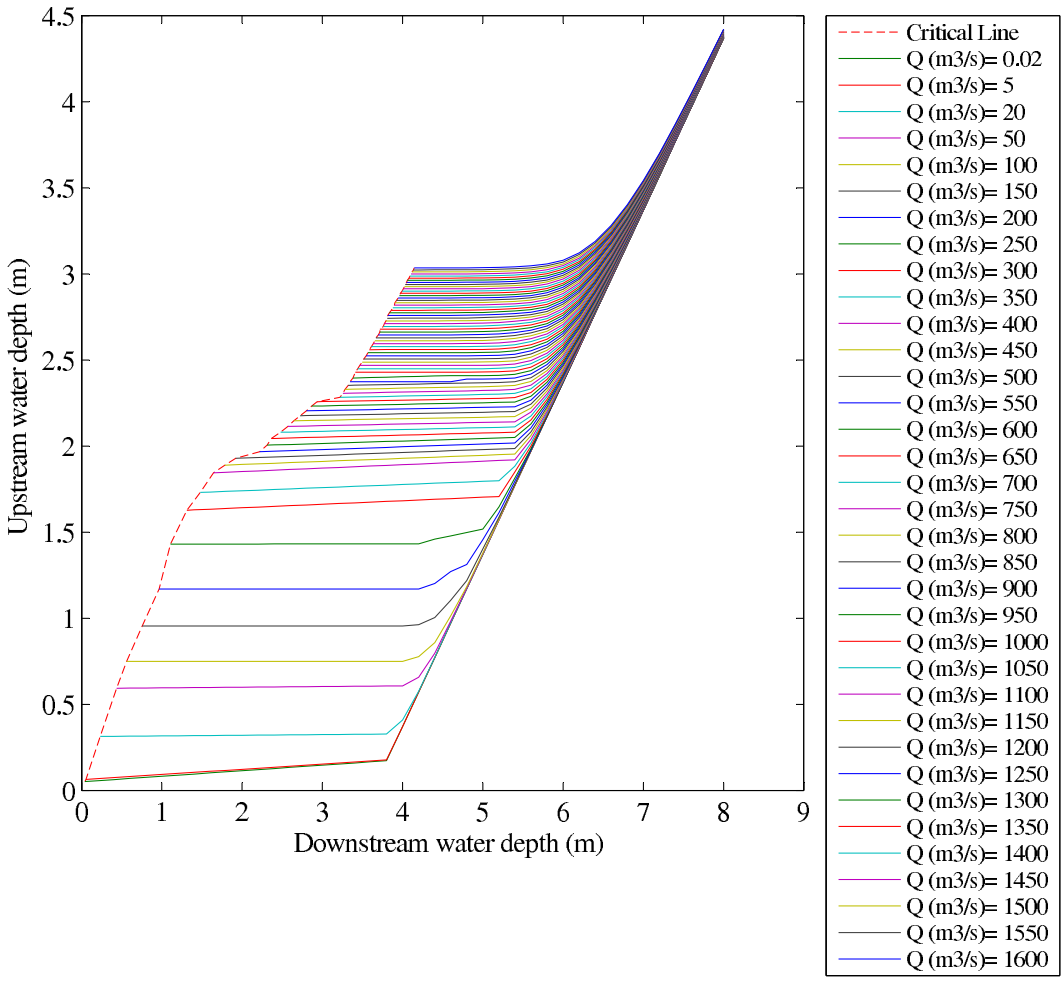

Figure A.7: Hydraulic Performance Graph - Reach R7

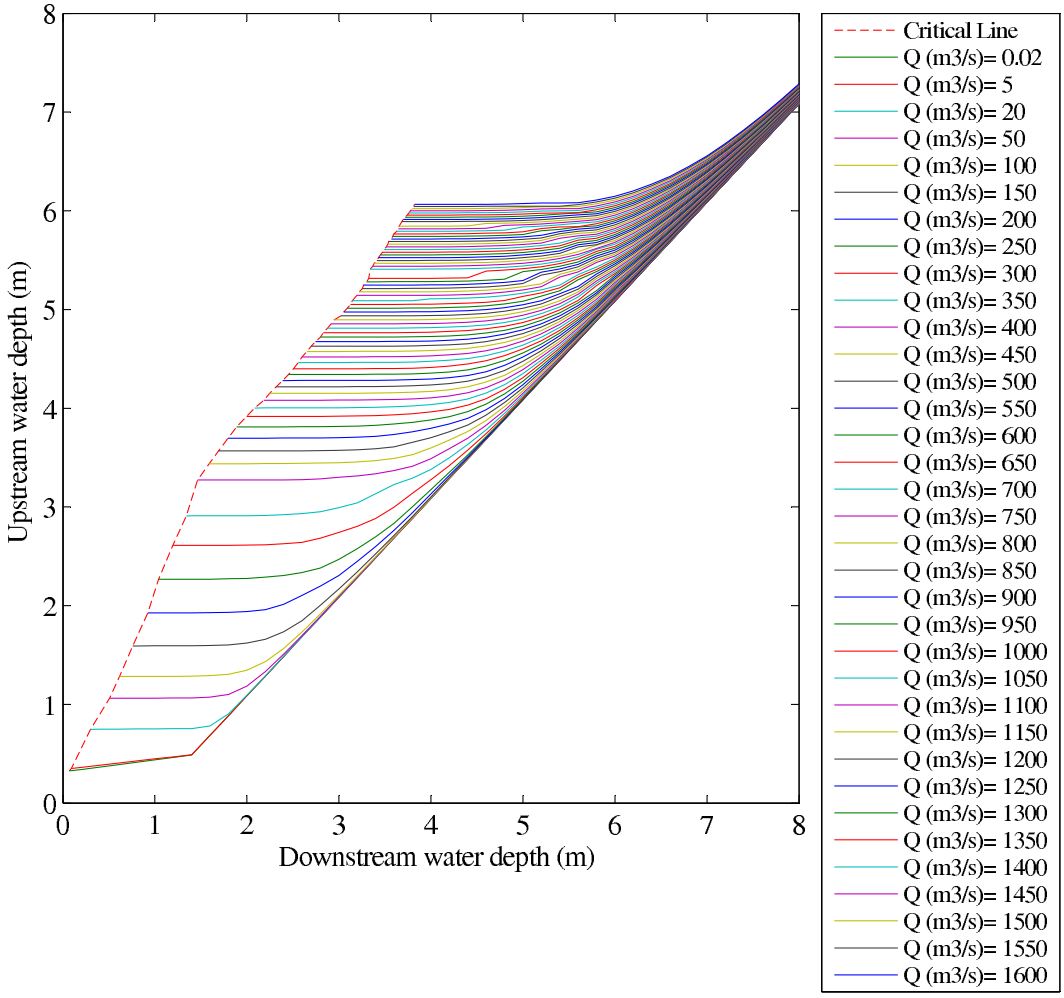

Figure A.8: Hydraulic Performance Graph - Reach R8

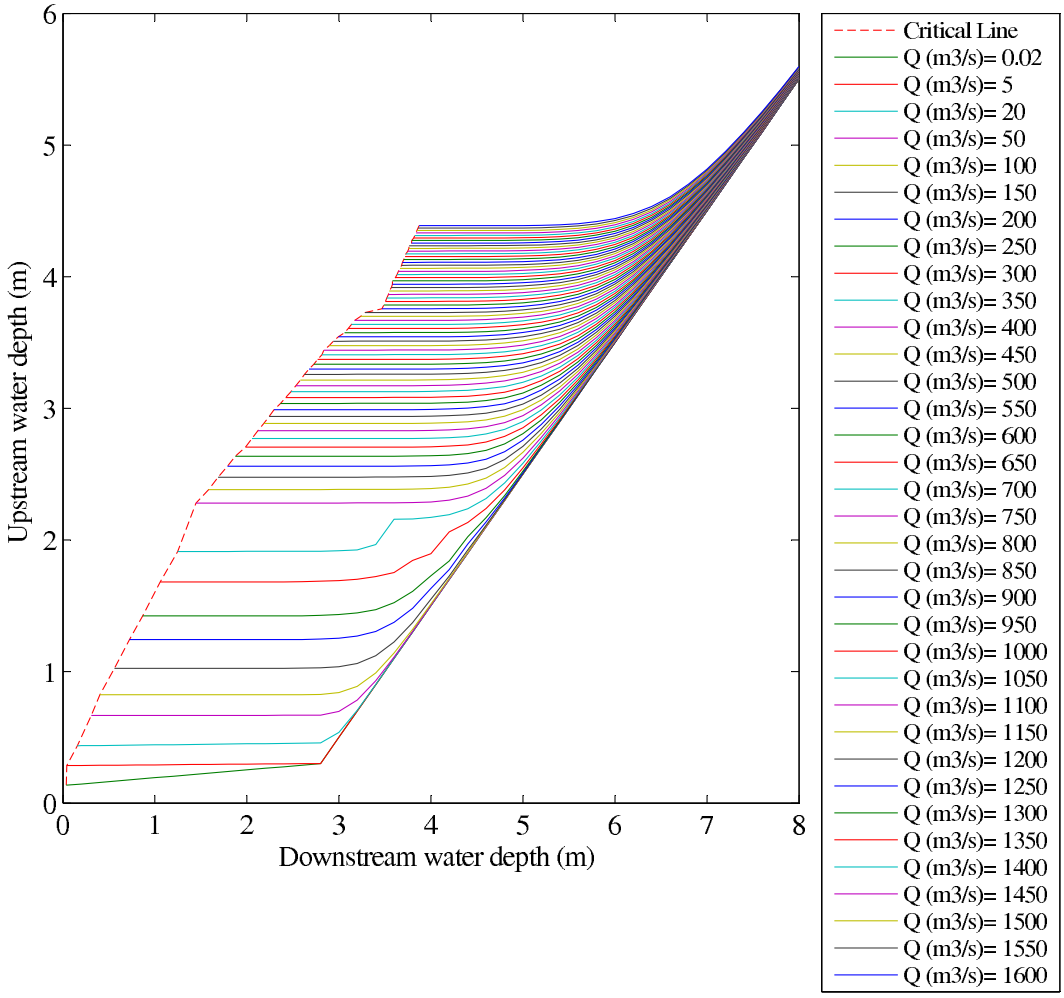

Figure A.9: Hydraulic Performance Graph - Reach R9

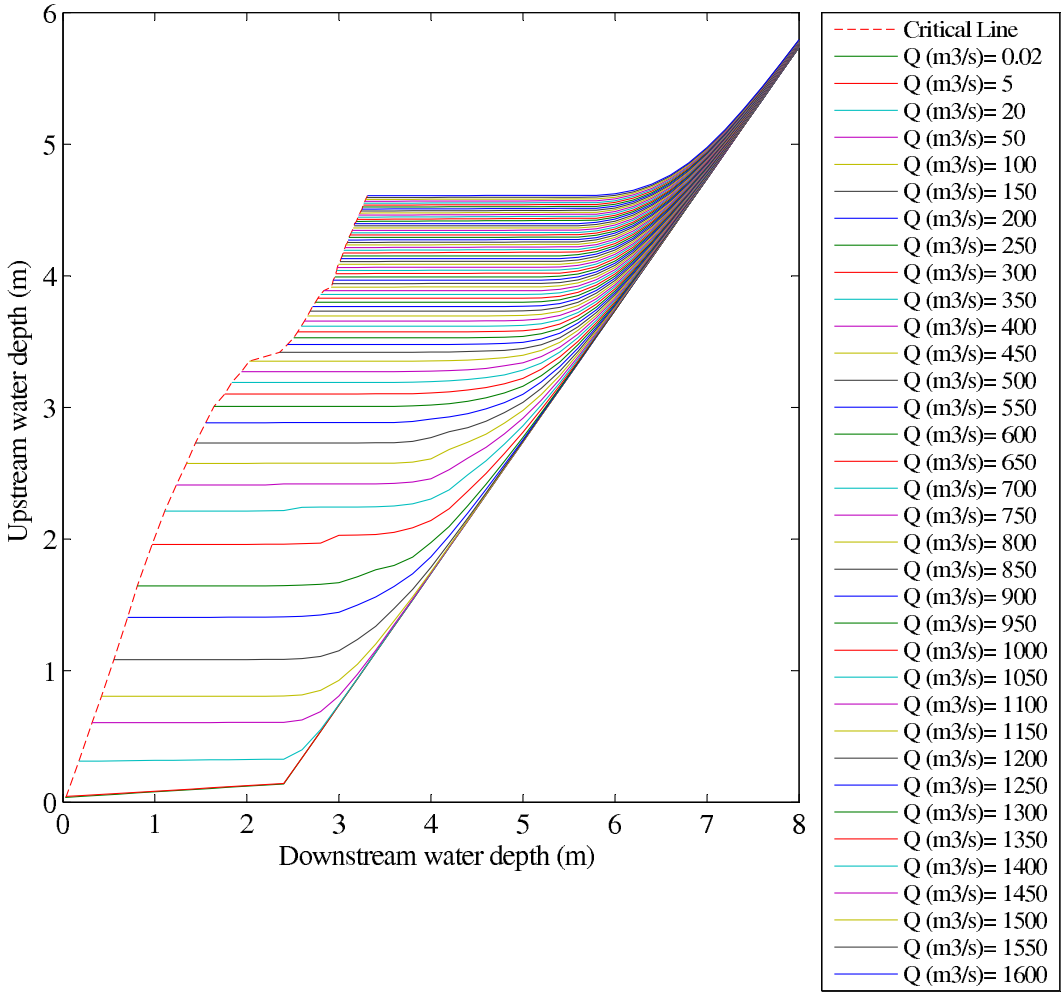

Figure A.10: Hydraulic Performance Graph - Reach R10

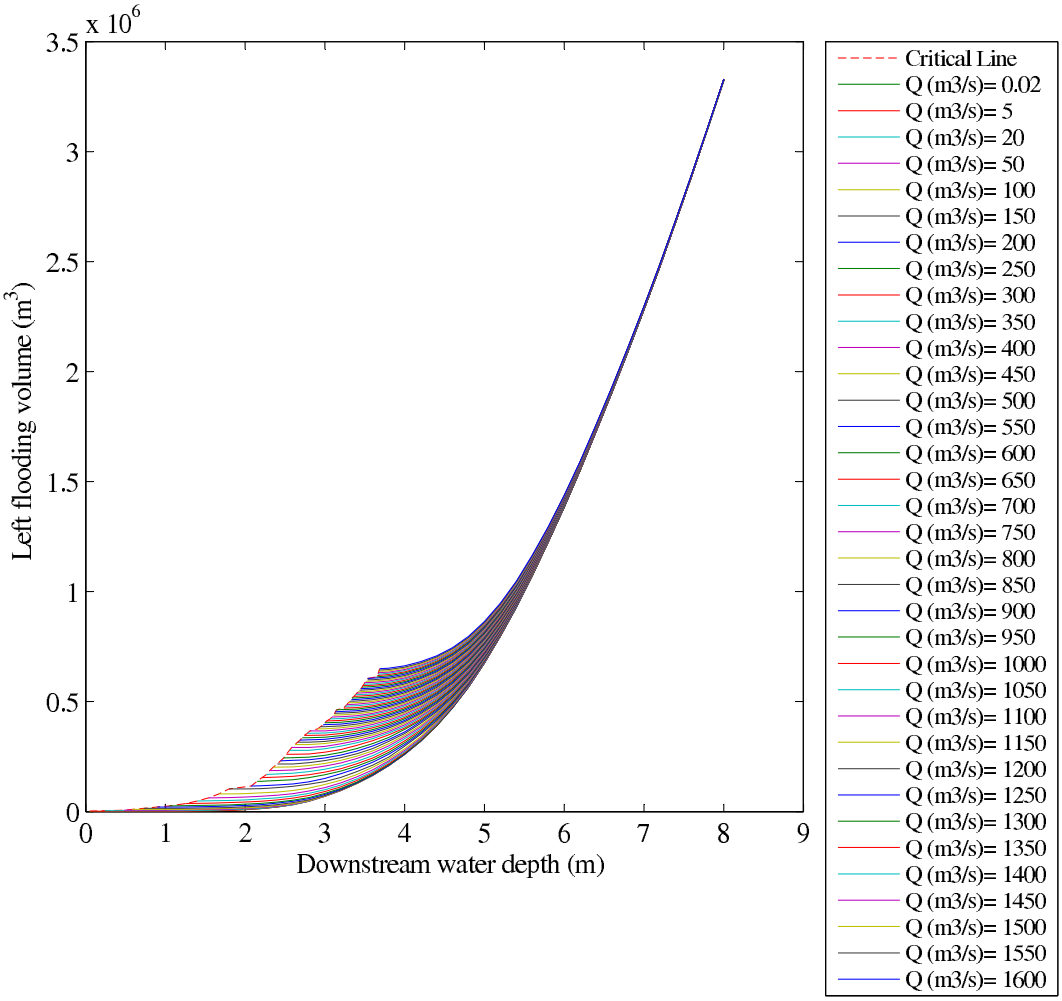

Figure A.11: Hydraulic Performance Graph - Reach R11

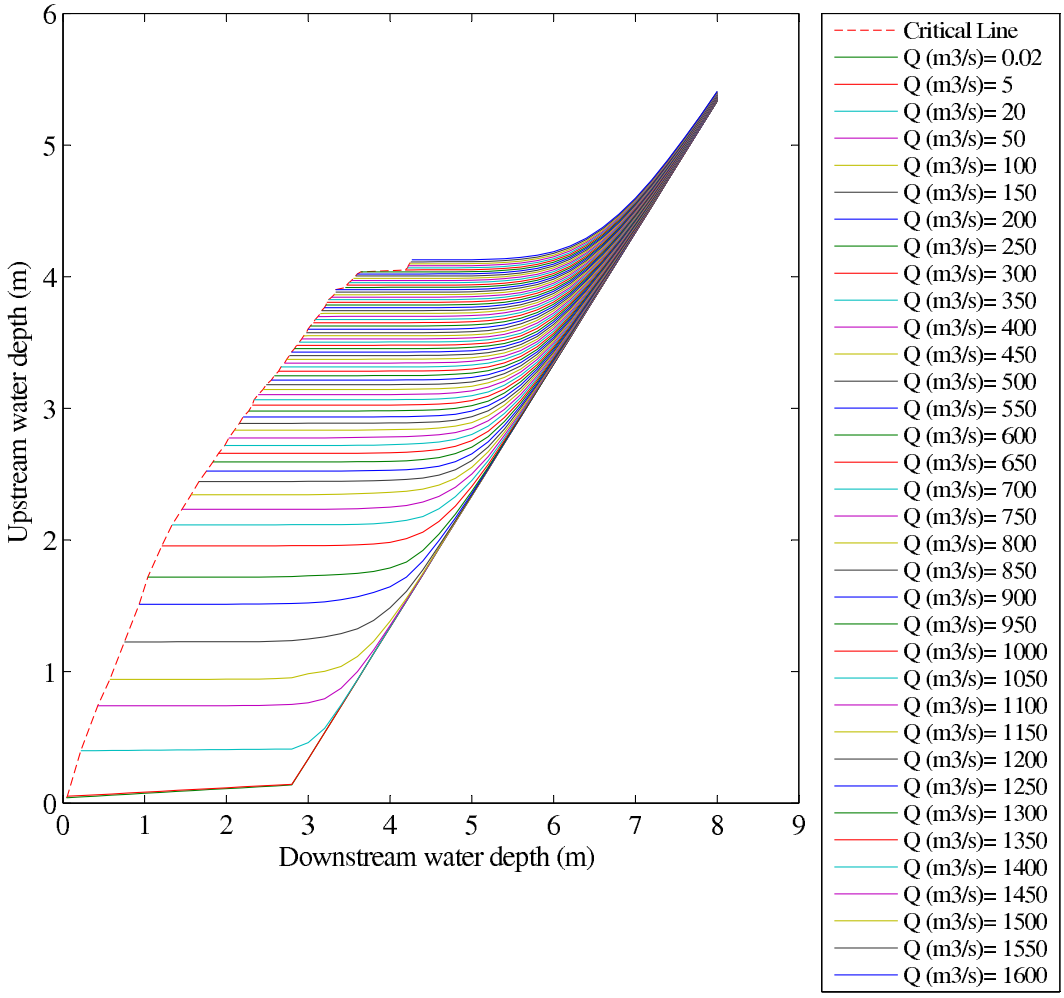

Figure A.12: Hydraulic Performance Graph - Reach R12

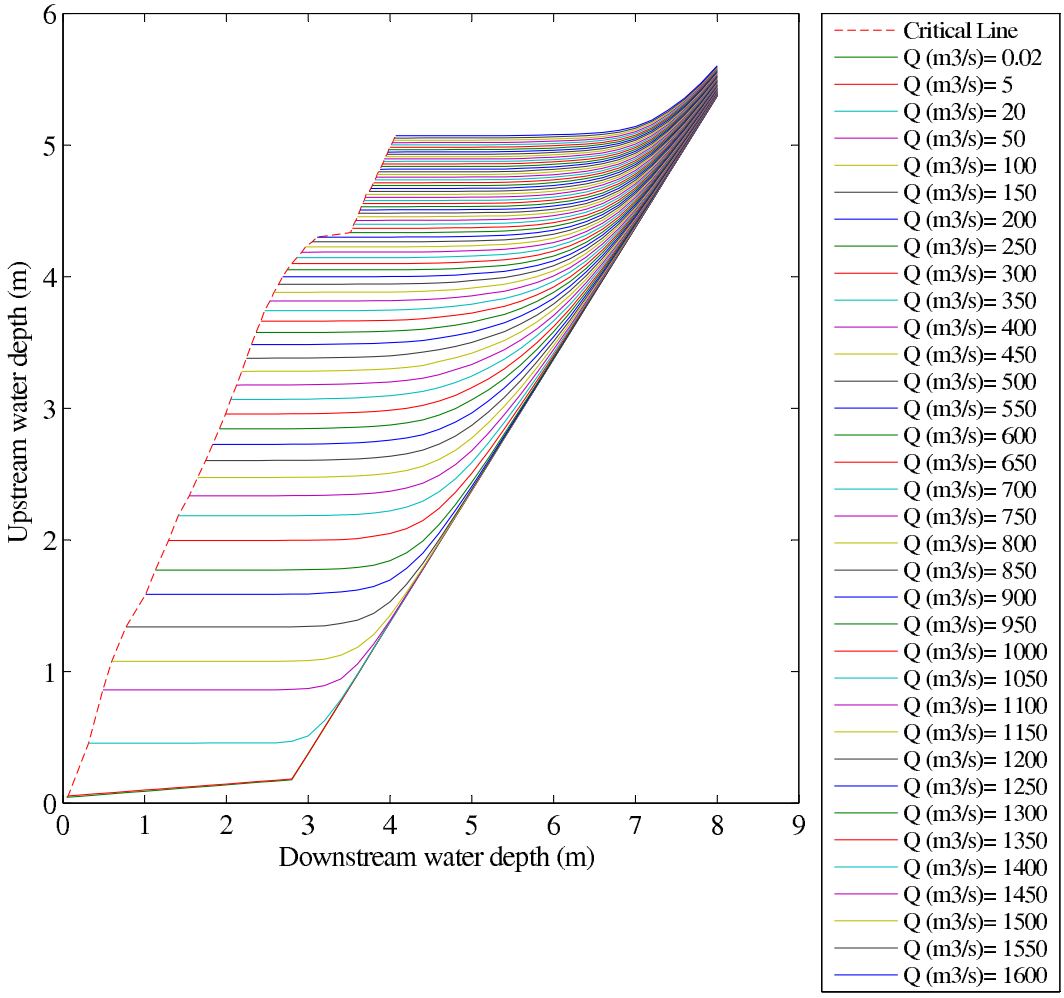

Figure A.13: Hydraulic Performance Graph - Reach R13

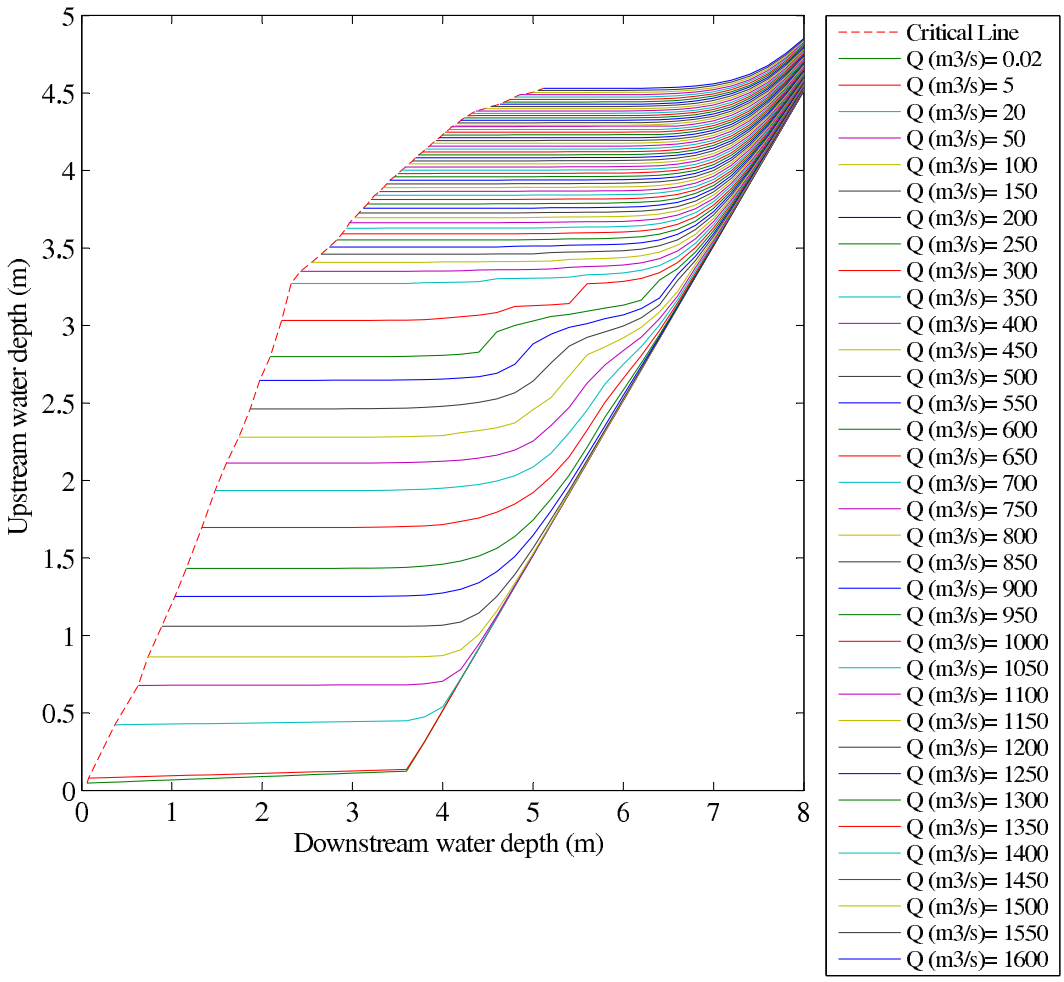

Figure A.14: Hydraulic Performance Graph - Reach R14

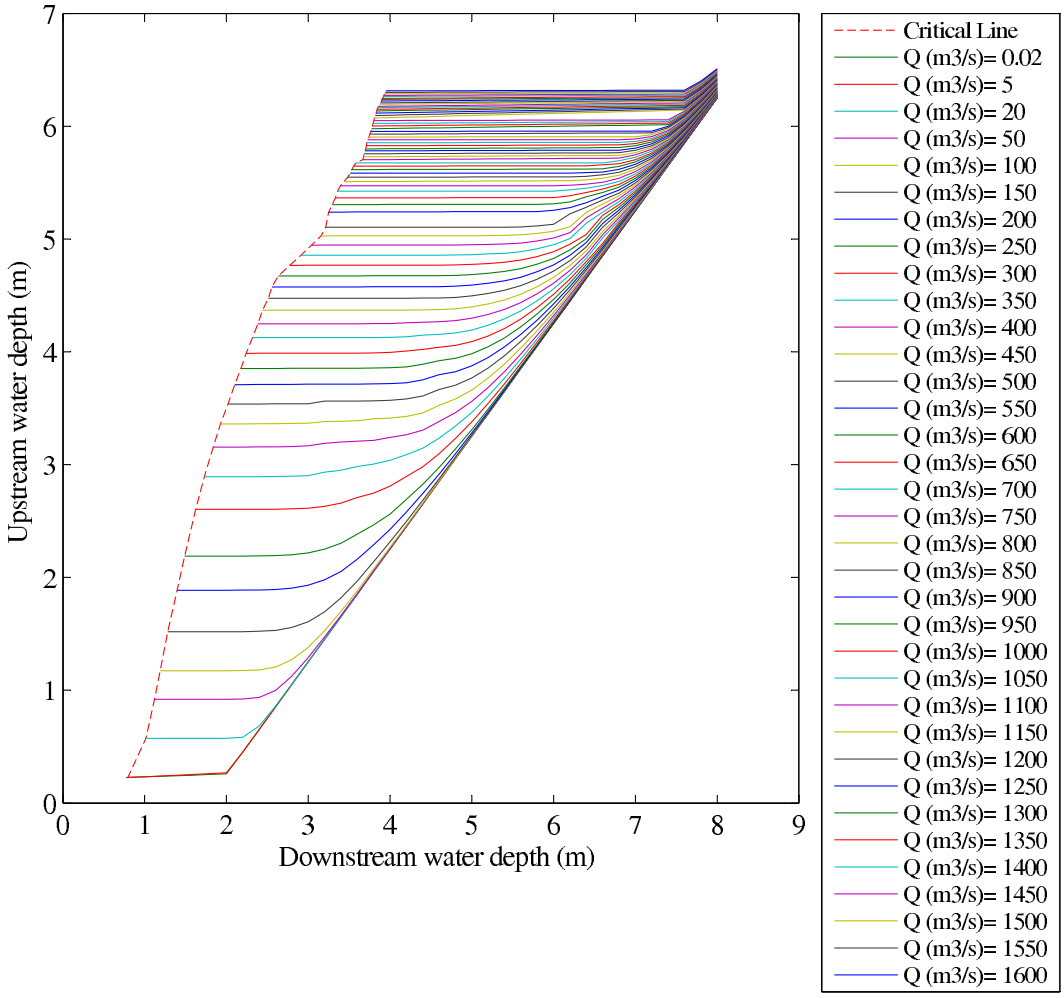

Figure A.15: Hydraulic Performance Graph - Reach R15

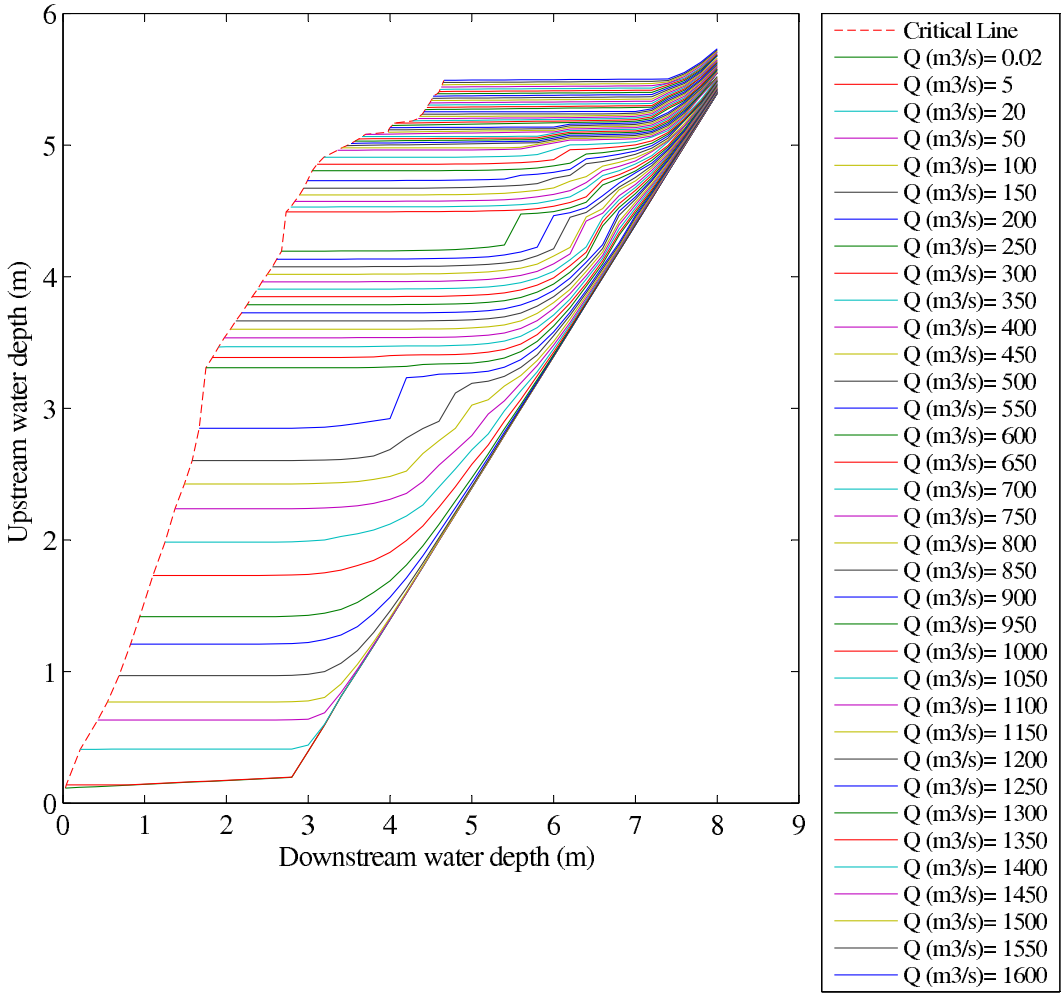

Figure A.16: Hydraulic Performance Graph - Reach R16

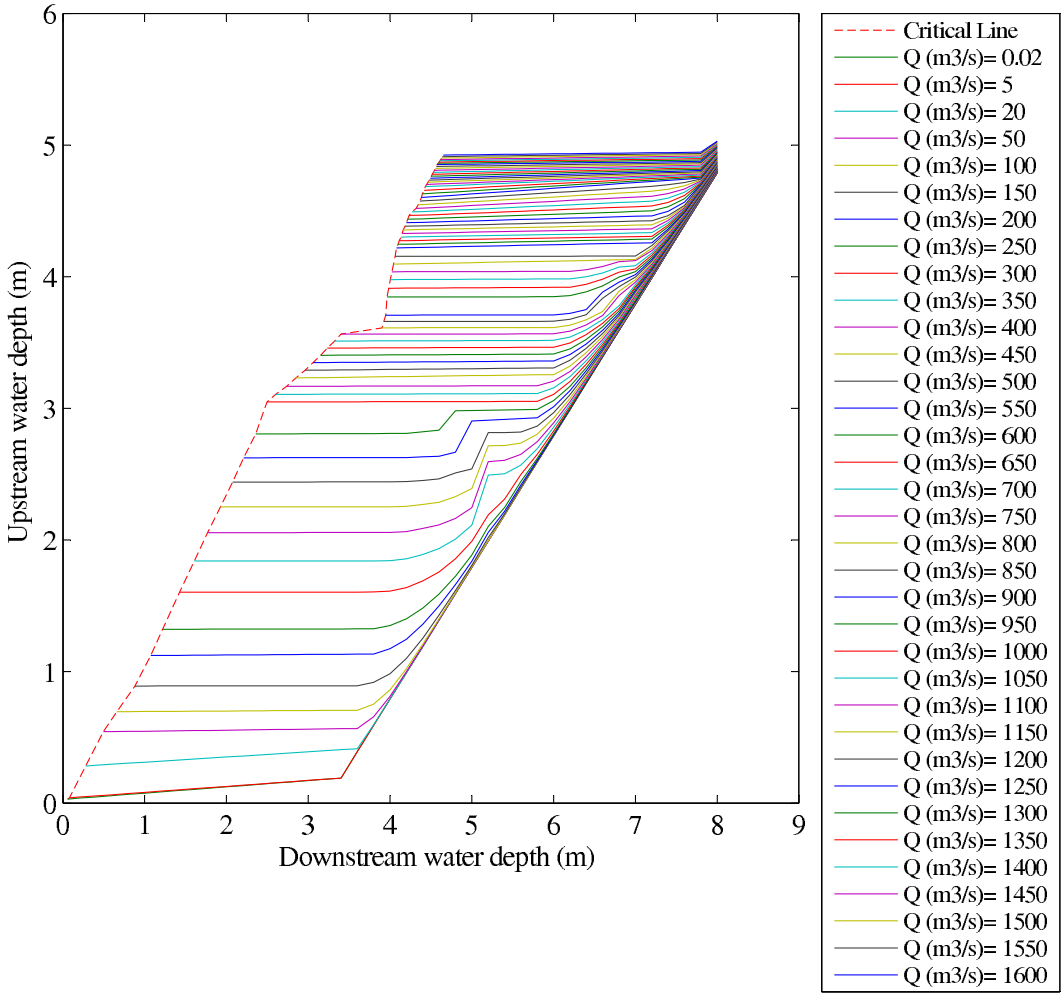

Figure A.17: Hydraulic Performance Graph - Reach R17

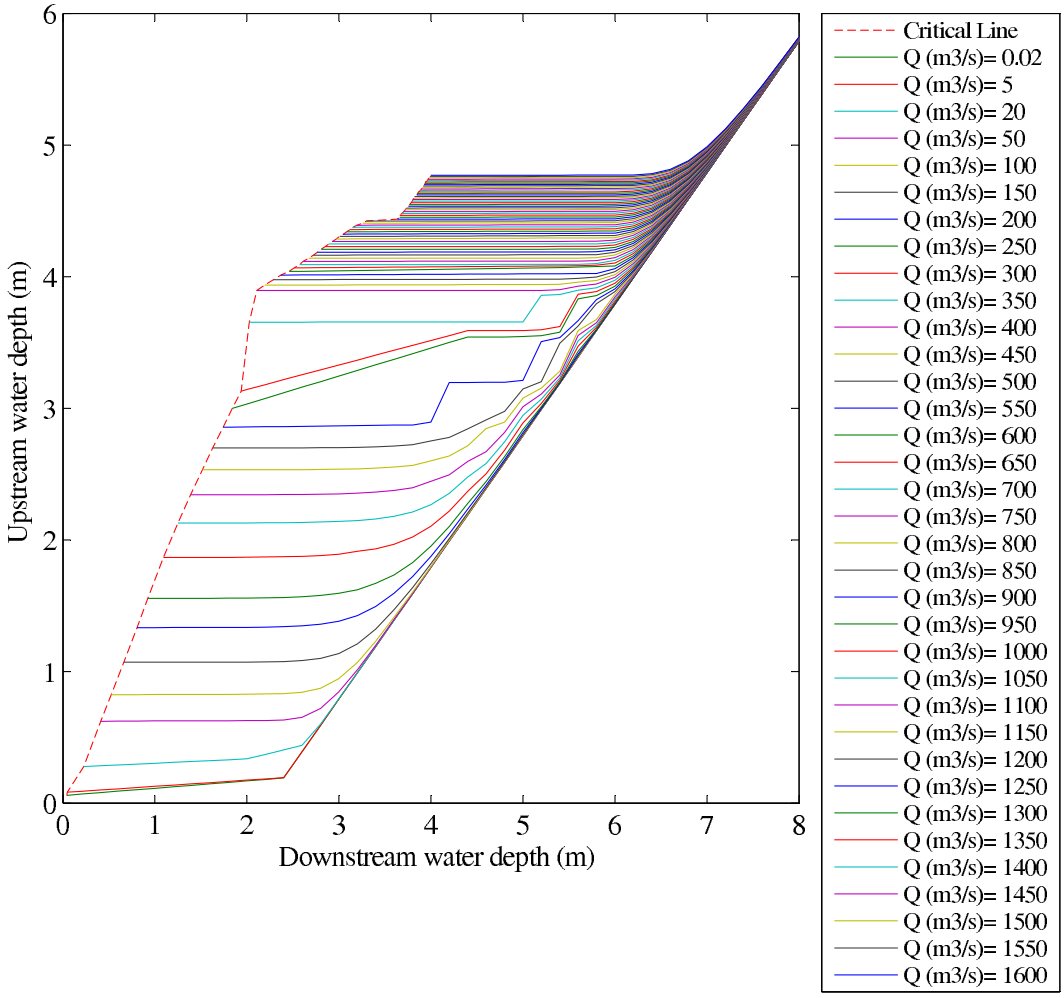

Figure A.18: Hydraulic Performance Graph - Reach R18

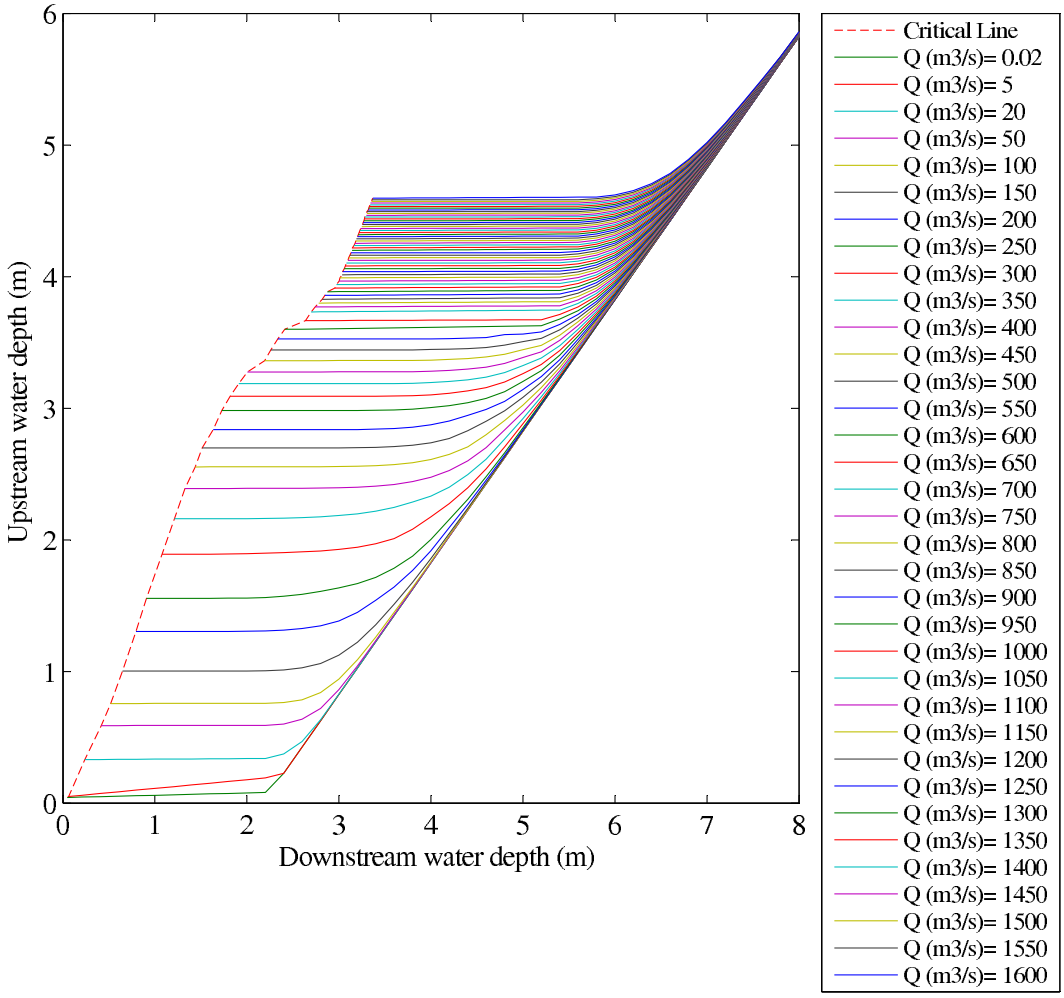

Figure A.19: Hydraulic Performance Graph - Reach R19

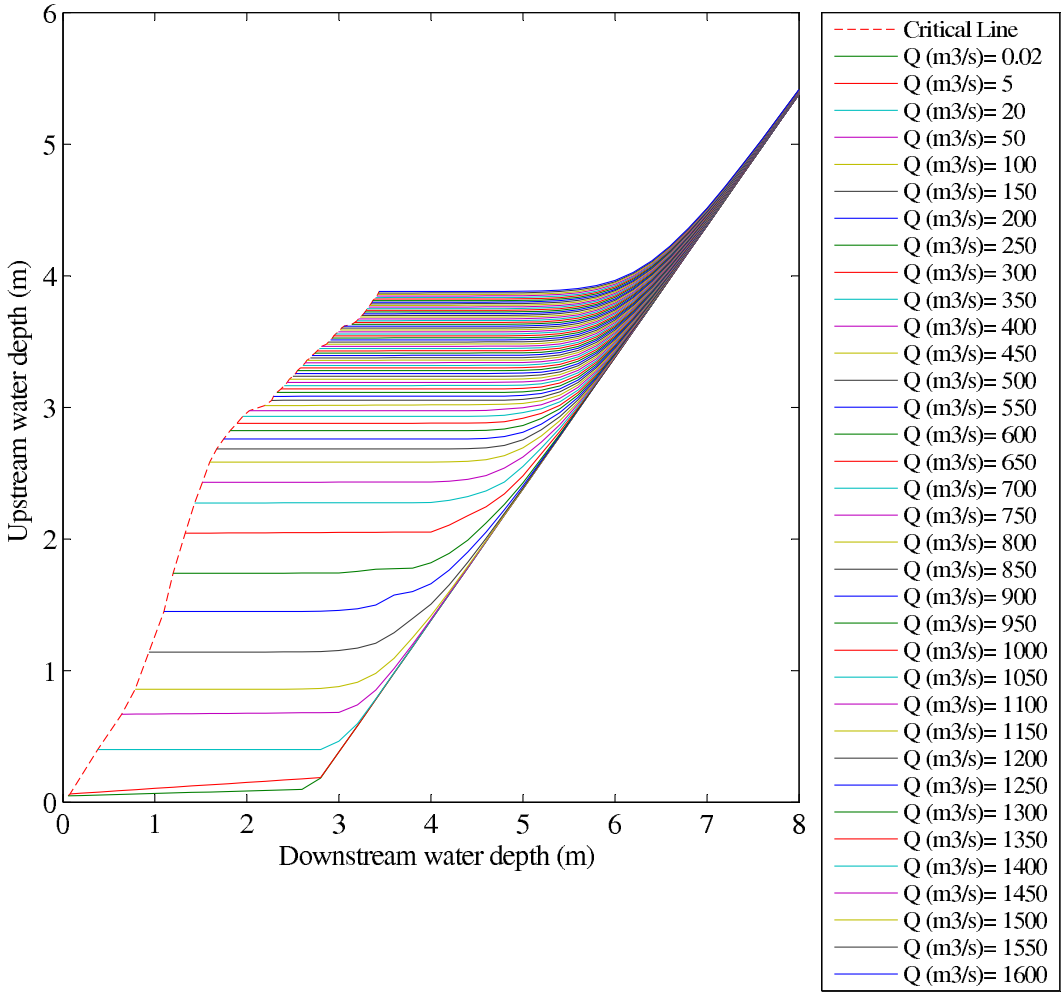

Figure A.20: Hydraulic Performance Graph - Reach R20

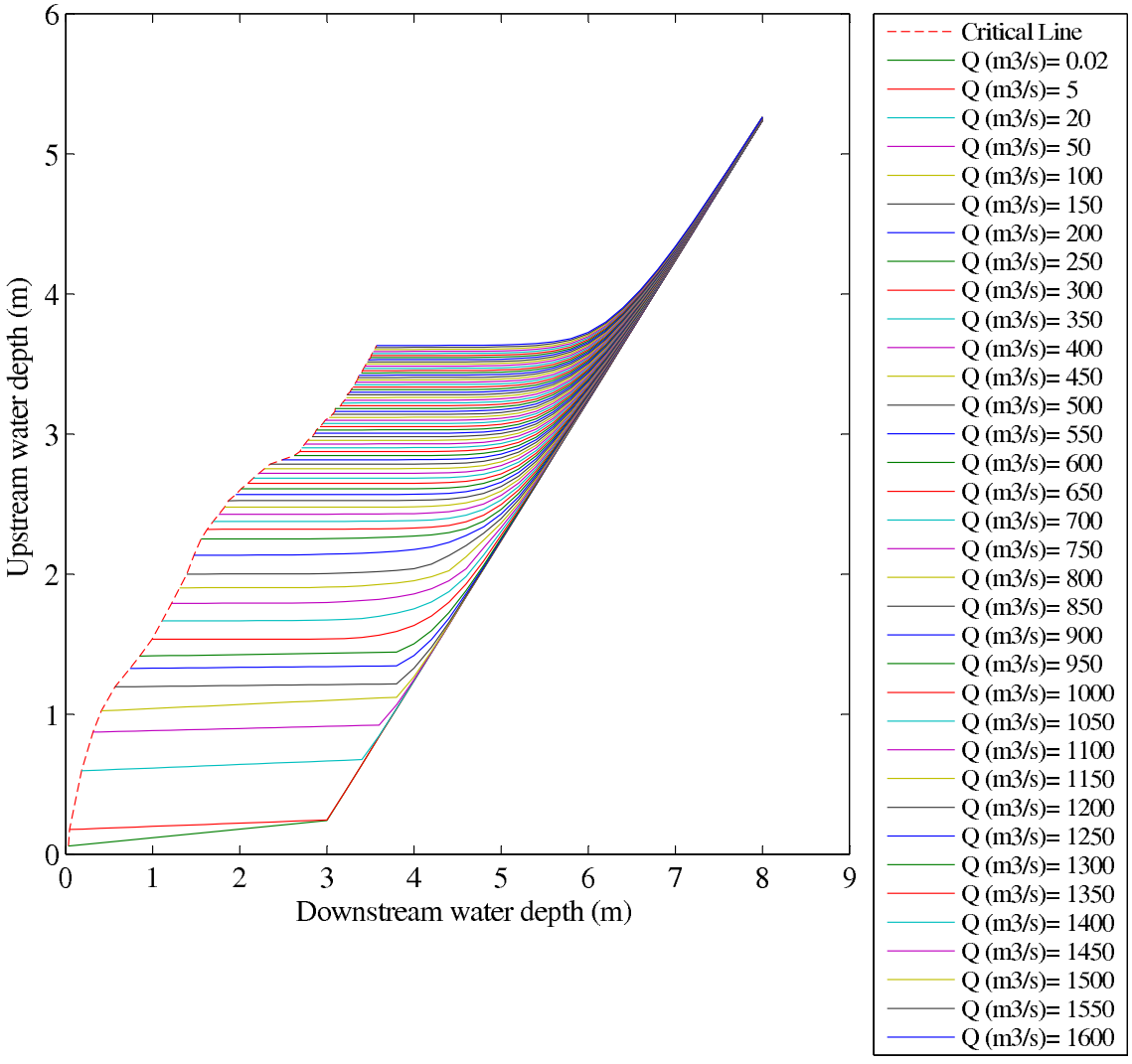

Figure A.21: Hydraulic Performance Graph - Reach R21

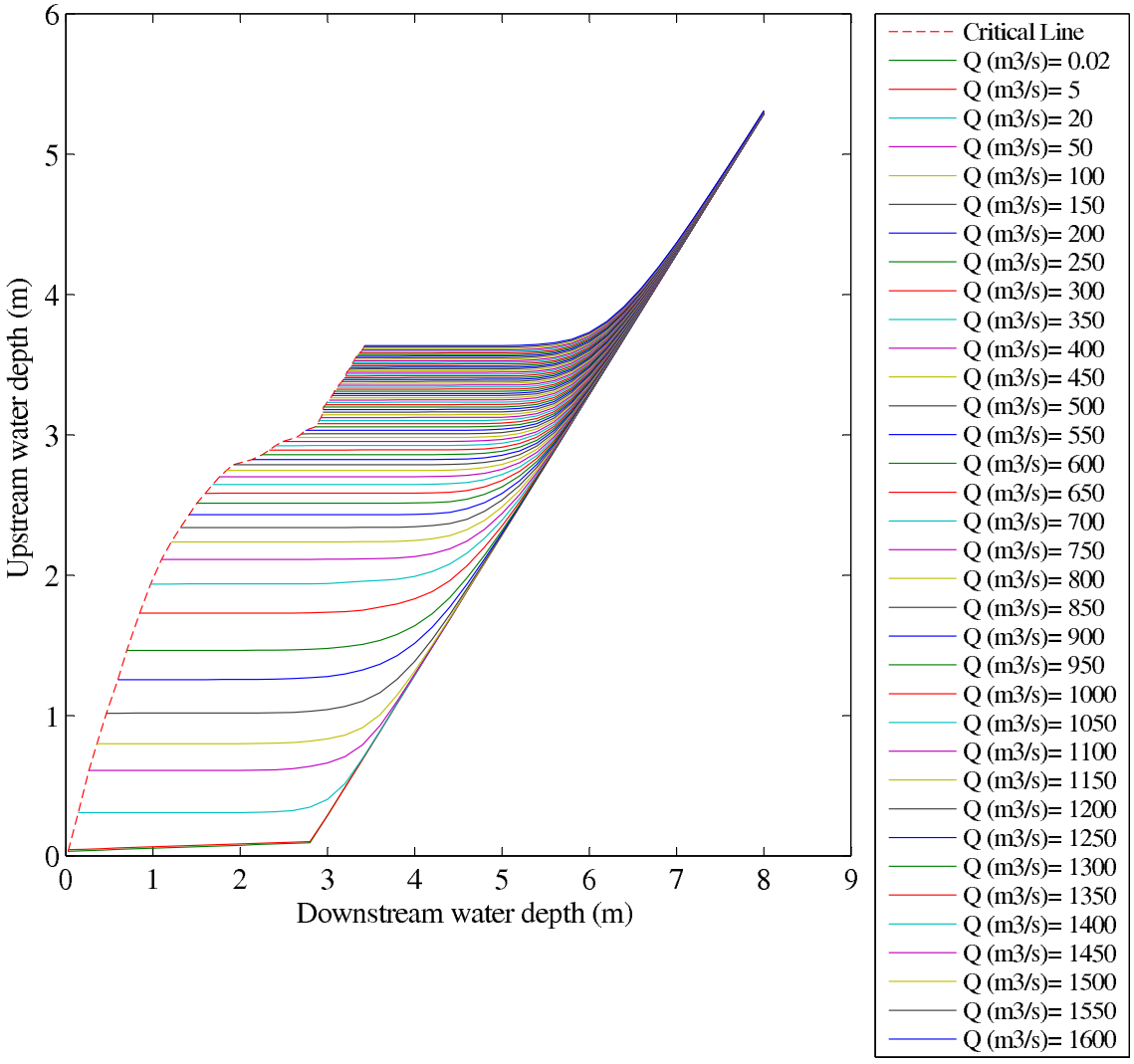

Figure A.22: Hydraulic Performance Graph - Reach R22

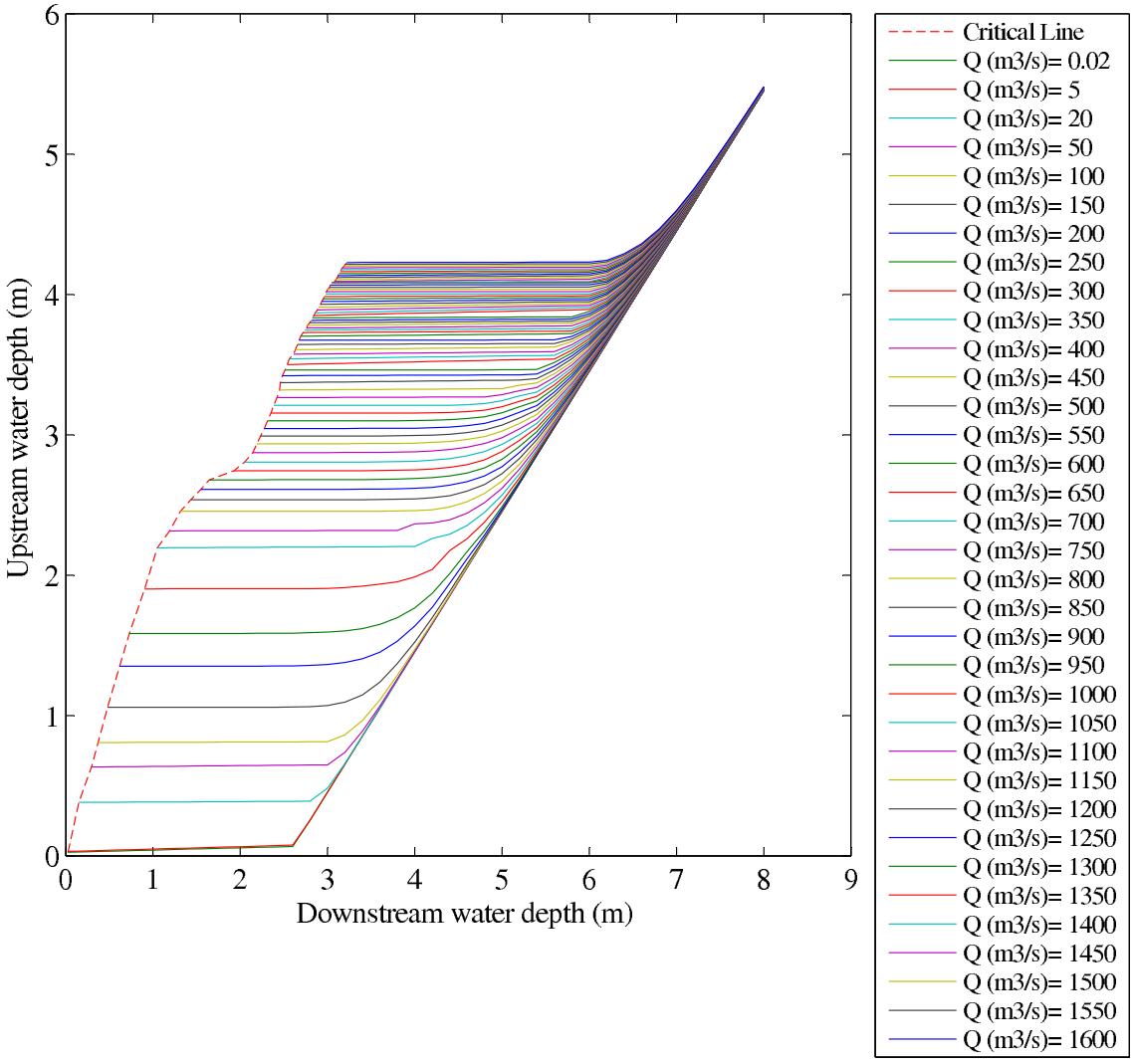

Figure A.23: Hydraulic Performance Graph - Reach R23

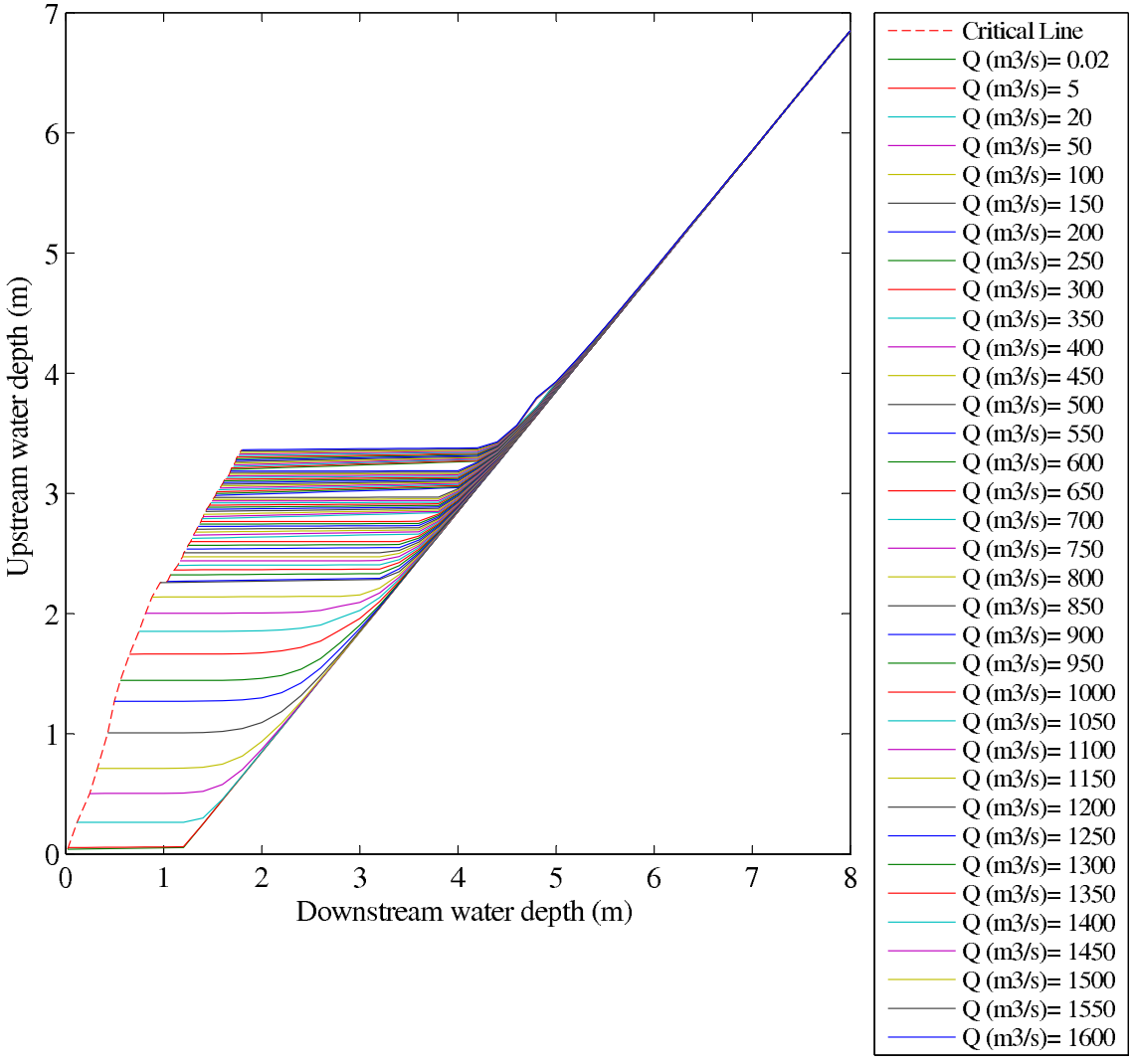

Figure A.24: Hydraulic Performance Graph - Reach R24

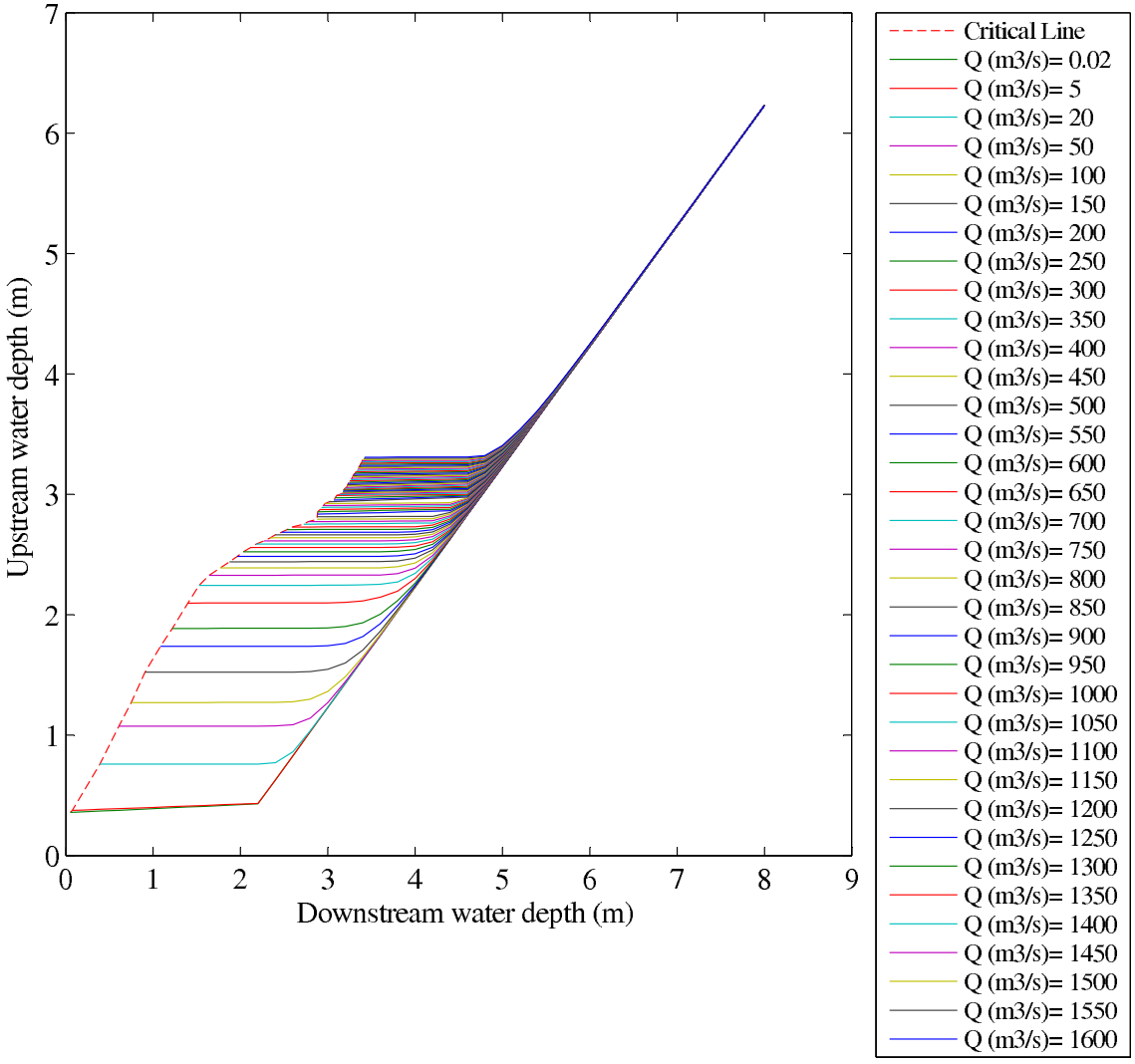

Figure A.25: Hydraulic Performance Graph - Reach R25

APPENDIX B

VOLUME PERFORMANCE GRAPH

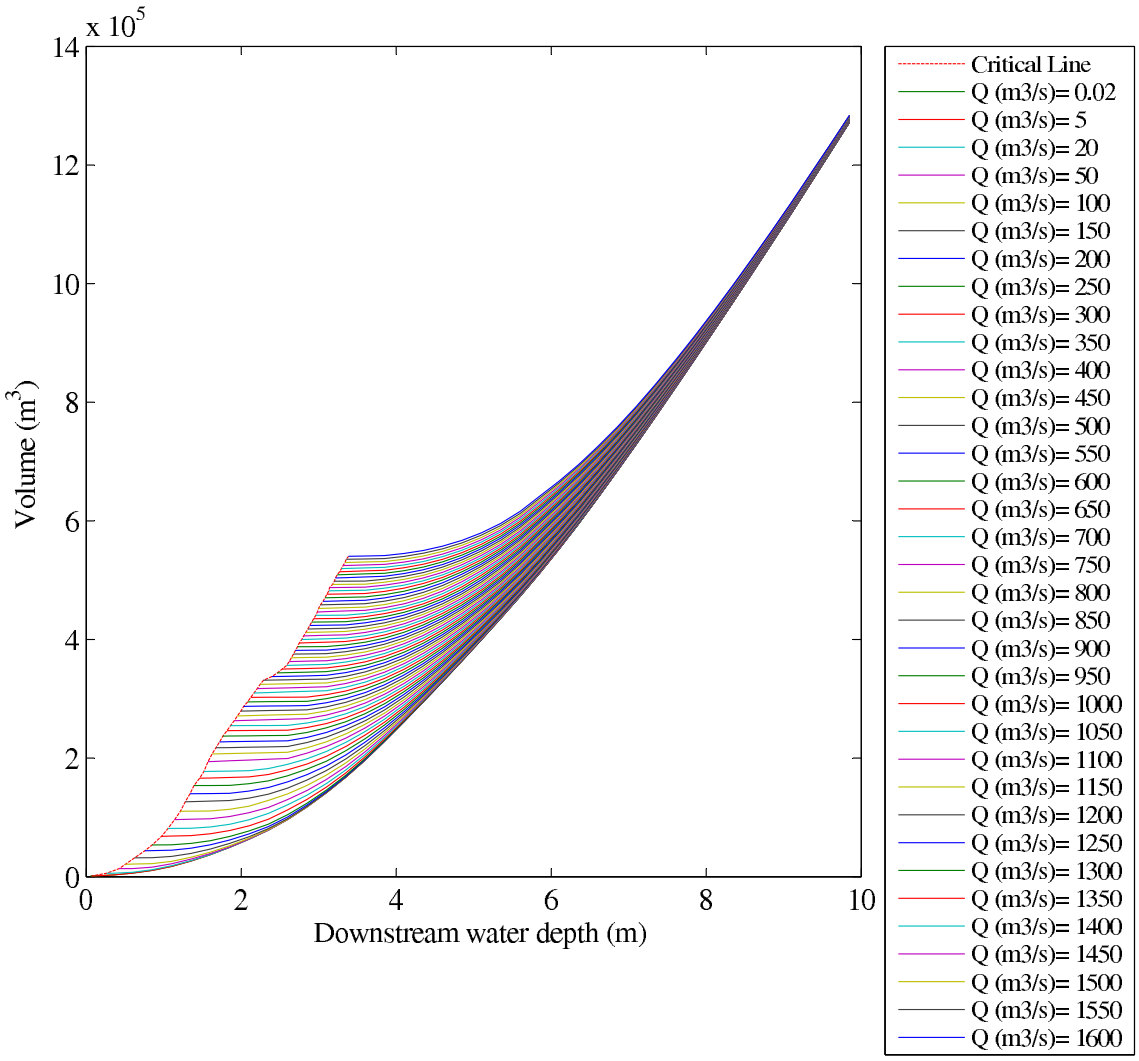

Figure B.1: Volume Performance Graph - Reach R1

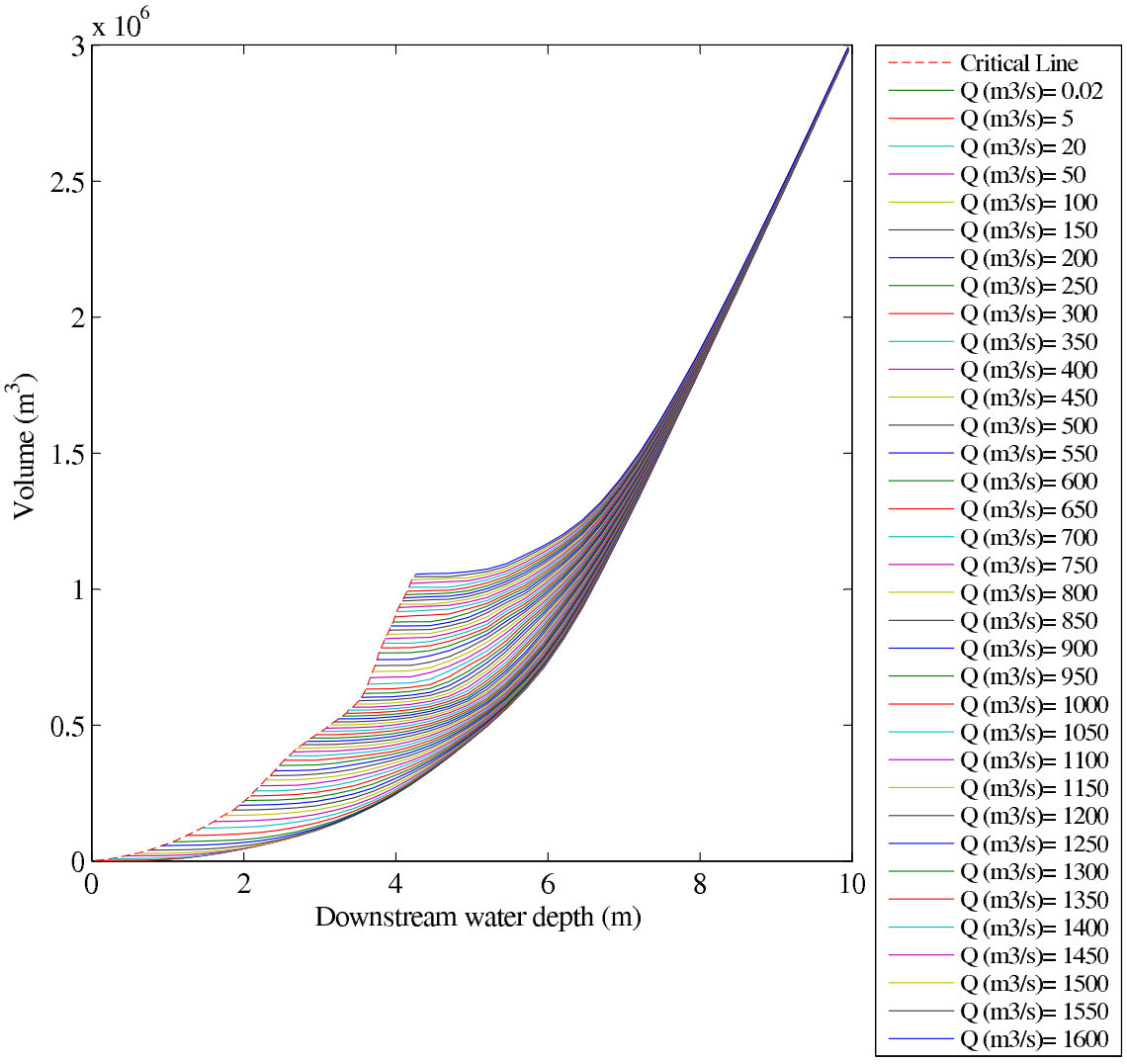

Figure B.2: Volume Performance Graph - Reach R2

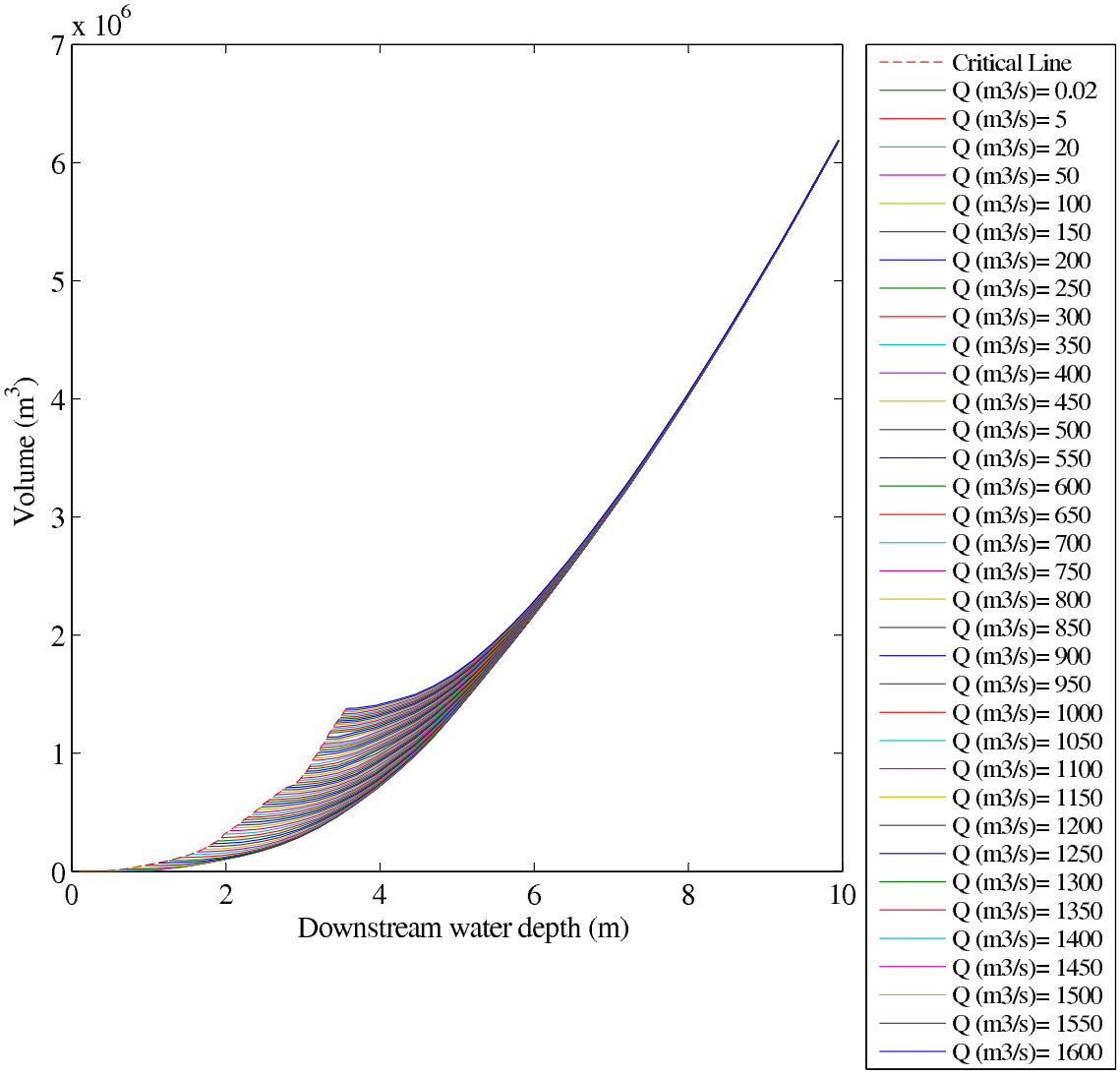

Figure B.3: Volume Performance Graph - Reach R3

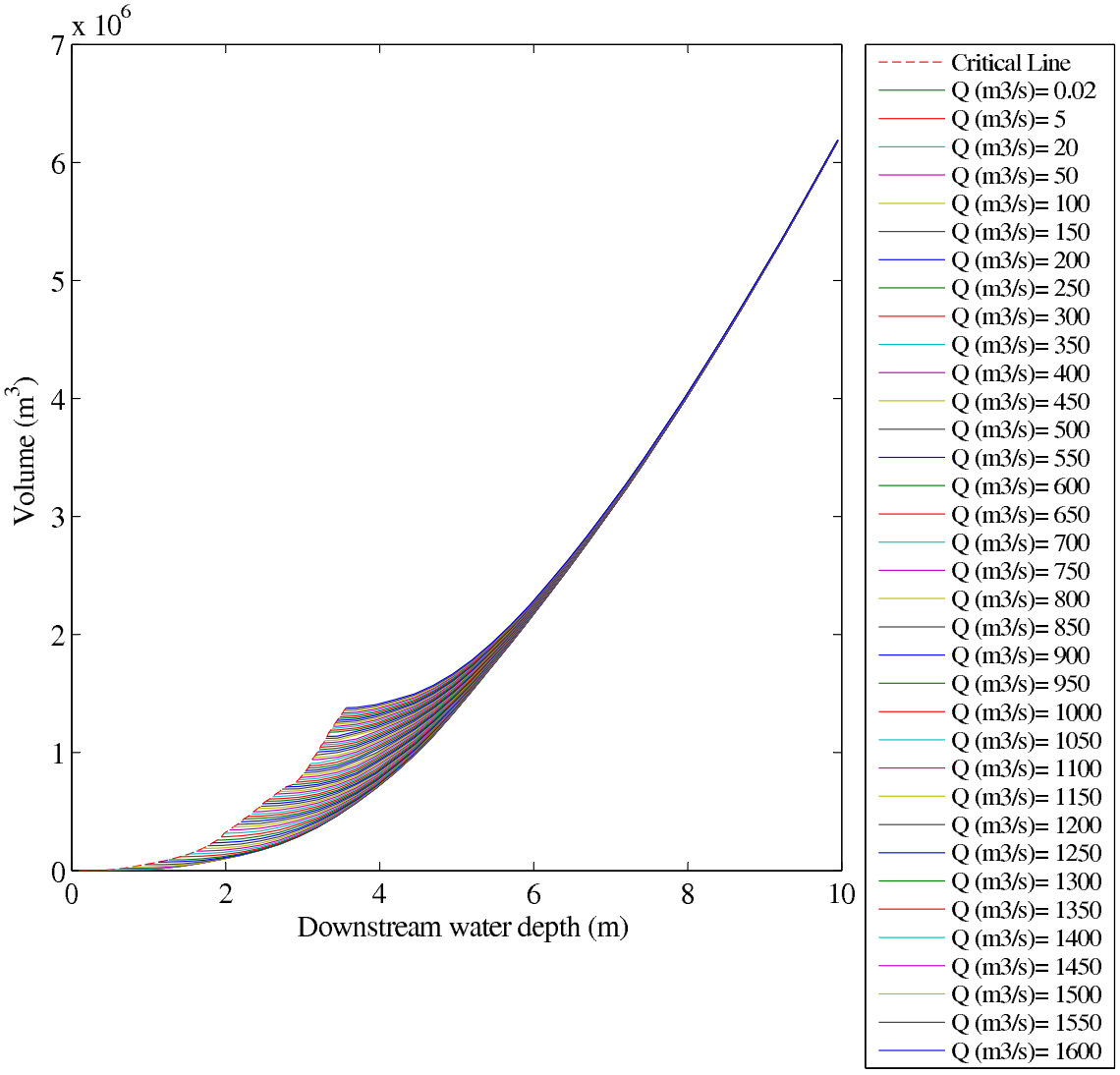

Figure B.4: Volume Performance Graph - Reach R4

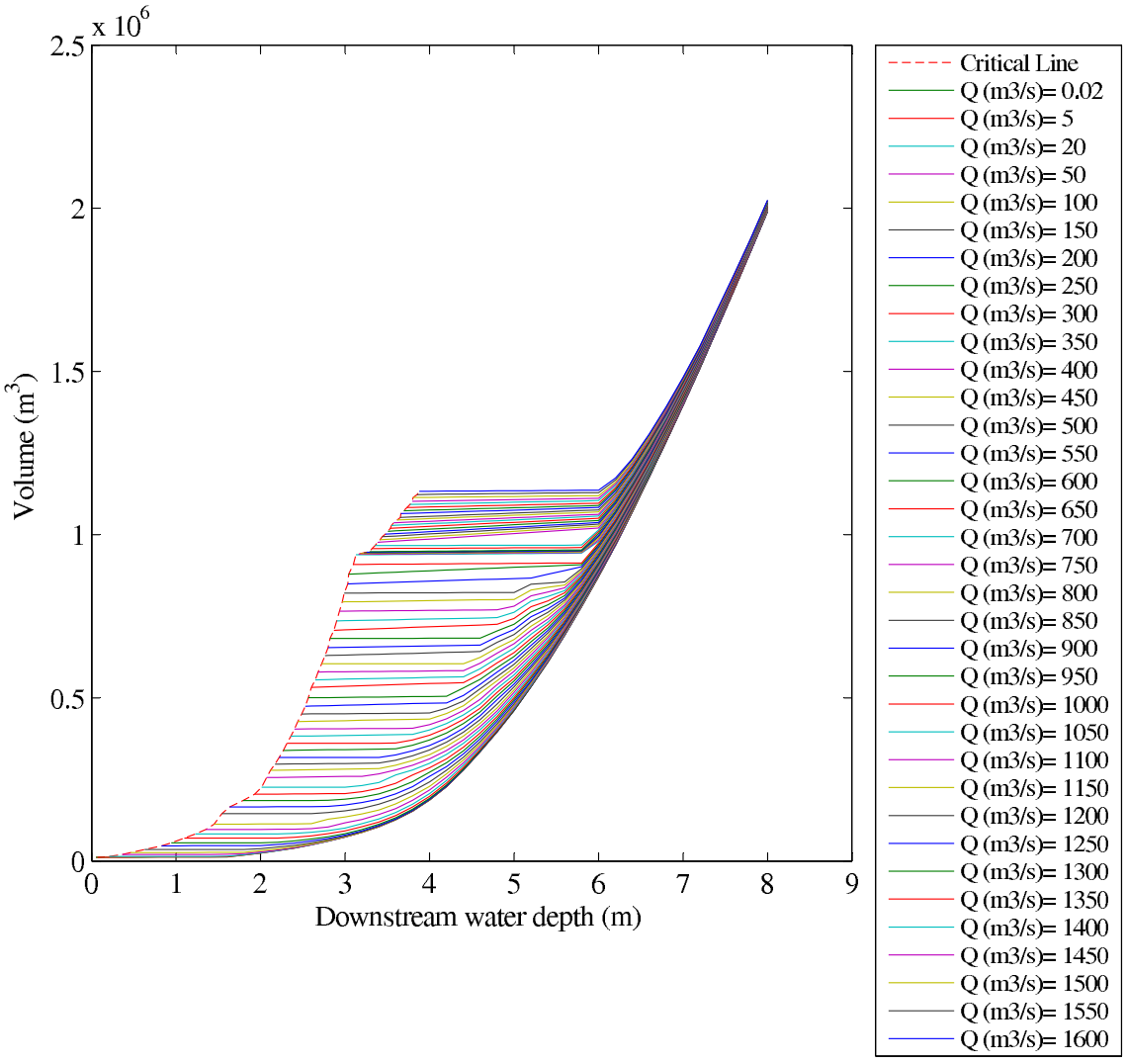

Figure B.5: Volume Performance Graph - Reach R5

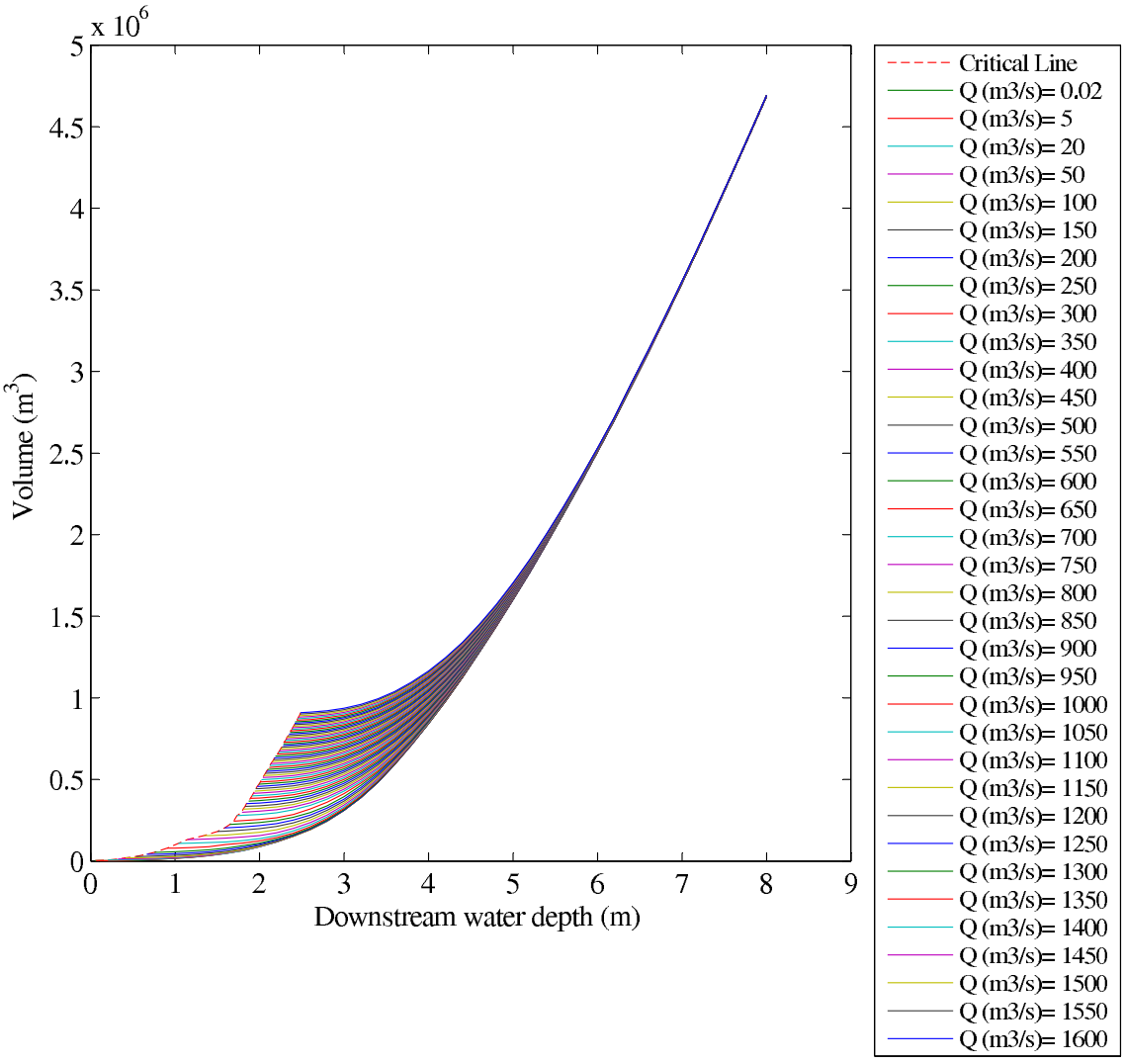

Figure B.6: Volume Performance Graph - Reach R6

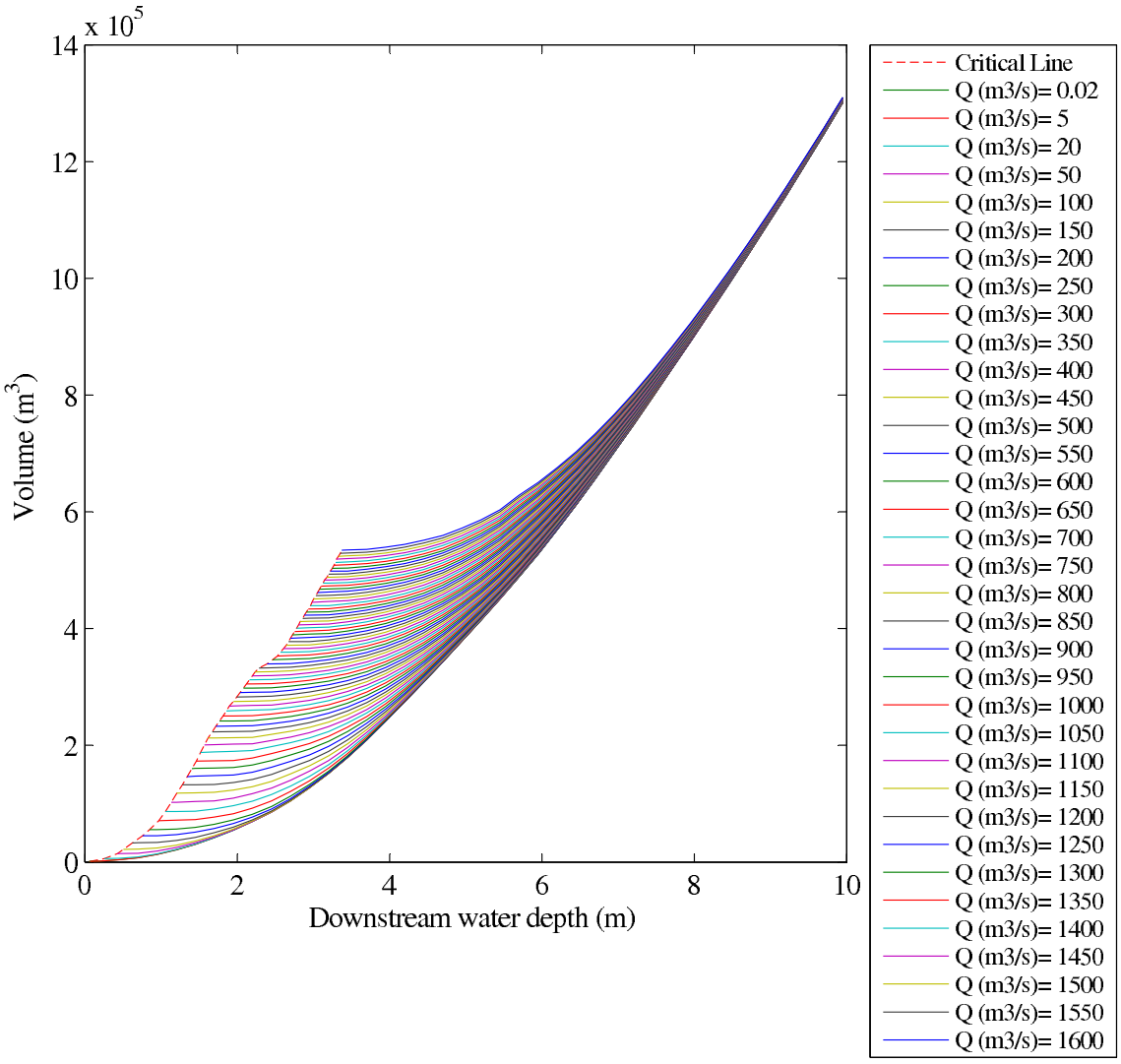

Figure B.7: Volume Performance Graph - Reach R7

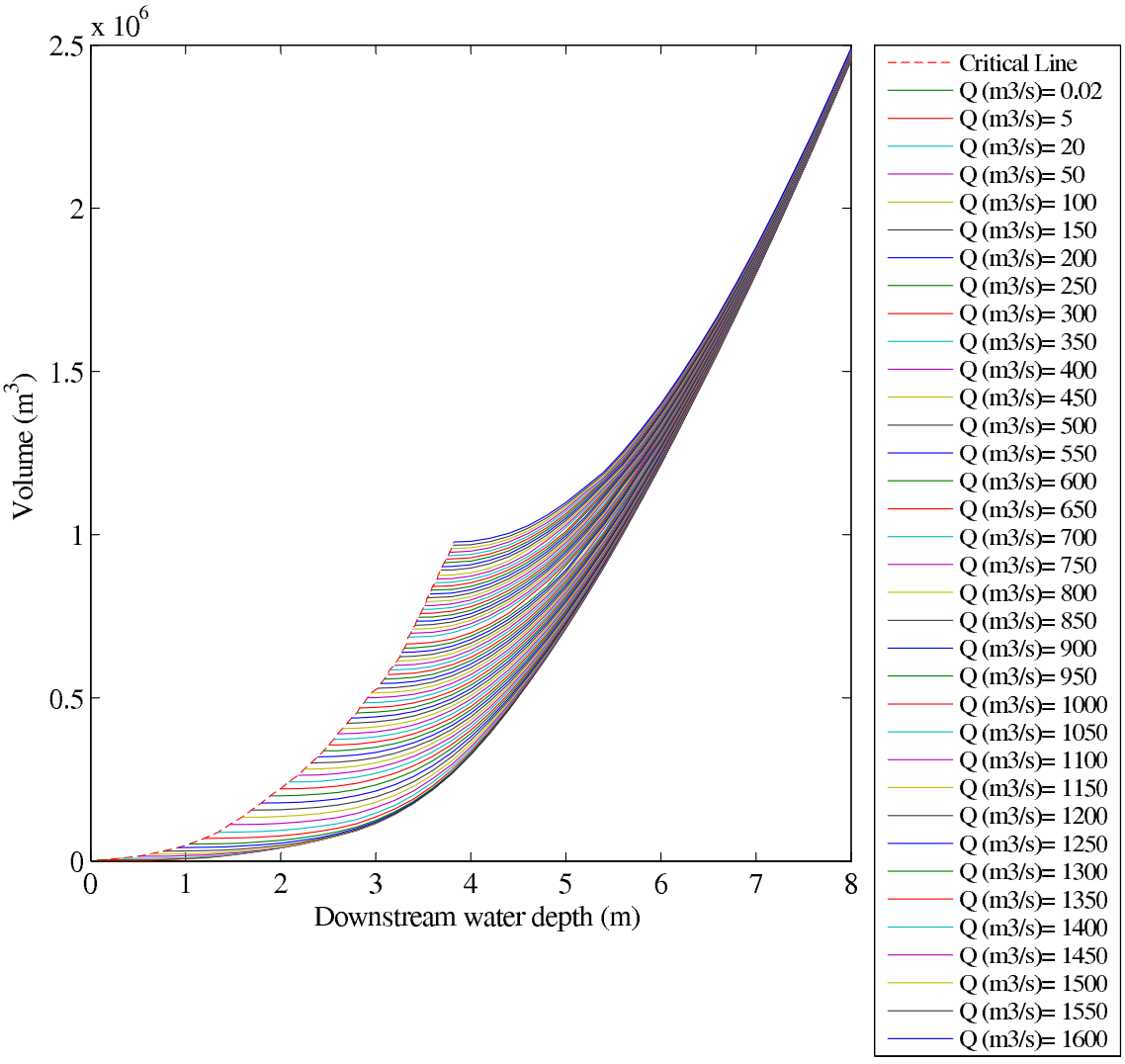

Figure B.8: Volume Performance Graph - Reach R8

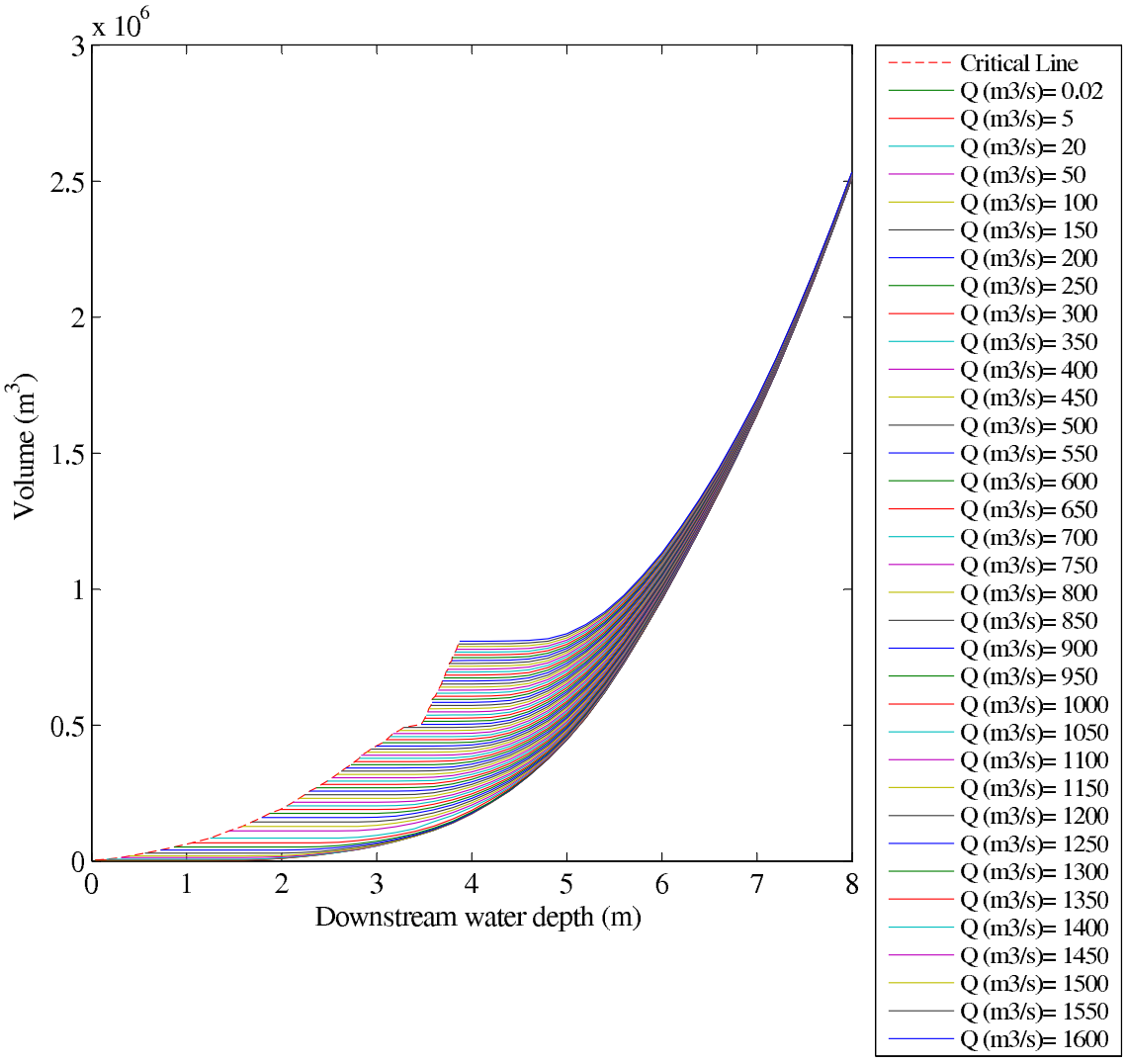

Figure B.9: Volume Performance Graph - Reach R9

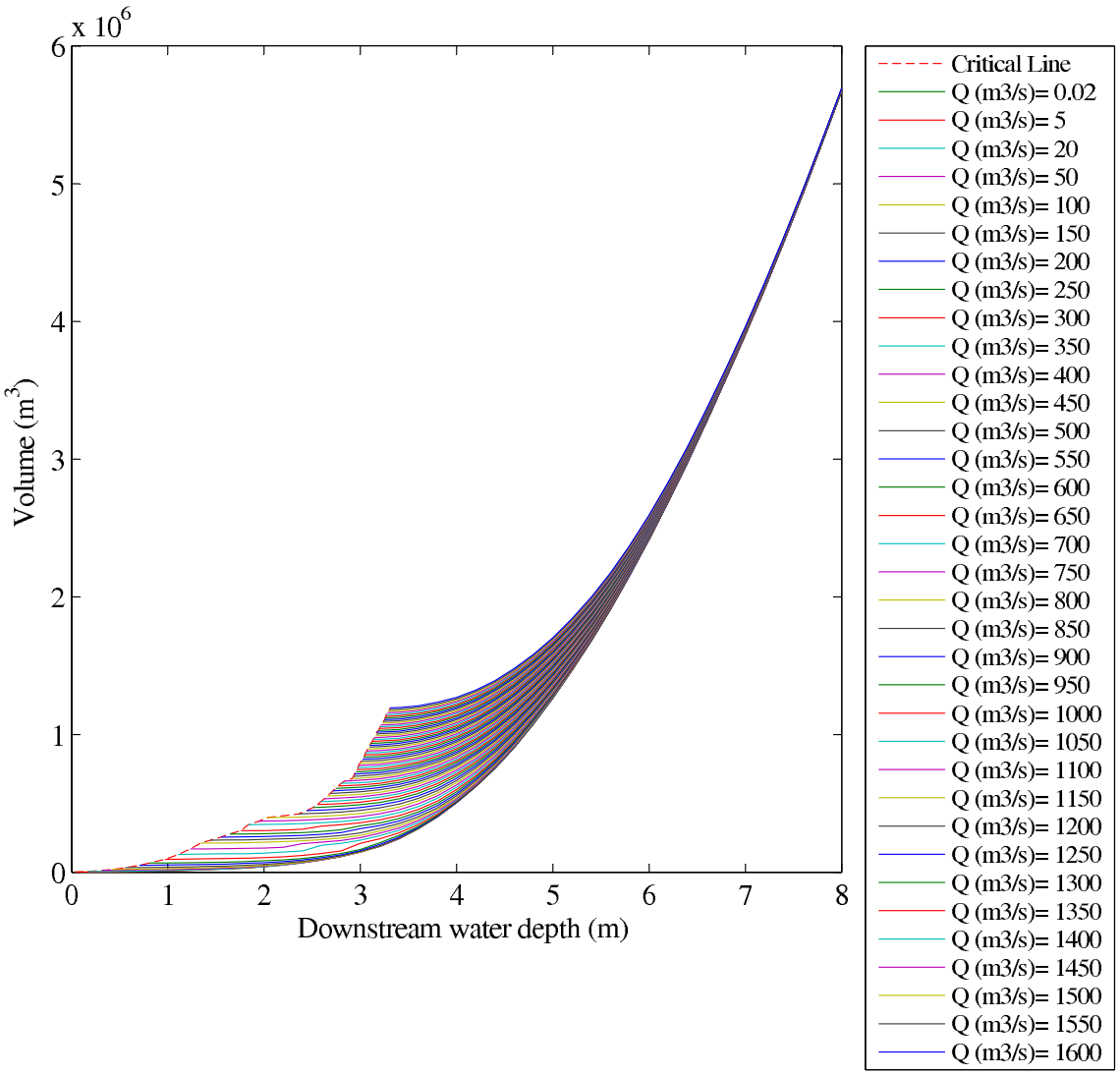

Figure B.10: Volume Performance Graph - Reach R10

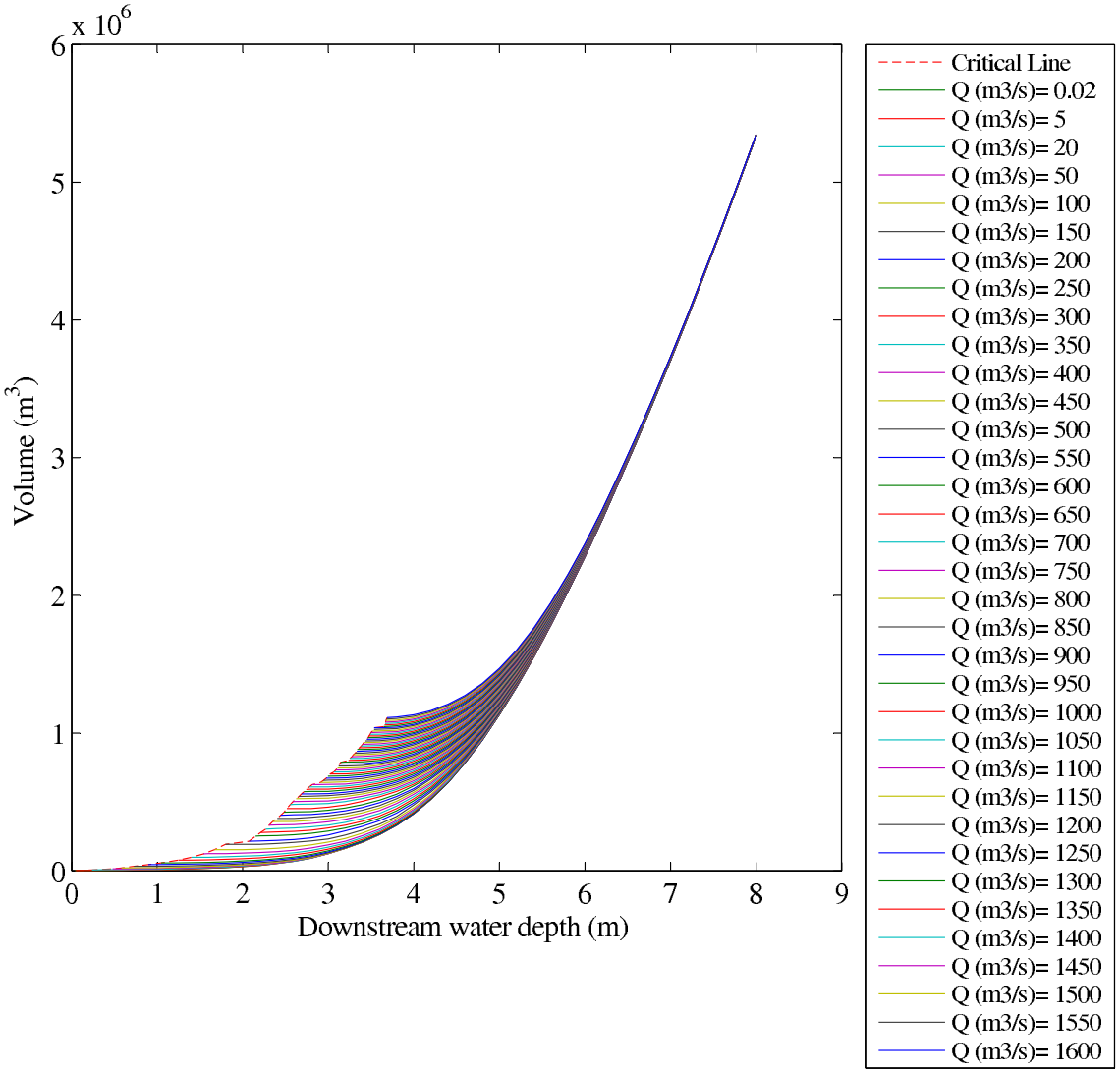

Figure B.11: Volume Performance Graph - Reach R11

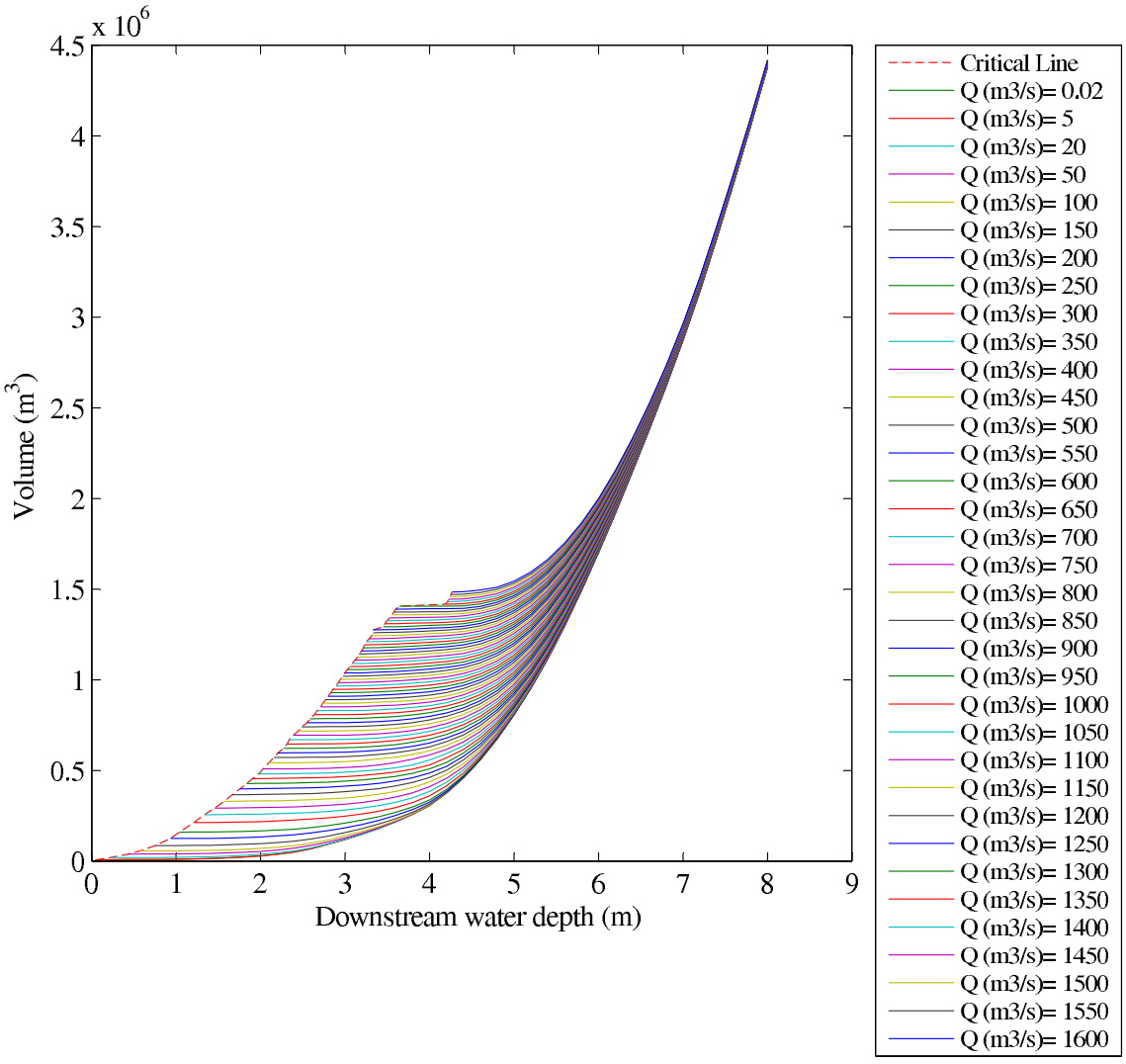

Figure B.12: Volume Performance Graph - Reach R12

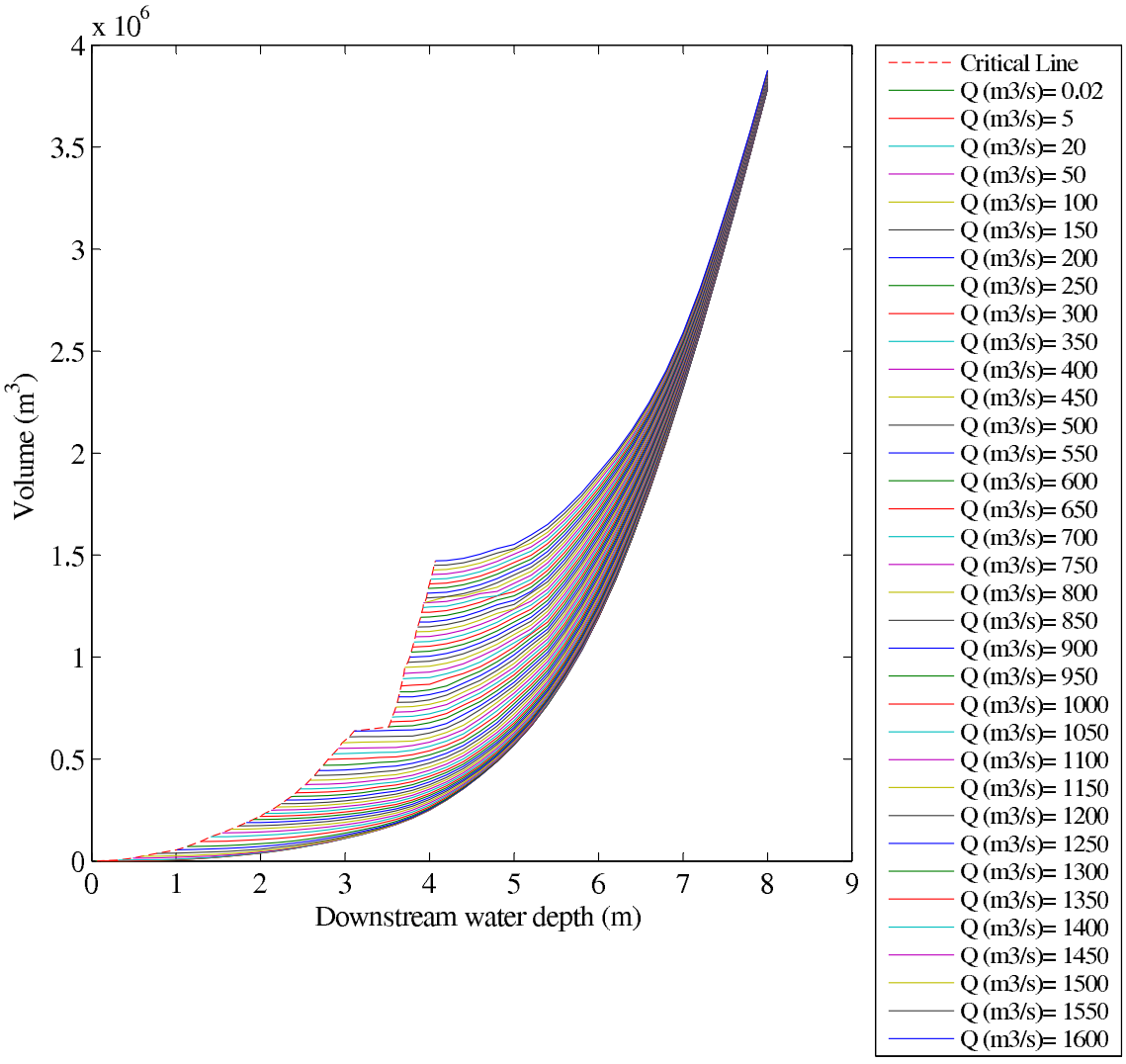

Figure B.13: Volume Performance Graph - Reach R13

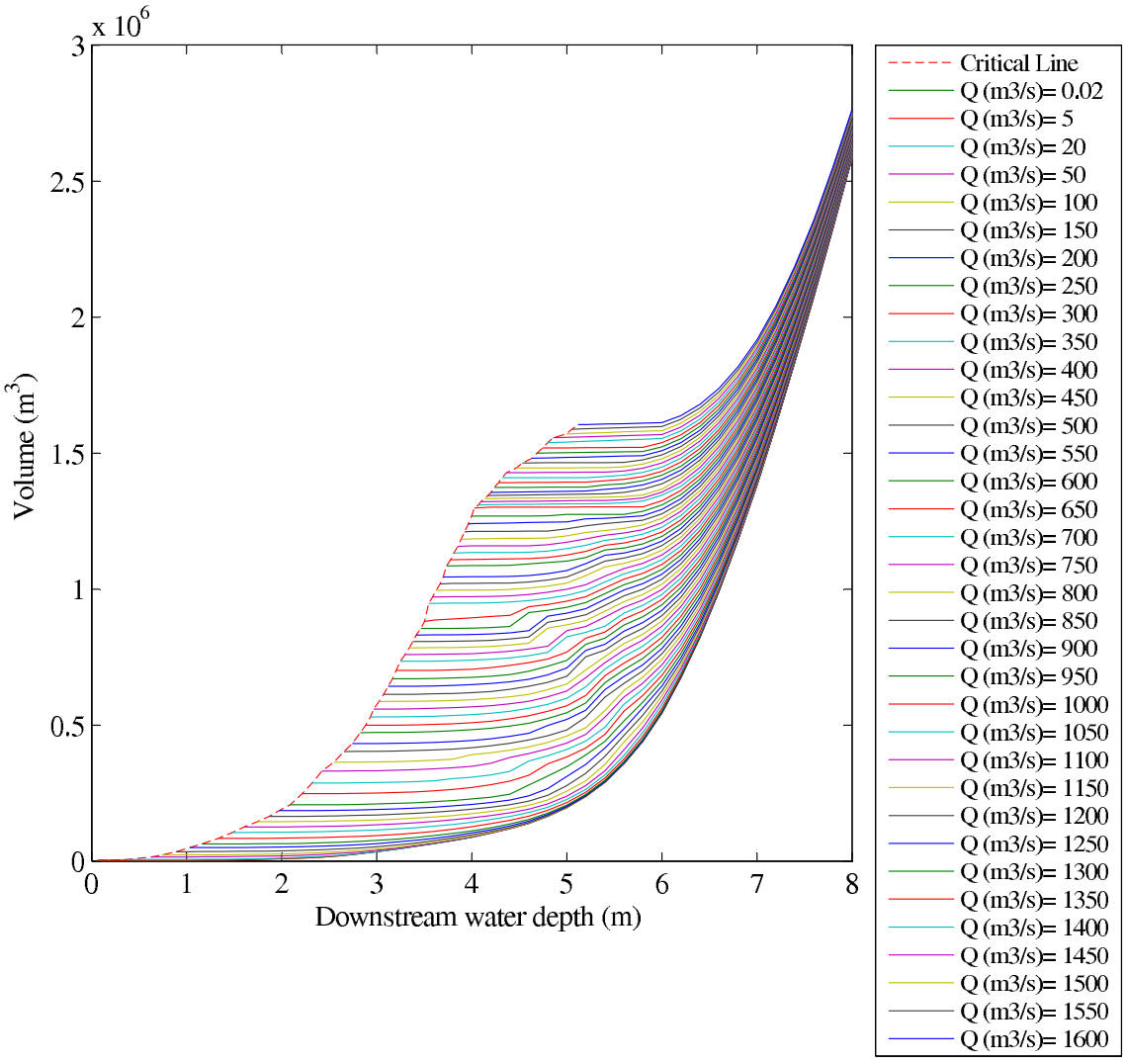

Figure B.14: Volume Performance Graph - Reach R14

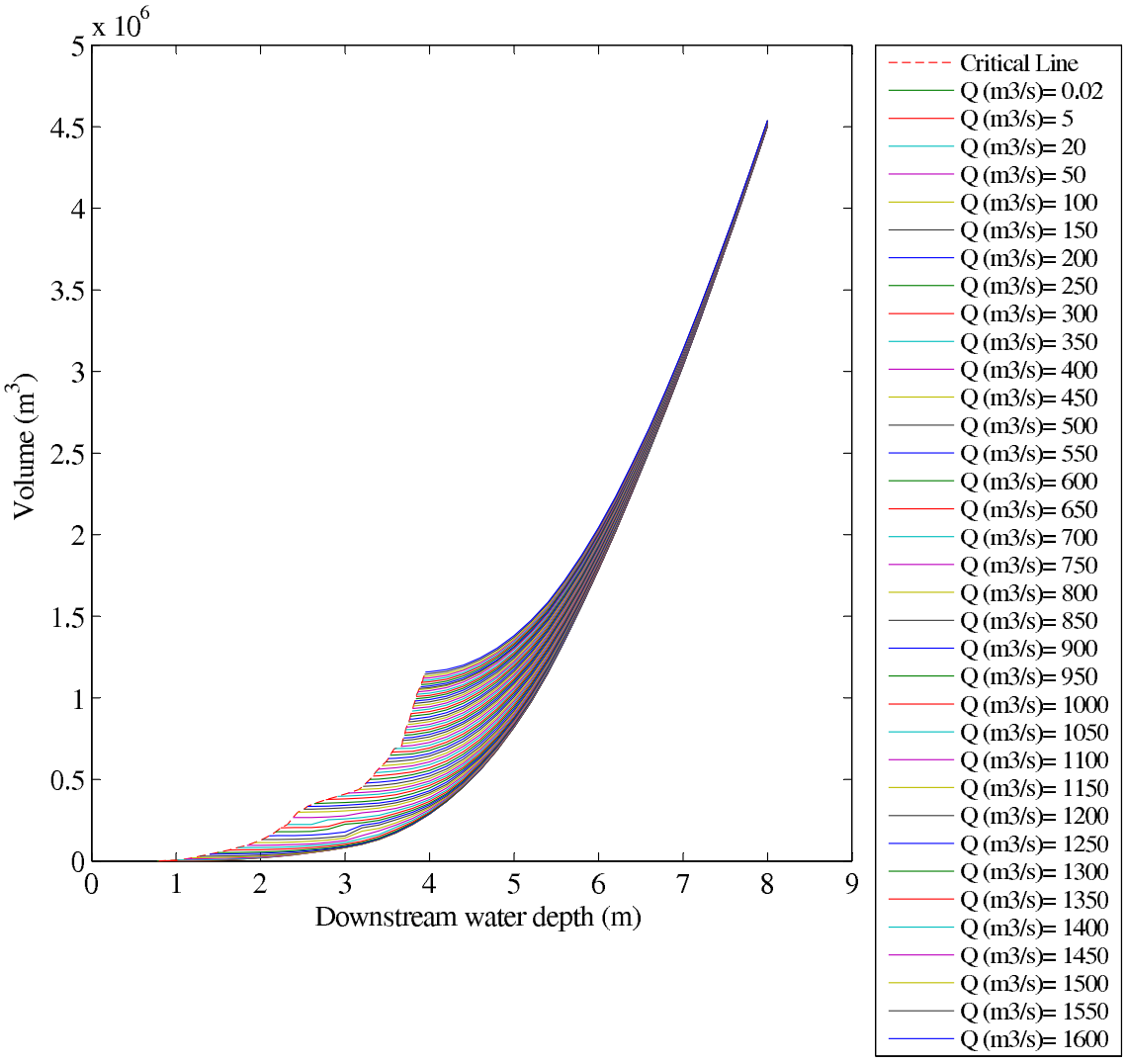

Figure B.15: Volume Performance Graph - Reach R15

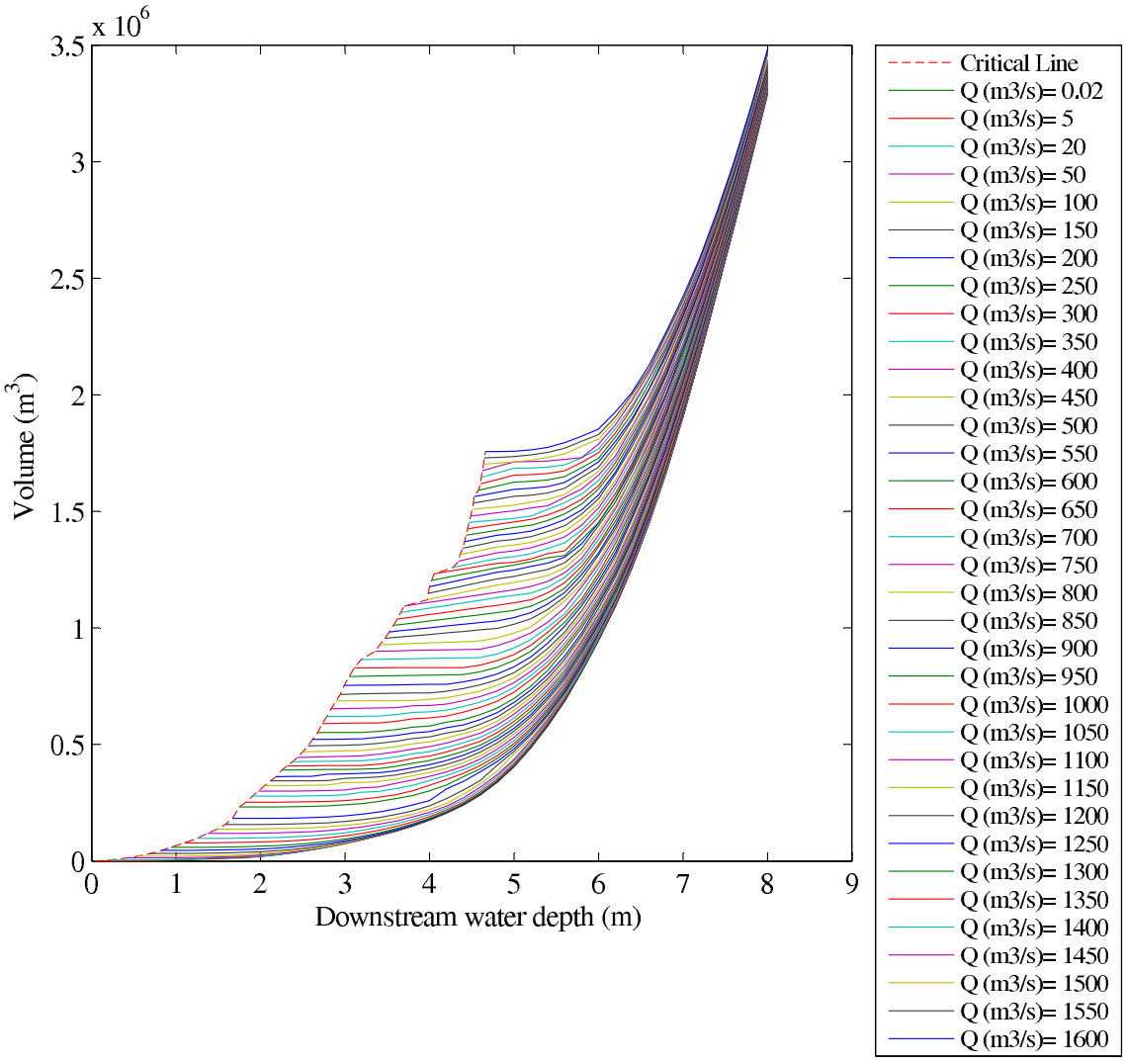

Figure B.16: Volume Performance Graph - Reach R16

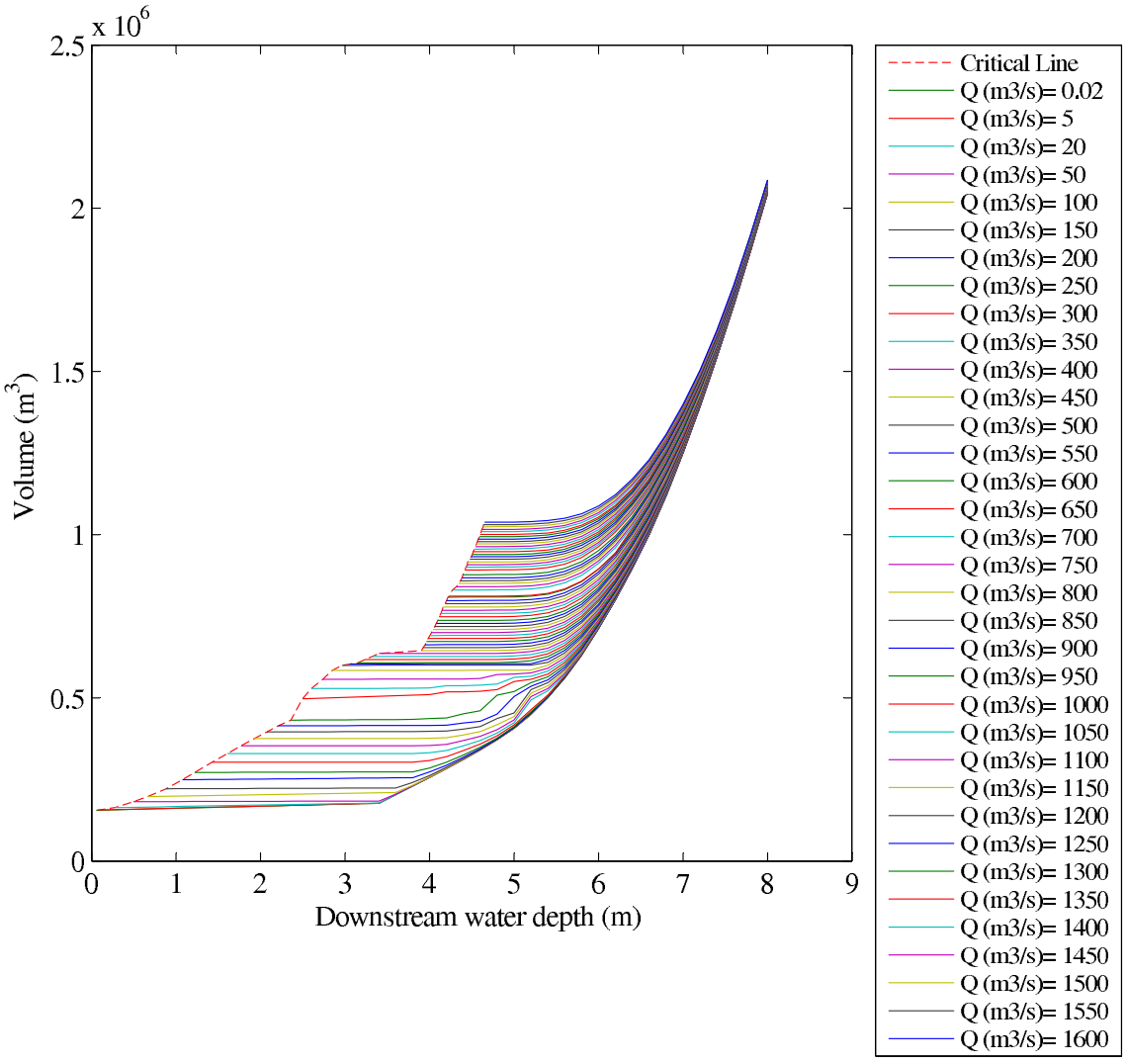

Figure B.17: Volume Performance Graph - Reach R17

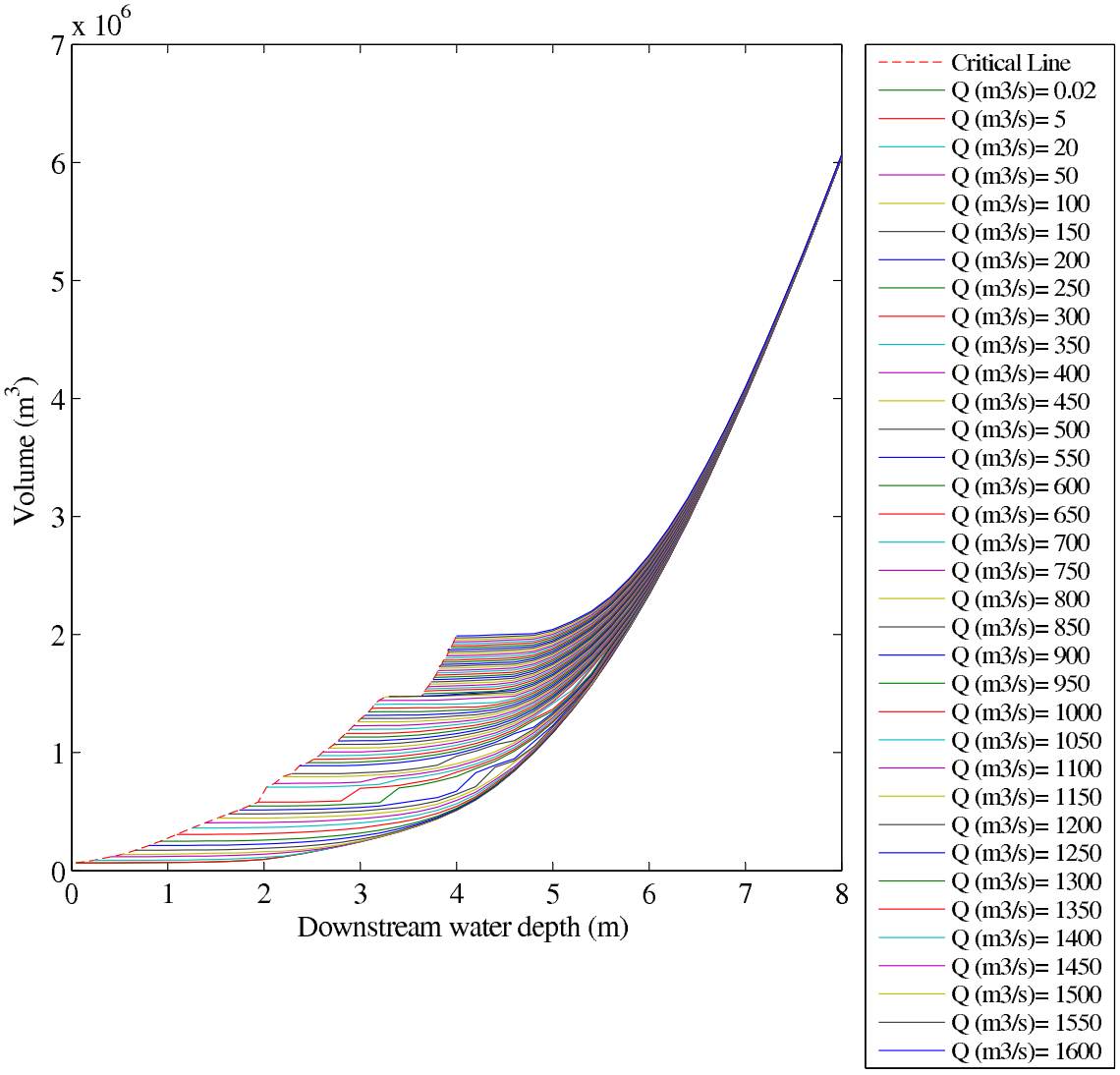

Figure B.18: Volume Performance Graph - Reach R18

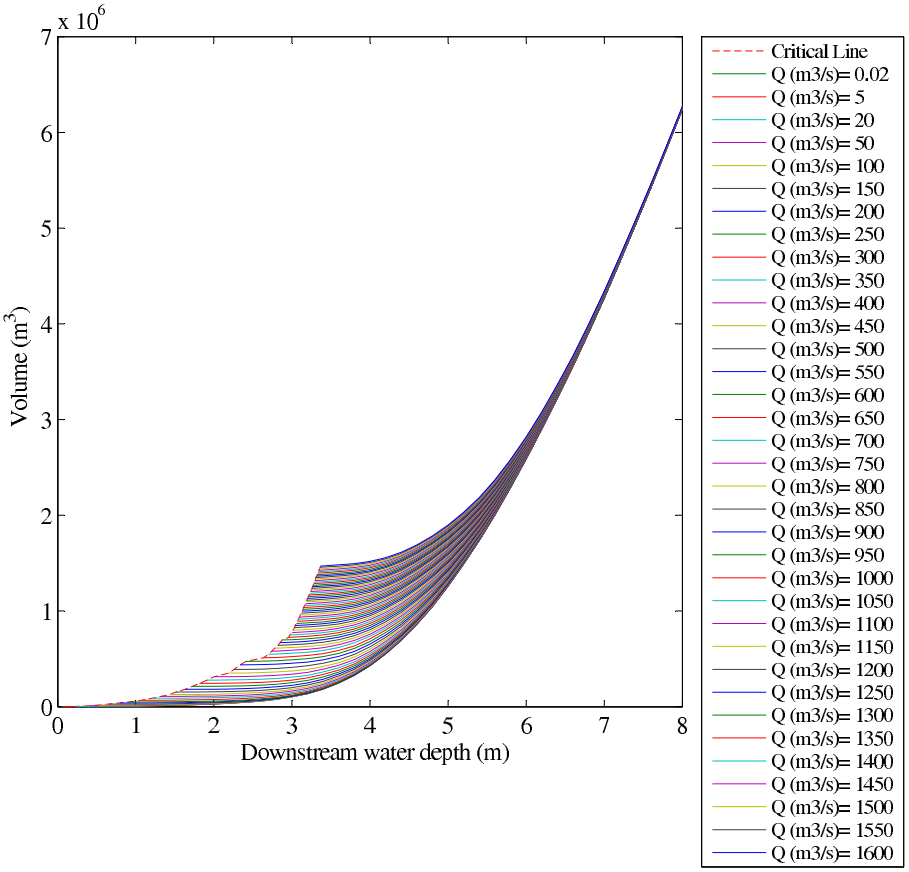

Figure B.19: Volume Performance Graph - Reach R19

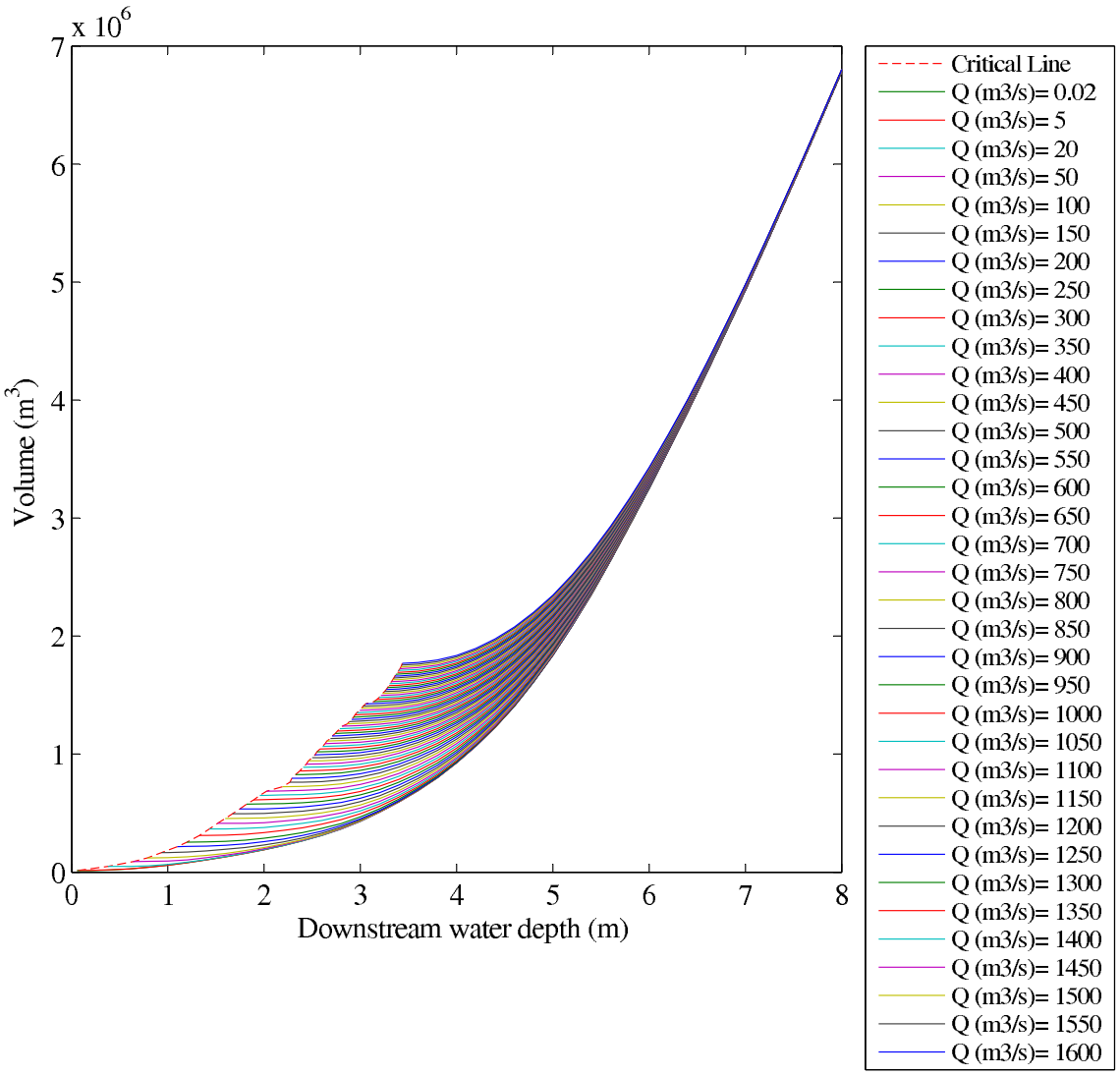

Figure B.20: Volume Performance Graph - Reach R20

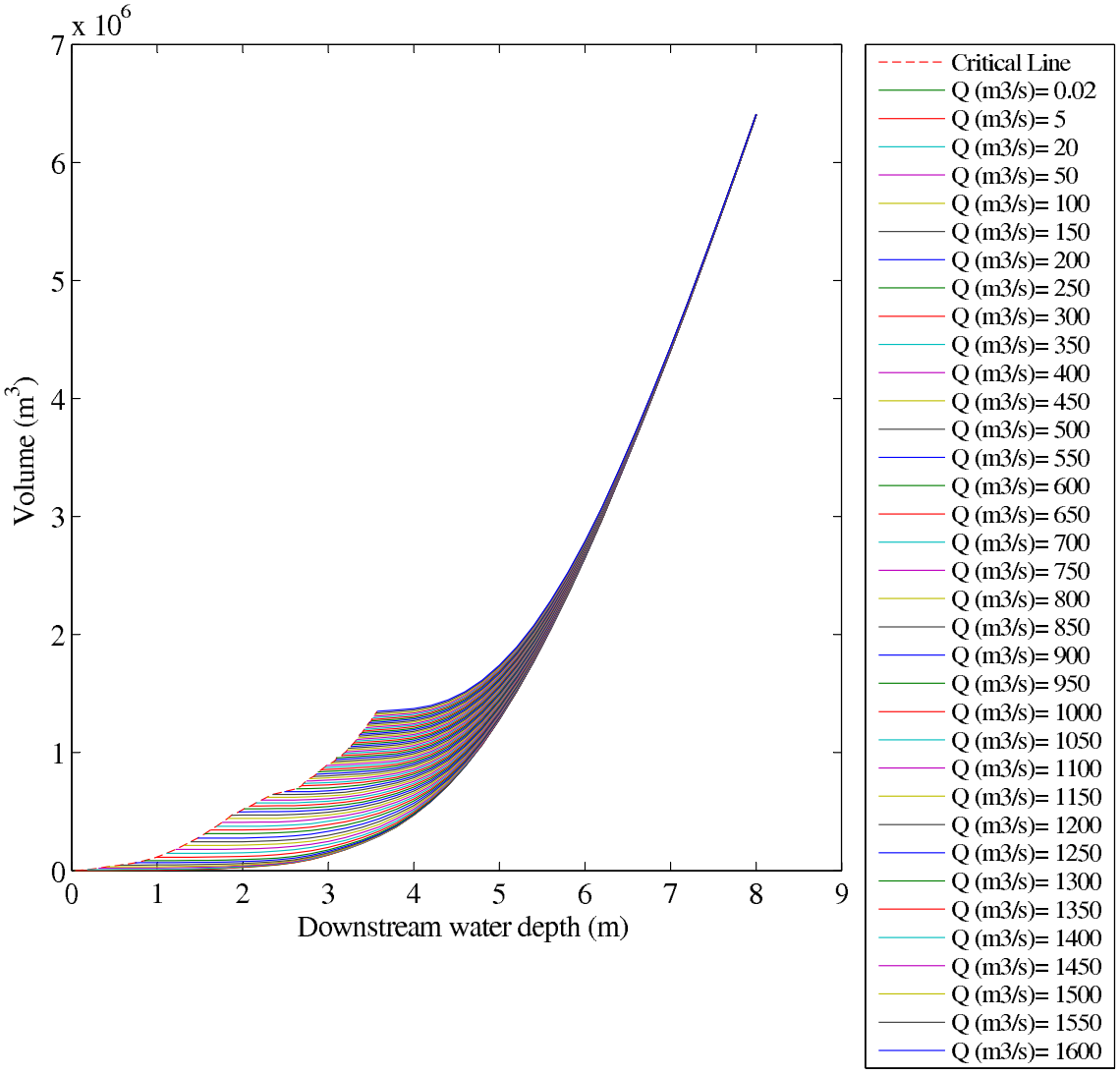

Figure B.21: Volume Performance Graph - Reach R21

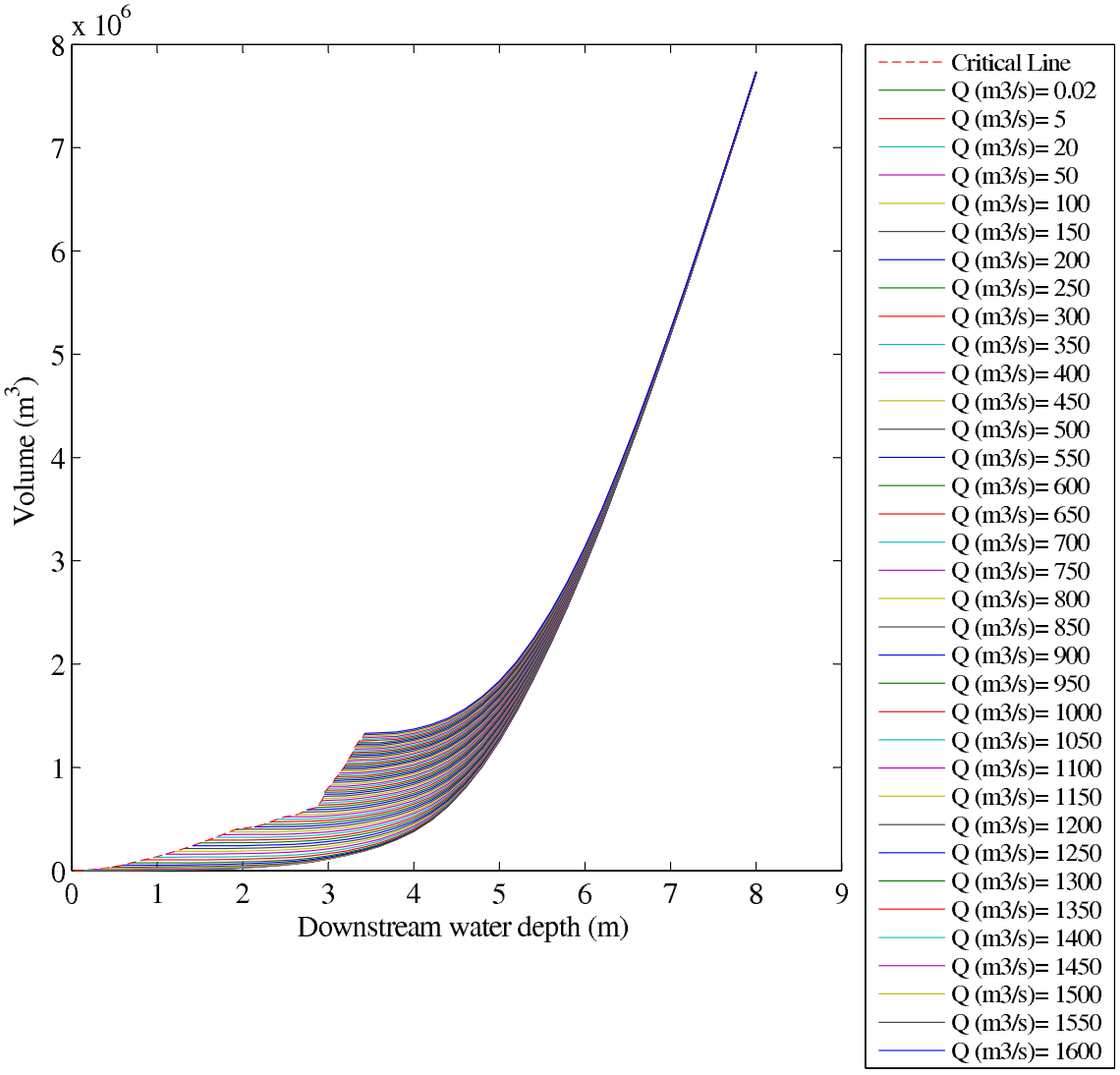

Figure B.22: Volume Performance Graph - Reach R22

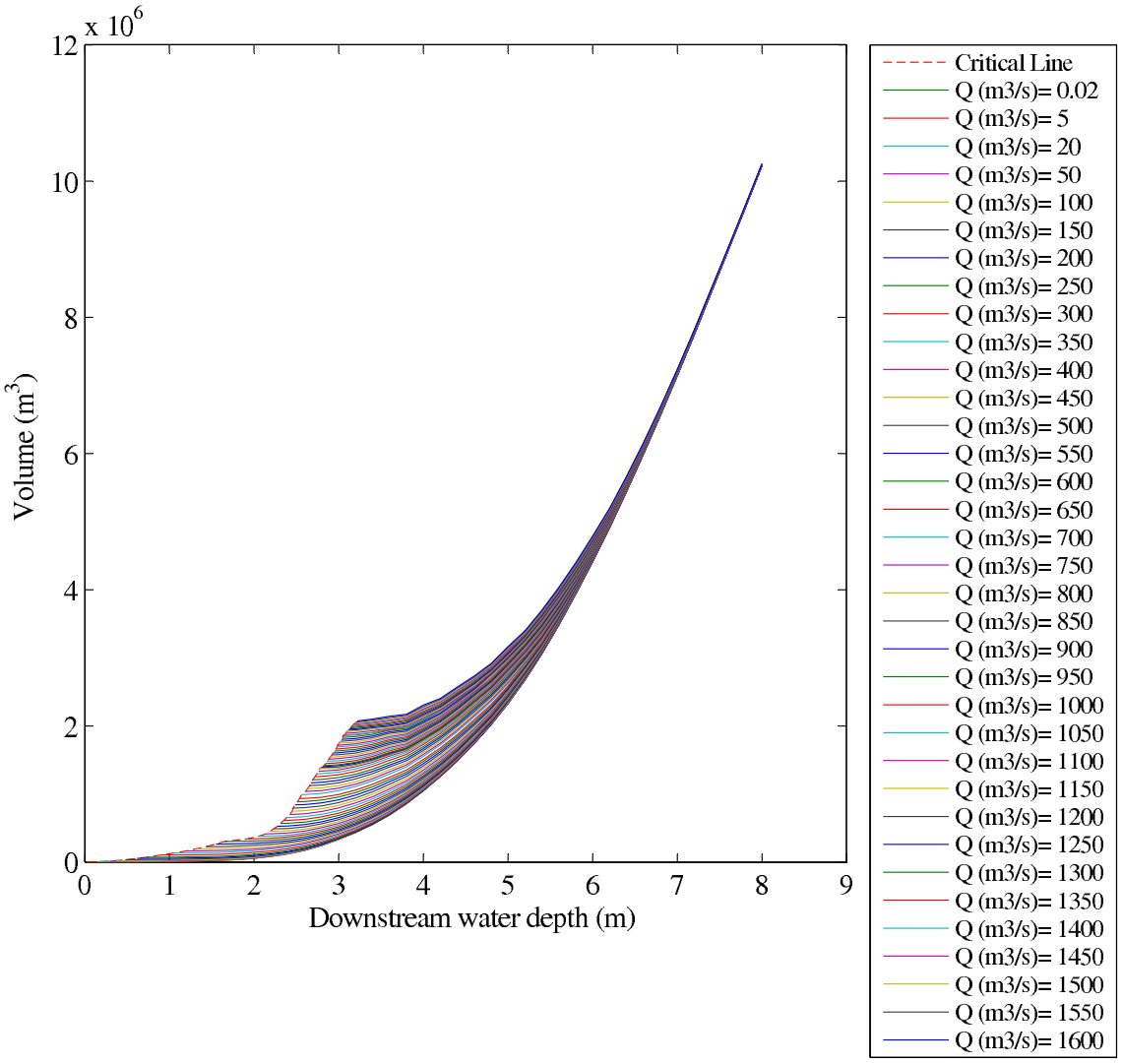

Figure B.23: Volume Performance Graph - Reach R23

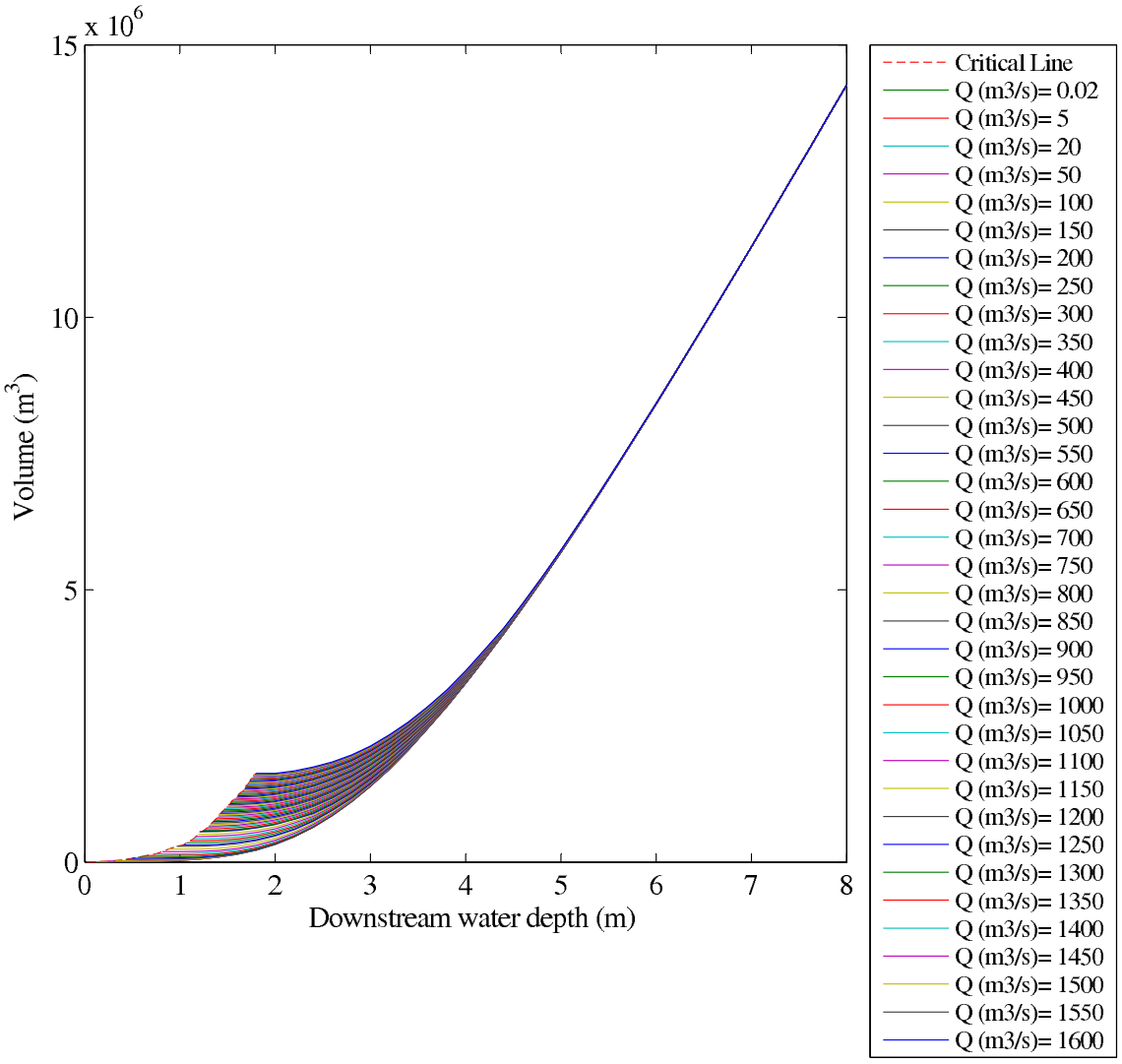

Figure B.24: Volume Performance Graph - Reach R24

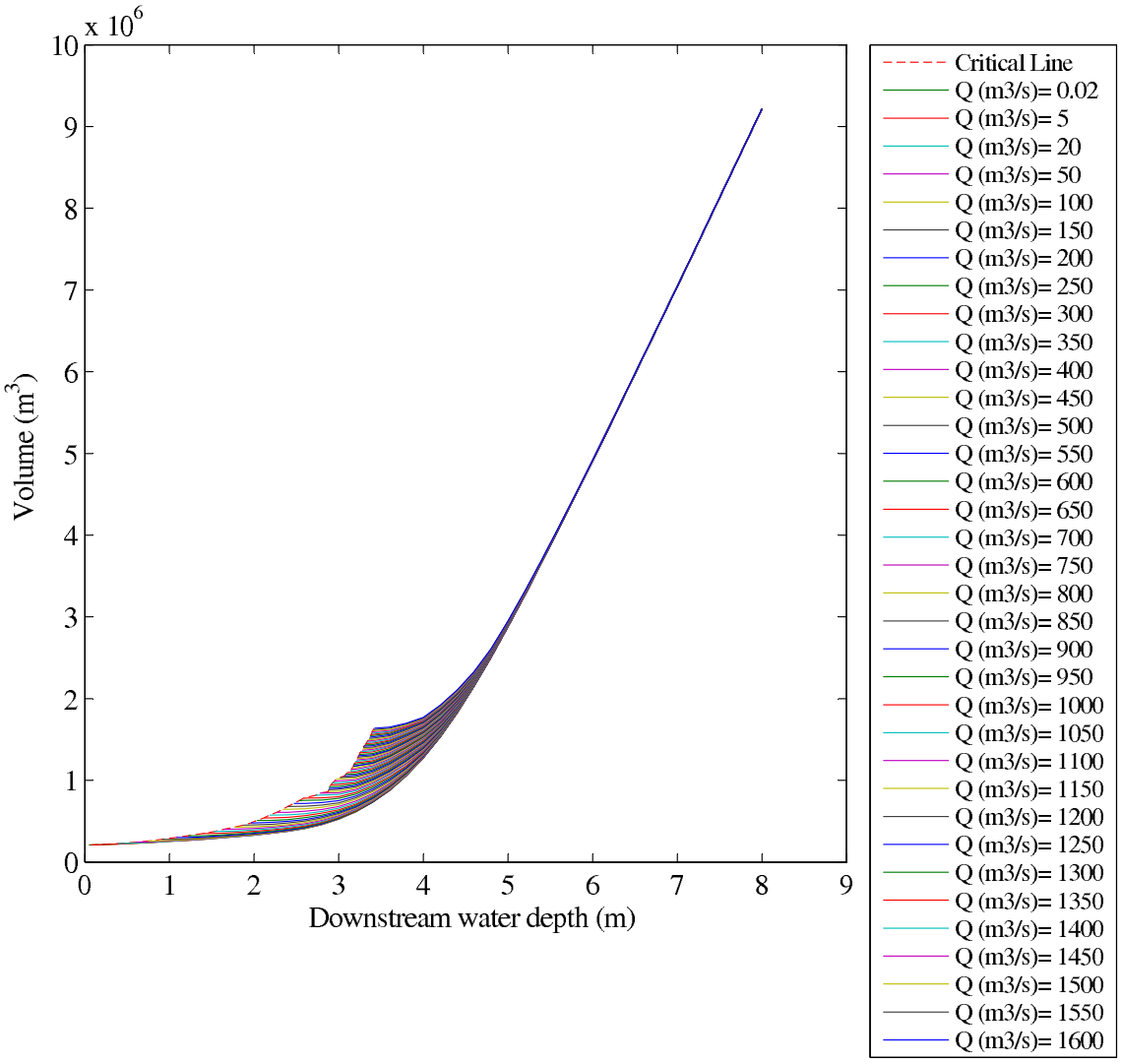

Figure B.25: Volume Performance Graph - Reach R25

APPENDIX C

LEFT FLOODING PERFORMANCE GRAPH

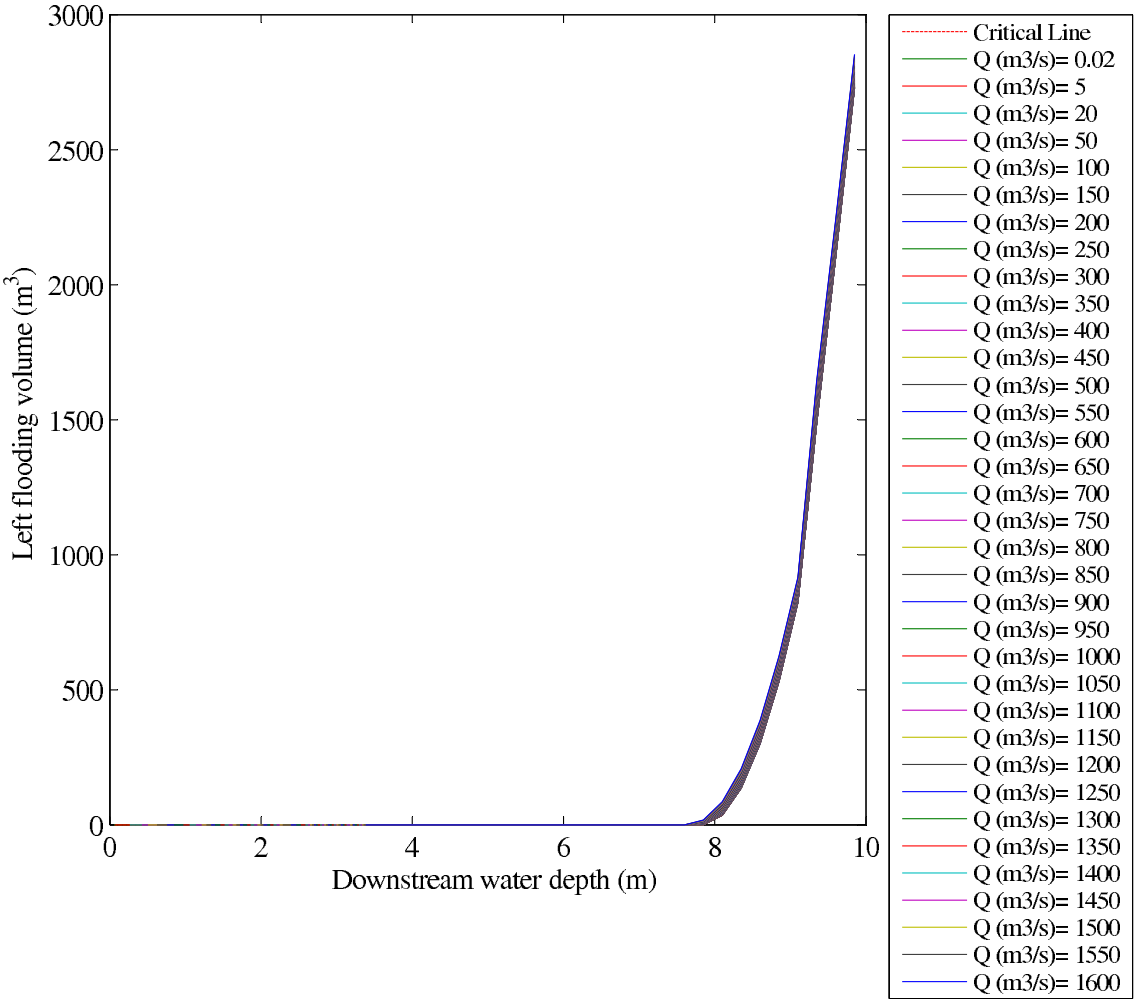

Figure C.1: Left Flooding Performance Graph - Reach R1

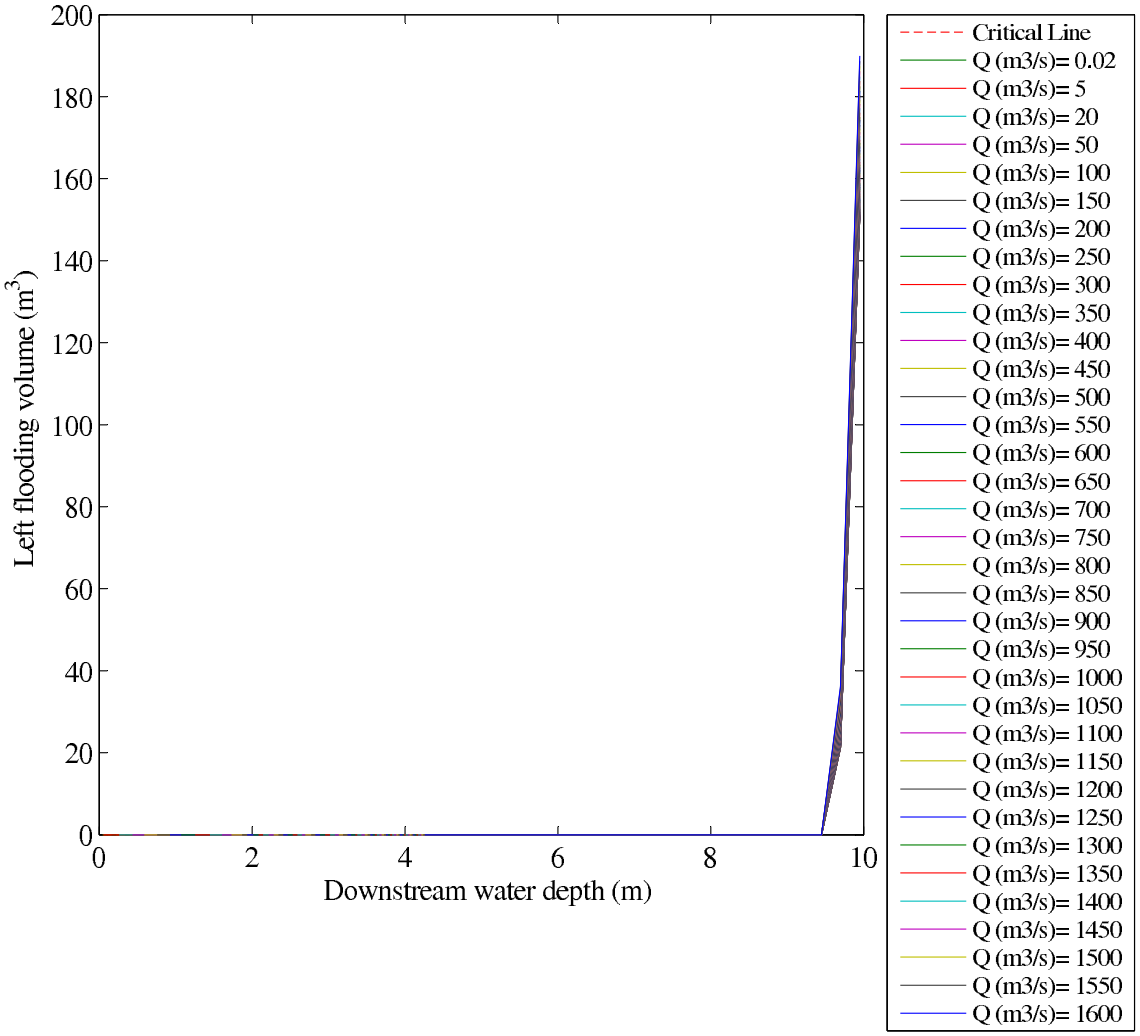

Figure C.2: Left Flooding Performance Graph - Reach R2

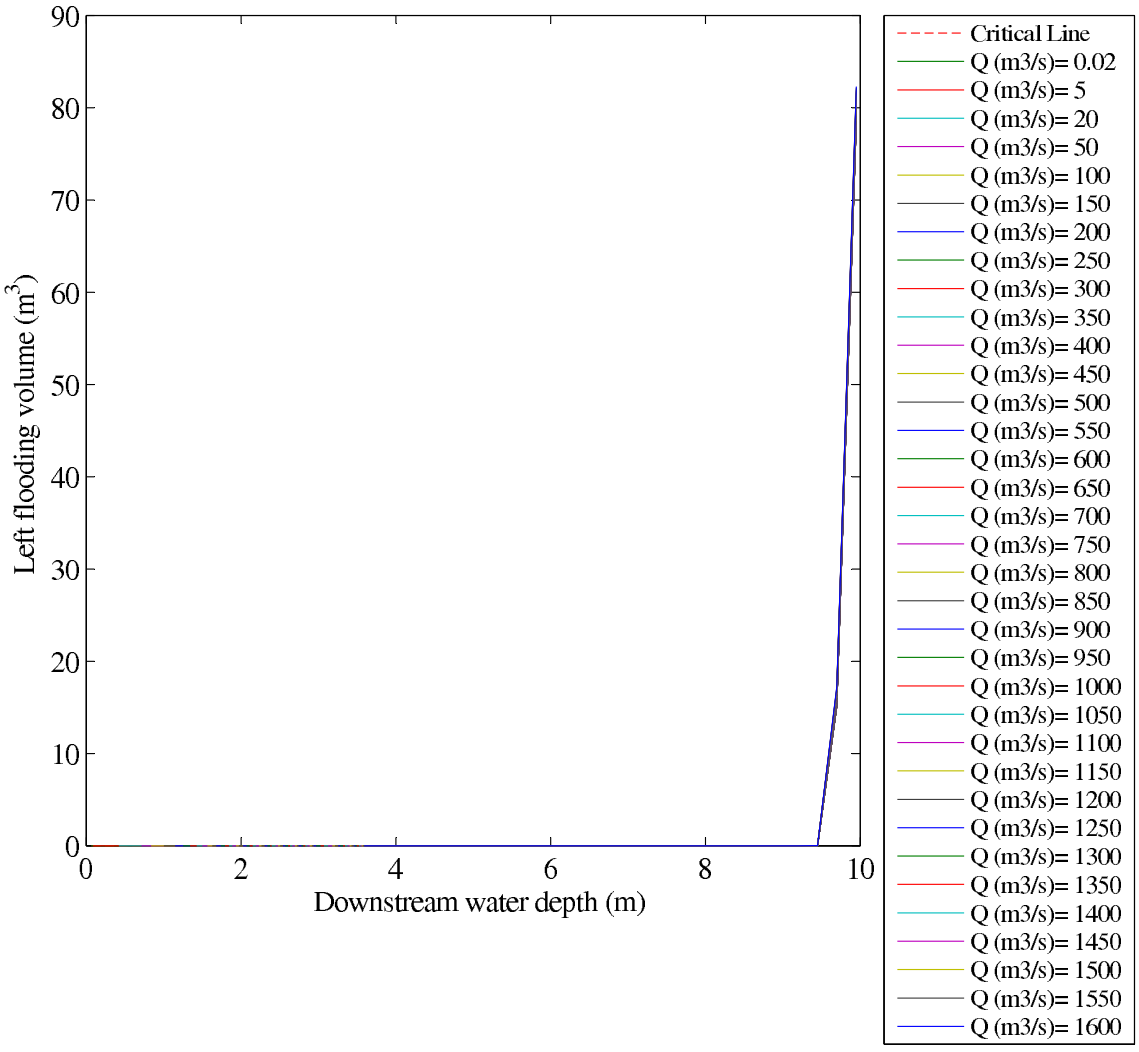

Figure C.3: Left Flooding Performance Graph - Reach R3

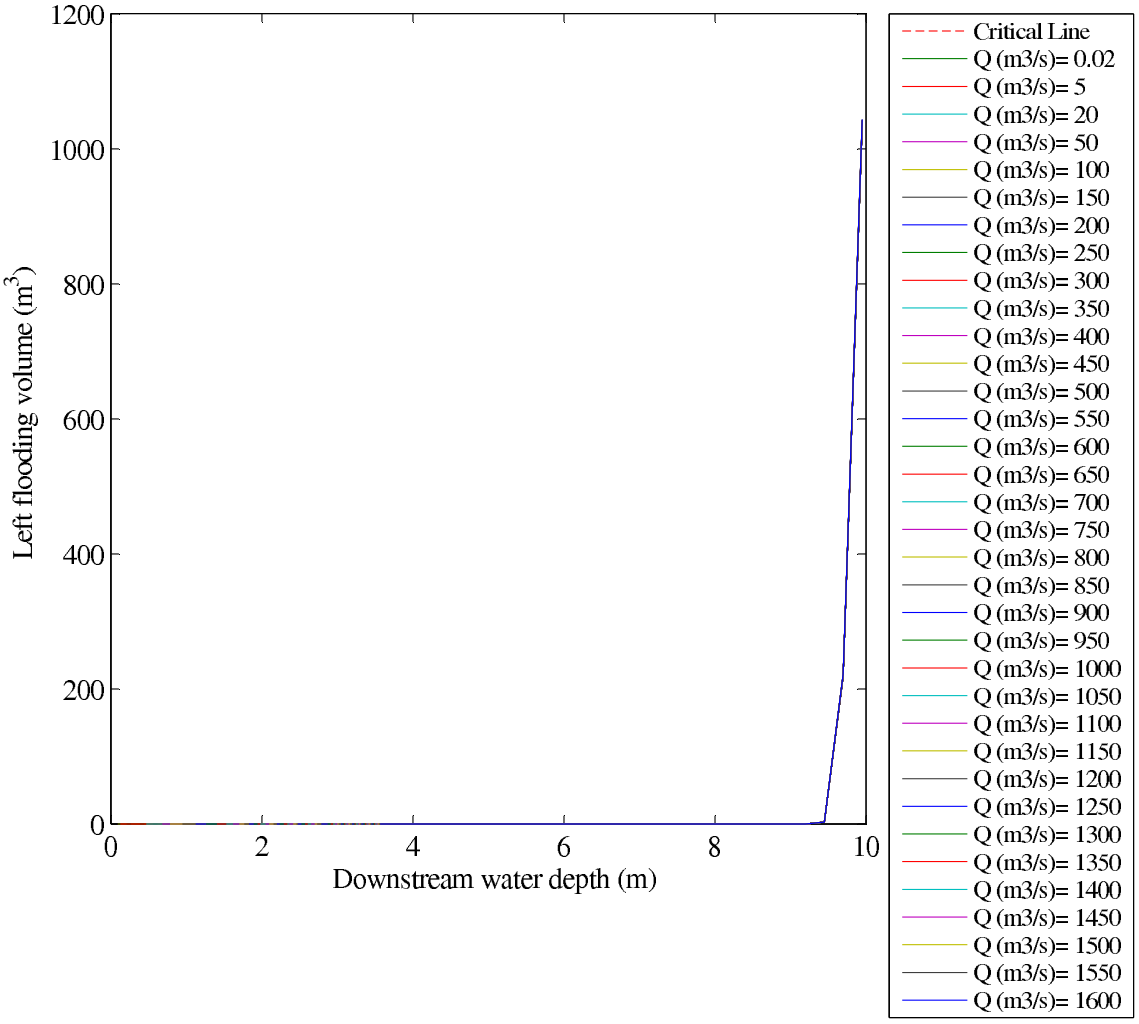

Figure C.4: Left Flooding Performance Graph - Reach R4

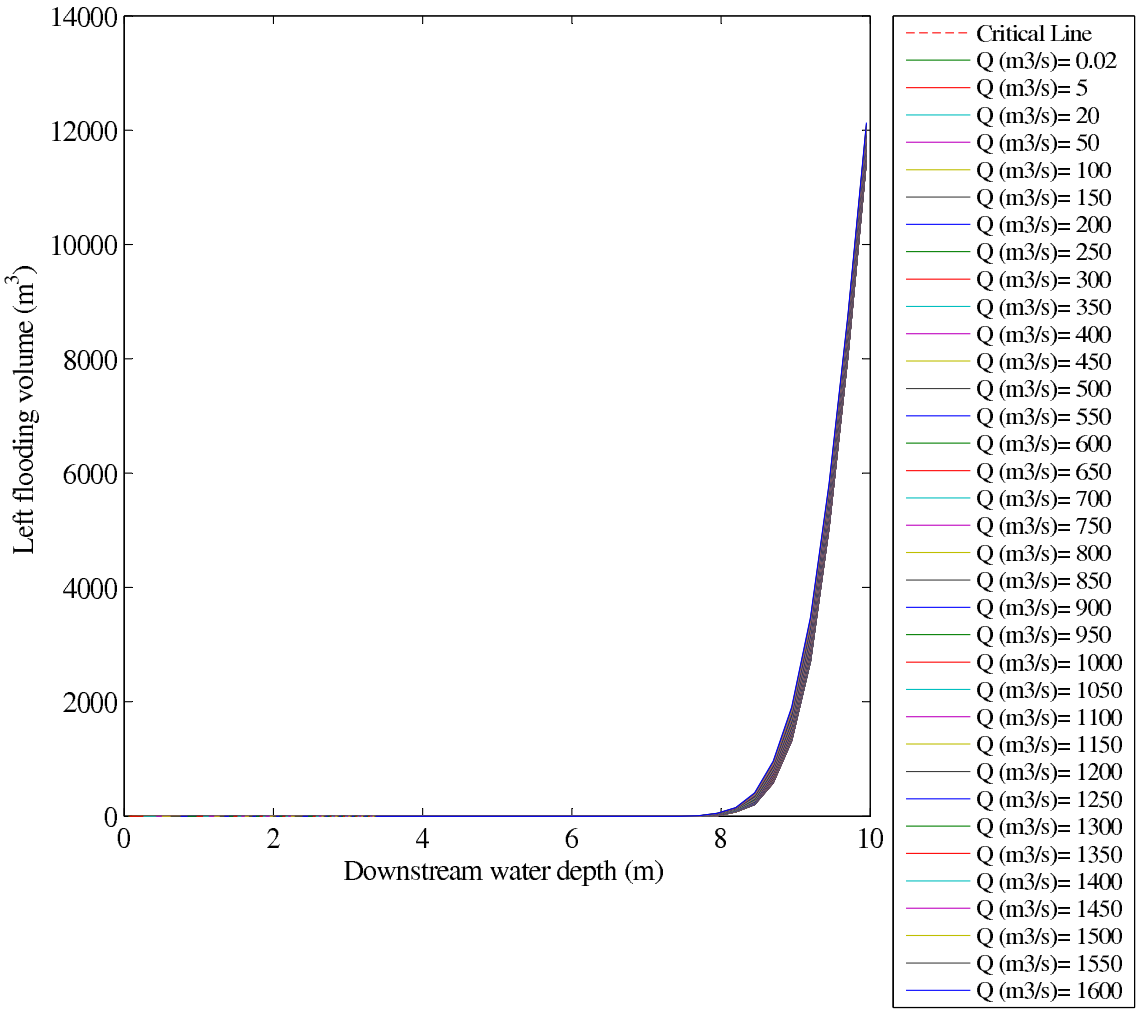

Figure C.5: Left Flooding Performance Graph - Reach R5

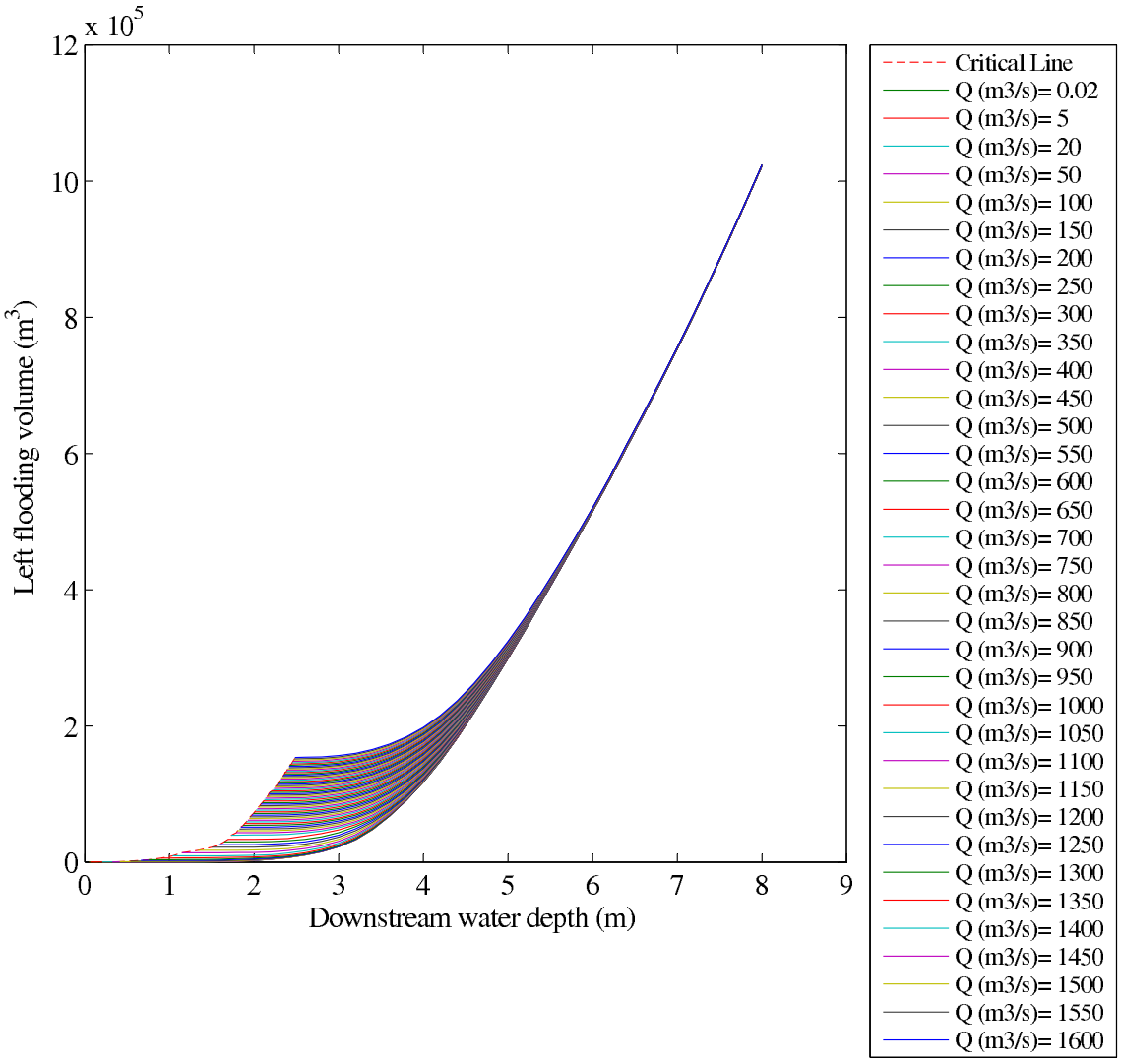

Figure C.6: Left Flooding Performance Graph - Reach R6

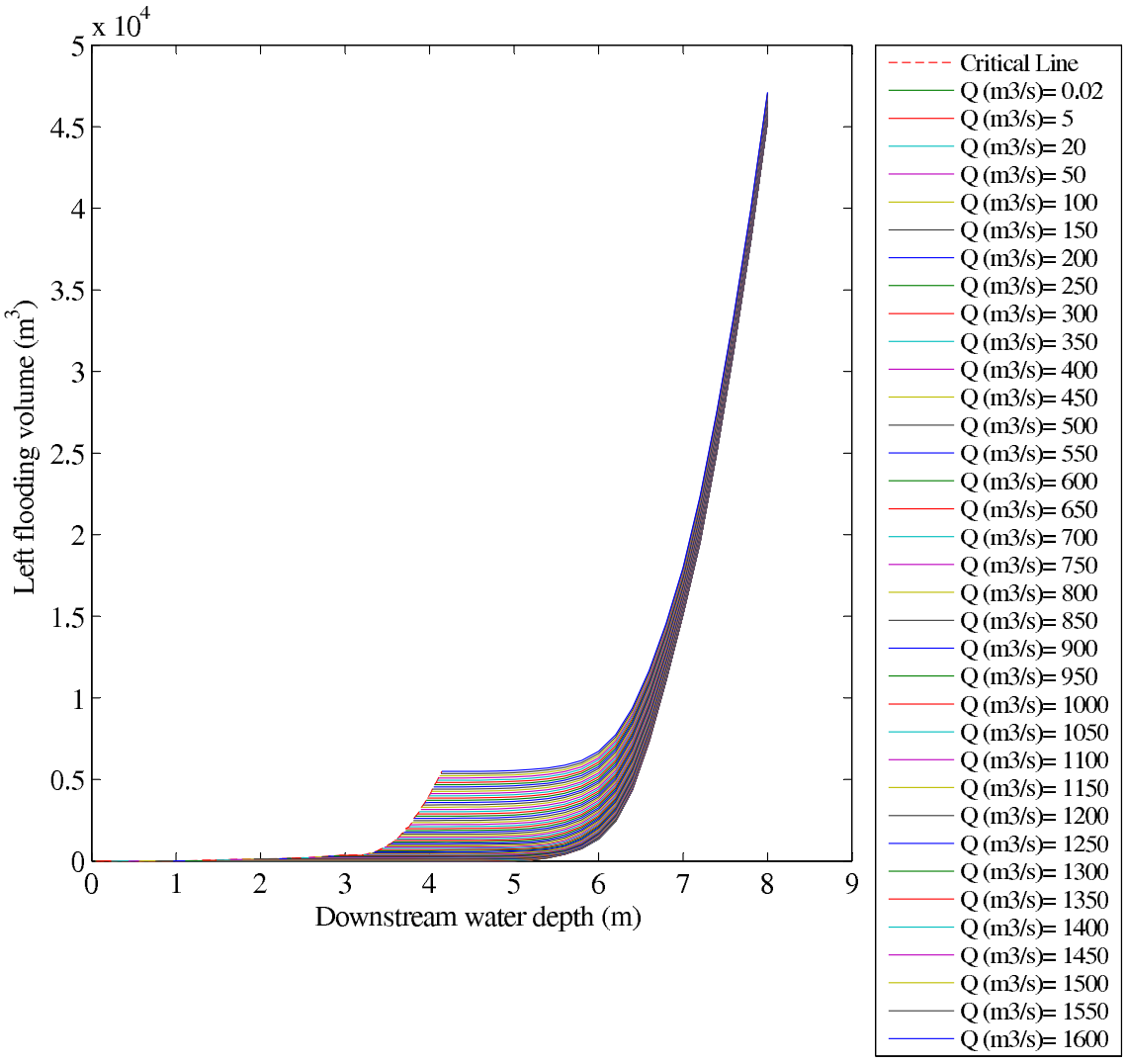

Figure C.7: Left Flooding Performance Graph - Reach R7

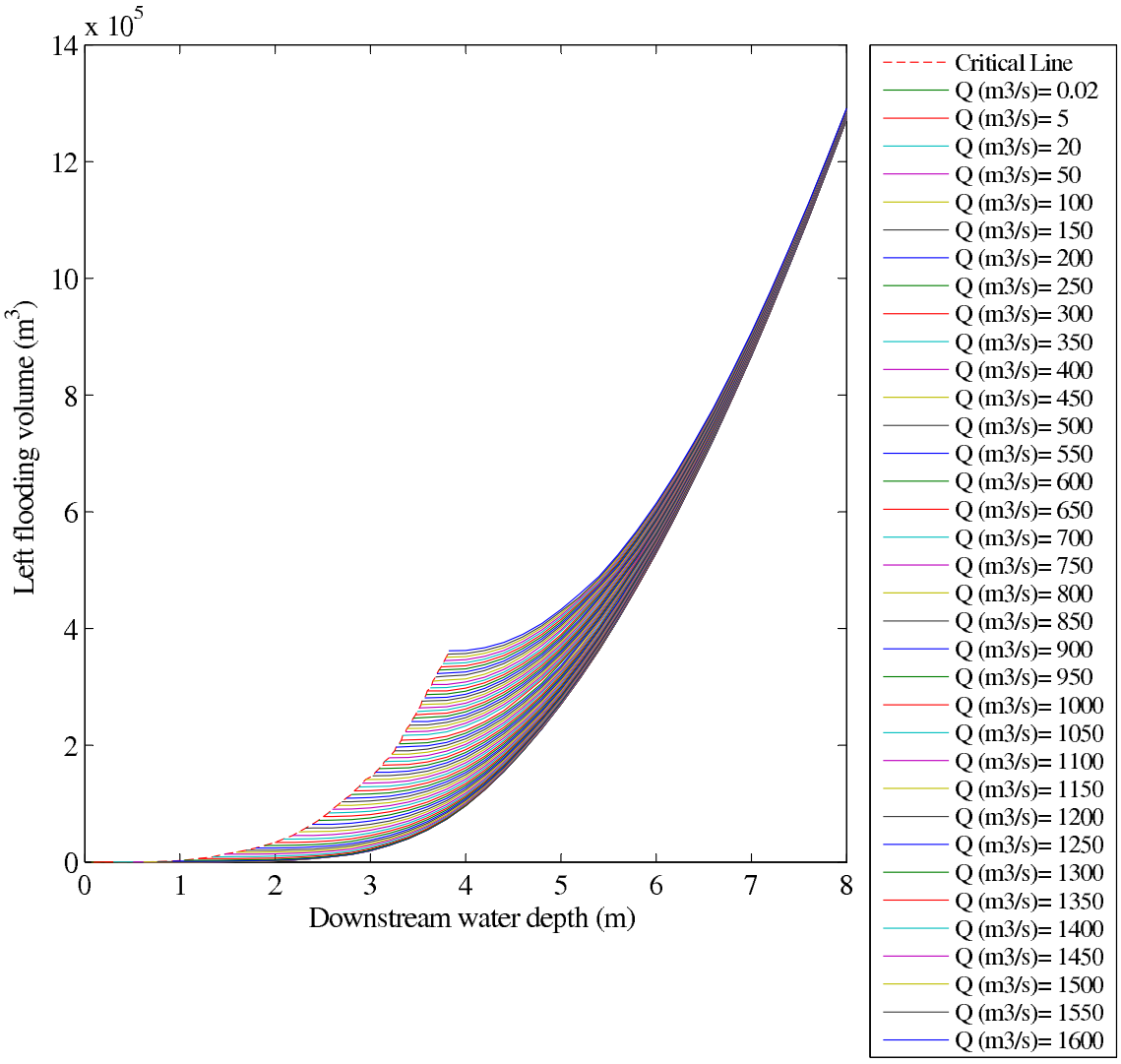

Figure C.8: Left Flooding Performance Graph - Reach R8

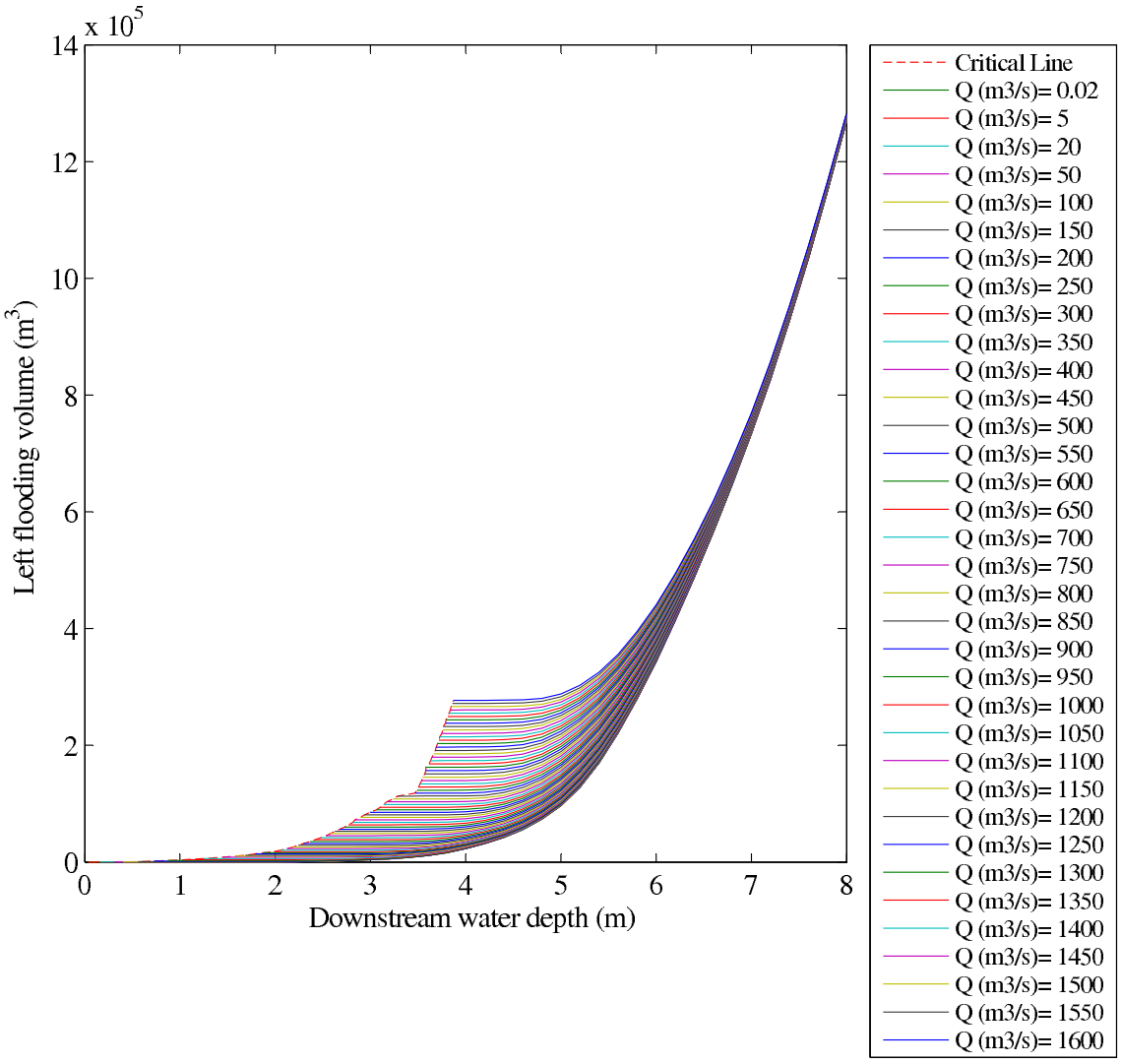

Figure C.9: Left Flooding Performance Graph - Reach R9

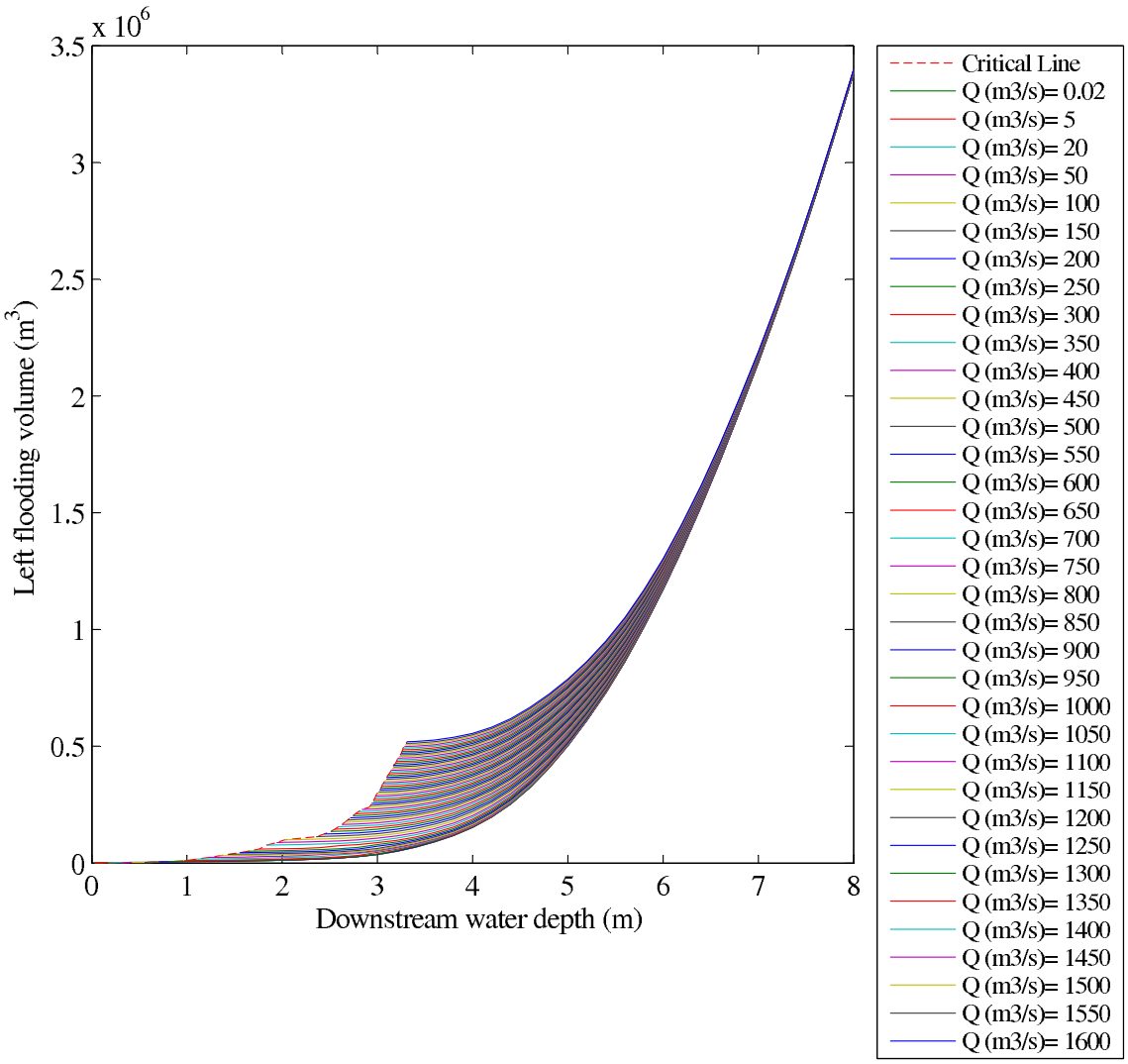

Figure C.10: Left Flooding Performance Graph - Reach R10

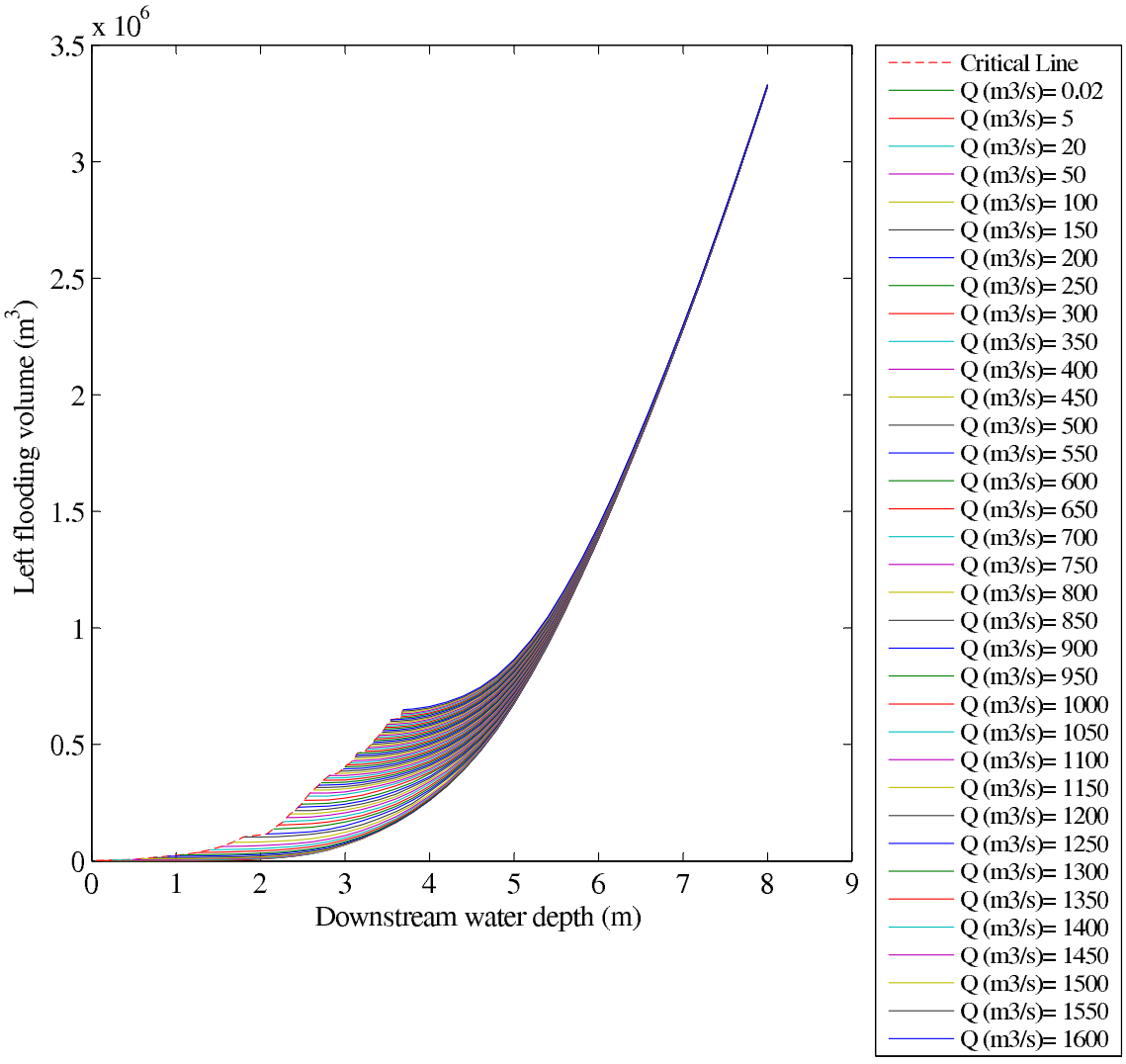

Figure C.11: Left Flooding Performance Graph - Reach R11

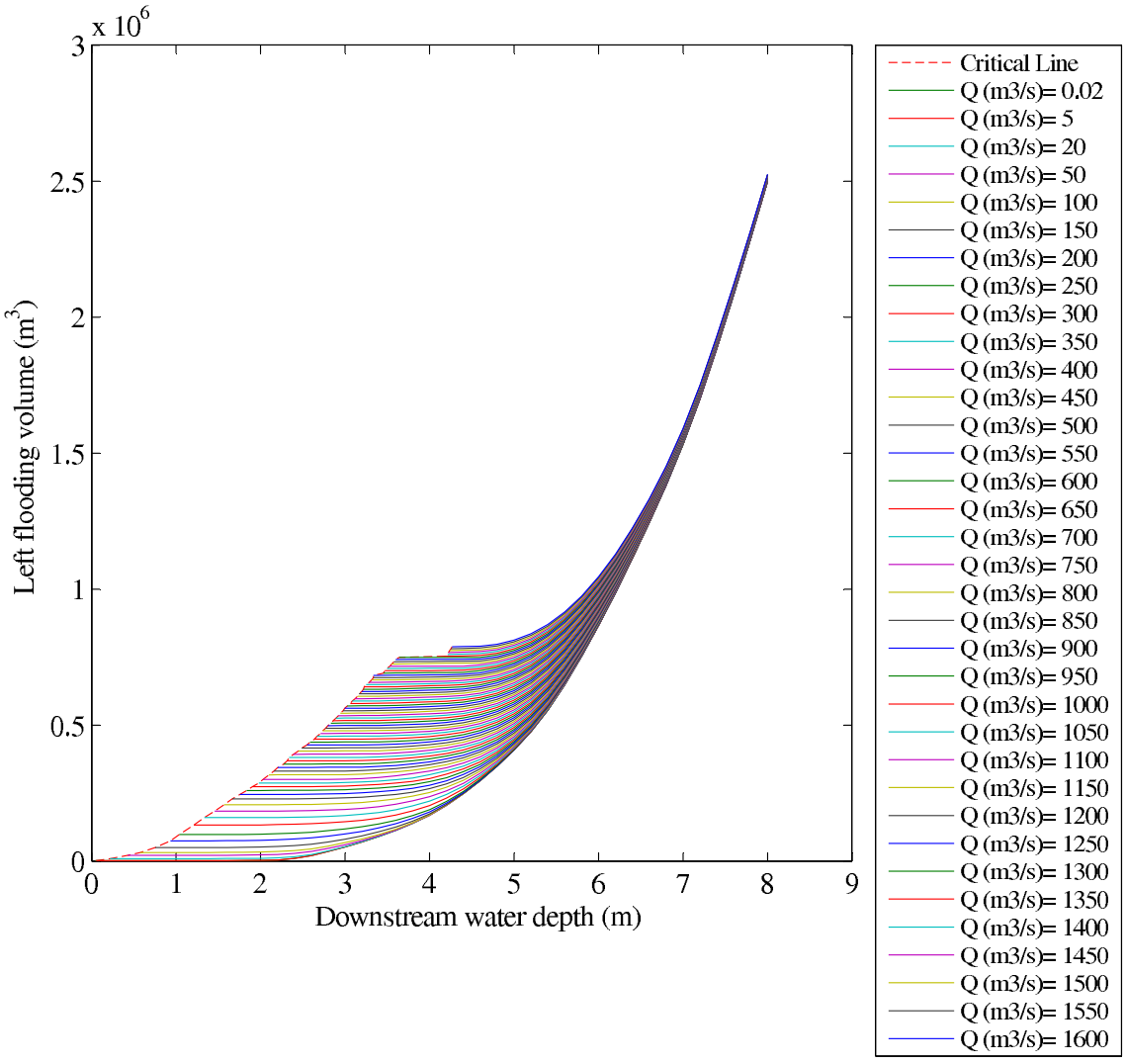

Figure C.12: Left Flooding Performance Graph - Reach R12

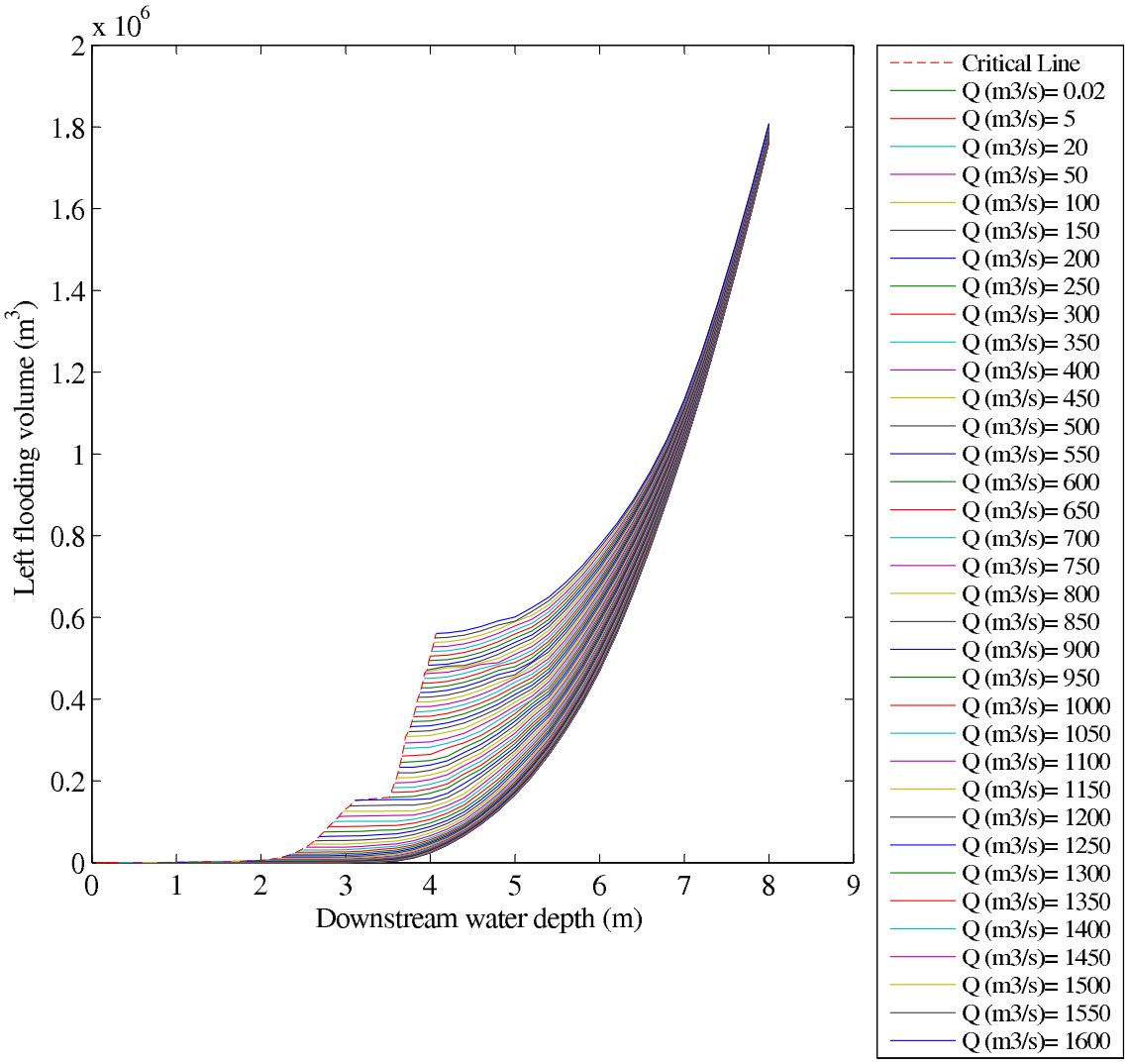

Figure C.13: Left Flooding Performance Graph - Reach R13

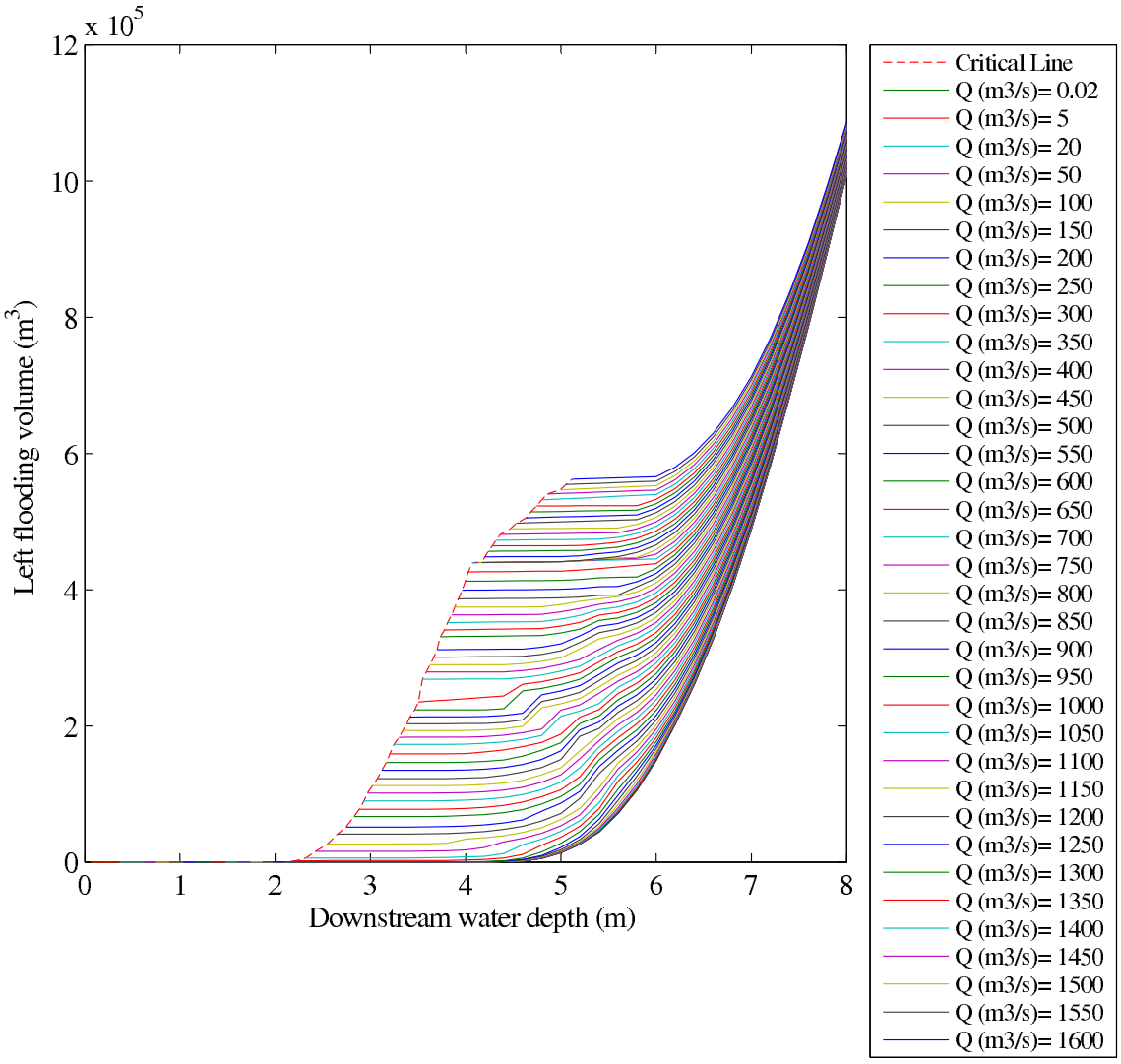

Figure C.14: Left Flooding Performance Graph - Reach R14

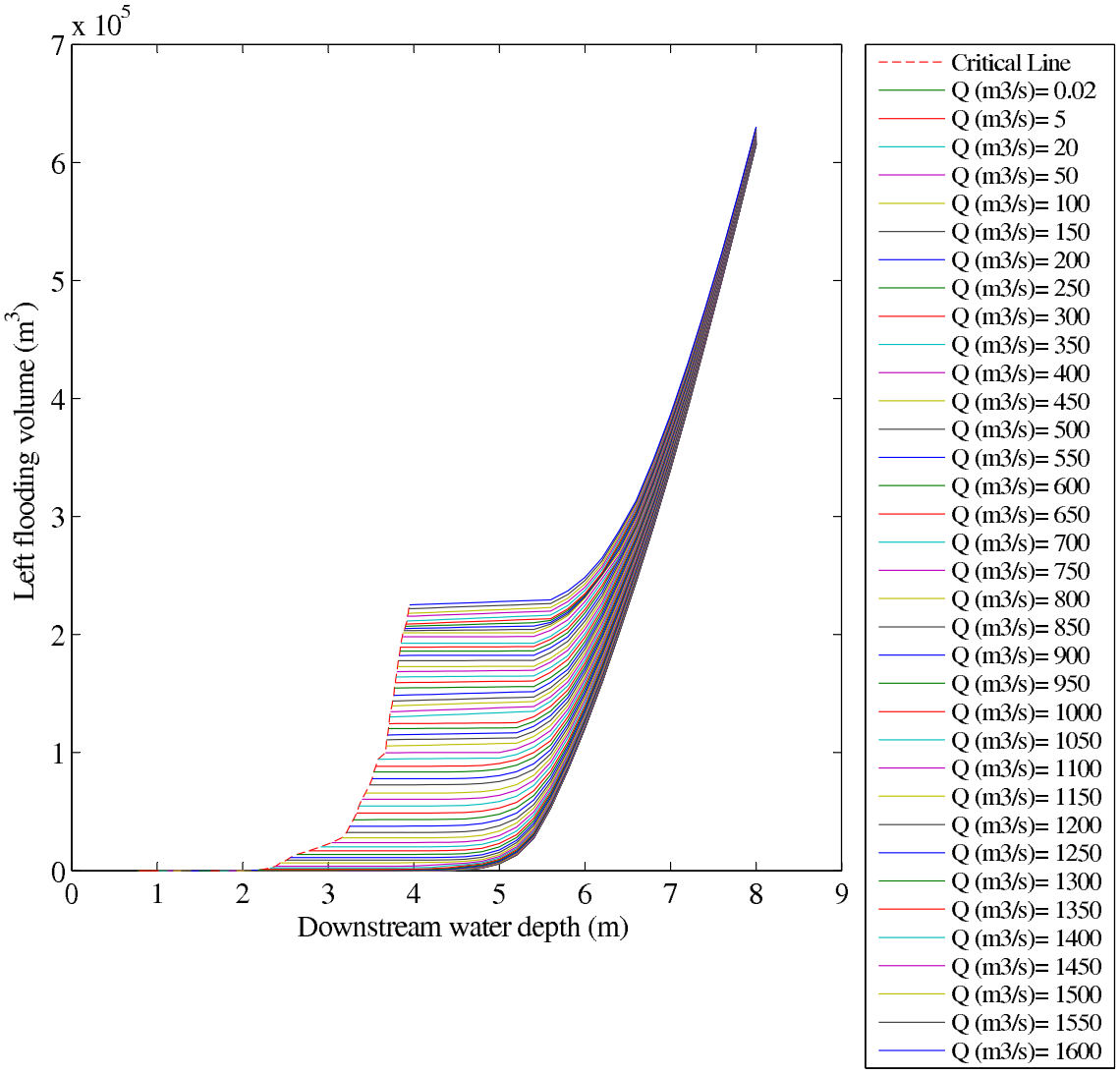

Figure C.15: Left Flooding Performance Graph - Reach R15

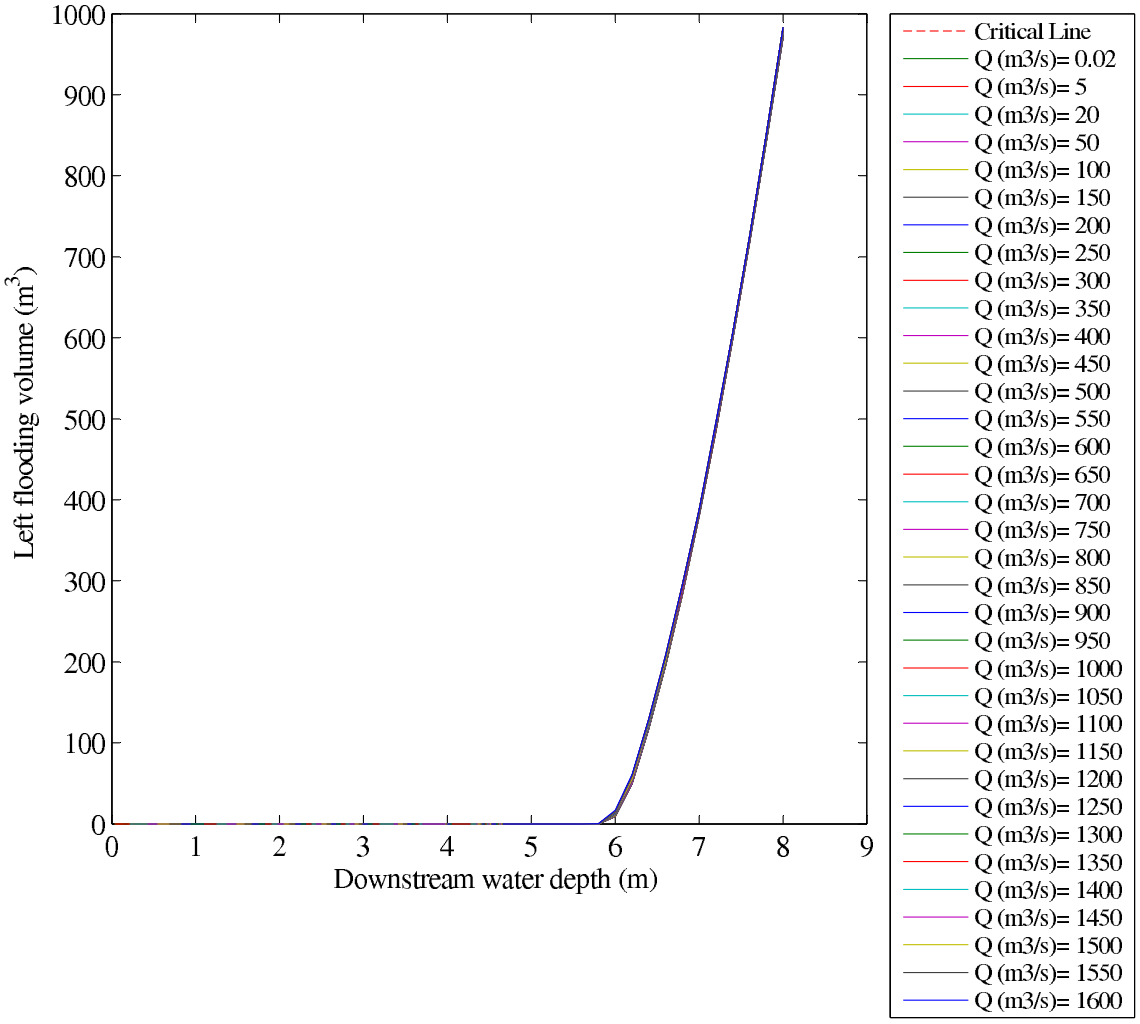

Figure C.16: Left Flooding Performance Graph - Reach R16

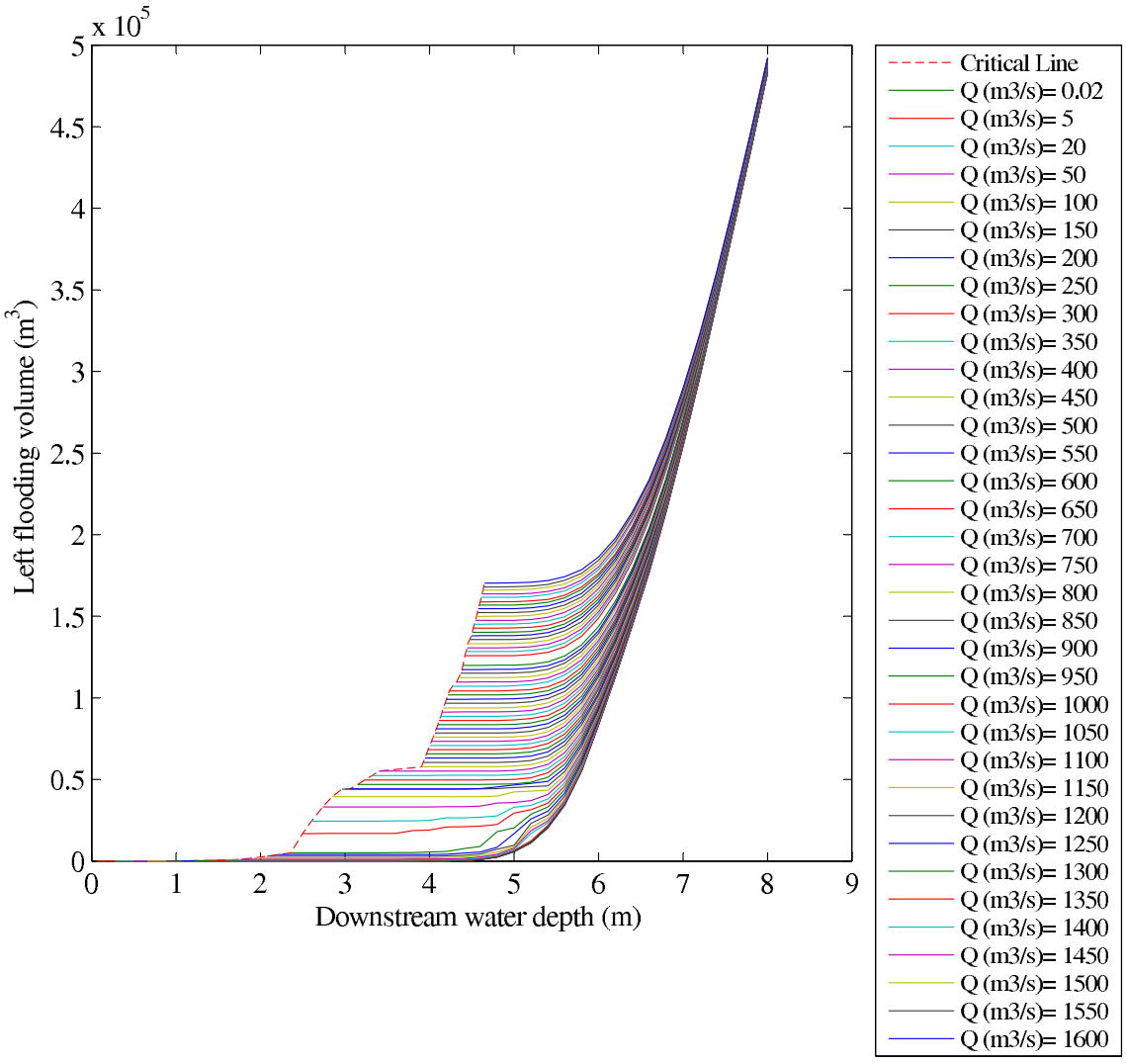

Figure C.17: Left Flooding Performance Graph - Reach R17

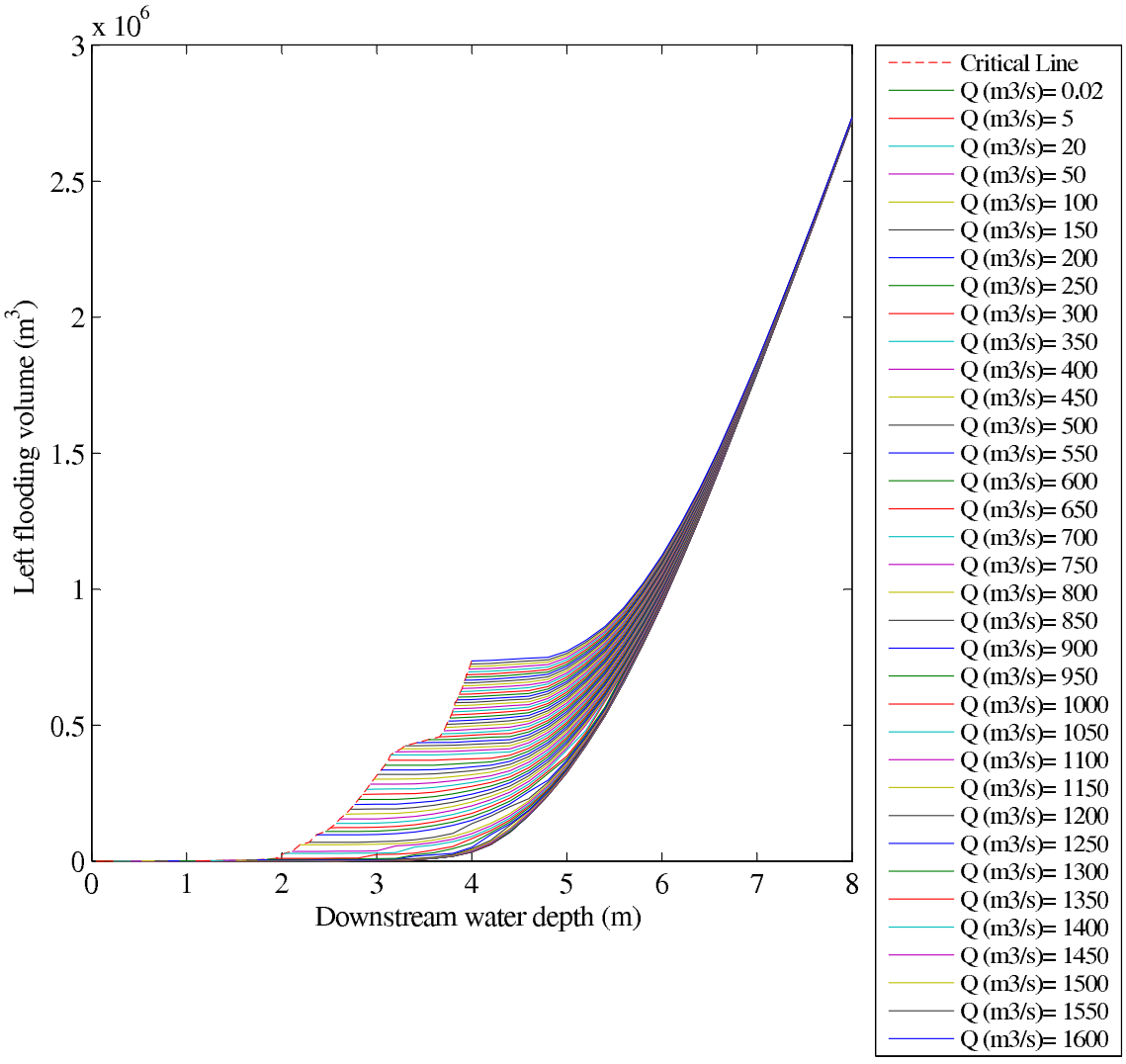

Figure C.18: Left Flooding Performance Graph - Reach R18

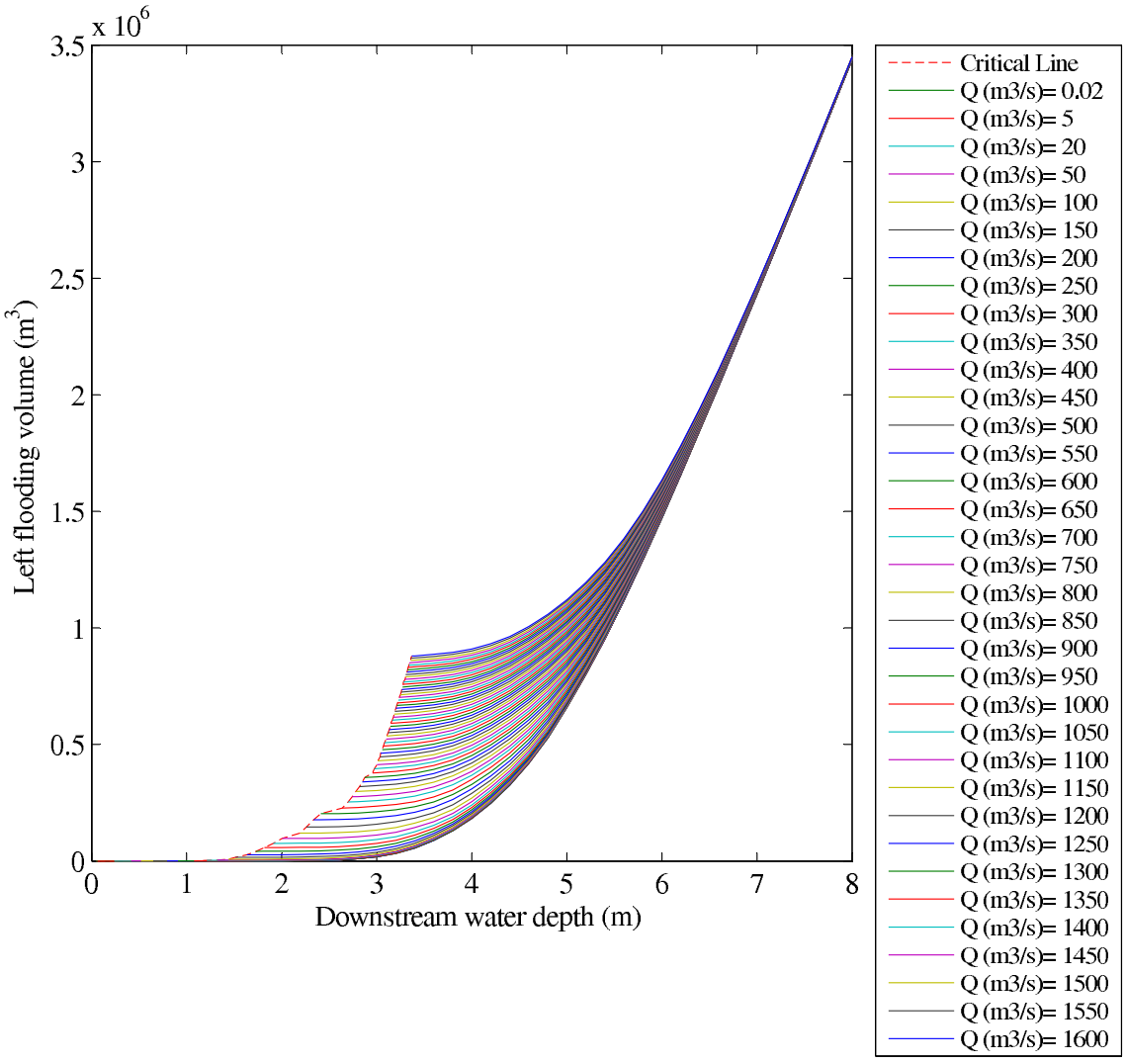

Figure C.19: Left Flooding Performance Graph - Reach R19

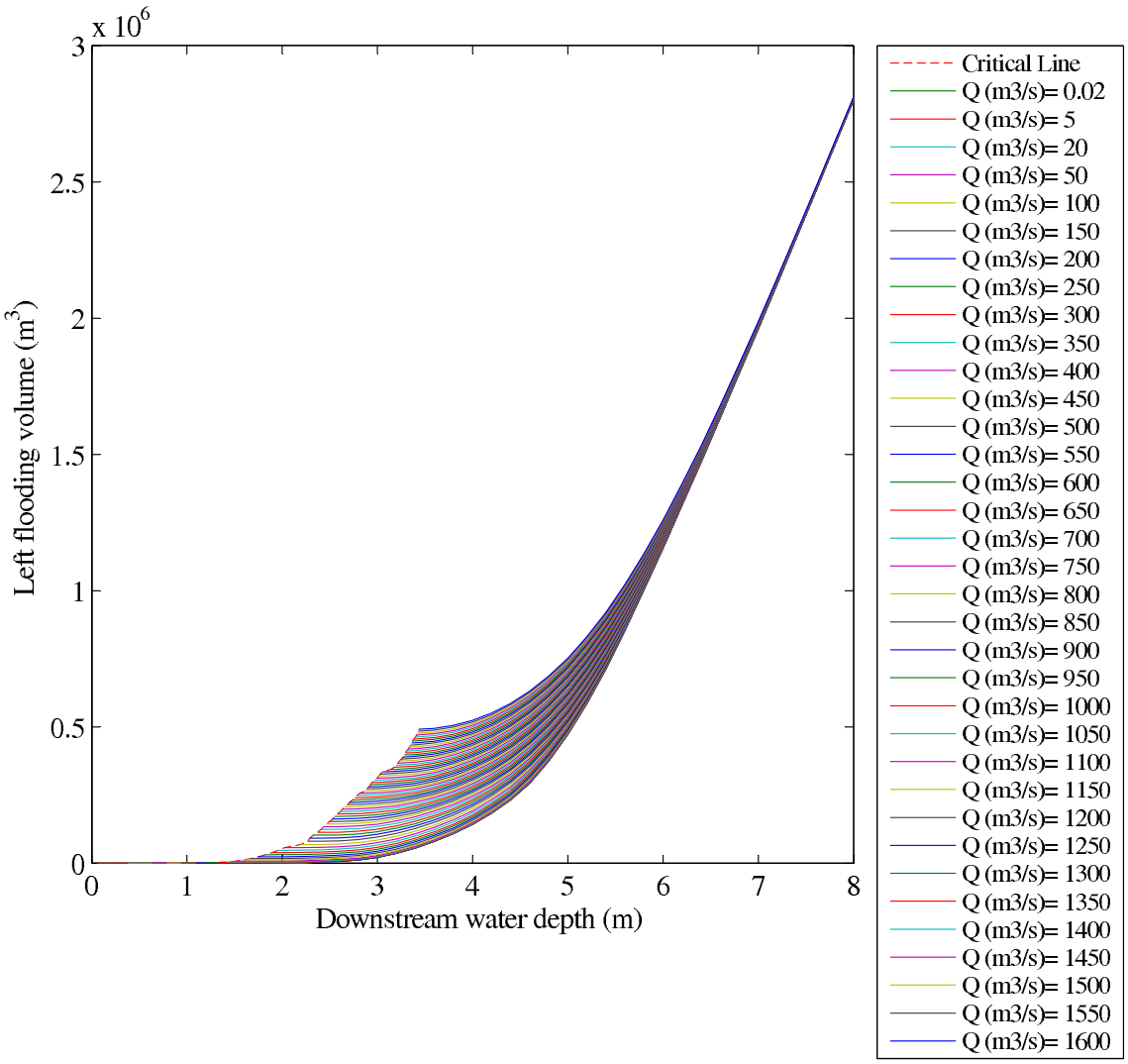

Figure C.20: Left Flooding Performance Graph - Reach R20

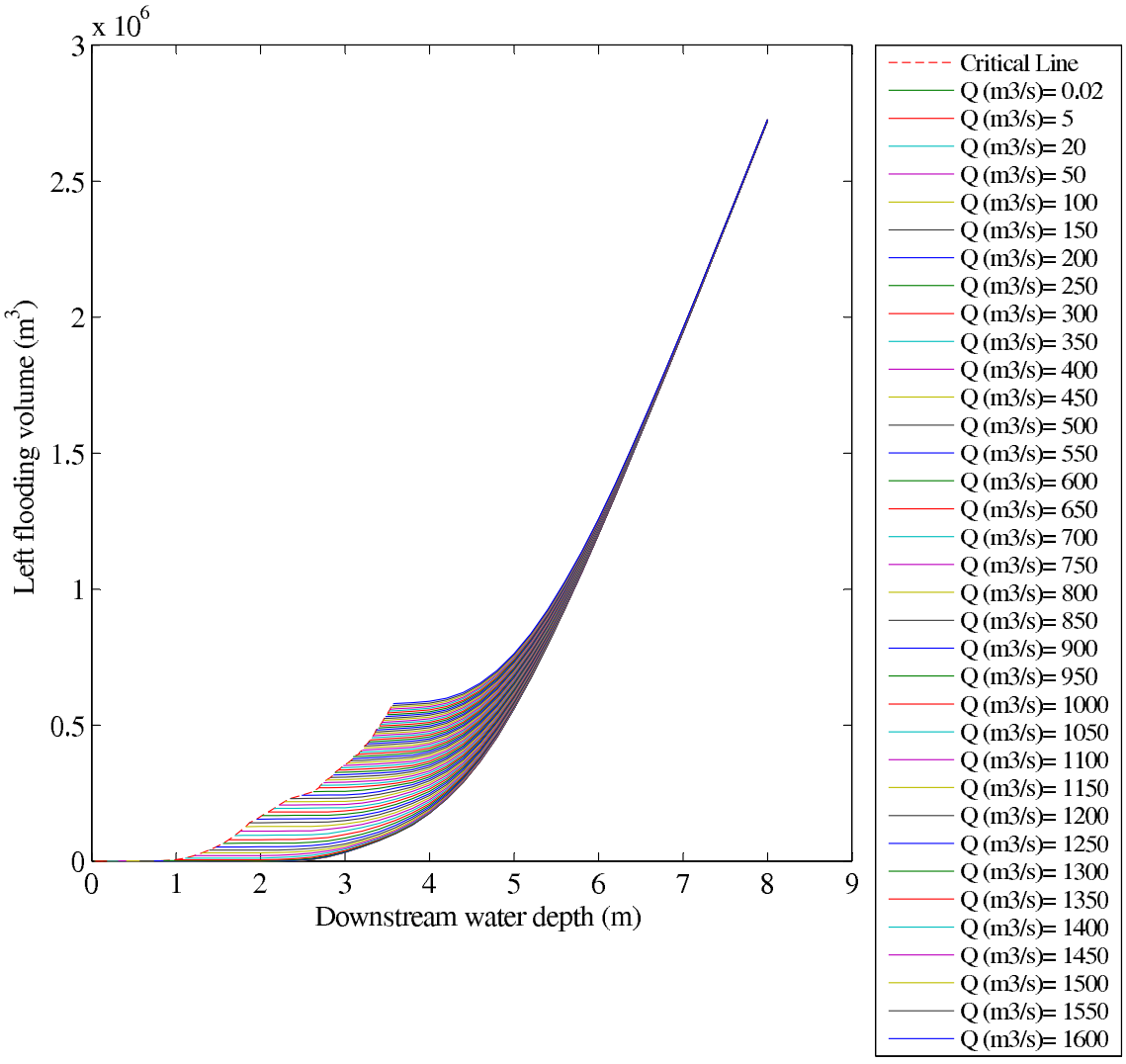

Figure C.21: Left Flooding Performance Graph - Reach R21

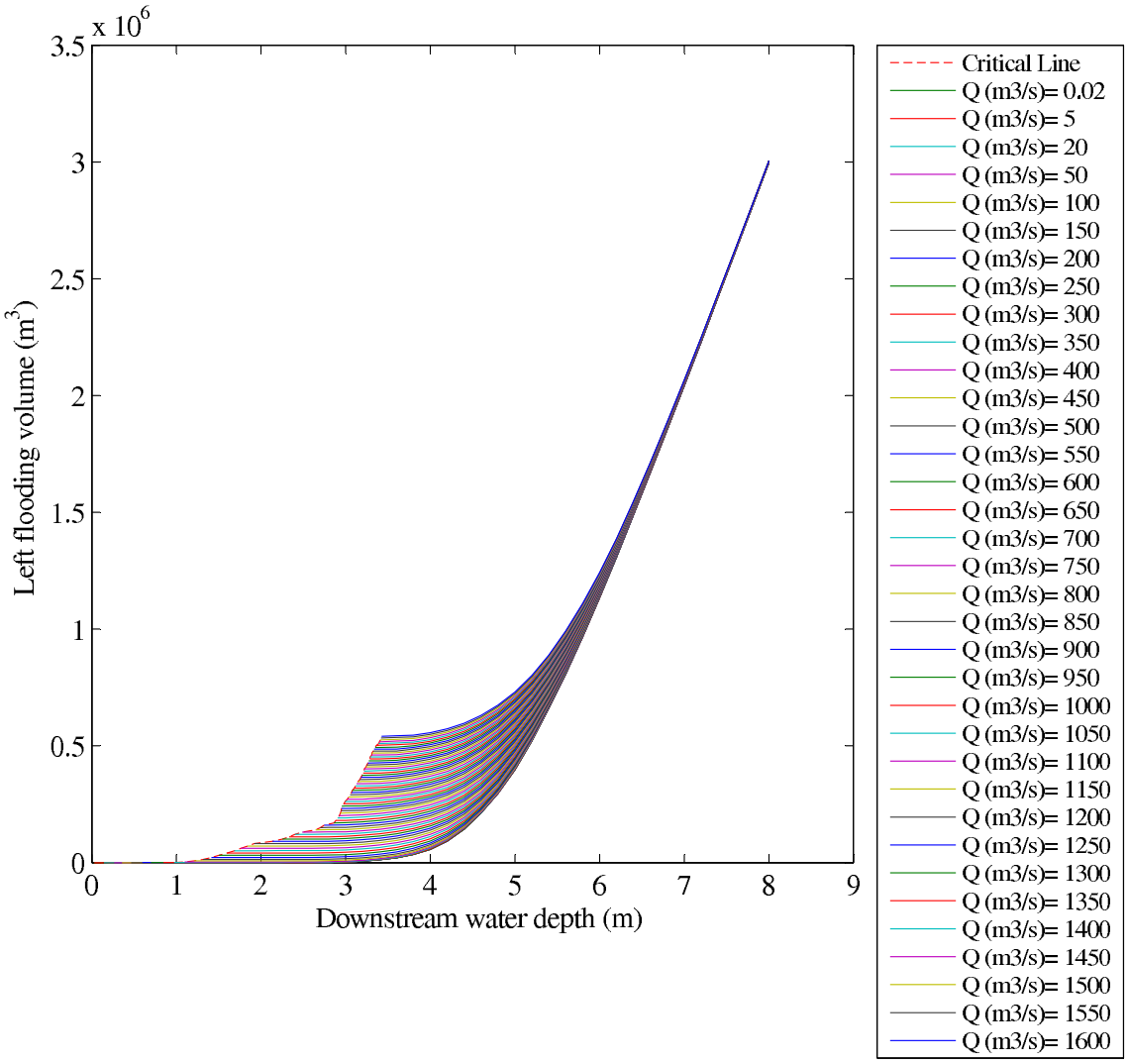

Figure C.22: Left Flooding Performance Graph - Reach R22

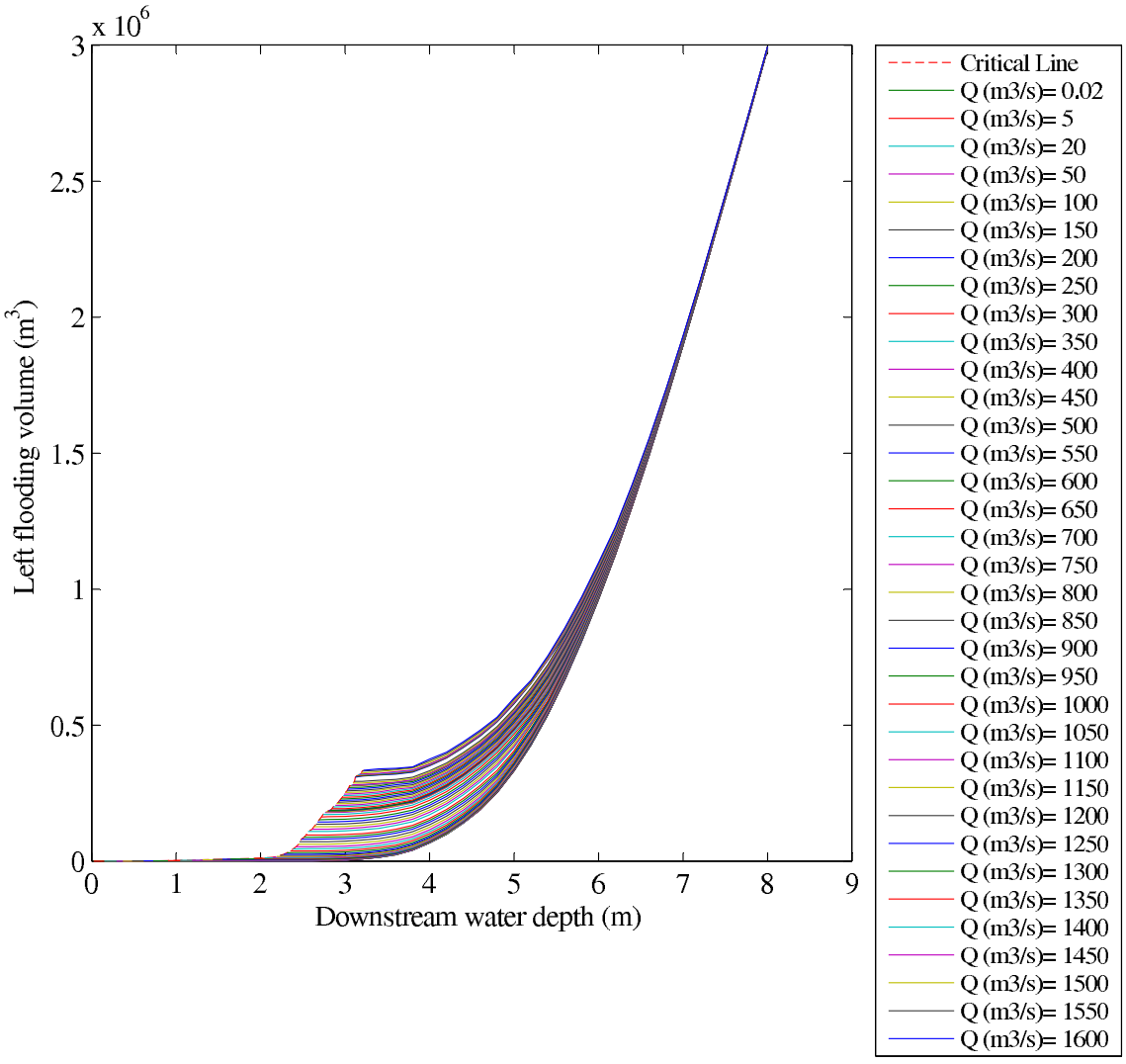

Figure C.23: Left Flooding Performance Graph - Reach R23

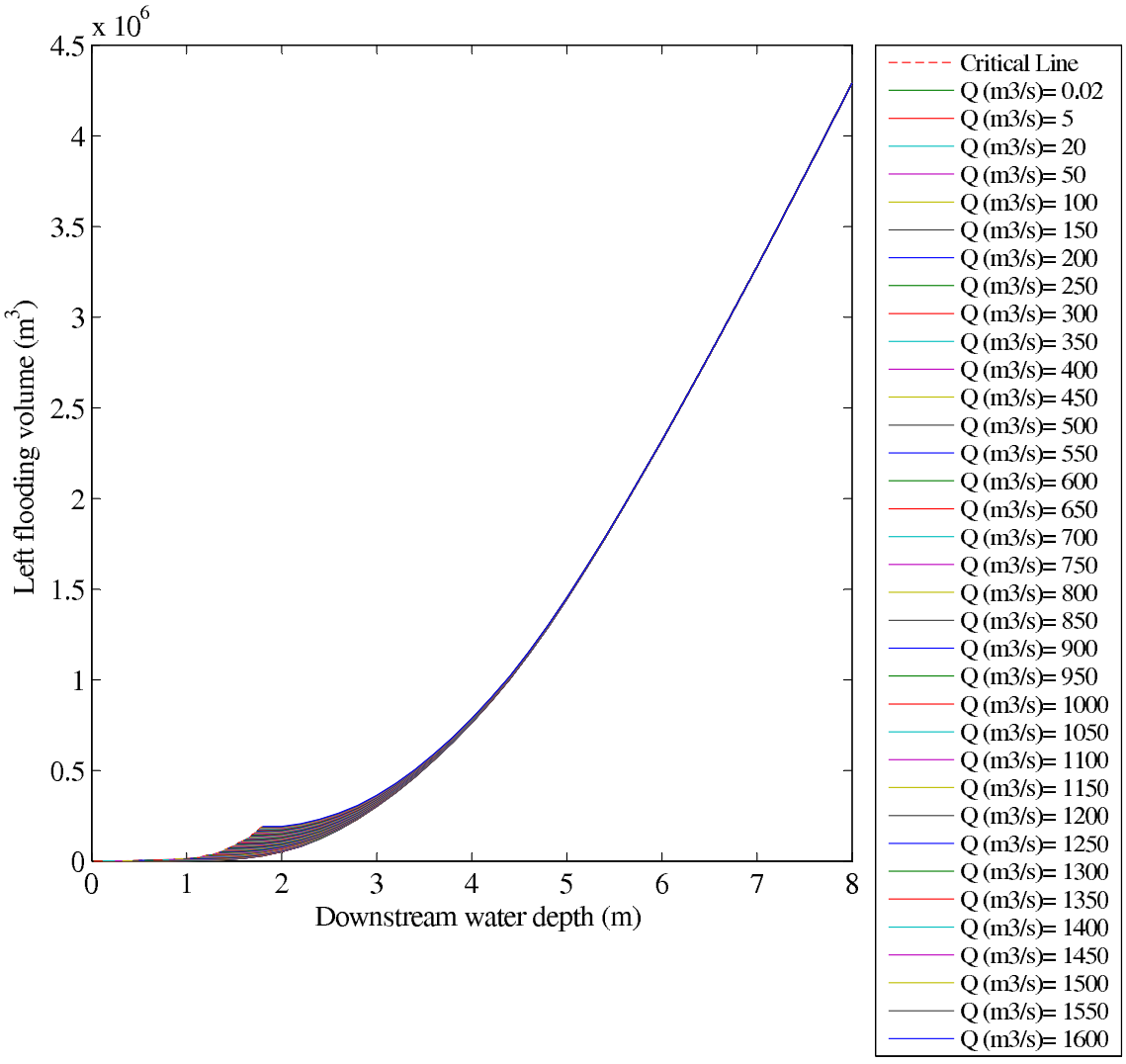

Figure C.24: Left Flooding Performance Graph - Reach R24

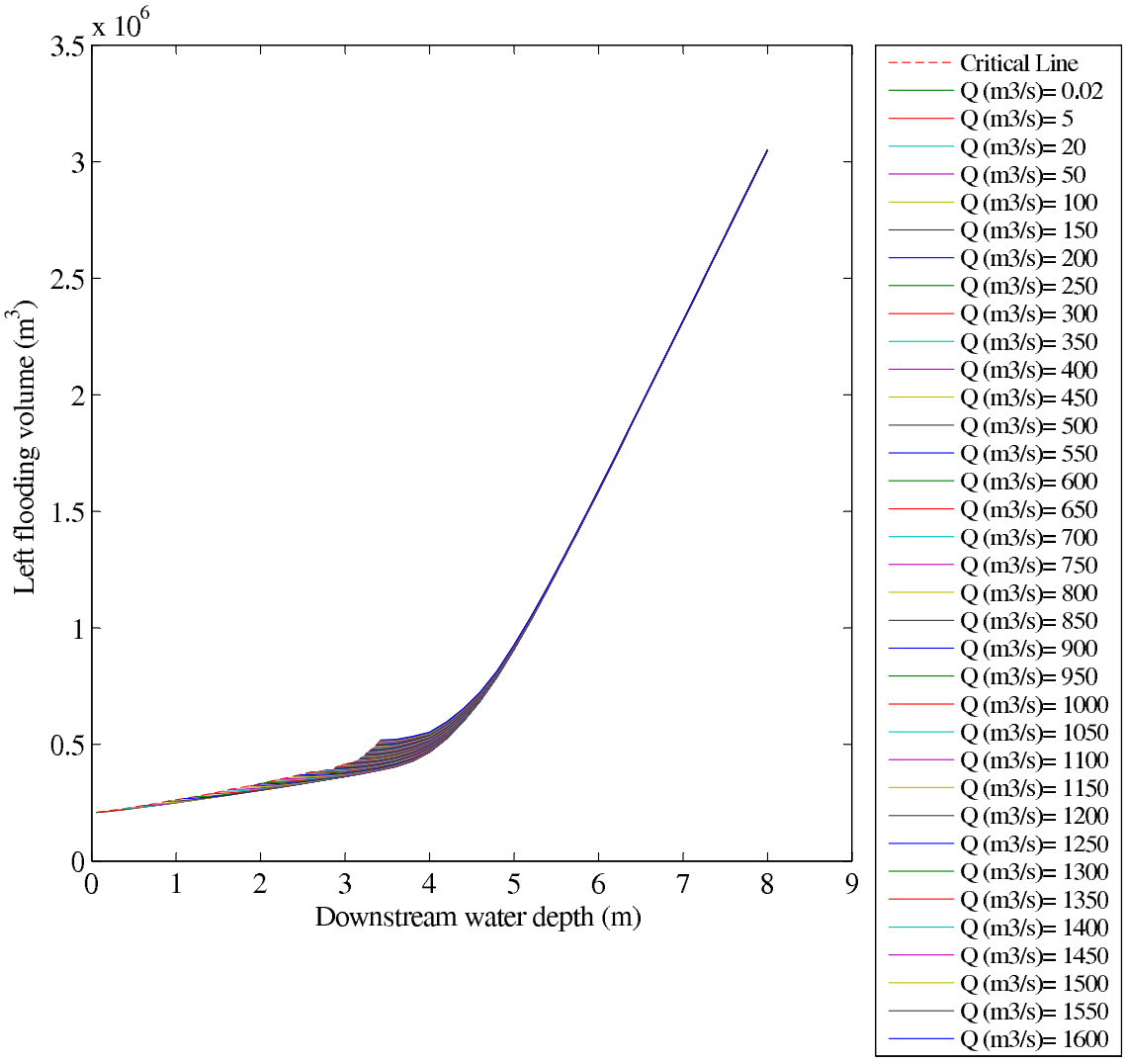

Figure C.25: Left Flooding Performance Graph - Reach R25

APPENDIX D

RIGTH FLOODING PERFORMANCE GRAPH

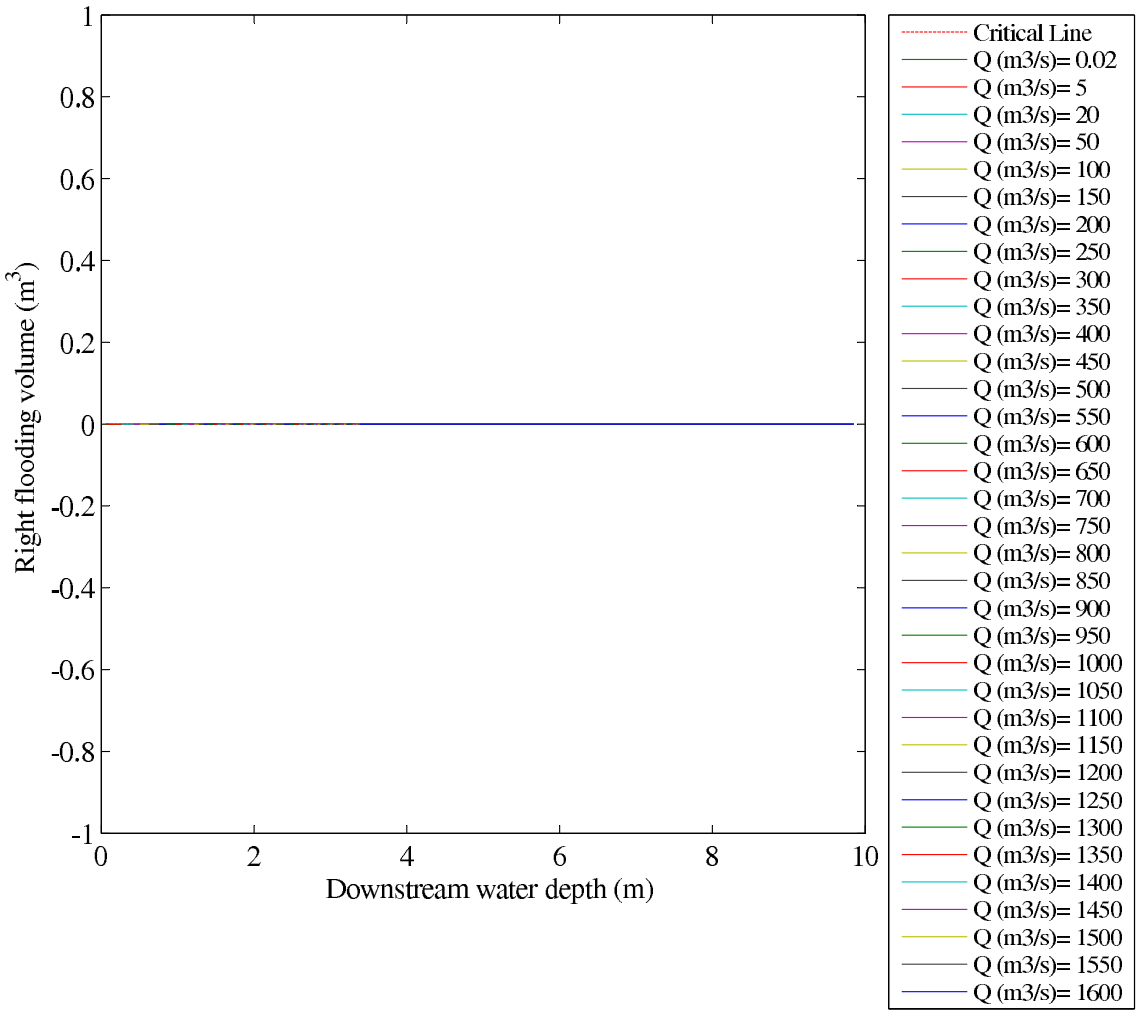

Figure D.1: Rigth Flooding Performance Graph - Reach R1

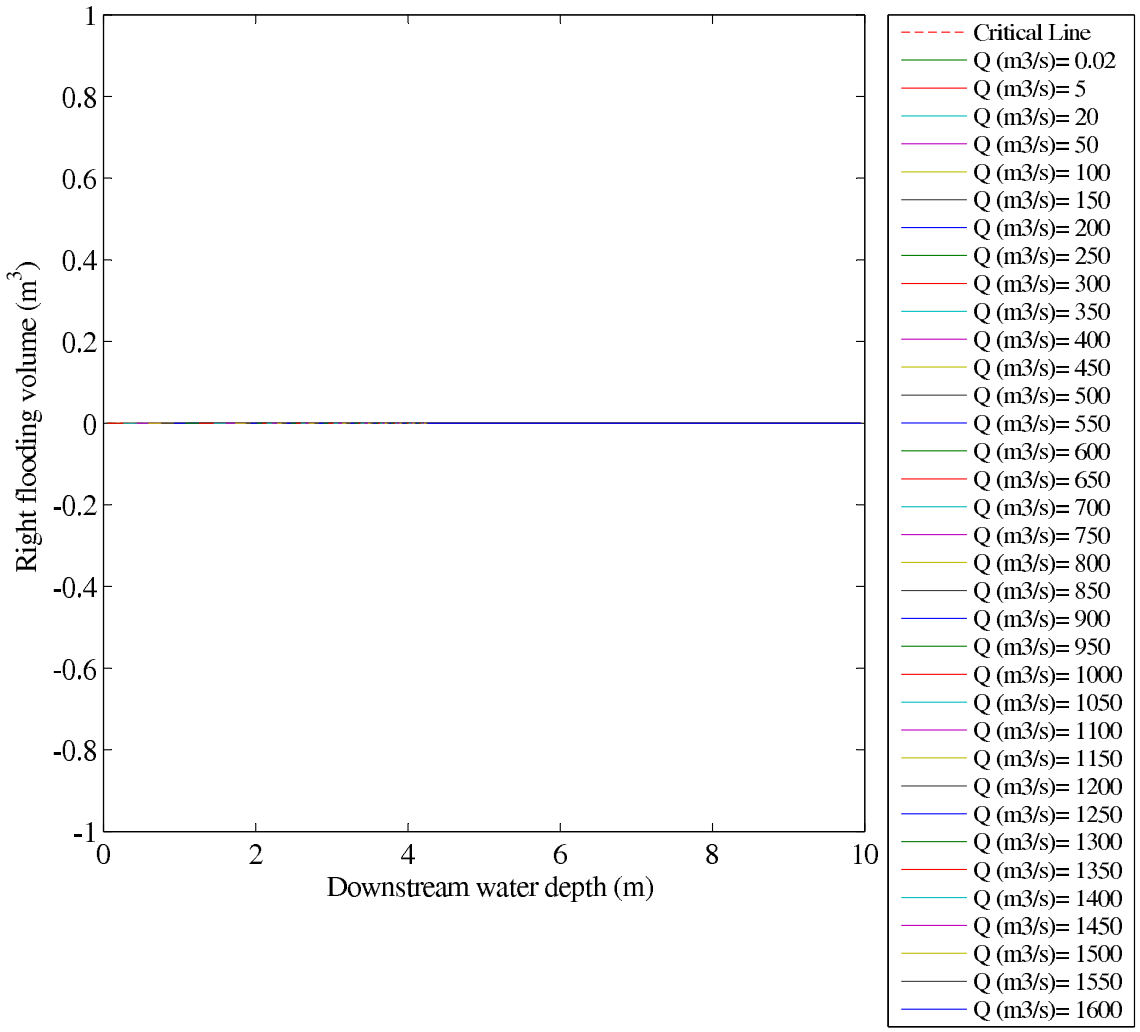

Figure D.2: Rigth Flooding Performance Graph - Reach R2

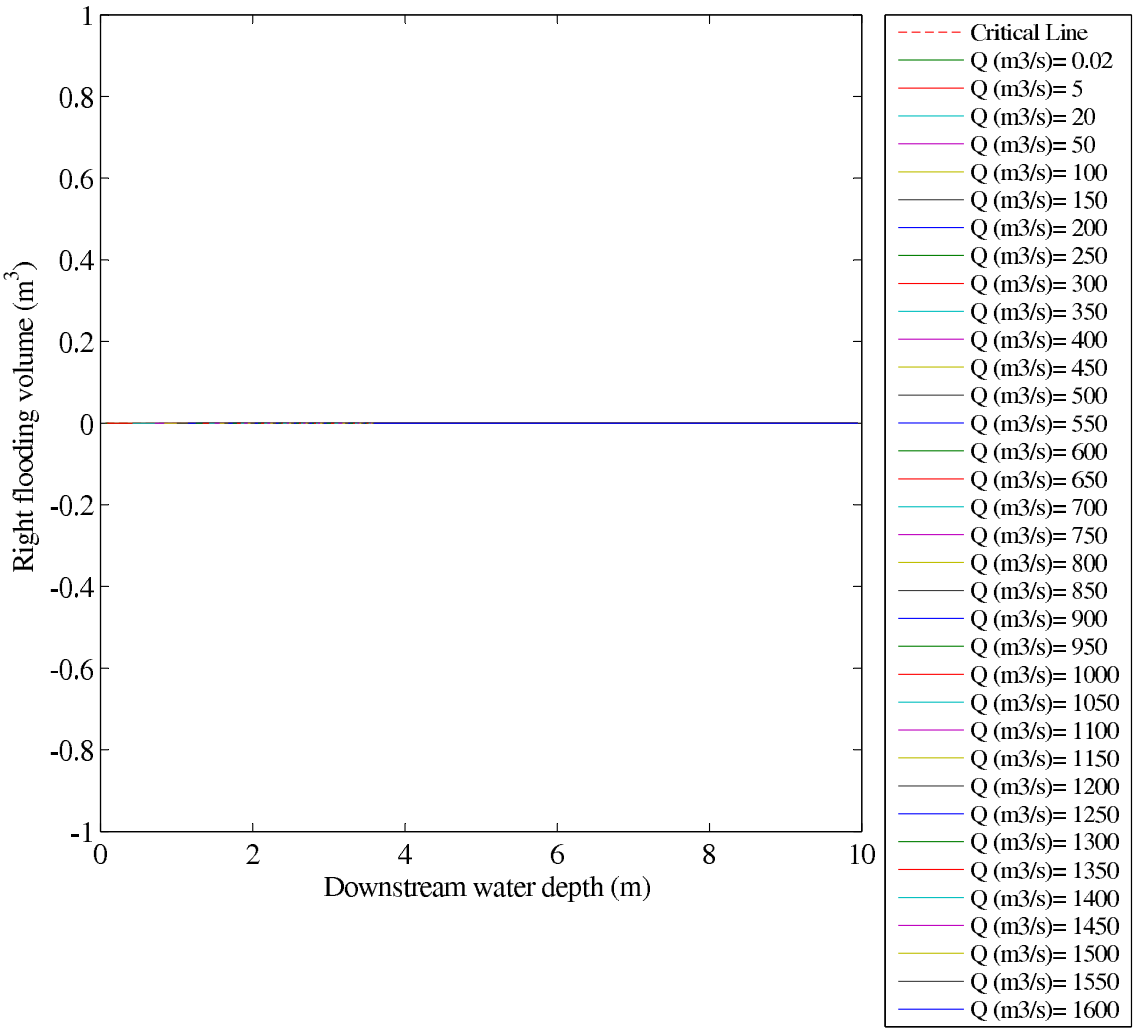

Figure D.3: Rigth Flooding Performance Graph - Reach R3

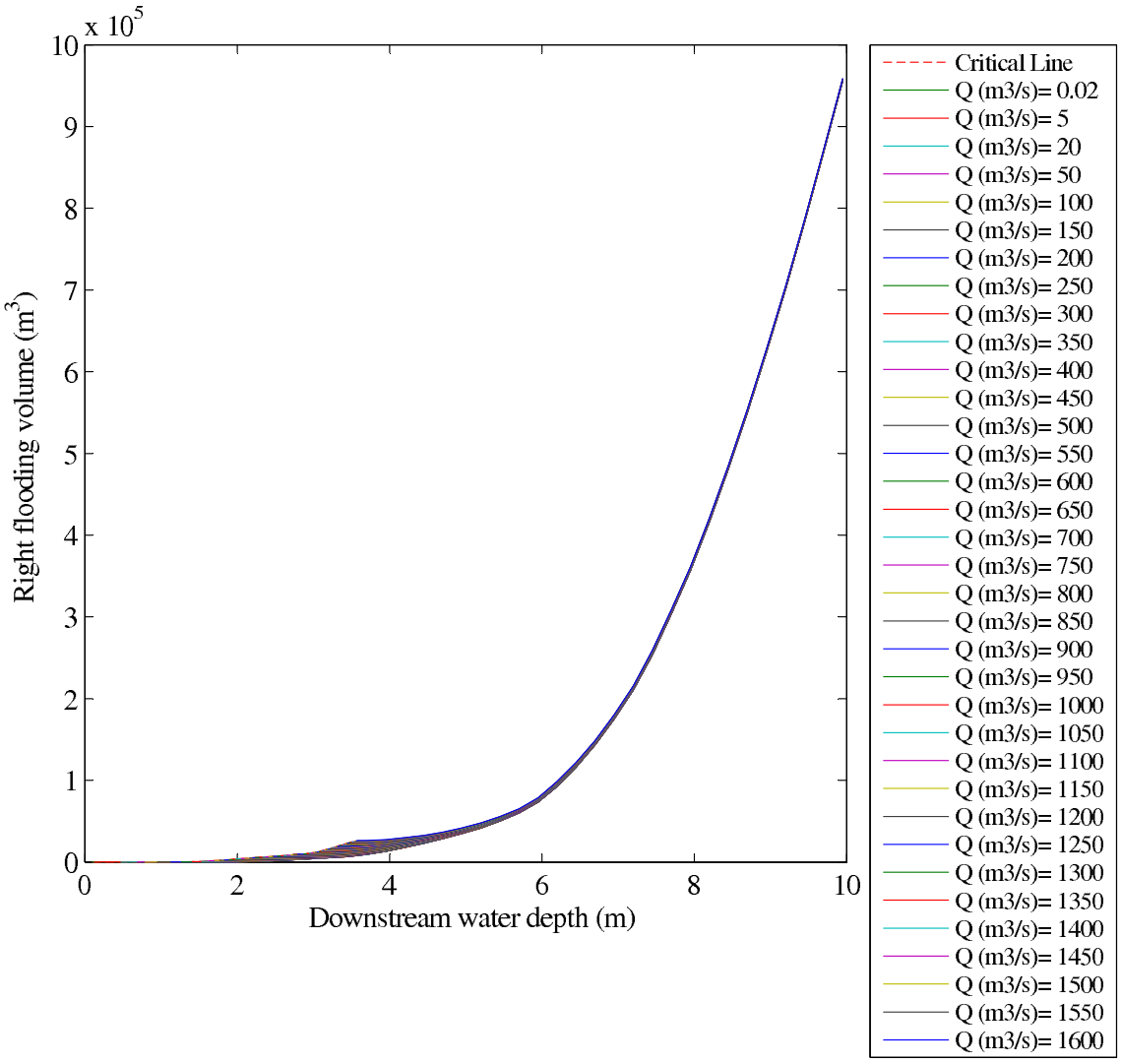

Figure D.4: Rigth Flooding Performance Graph - Reach R4

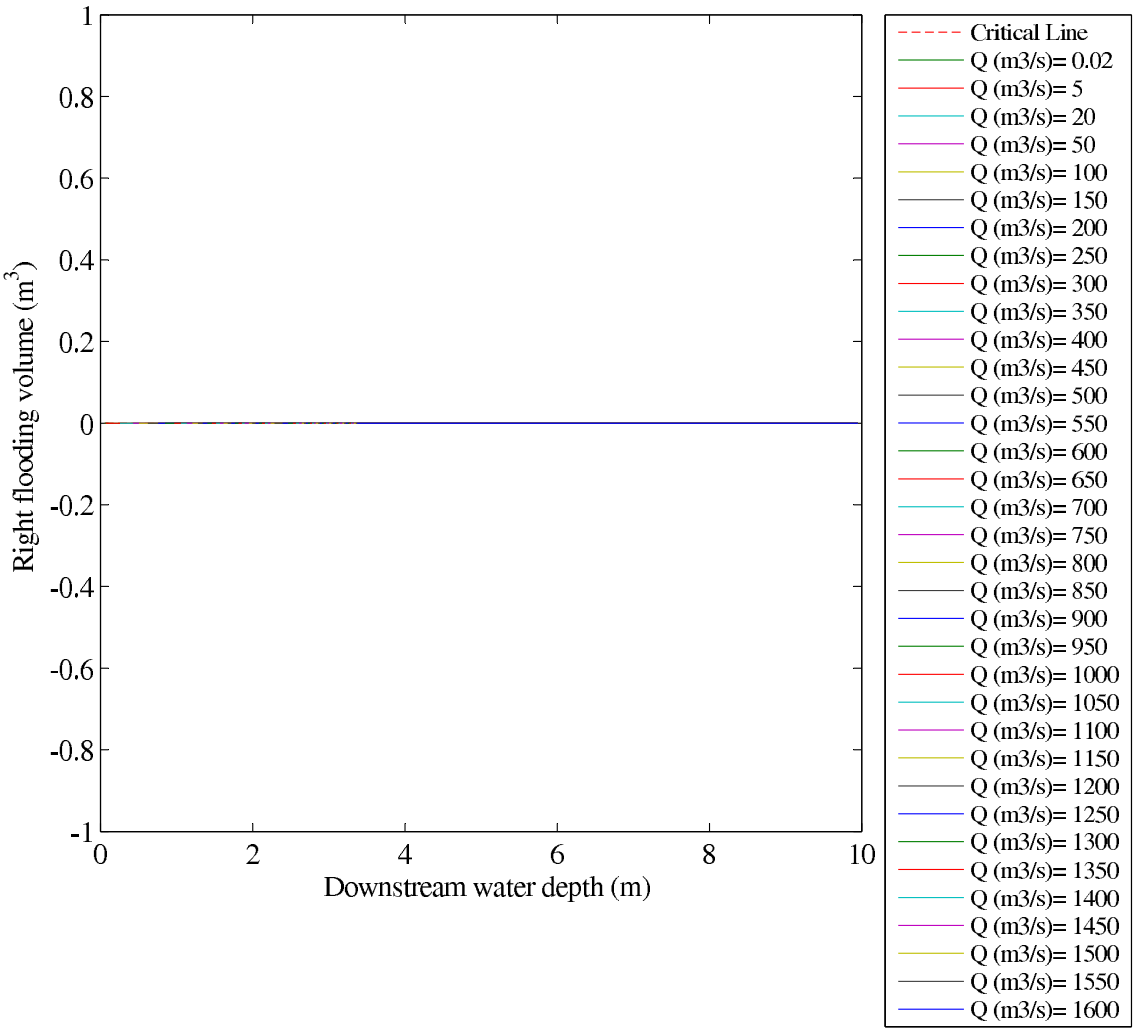

Figure D.5: Rigth Flooding Performance Graph - Reach R5

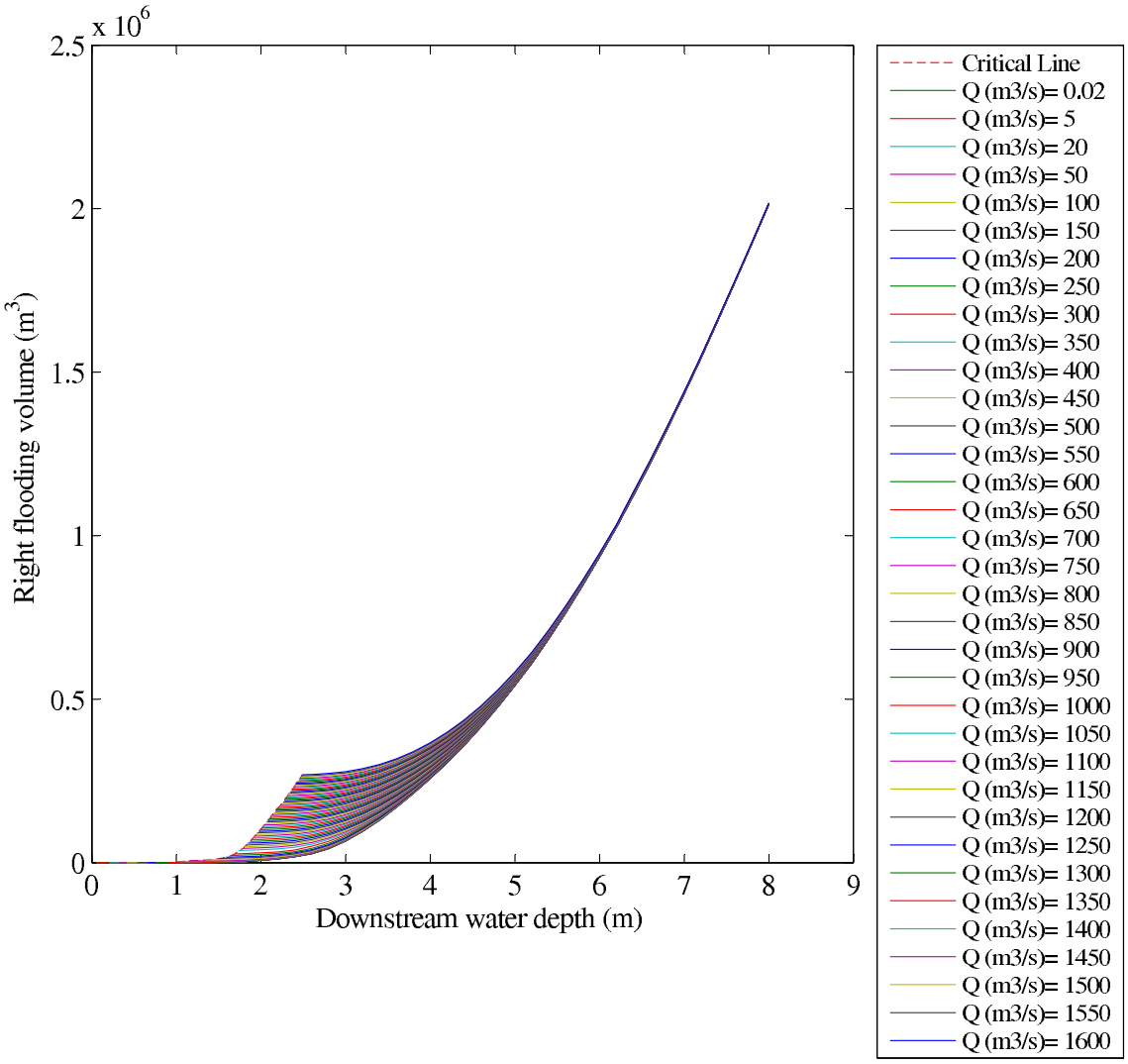

Figure D.6: Rigth Flooding Performance Graph - Reach R6

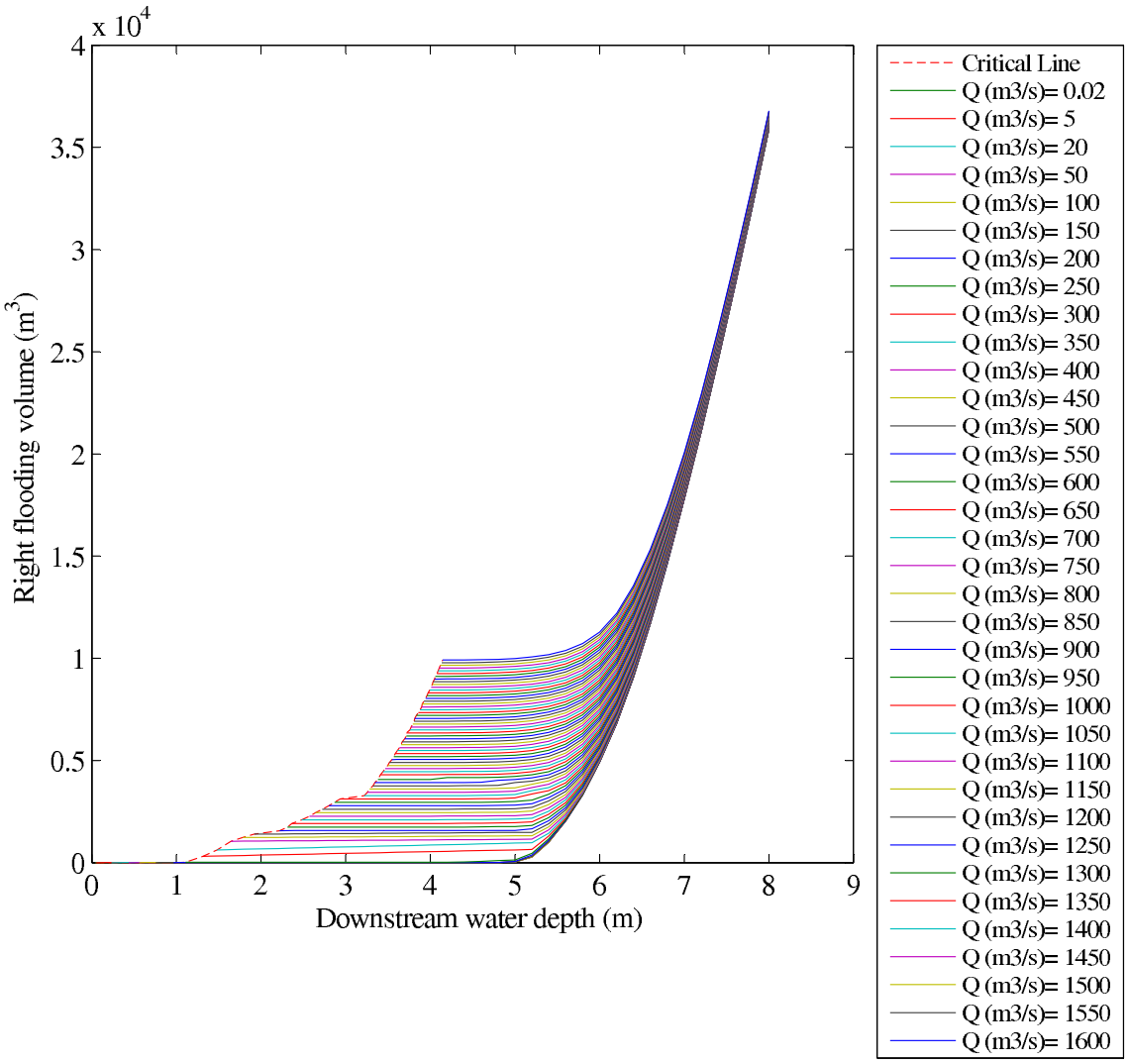

Figure D.7: Rigth Flooding Performance Graph - Reach R7

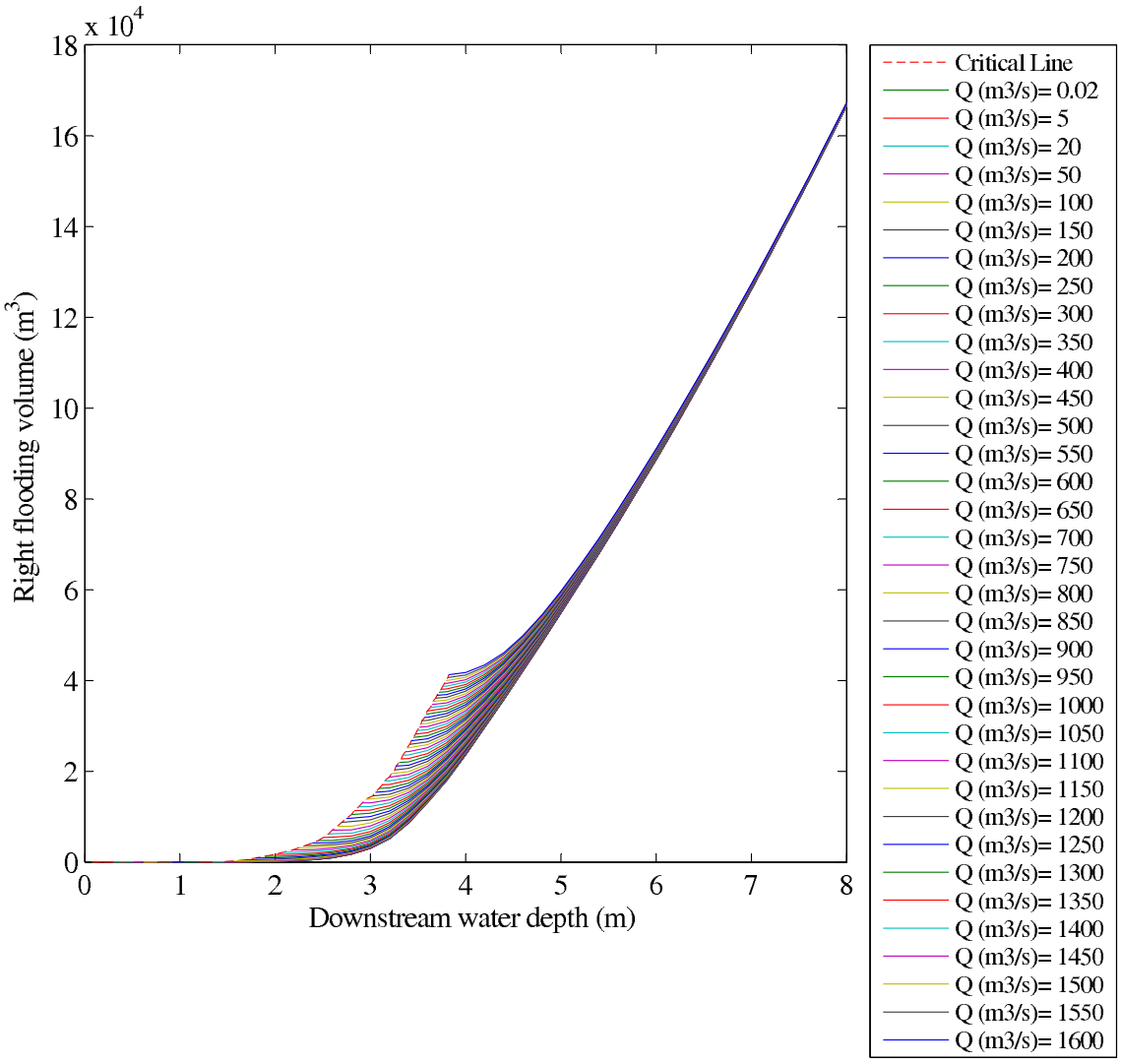

Figure D.8: Rigth Flooding Performance Graph - Reach R8

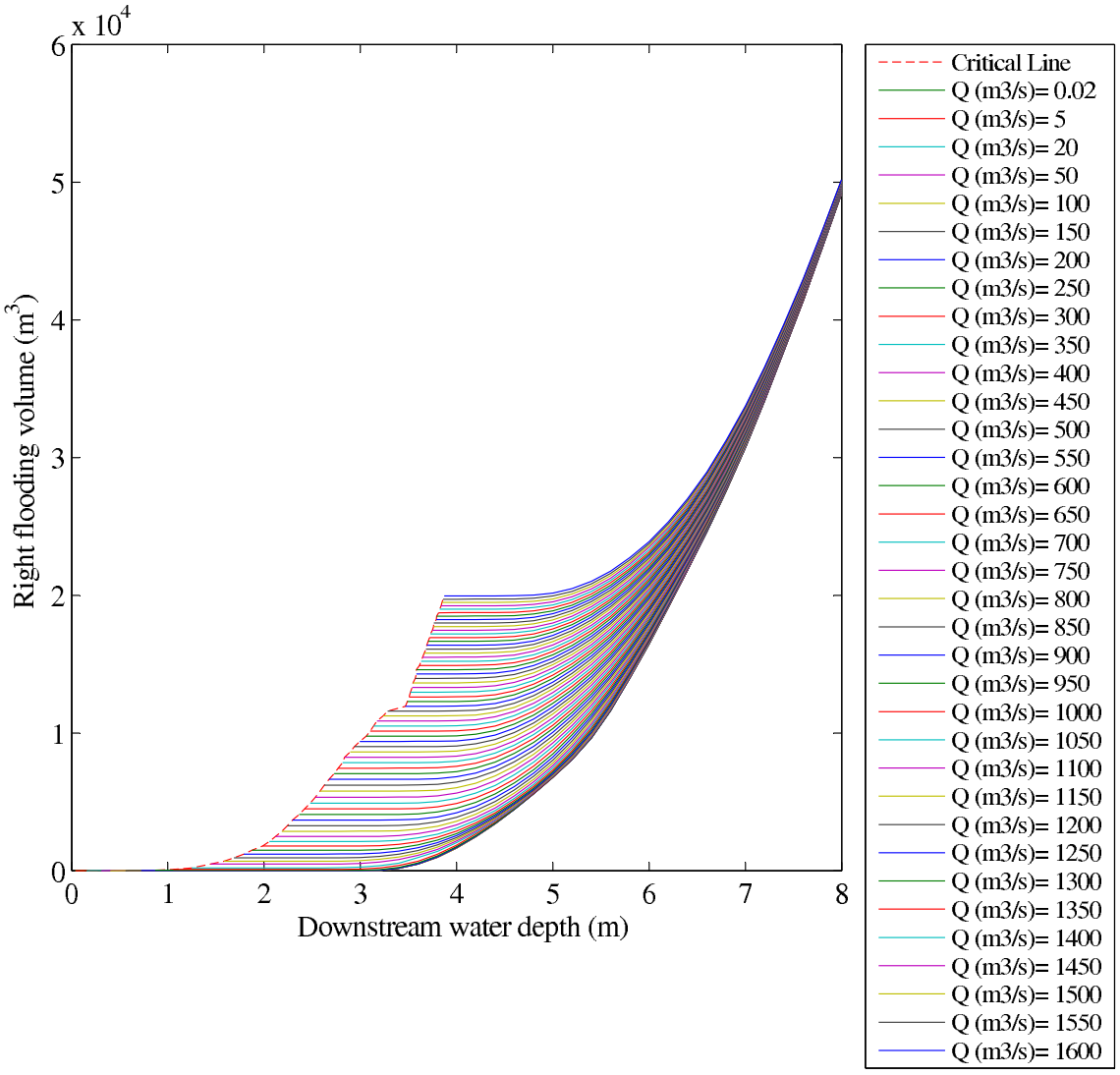

Figure D.9: Rigth Flooding Performance Graph - Reach R9

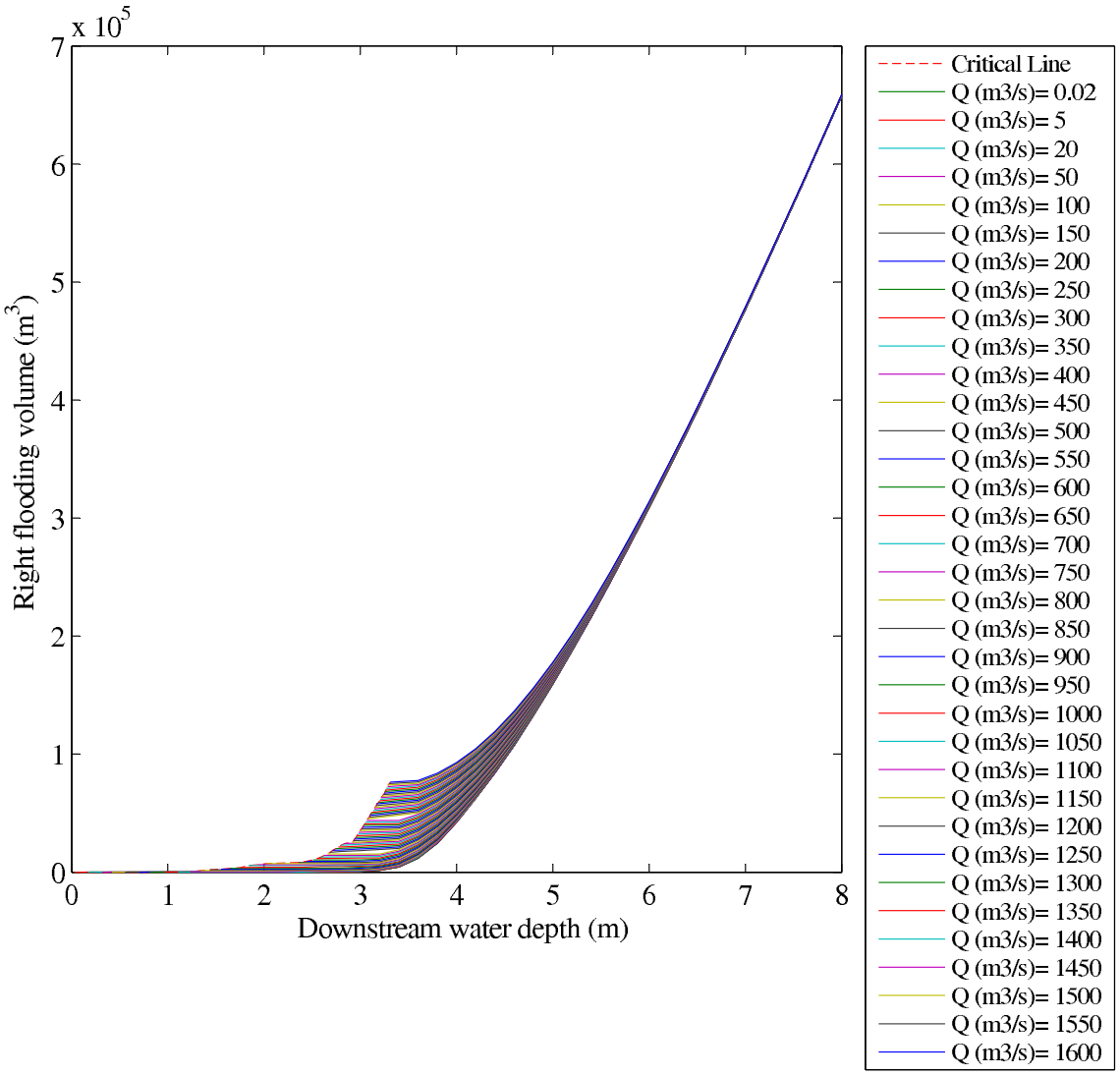

Figure D.10: Rigth Flooding Performance Graph - Reach R10

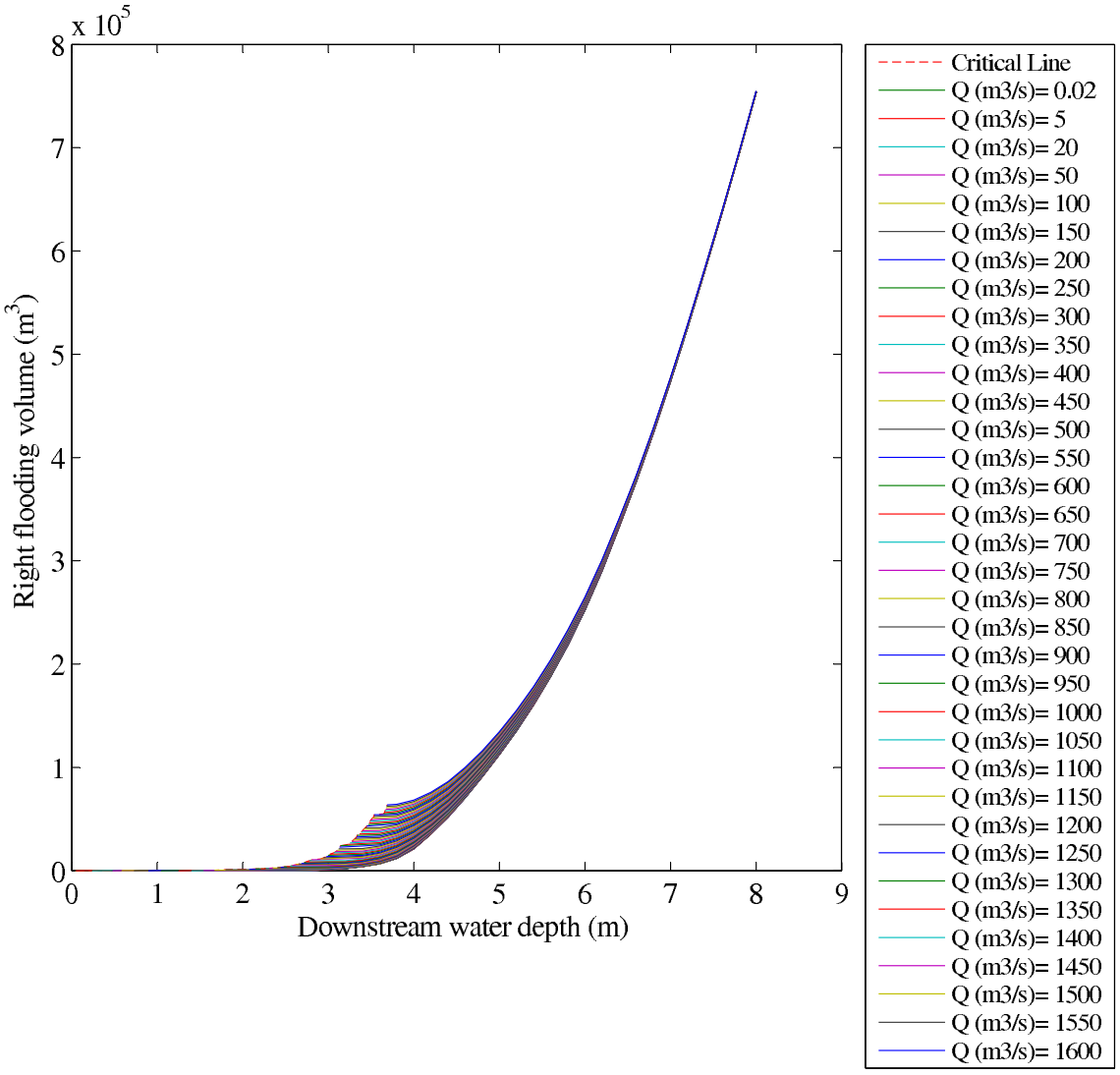

Figure D.11: Rigth Flooding Performance Graph - Reach R11

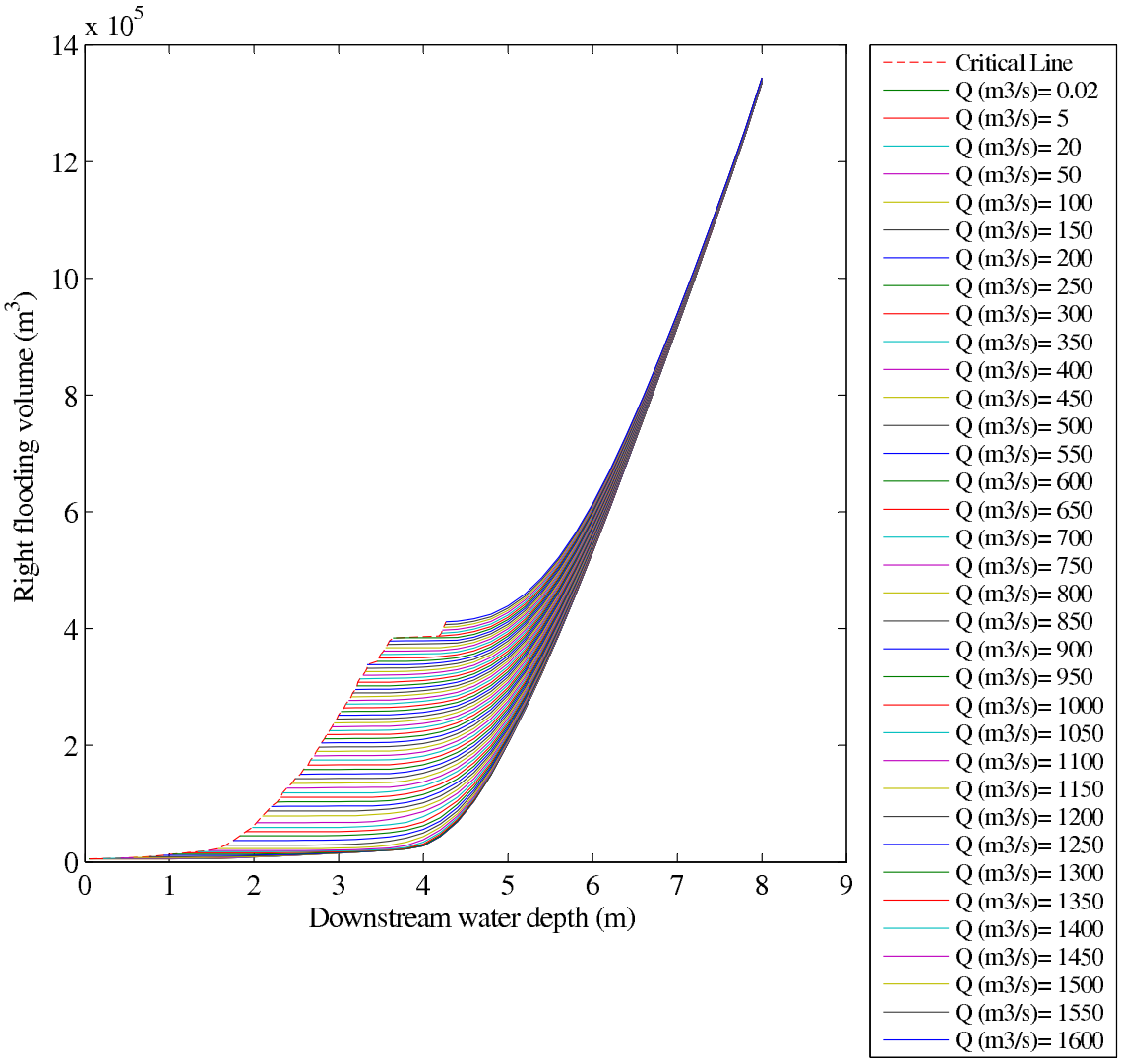

Figure D.12: Rigth Flooding Performance Graph - Reach R12

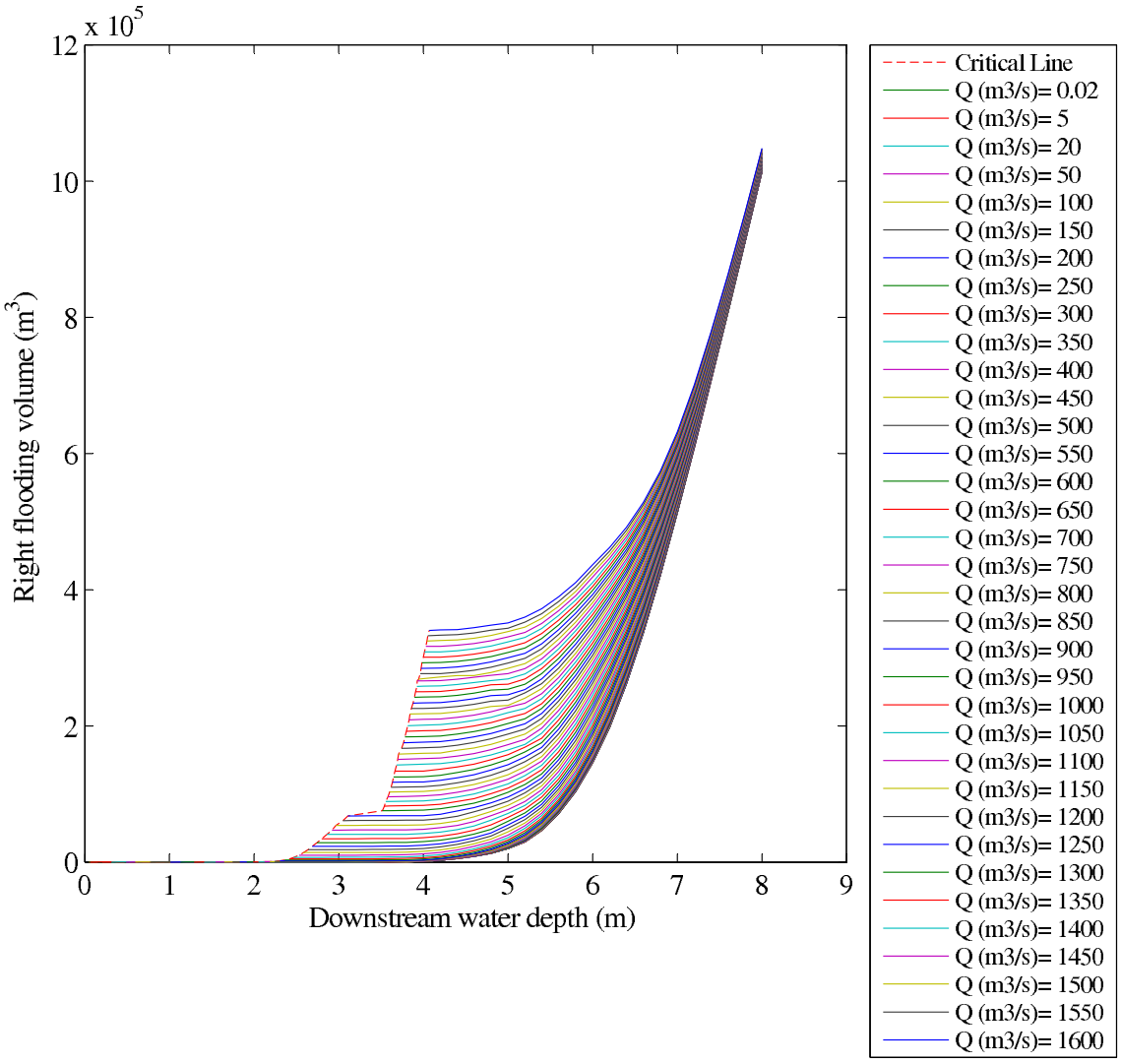

Figure D.13: Rigth Flooding Performance Graph - Reach R13

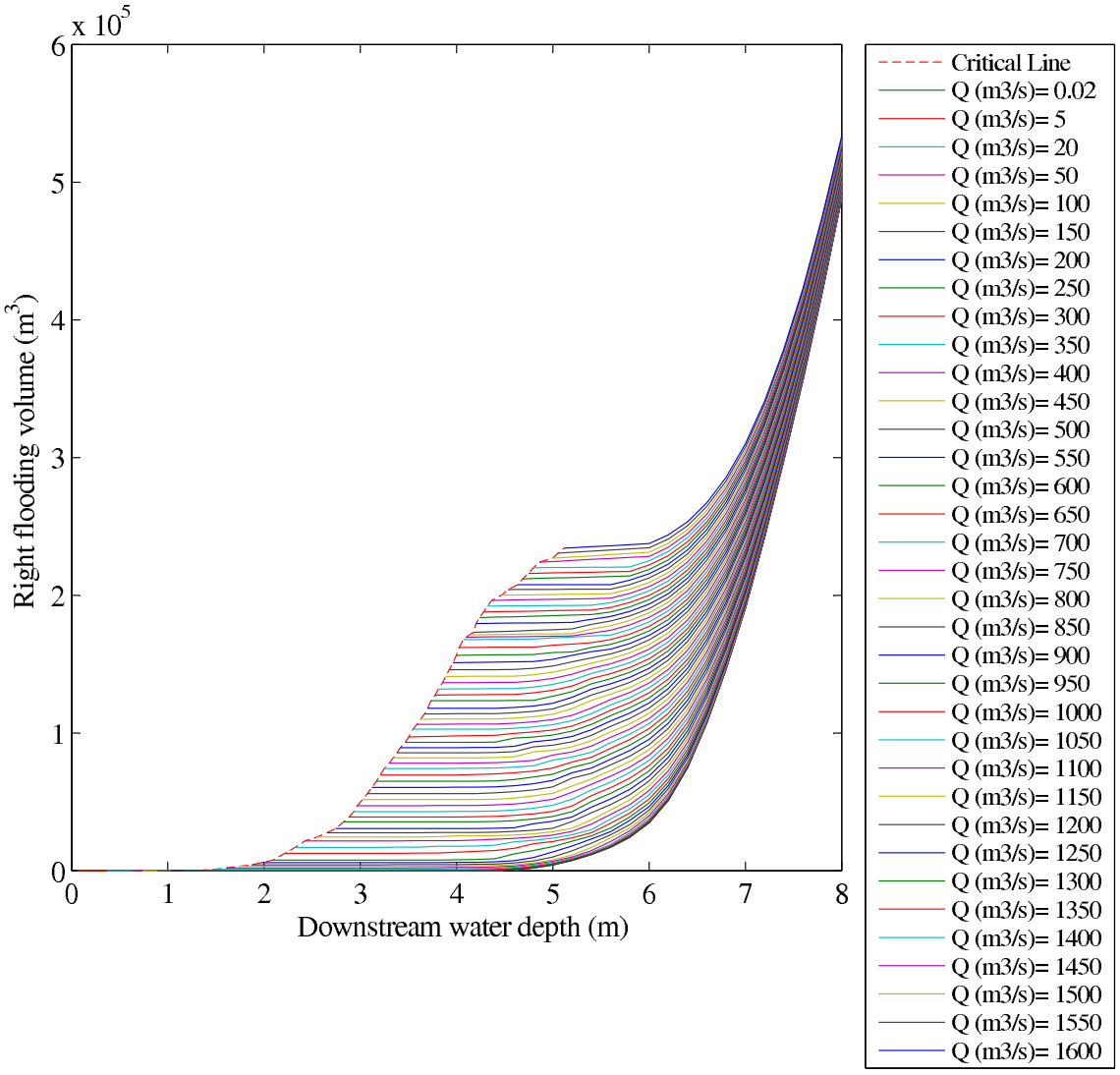

Figure D.14: Rigth Flooding Performance Graph - Reach R14

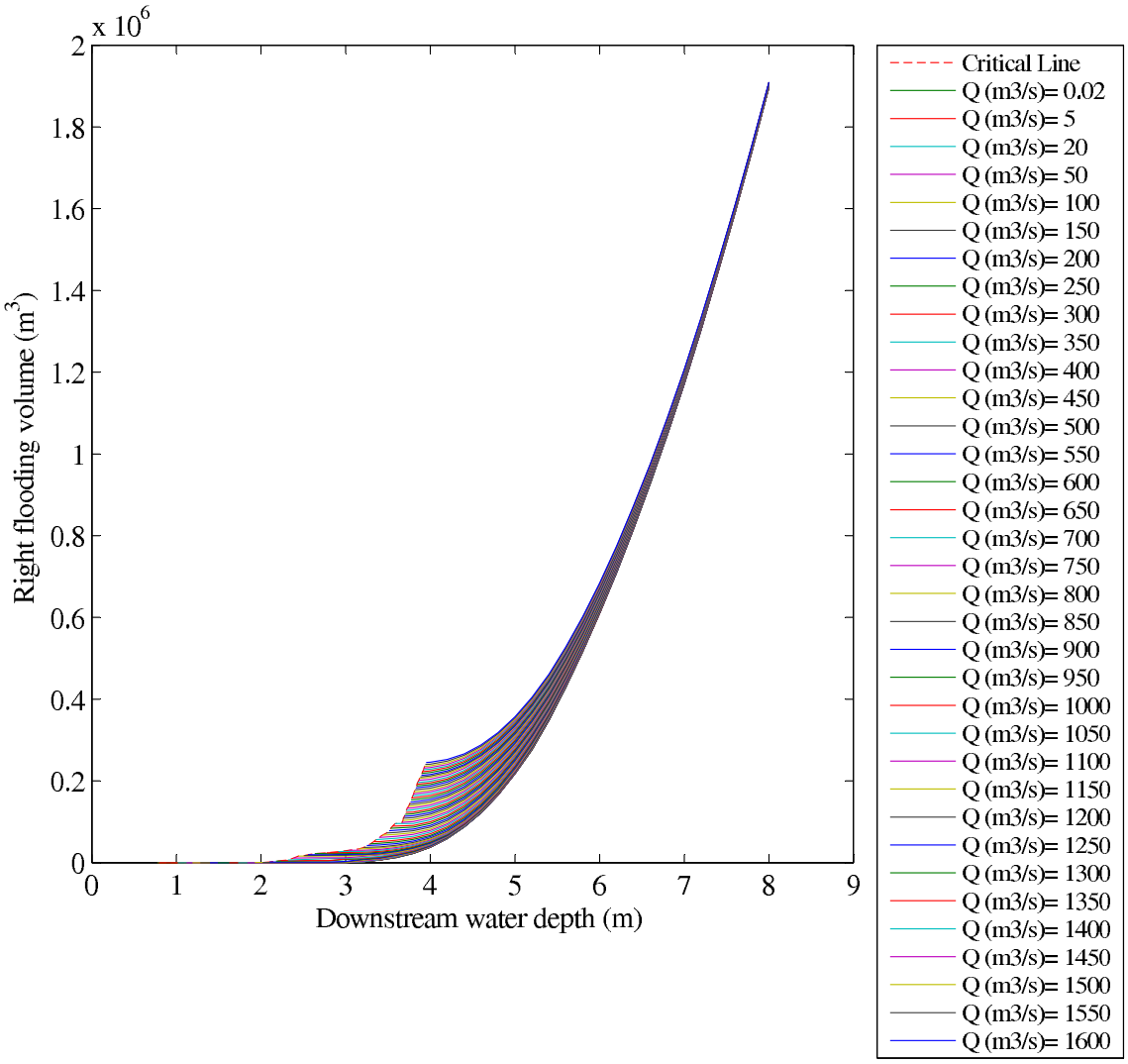

Figure D.15: Rigth Flooding Performance Graph - Reach R15

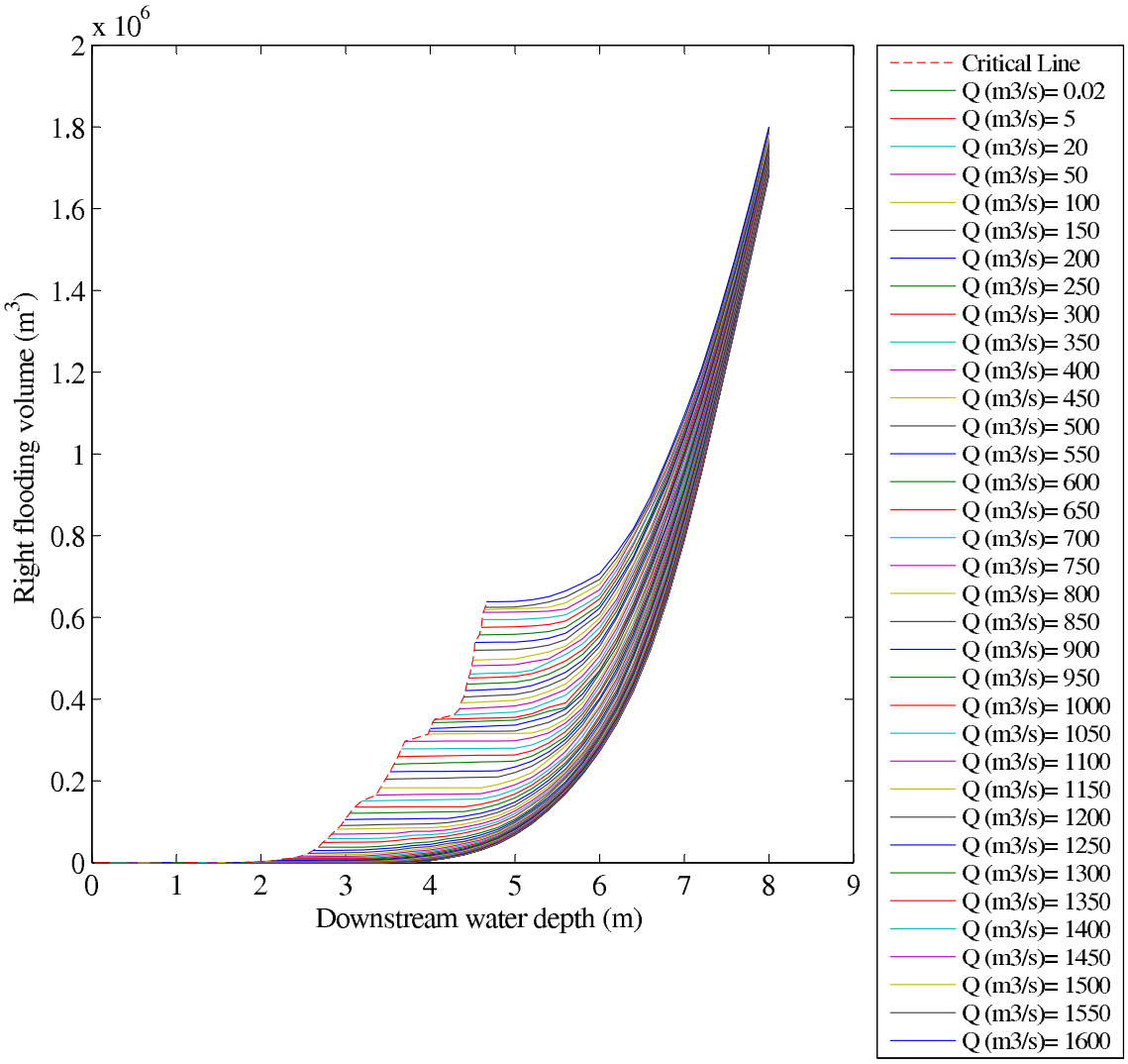

Figure D.16: Rigth Flooding Performance Graph - Reach R16

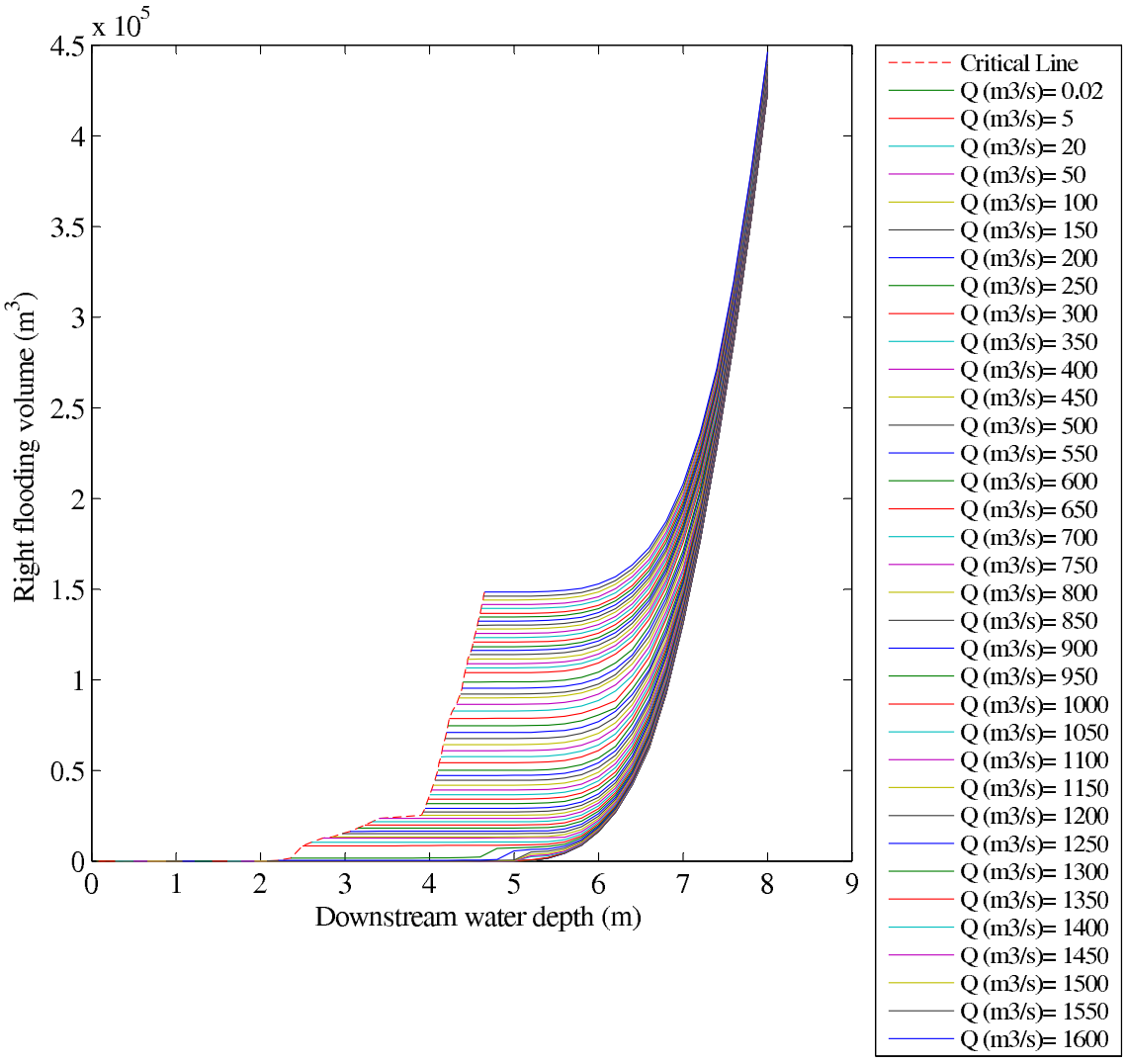

Figure D.17: Rigth Flooding Performance Graph - Reach R17

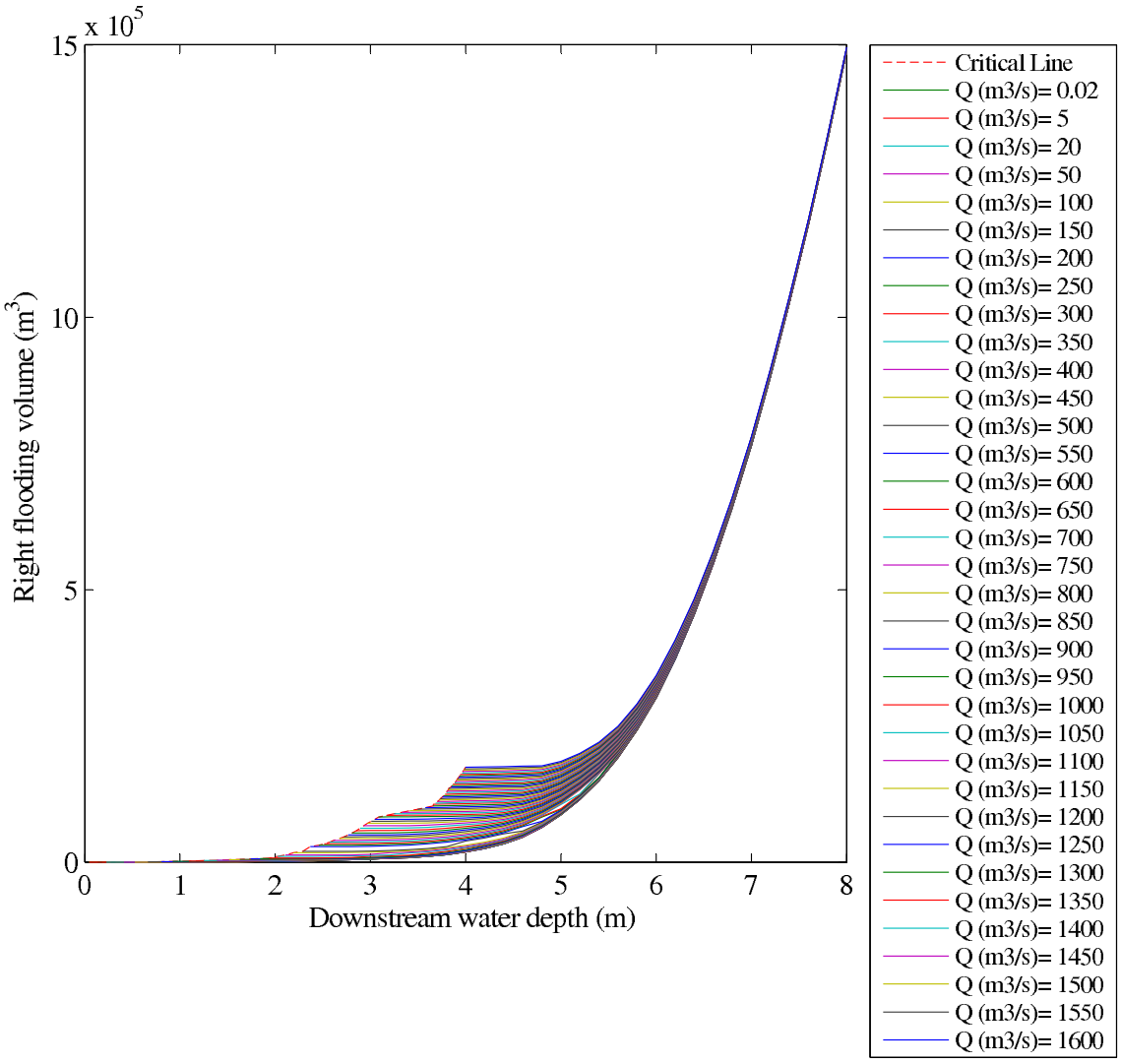

Figure D.18: Rigth Flooding Performance Graph - Reach R18

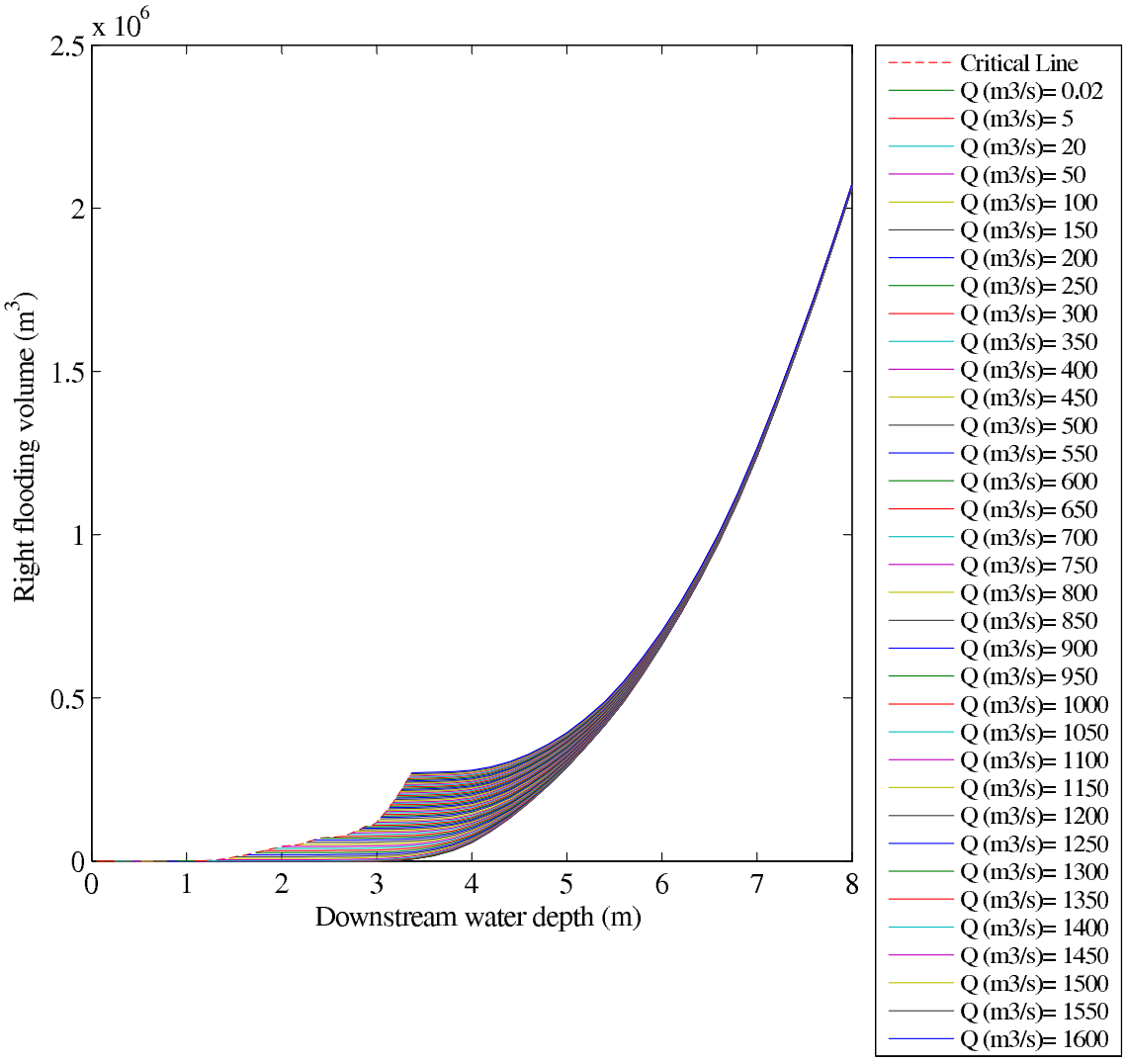

Figure D.19: Rigth Flooding Performance Graph - Reach R19

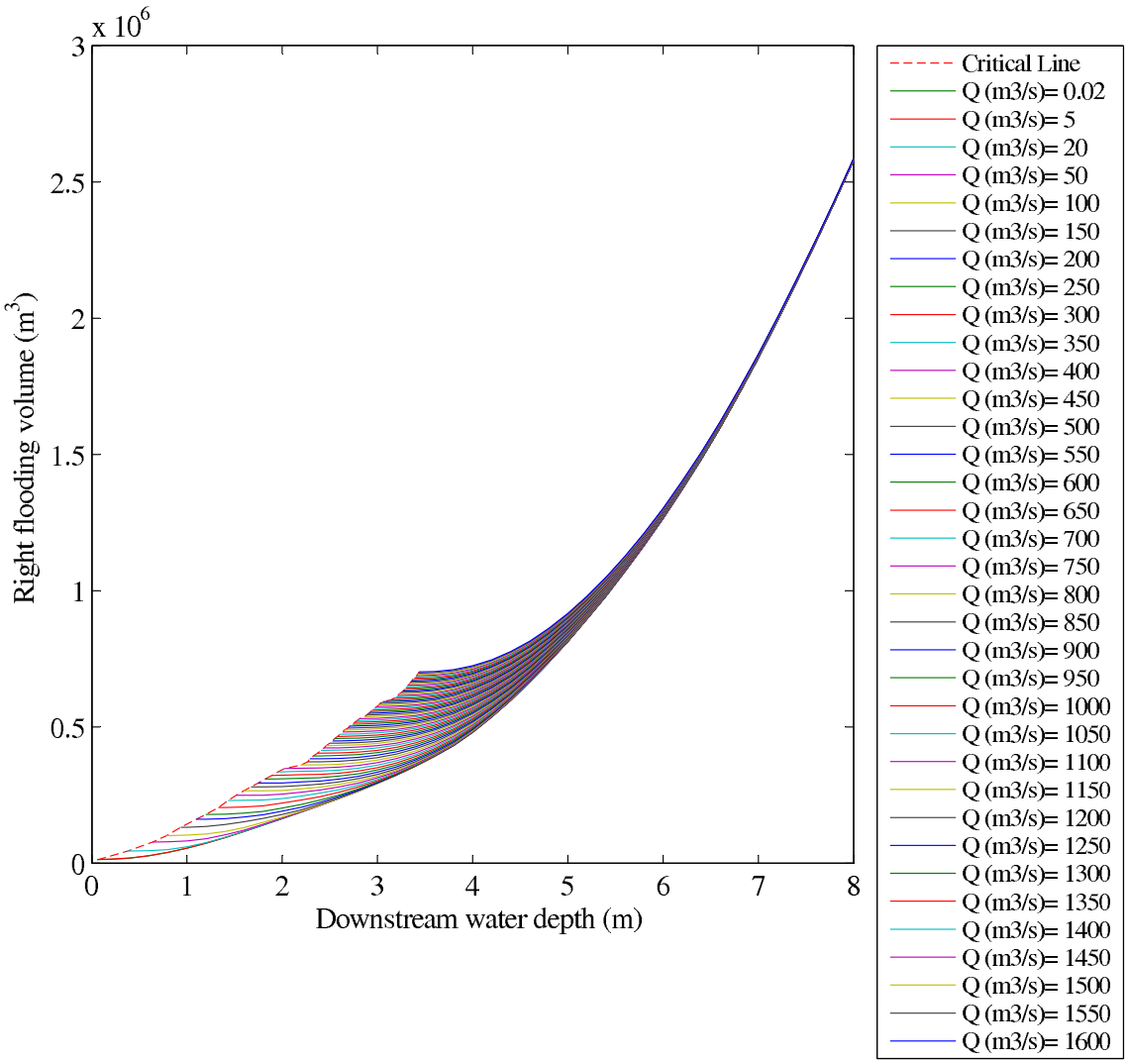

Figure D.20: Rigth Flooding Performance Graph - Reach R20

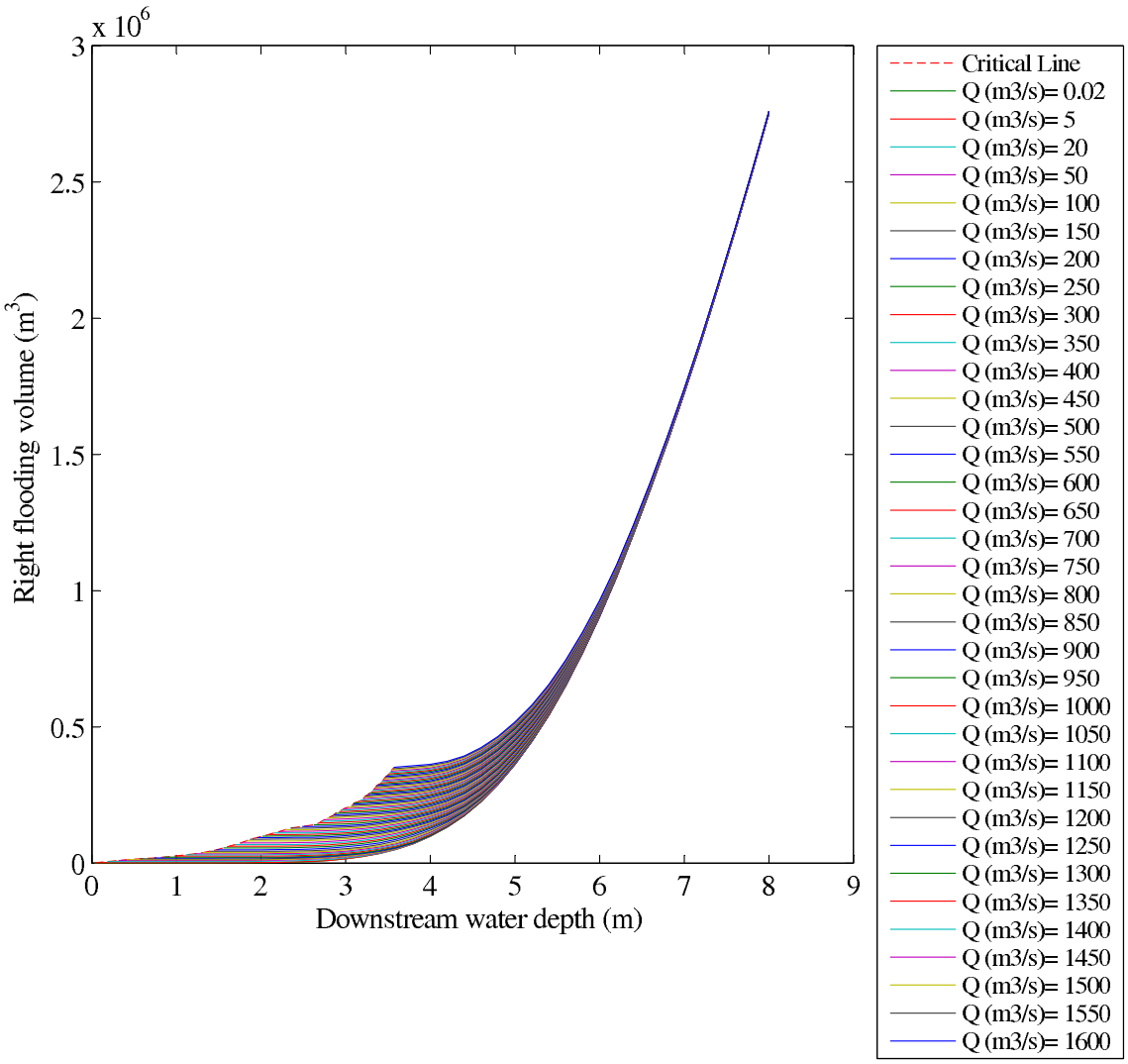

Figure D.21: Rigth Flooding Performance Graph - Reach R21

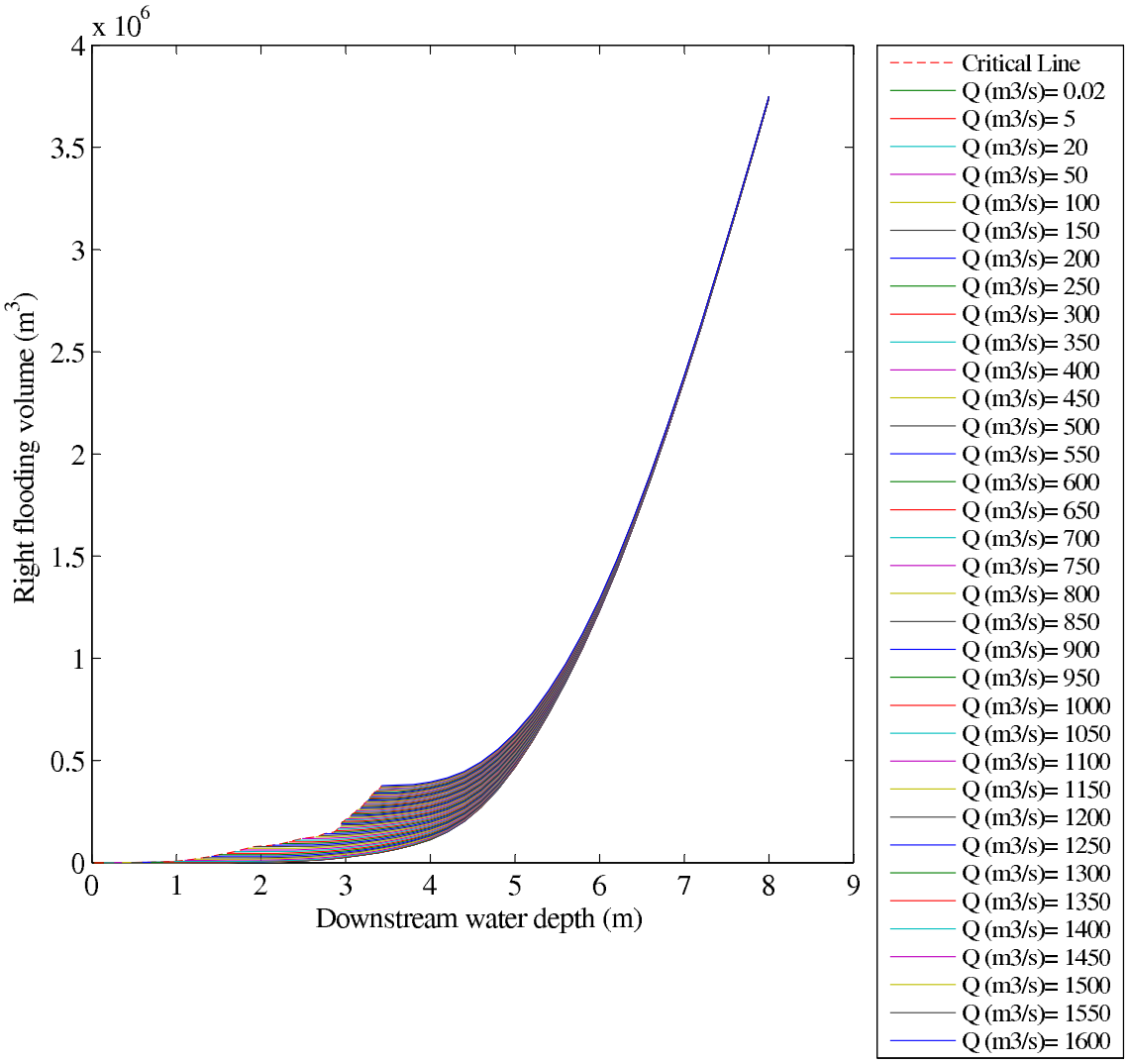

Figure D.22: Rigth Flooding Performance Graph - Reach R22

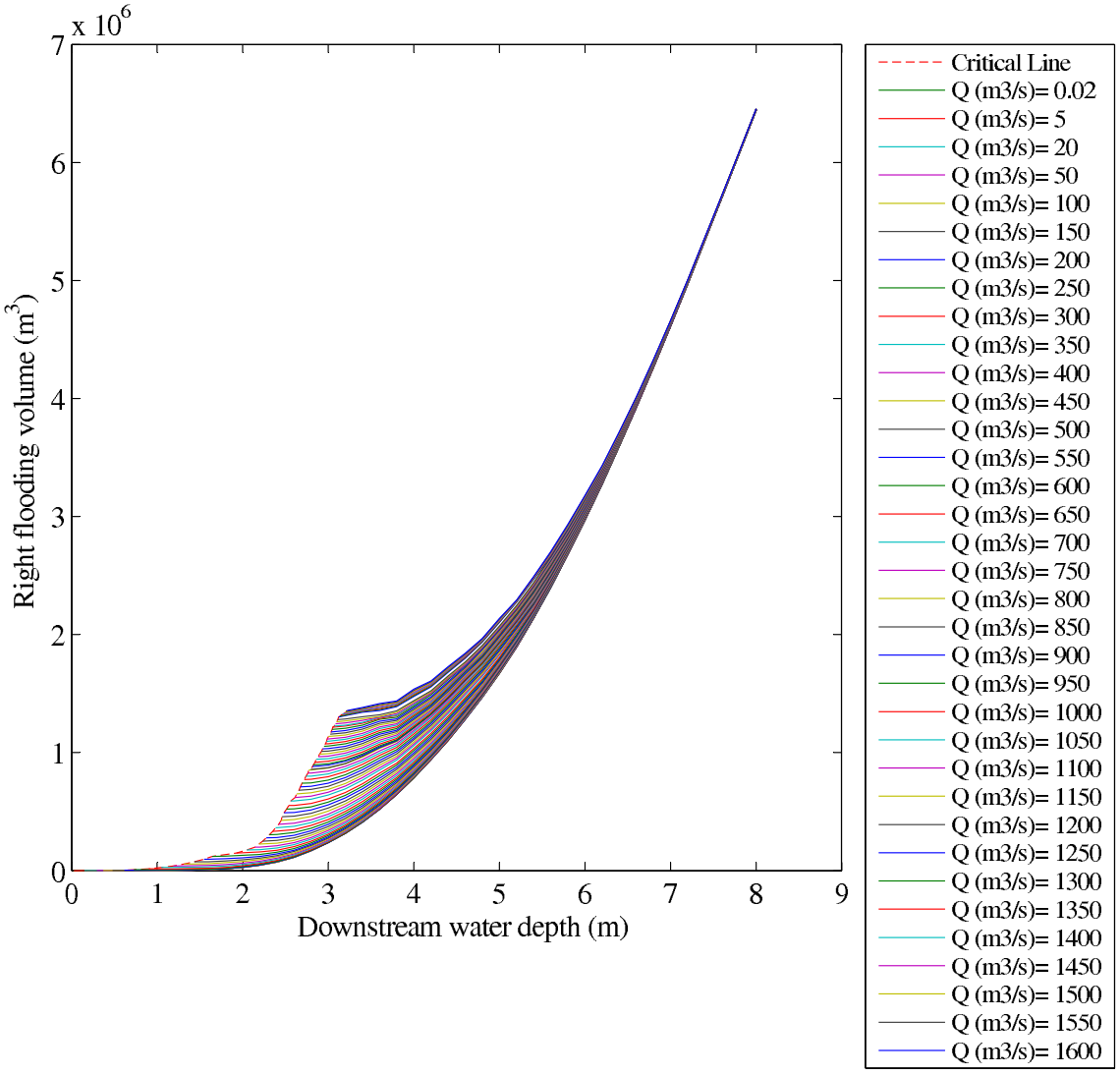

Figure D.23: Rigth Flooding Performance Graph - Reach R23

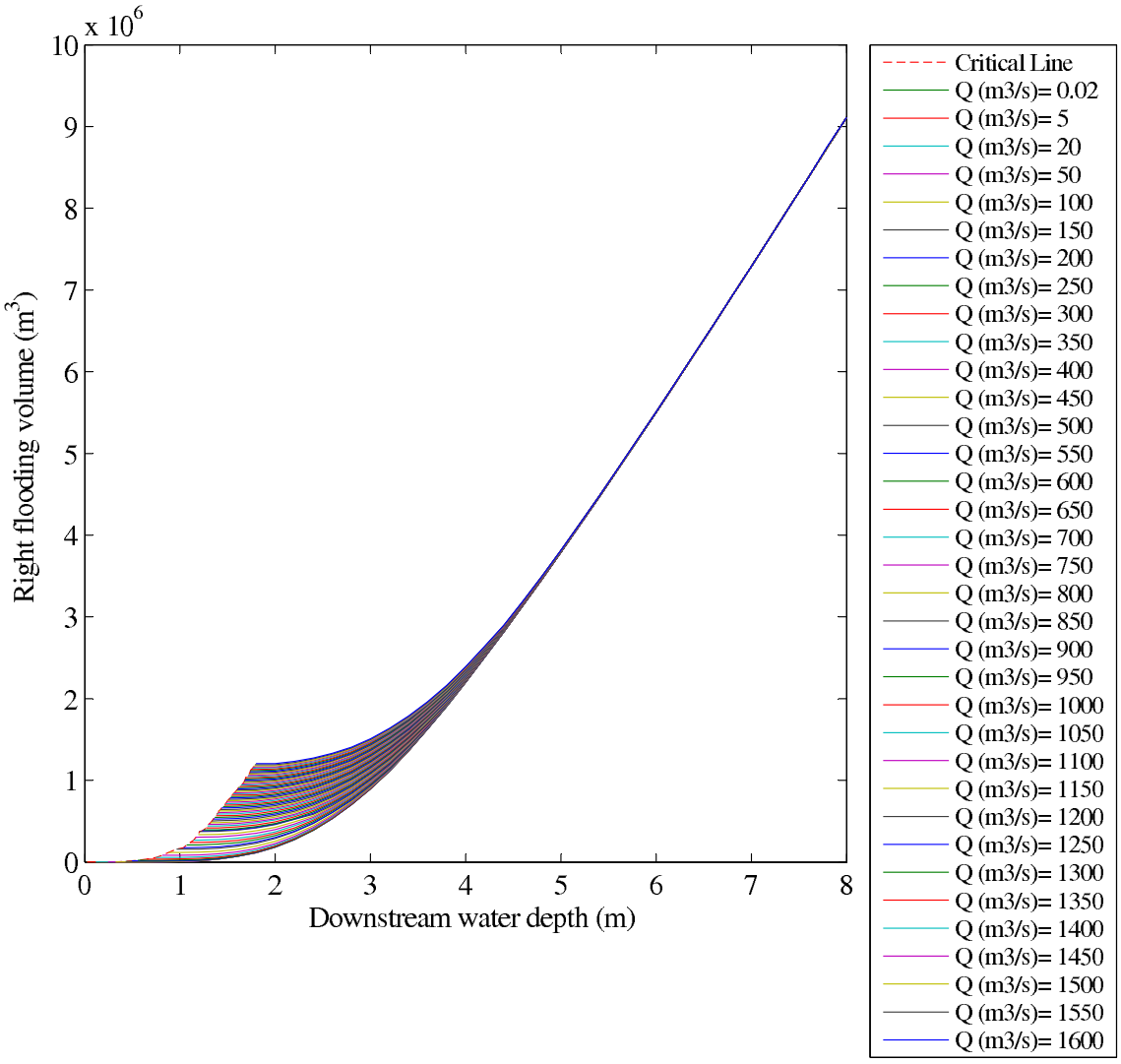

Figure D.24: Rigth Flooding Performance Graph - Reach R24

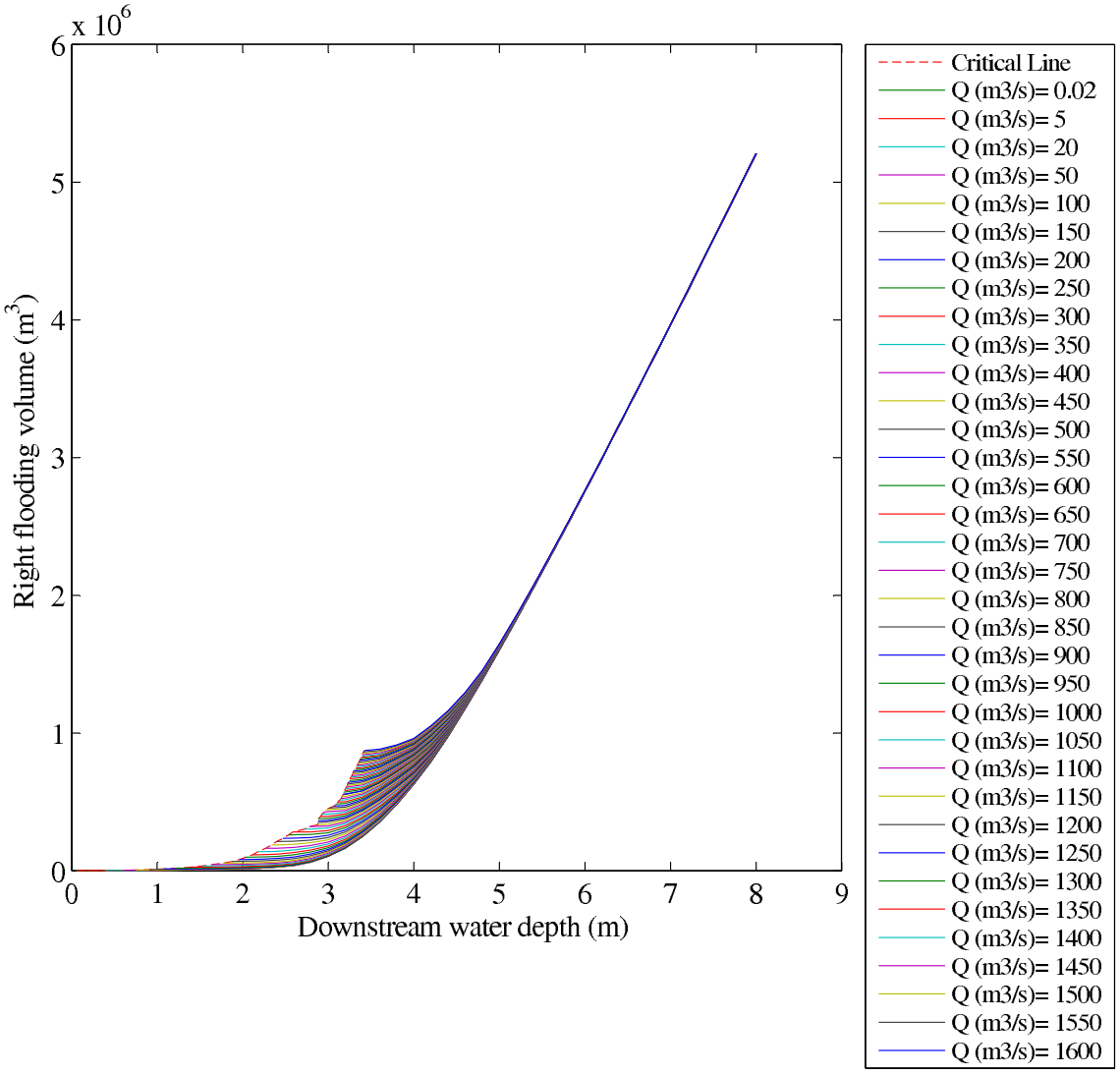

Figure D.25: Rigth Flooding Performance Graph - Reach R25